Scale Dependence of Flow and Transport Parameters in Porous Media

Der Fakultät für Bau- und Umweltingenieurwissenschaften
der Universität Stuttgart
zur Erlangung des Grades einer
habilitierten Doktorin

vorgelegte Habilitationsschrift
von
Dr. sc. nat. Insa Neuweiler

2006

Zusammenfassung

Motivation

Die vorliegende Arbeit befaßt sich mit der Skalenabhängigkeit von Modellen, die Strömungs- und Transportprozesse in porösen Medien beschreiben. Solche Prozesse sind für viele ingenieurwissenschaftlichen Fragestellungen relevant, wie beispielsweise die Grundwasserströmung in Gesteinsschichten oder geklüftetem Fels. Die Modellierung von Grundwasserströmung und Transport gelöster Stoffe ist notwendig für die Abgrenzung von Grundwasserschutzgebieten und die Sanierung von verunreinigten Grundwasserleitern. Eine weitere relevante Fragestellung ist die Förderung von Erdöl. Viele Förderungstechniken basieren auf der Verdrängung des Öls durch ein anderes, mit Öl nicht mischbares Fluid. Solch großskaligen Zweiphasenströmungsprozesse spielen bei der Speicherung von CO_2 in tiefen, geologischen Formationen eine Rolle. Eine solche Technik wird derzeit diskutiert bzw. in ersten Pilotprojekten angewandt mit dem Ziel, dem Anstieg von CO_2 in der Atmosphäre entgegenzuwirken. Zweiphasenprozesse müssen zudem für Risikoabschätzungen bei der Lagerung von gefährlichen Materialien, so wie radioaktiven Abfall, oder für die Gewinnung von geothermischer Energie abgeschätzt werden. Technische Anwendungen auf einer kleinen Längenskala sind beispielsweise die Strömung durch die Diffusionsschicht in einer Brennstoffzelle oder der Trocknungsprozess bei der Herstellung von Papier.

Strömungsprozesse in porösen Medien spielen außerdem eine wichtige Rolle für den terrestrischen Teil des Wasserkreislaufs. In der ungesättigten Bodenzone, der Bodenschicht zwischen der Erdoberfläche und einem tiefer liegenden Aquifer, fließen Wasser und Luft durch den Boden. Die ungesättigte Bodenzone hat eine entscheidende Bedeutung für die Bilanzierung von Energie- und Wasserflüssen und somit in der Klimamodellierung.

In dieser Arbeit werden Strömungsprozesse im Untergrund betrachtet. Diese Prozesse sind skalenabhängig, das heißt sie werden auf verschiedenen Längenskalen unterschiedliche stark von verschiedenen Kräften dominiert. Graviation ist zum Beispiel vernachlässigbar, wenn das poröse Medium nicht signifikant in vertikale Richtung ausgedehnt ist und die Druckgradienten in horizontale Richtung groß sind. Die Skalenabhängigkeit der Prozesse ist außerdem mit der Frage nach der typischen Längenskala von Heterogenitäten des porösen Mediums verbunden.

Mit den hier behandelten Modellen können poröse Medien, wie Ton, Kies, Sandsteine oder geklüfteter Fels abgebildet werden (siehe beispielsweise Abbildung 1). Die Abmessungen der Medien sind unterschiedlich. Es ist in Abbildung 1 deutlich sichtbar, dass natürlicher Untergrund in aller Regel heterogen ist und die typischen Längenskalen dieser Strukturen sich stark unterscheiden.

Um Zweiphasenströmungsprozesse sinnvoll abschätzen zu können, werden Modelle benötigt, die diese Prozesse auf den relevanten Längenskalen adäquat beschreiben. Eine Herausforderung an die Modelle stellt die Heterogenität der Parameter eines Mediums dar, mit welchen die Strömungs- und Transportprozesse interagieren. Als ein Beispiel

soll der Aufstieg einer Gasblase in einem wassergesättigten porösen Medium durch Auftriebskräfte herangezogen werden. Wenn die Gasblase auf eine Linse aus feinerem Material und somit höherem Eindringdruck als das umgebende Material trifft, kann sie in die Linse nicht eindringen solange der Eindringdruck nicht erreicht ist. Das Gas staut sich unter der Linse an oder umfließt sie. Die heterogene Struktur der Bodenparameter kann in aller Regel bei der Modellierung eines Prozesses nicht vernachlässigt werden. Ihr Einfluss muss daher von den Modellen sinnvoll erfasst werden.

Abbildung 1: Beispiele von Boden- und Felsmaterial.

Um einen Prozess in einem heterogenen Medium zu modellieren, müsste die heterogene Struktur demnach eigentlich detailliert dargestellt werden. Allerdings ist die Längenskala des Mediums, in dem ein Prozesses beschrieben werden soll, meist viel größer als die Längenskala der Heterogenitäten. Daraus ergeben sich zwei grundsätzliche Probleme:

- Da Messungen von Parametern für poröse Medien sehr aufwendig sind, ist die Struktur der Materialeigenschaften meist nicht hinreichend gut bekannt. Daher stellt sich bei unzureichender Datengrundlage die Frage: Wie können Eigenschaften von komplexen, strukturierten Medien mit geringer und nur lokaler Kenntnis der Parameter vorhergesagt werden?

- Andererseits ist es auch möglich, dass die Struktur eines Mediums sehr genau bekannst ist, beispielsweise durch tomographische Messungen kleiner Proben. Es ist jedoch mit der derzeitigen Rechnerleistung meist nicht möglich, einen Prozess in so einem komplexen System detailliert zu berechnen. Es ist unter Umständen auch nicht von Interesse die Prozesse räumlich hochaufgelöst darzustellen, da man an gemittelten Größen, wie beispielsweise einem Fluss durch eine Kontrollebene, interessiert ist.

Um die anfangs beschriebenen Anwendungen planen und vorhersagen zu können, benötigt man daher Modelle, die den Einfluß der Heterogenitäten in einem **gemittelten** Sinn wiedergeben, ohne eine detaillierte Beschreibung der Parameter zu verwenden. Die Modelle müssen die relevanten Prozesse in einer vereinfachten Weise beschreiben, aber dennoch

den Einfluss der Heterogenitäten erfassen.

Zielstellung der Arbeit

In dieser Arbeit werden Modelle entwickelt, die eine vereinfachte Prozessbeschreibung in einem komplexen System erlauben, um gemittelte Zielgrößen vorhersagen zu können. Solche Modelle werden **effektive Modelle** genannt und sie werden mit **upscaling** Methoden hergeleitet.
Um die Prozesse im Mittel wiedergeben zu können, wird das Modell mit heterogenen Parametern durch ein effektives Modell mit äquivalenten homogenen Parametern ersetzt. Ein solches Modell muss aus dem detaillierten heterogenen Modell hergeleitet werden. Die Parameter für ein effektives Modell werden effektive Parameter genannt.
Äquivalente homogene Modelle und deren effektive Modellparameter werden hier für Strömung und Transport in porösen Medien hergeleitet. Dabei werden drei Hauptfragestellungen verfolgt:

- Wie ändert sich die Prozessbeschreibung beim Übergang von einer kleineren auf eine größere Skala und welches Modell beschreibt den gemittelten Prozess auf einer größeren Skala adäquat? Man würde meist erwarten, dass die Prozesse in beiden Modellen die gleichen sind. Das ist jedoch nicht immer der Fall. Es kann sowohl vorkommen, dass Prozesse durch den Skalenübergang an Relevanz verlieren als auch dass neue Prozesse hinzukommen. Es muss bei einer Anwendung überprüft werden, ob die Annahmen, die für die Herleitung eines gemittelten Modells getroffen wurden, erfüllt sind.

- Wie wird die Information über kleinskalige Heterogenitäten in den effektiven Parametern auf der größeren Skala erfasst?

- Wie kann Heterogenität charakterisiert und quantifiziert werden? Welche Information der kleineren Längenskala wird für das effektive Modell benötigt?

Die hier entwickelten effektiven Modelle werden benötigt, um Prozesse sinnvoll abzuschätzen, Verfahren zu planen oder Daten auf den relevanten Skalen zu analysieren. Für viele Probleme existieren keine ausreichenden Modellkonzepte. Das gilt insbesondere für die Abbildung nichtlinearer Prozesse, wie zum Beispiel Zweiphasenströmung.
Die vorliegende Arbeit vergleicht und schätzt upscaling Methoden ein und legt effektive Modelle und Modellparameter für ausgewählte Zweiphasenströmungsprobleme vor. Sie diskutiert außerdem die Frage, wie Heterogenität quantifiziert werden kann, und wie solche Quantifizierungen zur Berechnung von effektiven Parametern verwendet werden kann. Dabei liegt der Fokus weniger auf der Anwendung der effektiven Modelle, als vielmehr auf der Entwicklung von Prozessverständnis. Im folgenden wird ein Überblick über die in den einzelnen Kapiteln der Arbeit behandelten Aspekte gegeben.

Verwendete Methoden

Die ersten beiden Kapitel der Arbeit nach der Einleitung (Kapitel 2 und 3) geben einen Überblick über die hier verwendeten Methoden und Konzepte. In Kapitel 2 werden verschiedene Quantifizierungsmodelle für heterogene Strukturen besprochen. Im ersten Teil wird die stochastische Beschreibung eines heterogenen Parameterfeldes ausgeführt. Das Parameterfeld wird dabei als ein Zufallsfeld mit einer gegebenen multivariaten Verteilung beschrieben. Da in der Regel nur zweite Momente der Verteilung verwendet werden, wird Heterogenität hier im wesentlichen durch den Erwartungswert, die Varianz und die Zweipunktkovarianz des Parameterfeldes quantifiziert. Anisotropie eines Feldes kann durch eine Richtungsabhängigkeit der Integralskala oder Korrelationslänge definiert werden. Falls es keine endliche Korrelationslänge für ein Feld gibt, sind die stochastisch gemittelten Größen nicht represäntativ für das einzelne Feld.

Die Charakterisierung eines Feldes durch seine ersten und zweiten Momente ist nur dann vollständig, falls das Feld Gauss-verteilt ist. Dies ist in natürlichen porösen Materialien jedoch oft nicht der Fall. Strömung und Transport wird oft durch räumlich zusammenhängende Bereiche mit extrem hoher oder extrem niedriger Permeabilität bestimmt. Im zweiten Teil werden deshalb Quantfizierungskonzepte für räumlich verbundene Strukturen bestimmter Parameterbereiche eines Feldes besprochen. Zwei Beispiele für Felder die sich in dieser Eigenschaft unterscheiden sind in Abbildung 2 gezeigt. Charakteristische Größen können aus Indikatorfeldern bestimmt werden.

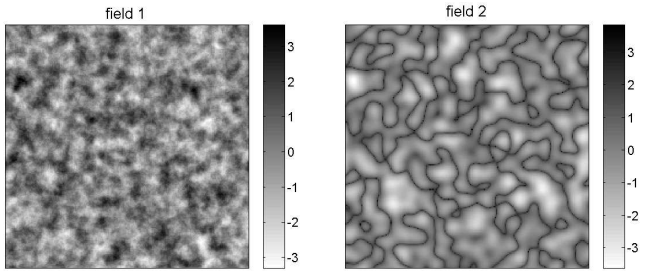

Abbildung 2: Multi-Gauss verteiltes Feld, in dem mittlere Parameterwerte räumlich verbunden sind (links) und nicht mulit-Gauss verteiltes Feld, in dem extrem hohe Parameterwerte räumlich verbunden sind (rechts). Beide Felder haben den gleichen Mittelwert, die gleiche Varianz und die gleiche Autokovarianz.

In Kapitel 3 werden Methoden zur Herleitung effektiver Modelle und effektiver Modellparameter dargestellt. Mit der Homogenisierungstheorie kann ein effektives Modell für den Grenzfall, dass das Verhältnis der Längenskala der Heterogenitäten und der des Modellgebietes (diese Verhältnis wird als ε bezeichnet) gegen null geht, abgeleitet werden (siehe Abbildung 3).

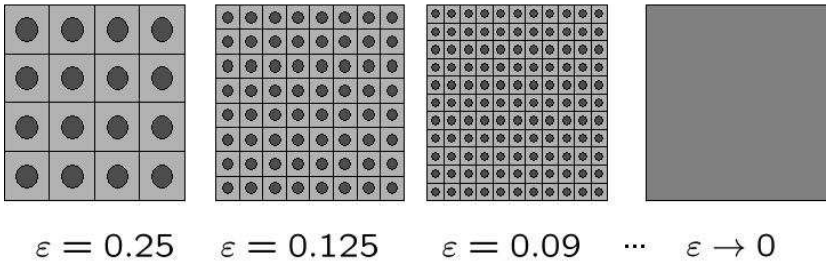

Abbildung 3: Periodisches Feld im Limes $\varepsilon \to 0$.

Die Methode basiert auf einer Skalenentwicklung im Parameter ε. Das resultierende Modell unterliegt deshalb der Annahme einer Skalentrennung. Weitere Annahmne werden getroffen, indem die typische Zeitskala und die dimensionslosen Größen des Problems ins Verhältnis zum Entwicklungsparameter ε gesetzt werden. Das effektive Problem gilt nur für den so abgegrenzten Bereich. Die effektiven Parameter des Modells ergeben sich für ein deterministisches Parameterfeld aus der Homogenisierungstheorie. Da das Parameterfeld jedoch meist nicht deterministisch bekannt ist, werden Methoden zur Abschätzung der Parameter besprochen, die auf einer vereinfachten Quantifizierung von Heterogenitäten basieren. Zum einen werden verschiedene Methoden der Theorie effektiver Medien besprochen, bei denen die Parameter aus der univariaten Verteilungsfunktion der Parameter bestimmt werden. Zum anderen werden stochastische Modelle verwendet, bei denen die Parameter in einer Störungsentwicklung in der Varianz des Parameterfeldes bis zur zweiten Ordnung angenähert werden. Solche Modelle können im Prinzip ebenfalls verwendet werden, um effektive Modelle direkt abzuleiten. Die stochastischen Differentialgleichungen werden dabei stochastisch gemittelt. Dieses Vorgehen erfordert die Lösung von Schließungsproblemen, die in der Regel in Störungsentwicklungen genähert werden.

Anwendung der Upscaling-Methoden auf unterschiedliche Strömungsprozesse im Untergrund

In den Kapiteln 4 bis 7 werden Anwendungen der oben dargestellten Methoden für ausgewählte Zweiphasenströmungsprobleme beschrieben. Es werden dabei ausschließlich nicht mischbare Fluide betrachtet. Dabei werden die drei oben aufgeführten Fragen verfolgt. Kapitel 4 behandelt die Modellbildung. Es werden instabile Strömungsprozesse diskutiert, für die die Beschreibung mit effektiven Modellen problematisch ist. In Kapitel 5 wird die Strömung von Wasser und Luft in der ungesättigten Bodenzone besprochen, ein Zweiphasenprozess, der mit der Richards Gleichung in einer vereinfachten Weise beschrieben wird. Die relevante charakteristische Längenskala beträgt hier typischerweise einige Meter. Auf dieser Skala dominieren Gravitations- und Kapillarkräfte. In Kapitel 6 wird ein Zweiphasenströmungsproblem auf der gleichen Längenskala diskutiert. Die Fluide besitzen jedoch eine ähnliche Viskosität und Dichte, was die Komplexität des Prozesses erhöht. Die in Kapitel 5 und 6 betrachteten Prozesse können als unterschiedliche

Zweiphasenströmungsprozesse auf der gleichen charakteristischen Längenskala betrachtet werden. In den Kapiteln 5 und 6 wird die Quantifizierung von Heterogenitäten diskutiert. Die Verdrängung eines Fluides durch ein anderes auf einer großen Längenskala von mehreren Kilometern wird in Kapitel 7 behandelt. Auf dieser Skala dominieren Gravitations- und viskose Kräfte, während Kapillarkräfte vernachlässigt werden können. Im weiteren werden die wesentlichen Ergebnisse der Kapitel 4 bis 7 beschrieben.
In **Kapitel 4** wird die Frage behandelt, ob und wie gegebenenfalls gemittelte Größen für instabile Strömung modelliert werden können. Dabei werden sowohl viskose Instabilitäten betrachtet, als auch Instabilitäten, die bei kapillar dominierter Strömung in einem heterogenen Feld auftreten können. Viskose Instabilitäten spielen eine Rolle bei Verdrängungsprozessen auf großen Längenskalen. Die Mobilität des verdrängenden Fluides muss größer sein als die des verdrängten Fluides. Solche Szenarien sind beispielsweise bei der Erdölförderung oder bei der Injektion von CO_2 in großskaligen Gesteinsformationen relevant. Instabilitäten bei kapillar dominierter Strömung treten bei der Verdrängung eines benetzenden durch ein nicht-benetzendes Fluid in stark heterogenen Feldern auf. Solche Prozesse sind beispielsweise relevant, wenn in Gesteinsformationen eingelagerter nuklearer Abfall korrodiert und das entstehende Gas durch das umgebende poröse Medium migriert.
Der Fall von kapillar instabiler Strömung wird mit einer Analogie zur Verdrängung eines Fluides durch ein anderes in einer offenen, rauhen Kluft behandelt. Die Kluft wird dabei als ein vereinfachtes, qualitatives Modell für ein poröses Medium betrachtet. Dabei entstehen durch Einschlüsse der benetzenden Phase durch die nichtbenetzende Phase eine räumliche Fluidanordnung, die keine spezifische Längenskala aufweist. Der Strömungsprozess in der Kluft wurde mit einem Invasionsperkolationsmodell und mit einem Laborexperiment untersucht. Beim Invasionsperkolationsmodell handelt es sich um eine Weiterentwicklung des in der Literatur gebräuchlichen, da die Krümmung der Grenzfläche zwischen den Fluiden in der Kluft reproduziert werden muss. Es wurden zwei Kluftöffnungsweitenfelder mit verschiedenen Korrelationsstrukturen untersucht. Im einen Fall hatte das Feld eine endliche Korrelationslänge, im anderen Fall existierte eine solche Skala nicht. Die wesentlichen Ergebnisse aus diesem Kapitel lassen sich wie folgt zusammenfassen:

- Das Invasionsperkolationsmodell hat gezeigt, dass die Verteilung der Front zwischen den Fluiden irregulär ist. Dies lässt sich mit der Korrelationsfunktion der räumlichen Sättigungsverteilung quantifizieren. Die Korrelationsfunktion besitzt keine endliche Korrelationslänge. Dies ist weitestgehend unabhängig von der zu Grunde liegenden Struktur des Feldes der Kluftöffnungsweiten.

- Das Invasionsperkolationsmodell reproduziert die wesentlichen Fließprozesse in einer offenen rauhen Kluft. Die Simulation reproduzierte das Experiment mit einer guten Übereinstimmung.

- Es wurde dargelegt, dass für instabile Prozesse kein repräsentatives Elementarvolumen existiert. Die Verwendung von Kontinuumsskalenmodellen für solche Prozesse

ist deshalb oft nicht sinnvoll.

- Gemittelte Größen, wie beispielsweise Sättigungen, dürfen für instabile Prozesse in porösen Medien nur für ausgewählte Fragestellungen herangezogen werden. Die gemittelten Größen geben den Prozess in einer einzelnen Realisation des porösen Mediums nicht wieder, stellen jedoch unter Umständen sinnvolle Maße für Risikoabschätzungen dar.

Kapitel 5 behandelt ein effektives Modell für Strömungsprozesse in der ungesättigten Bodenzone, die durch die Richards Gleichung beschrieben werden. Die Richards Gleichung ist die Kontinuitätsgleichung für die Wasserphase unter der Annahme, dass der Druck in der Luft räumlich und zeitlich konstant ist.
Strömung in der ungesättigten Bodenzone bestimmt den Transportweg von im Wasser gelösten Stoffen (Schadstoffe oder Nährstoffe), die von der Landoberfläche mit der Infiltration von Niederschlägen in tieferliegende Aquifere eingetragen werden. Die Strömung bestimmt die charakteristischen Transportzeiten, die wiederum den Abbau solcher Schadstoffe beeinflussen. Auf einer regionalen Skala sind die Strömungsprozesse in der ungesättigten Bodenzone wichtig für Wasser- und Energiebilanzen und für die Trennung von Niederschlagswasser in Oberflächenabfluss, Infiltration und Evapotranspiration des Wassers. Gerade auf der regionalen Skala ist eine räumlich detaillierte Modellierung der Strömung in aller Regel nicht möglich und man ist auf effektive Modelle angewiesen.
Ein effektives Modell wurde mit Homogenisierungstheorie für langsame Strömungsprozesse abgeleitet. Effektive Parameter wurden für kapillar dominierte und gravitationsdominierte Strömungen mit verschiedenen Methoden angenähert. Gravitationsdominierte Strömung wurde außerdem für den quasi-eindimensionalen Fall einer vertikalen Strömung in einem horizontal geschichteten Medium untersucht. Die wesentlichen Ergebnisse sind hier:

- Für den Fall von langsamer, kapillar dominierter Strömung hat das effektive Modell die gleiche Form wie die ursprüngliche Richards Gleichung, mit einer effektiven Retentionsfunktion und einer effektiven Durchlässigkeit, die jeweils vom gemittelten Druck in der Wasserphase abhängen.

- Für das geschichtete Modell wurde gezeigt, dass die Form der Richards Gleichung auch beim Übergang zu gravitationsdominierter Strömung beibehalten wird. Die Auswertung verschiedener Testfälle ergab, dass die effektiven Parameter sich nicht stark von denen unterscheiden, die sich für den kapillar dominierten Fall ergeben. Daraus lässt sich schließen, dass die Annahme von kapillar dominierter Strömung auch dann zu sinnvollen Ergebnissen führt, wenn Gravitationskräfte die Kapillarkräfte dominieren.

- Es konnte für das geschichtete System ebenfalls gezeigt werden, dass das effektive Modell nicht mehr die gleiche Form wie die Richards Gleichung hat, falls eine Skalenseparation im porösen Medium nicht mehr gut erfüllt ist.

- Für den Fall langsamer, kapillar dominierter Strömung wurden die effektiven Modellparameter mit stochastischer Theorie explizit in einer Störungsnäherung berechnet. Der kapillare Eindringdruck ist in den effektiven Parametern nicht mehr vorhanden.

- Es wurde gezeigt, dass die effektiven Modellparameter in Feldern mit räumlich verbundenen extremen Parameterwerten nicht gut mit einer Störungsnäherung zweiter Ordnung abgeschätzt werden können. Die effektive Retentionsfunktion des Mediums ist zwar nicht sensitiv gegenüber der räumlichen Struktur der Parameter, es ergeben sich jedoch deutliche Unterschiede zwischen Gauss'schen und nicht-Gauss'schen Feldern bei der effektiven Durchlässigkeit des Mediums.

- Methoden der Theorie effektiver Medien, die auf einer Hintergrunds-Inklusions Beschreibung des Mediums basieren, wurden verwendet, um effektive Durchlässigkeiten abzuschätzen. Falls das Parameterfeld des Mediums räumlich verbundene Extremwerte hat, reproduzieren die so abgeschätzten effektiven Durchlässigkeiten die tatsächlichen Kurven besser, als die mit stochastischer Theorie abgeschätzten.

Ein Zweiphasenströmungsproblem mit zwei Fluiden mit ähnlicher Viskoität und Dichte (gravitationserzeugte Gegenströmung in einem abgeschlossenen porösen Medium) wird in **Kapitel 6** behandelt. Es wird angenommen, dass die Bedingungen für kapillares Gleichgewicht erfüllt sind. Gleich der Strömung in der ungesättigten Zone, findet der Prozess auf einer Längenskala im Meterbereich statt.
Gravitationsgetriebene Gegenströmung ist relevant, wenn aus im Untergrund eingelagerten Deponien unter Einfluss von Gravitation Fluide auslaufen. Die Anwendungen sind hier ähnlich wie die in Kapitel 4 erwähnten Anwendungen für kapillar instabile Strömung. Die Unterschiede sind jedoch, dass die hier betrachteten Strömungsprozesse durch Kapillar- und Gravitationskräfte dominiert sind, und dass das Medium keine allzu grossen Heterogenitäten aufweisen darf, damit es nicht zu Instabilitäten kommt. Eine weitere Anwendung ist die Strömung von CO_2, das in eine Gesteinsformation injeziert wurde, die eine vertikale Ausdehnung von einigen Metern hat. Nach der Injektion ist das System geschlossen, das CO_2 fliesst durch die Auftriebskräfte aufwärts, während das Wasser in die entgegengesetzte Richtung verdrängt wird.
Die wichtigsten Ergebnisse dieses Kapitels sind die folgenden:

- Ein effektives Modell für gravitationsgetriebene Gegenströmung wurde abgeleitet. Das Modell besitzt keinen viskosen Term mehr. Der lokale viskose Term wird im effektiven Modell in einem gemittelten Gravitationsterm erfasst. Die effektiven Parameterfunktionen werden von den separaten Strömungsgleichungen für beide Phasen getrennt berechnet, wobei die jeweils andere Phase als stagnierend betrachtet wird. Das Modell wurde mit numerischen Simulationen validiert.

- Die stochastisch gemittelten Parameterfunktionen für das effektive Modell wurden explizit berechnet. Es konnten nur arithmetische Mittelwerte verwendet werden, da

die nicht-benetzende Phase lokal verschwindende Durchlässigkeiten aufweist. Mittelwerte wie das geometrische Mittel ergeben damit keine sinnvollen Ergebnisse. Die effektive Mobilität des Systems wird allerdings mit den arithmetischen Mitteln überschätzt. Abschätzungen mit der Theorie effektiver Medien ergeben bessere Ergebnisse als stochastische Mittel.

- Die effektiven Parameterfunktionen des Modells wurden für Felder analysiert, in denen extreme Parameterwerte räumlich verbunden waren. Stochastische Mittelwerte ergeben hier keine guten Schätzwerte für die effektiven Parameter. Dies gilt insbesondere für die nicht-benetzende Phase. Ihre makroskopische Restsättigung hängt stark vom Auftreten von präferentiellen Fließpfaden ab.

- Methoden der Theorie effektiver Medien, die auf einer Hintergrund-Inklusions Beschreibung des Mediums basiert, sind besser geeignet als Methoden der stochastischen Theorie, um die effektiven Parameter abzuschätzen, falls das Parameterfeld gut verbundene Extremwerte aufweist.

In **Kapitel 7** werden Zweiphasenströmungen auf einer grossen Längenskala betrachtet, auf der Kapillarkräfte vernachlässigbar sind. Ein solcher Strömungsprozess ist bekannt als das Buckley-Leverett Problem, in dem Gravitationskräfte und viskose Kräfte berücksichtigt werden.
Das Buckley-Leverett Problem ist hauptsächlich für großskalige technischen Anwendung relevant. Das wichtigste Beispiel ist sicherlich die Gewinnung von Erdöl aus einem Reservoir durch Verdrängung durch ein anderes Fluid.
Für neutral stabile Strömungen wurde das effektive Modell mit den folgenden Ergebnissen ausführlich analysiert:

- Ein effektives Modell für den Strömungsprozess wurde abgeleitet. Das effektive Modell reproduziert die gemittelte Sättigungsverteilung. Der Prozess in einem realen porösen Medium würde nur dann durch das effektive Modell reproduziert, wenn ein Diffusionsterm in den ursprünglichen Strömungsgleichungen vorhanden wäre. Es ist jedoch im Gegenteil der Fall, dass die Übergangszone zwischen den beiden Phasen selbstaufsteilend ist. Das effektive Modell reproduziert daher nicht den realen Prozess, sondern nur ein räumliches oder stochastisches Mittel. Für Anwendungen sind diese effektiven Modelle relevant, wenn groß-skalig gemittelte Sättigungsverteilungen oder Flüsse über eine Kontrollfläche von Interesse sind.

- Die effektiven Parameter für das effektive Modell wurden explizit berechnet. Ein nichtlinearer Dispersionsterm, der im ursprünglichen Problem nicht enthalten war, wurde abgeleitet. Ein Dispersionskoeffizient wurde in einer Approximation zweiter Ordnung in der Varianz des Feldes mit stochastischen Methoden berechnet.

- Der Dispersionskoeffizient wurde für ein radiales und für ein gleichförmiges Strömungsfeld berechnet. Dabei wurde eine verallgemeinerte Momentenmethode verwendet, um die Übergangszone zwischen den beiden Fluiden zu quantifizieren, aus

denen der Dispersionskoeffizient abgeleitet werden kann. Der Makrodispersionskoeffizient ähnelt dem für ein Transportmodell.

- Die Ergebnisse wurden mit numerischen Simulationen bestätigt.

Abschließende Bemerkungen

Die in den Kapiteln 4 bis 7 behandelten Beispiele tragen zum Verständnis des Einflusses von Struktur auf Zweiphasen-Strömungsprozesse auf verschiedenen Längenskalen bei. Diese Arbeit trägt zur Einschätzung und zum Vergleich verschiedener Upscalingmethoden bei. Die effektiven Modellparameter wurden mit verschiedenen Methoden abgeschätzt. Dabei wurde die Limitierung von stochastischen Methoden in störungstheoretischer Näherung diskutiert und alternative Methoden zur Abschätzung von Modellparametern aufgezeigt. Die Arbeit trägt daher zum sowohl zum Prozessverständnis von Strömungsprozessen in heterogenen Medien, als auch zum Verständnis der relevanten Charakteristiken von Heterogenitäten von Parametern bei.
Abschließend seien die wichtigsten offenen Fragestellungen erwähnt.
Die effektiven Modelle wurden stets unter der Annahme abgeleitet, dass die Skalen im porösen Medium strikt getrennt sind. In natürlichen porösen Medien ist das oft nicht gegeben. Es gibt wenige Untersuchungen von Methoden, die langreichweitige Korrelationen von Parametern erfassen können. Besonders für nichtlineare Prozesse sind solche Methoden kaum anzuwenden. Fortschritte auf diesem Feld sind notwendig, um effektive Modelle besser auf Feldanwendungen übertragen zu können.
Die Frage nach der Unsicherheit der effektiven Parameter wurde hier nicht angesprochen. Für die Anwendbarkeit von effektiven Modellen ist es jedoch wichtig, Abschätzungen über die Verlässlichkeit der Parameter zu haben. Für Zweiphasenströmungen ist dies ein offenes Feld für zukünftige Forschung.
Die effektiven Modelle wurden hier stets für langsame Prozesse abgeleitet. Für viele Anwendungen sind schnelle Prozesse wichtig. Beispielsweise Infiltration von Wasser in den Boden nach einem Niederschlagsereignis geschieht in der Regel auf einer kleinen Zeitskala. Die effektiven Modelle sind für diese Prozesse vermutlicherweise komplexer als die hier besprochenen. Dynamische Effekte in effektiven Modellen ist ein relativ junges Forschungsfeld, das derzeit kontrovers diskutiert wird.

Contents

Chapter 1

Introduction

Flow and transport processes in porous media are relevant for a variety of engineering applications, ranging from biomechanical to technical fields or from flow in fuel cells to water balances in catchments. Examples are shown in Figure 1.1. Single phase flow processes in porous media are typically related to water flow in aquifers. The transport of solutes, such as contaminants, in the groundwater can only be estimated if the flow process in the aquifer is understood. Modelling of single phase flow and transport of contaminants is relevant for water management plans, for groundwater protection and for the planning of remediation of contaminated aquifers. These are important tasks, as groundwater is one of the most important resources for drinking water and considered on a global scale it is getting scarcer due to the increasing demand.

Often the flow of more than one fluid in the porous medium has to be considered. For example, different methods for oil recovery are based on displacement of oil from the reservoir by another, immiscible fluid. The modelling of large-scale two-phase flow processes in the subsurface continues also to gain profile in the light of the ongoing discussion about CO_2 sequestration. This is true also for other problems of storage of hazardous material, such as nuclear waste. Two-phase flow is also important for the exploitation of geothermal energy and geotechnical applications.

Two-phase flow in porous media has also technical applications on a much smaller length scale. One example is the drying procedure in paper production, which is based on the flow of water and air through the porous material paper. Recently the application of two-phase flow models and transport of components in the phases is discussed for medical applications, as tissue and bone material is porous. As an example, the liver can be considered as a porous material which has a filter function. The field of applications of multi-phase flow and transport models for medical research is however only at the beginning stage.

The flow of water and air in the soil is important for the flow processes taking place in the unsaturated zone, which is the soil zone inbetween the land surface and underlying aquifers. The unsaturated zone plays is an important part in the terrestrial part of the global water cycle and regional water balance models. It is the central medium for vegetation and fauna and it is crucial for the balance of energy and water fluxes. As such it is

under strong anthropogenic influence. The unsaturated zone plays an important role for climate research, which in times of shifting climate conditions becomes increasingly important. Yet, the unsaturated zone is a highly complex system. The models which describe the fluxes are well established for porous media on a meter scale and are tested mainly under equilibrium conditions in the laboratory. Their applicability for water balance models on a much larger scale, which can stretch over kilometers, is discussed controversely in the literature (e.g. Harter and Hopmans (2004)).

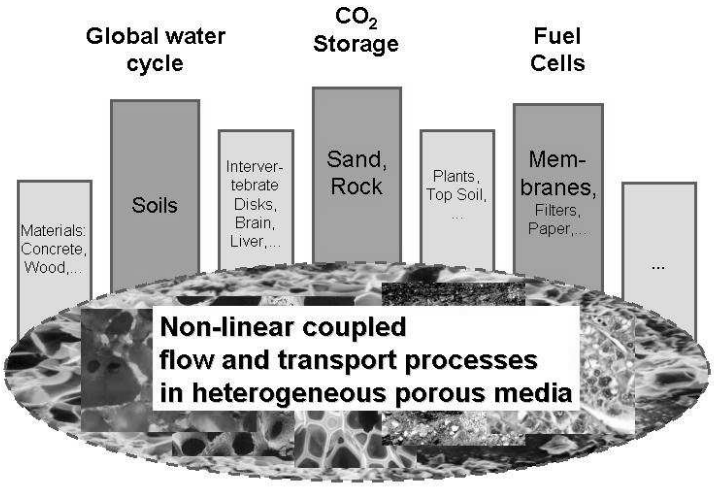

Figure 1.1: Applications of flow and transport in porous media.

1.1 Heterogeneous materials and soil structure

Flow and transport in the subsurface is scale dependent, as different forces are predominant on different length scales. The scale dependence is also strongly related to the question of the length scales of heterogeneities of the material properties.

A variety of heterogeneous media which are important for technical, environmental and medical purposes are shown in Figure 1.2 below. The figures illustrate the variability of structures and length scales in heterogeneous media. Media with a heterogeneous structure on a very small length scale such as bones or paper have similar features to the soil material of an aquifer.

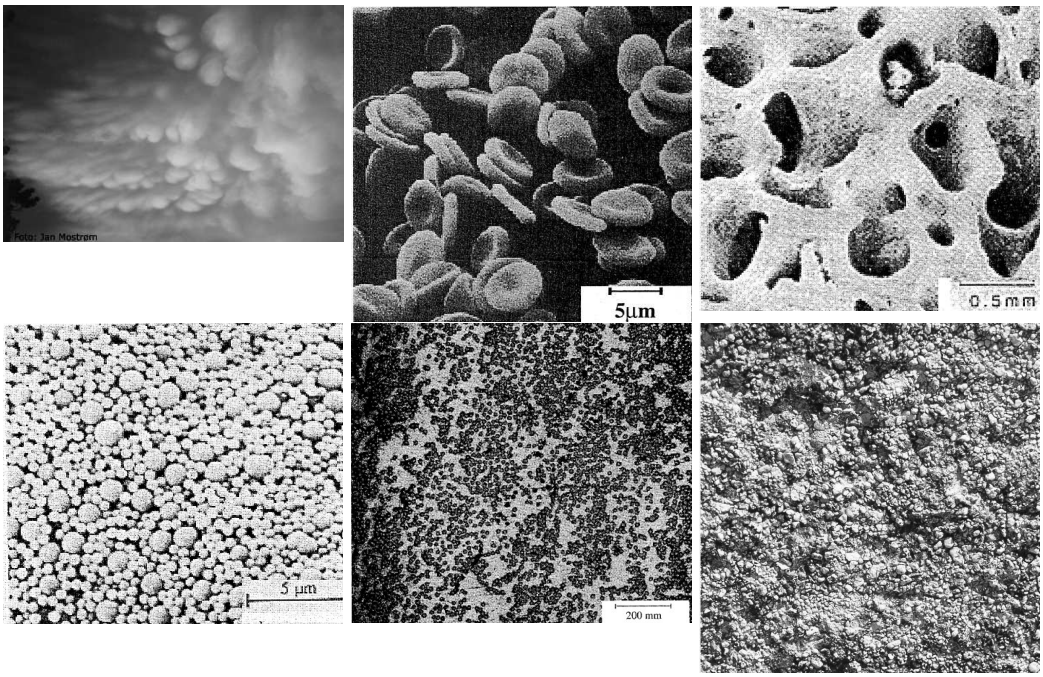

Figure 1.2: Heterogeneous materials. Upper row from left to right: Clouds, blood cells, deseased bone material. Lower row from left to right: Colloidal system, fiber-enforced cement, mixture of carbonate and rock. Second and third picture in the upper row and first and second picture in the lower row taken from Torquato (2002).

This work is dedicated to the treatment of flow and transport processes in the subsurface. The porous media considered are soil, gravels, sandstones or fractured rock formations. Some pictures of porous media occuring in the subsurface are shown in Figure 1.3. The variety of structures and length scales is wide in this selection. The soil, which is important for the infiltration of water into the subsurface, can have small vertical extensions, such as several meters. An oil reservoir which is exploited can extend over kilometers. A gravel aquifer has a structure which is mainly determined by the gravels and the filling material in between. Such a structure can be isotropic. A reservoir in a very deep formation typically has a layered structure which is not necessarily horizontally oriented. Such a medium is highly anisotropic. The structures in an aquifer may be represented as a background material including loamy lenses. The lenses can be represented as ellipsoidal. A fractured rock can be represented as impermeable rock with highly permeable inclusions, which represent the fractures. The inclusions are then better represented as needles or disks.

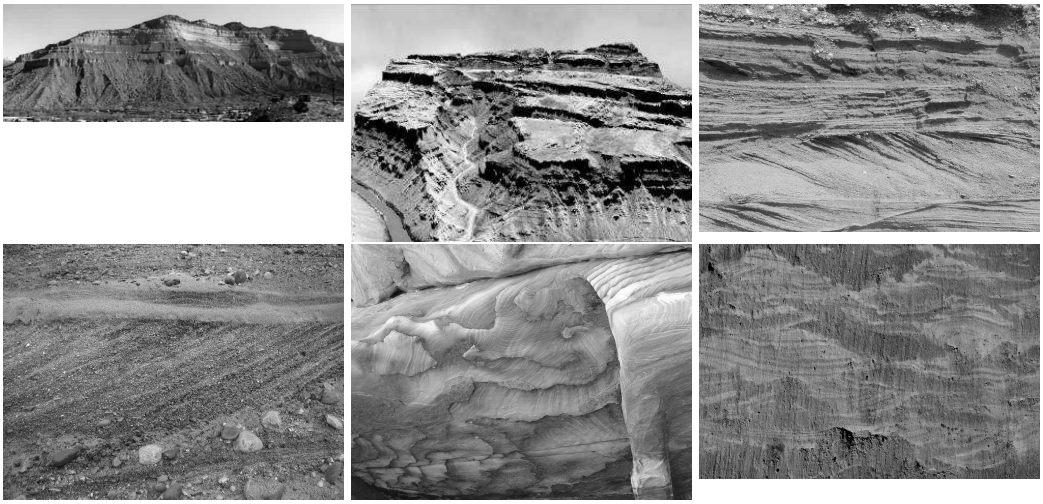

Figure 1.3: Samples of soil and rock. Second picture in the lower row courtesy of Arne Färber.

A heterogeneous porous medium can be considered a composite of different materials. The medium consists either of different composits which have clear interfaces, and the property in one phase is constant. However, the properties of the medium may change continuously, so that no interfaces can be defined. Examples for such parameter fields are shown in Figure 1.4.

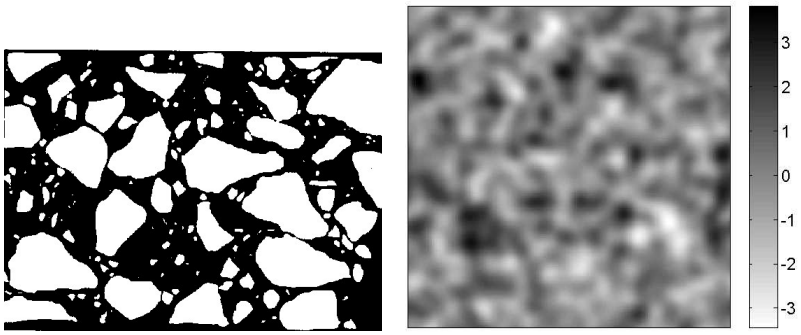

Figure 1.4: Heterogeneous composite and continuous field

The heterogeneous distribution of the material properties is characterized by typical length scales. If, for example, a medium is composed of two different materials, one of them being the background while the other one forms an isolated inclusion, a length scale for the heterogeneity would be the typical length scale of an inclusion. In a layered medium, the typical length scale of the heterogeneity is a typical layer thickness. A medium can be considered macroscopically homogeneous if there is one typical length scale of heterogeneities which is much smaller than the typical length scale of the medium

itself. It is, however, often also the case that there is not one typical length scale of heterogeneities. Structures exist on a large variety of length scales, often up to that of the medium itself (cf. Chapter 3).

1.2 Processes in heterogeneous materials

Often, we want to make predictions about flow and transport processes in porous media. For example, we might want to estimate the flow velocity in an aquifer in order to estimate the travel time of a contaminant in the groundwater.
The processes which cause the flow of fluid through a porous medium are scale dependent. Gravity forces, for example, are negligible if the medium does not extend much in vertical direction and the pressure gradients in a horizontal direction are high. The relevant mechanisms can be estimated by dimensionless numbers, which relate the different driving forces to each other. If such a dimensionless number is much smaller or larger than one, the forces which contribute to a smaller extent may be neglected.
When a process in a heterogeneous medium is modelled, the parameters of the equations describing the process depend on space. Flow and transport processes interact with the heterogeneous structures. For example, the concentration distribution of a solute transported with the water flow field in an aquifer is distorted due to the heterogeneous streamlines of the flow field. The heterogeneity of the streamlines is due to the heterogeneity of the permeability field. For another example, if gas rises in a partly water-saturated porous medium and the gas bubble hits a lens with a higher entry pressure, it cannot enter the lens and pools underneath it. The pooling leads to bypassing of the lens. The example illustrate, that heterogeneous structure of the soil parameters cannot be neglected, but has to be captured by the model.
To model a process in a heterogeneous medium accurately, the parameter distribution has to be mapped exactly. However, the length scale of the medium is mostly much larger than the scale of the heterogeneities, so that the modelling of the process becomes very complex.
In order to predict and plan the applications described above, we need models which are capable of incorporating the effects of the heterogeneous structure on the flow process in average without requiring the detailed description of the parameter distribution and without attempting to model the exact processes in all detail. Such models have to describe the process in a simplified way, but still capture the influence of the heterogeneity as far as possible. In order to deal with complex systems, the development of such models is crucial and is therefore an important field of research.

1.3 Coping with heterogeneity

The topic of heterogeneity is set in a very broad general framework, which goes beyond flow in the subsurface. The question of the interplay between the disorder and structure of material properties and observations on a scale where the structure is no longer resolved

appears in such varying fields as gas theory, meteorology, medicine, and also fluid dynamics. The methods for dealing with structure and heterogeneity have been transferred from one discipline to the other. This study can therefore be considered one exemplary application of the general question: How does the structure or disorder of material properties on different scales affect the processes in such media?

1.3.1 Averaged properties

There are two aspects to this question. When dealing with flow and transport in the subsurface the situation is often such that the structure of material properties is not well known and data are only available from limited samples. The question is then: how can properties of complex, structured systems be predicted with only little and local knowledge of the structure? It may, however, also be the case that every detail of the structure of the medium is known. For example, the structure of tissue can be measured with CT scans. However, it is not feasible to describe the structure in every detail. Or even if it were, we are probably not interested in the detailed process.
A well known example for a large heterogeneous system, where it is not necessary to resolve the heterogeneities, is an ideal gas in a closed volume. If the gas properties on a scale where each gas molecule is captured were resolved, the gas would be described by the equations of motion for each molecule at a given location and momentum of each molecule at a certain time. On a larger scale, it is impossible to describe the gas in this way as it consists of too many molecules. However, on a larger scale, the motion of each molecule is not of interest. The gas on this scale is described by thermodynamic equations, which relate the temperature, pressure and volume of the gas to each other. The thermodynamic equations are derived from the molecular gas equations.
The systems considered in the following are heterogeneous materials rather than gases. The properties of the materials are heterogeneously distributed in space and do not depend on time. Due to the spatial fluctuations of the parameters in a heterogeneous medium, the solution of the models (such as the flow velocity in an aquifer or the flux of oil in an oil reservoir) also fluctuates in space. If the length scale of the medium is much larger than the scale of the heterogeneities, the solution will also be very complex in its detailed resolution. However, in practice one is usually not interested in the detailed solution, but rather in averages of the solution over a certain averaging volume. In an oil reservoir, for example, the flow velocity of the oil at each location is not of interest. What is interesting is only the oil flux over a certain control area. Again, the exact distribution of the contaminant in an aquifer is not of concern, but we do need to know the average solute concentration in the water which is drawn from a well at a certain distance from a contamination site.
The question is then: how can predictions of processes be made without describing them in detail? How can models for a certain scale be simplified while the influence of the heterogeneous structure is still captured?
In both cases we want to model the processes in an averaged sense. We need models which allow to make predictions for the averaged quantities. Such models are calles **upscaled**

models and their derivation is called **upscaling**.

1.3.2 Upscaled models

If we are not interested in the detailed processes inside a heterogeneous porous medium, it is not a good approach to try to model the processes in the detail. Instead, equivalent models are used, which describe the process in average. The heterogeneous model is thus replaced by an equivalent homogeneous model. The upscaled model has to be derived from the knowledge we have about the detailed processes in the heterogeneous model. This upscaled model incorporates certain processes and has parameters which are no longer heterogeneously distributed. These homogeneous parameters are called **equivalent parameters** of **effective parameters**. Equivalent parameters reproduce one certain flow scenario, while effective parameters are general and do not depend on the large-scale boundary conditions (see Renard and de Marsily (1997)).
The picture of upscaled models with homogeneous parameters is not complete. In some approaches, the upscaled model is not homogeneous, but the heterogeneities are averaged out only in part. The parameters of the upscaled model are still heterogeneous, but the characteristics of the heterogeneity have changed. This procedure is called **coarse graining** (see Hristopulos (2003), King and Neuweiler (2002) and Attinger (2003)). It is here however not considered.
There are three important questions when deriving an upscaled model. The first one is: what does the upscaled model look like? Which processes link the averaged input to the averaged output? Naturally, one would mostly expect the processes in the upscaled model to be identical to the processes in the detailed small-scale model. However, this is not always the case. Sometimes, certain processes can be neglected in the averaged model. It can, however, also be the case that processes not present in the heterogeneous model are required to model the averaged quantities correctly. The upscaled model has to be derived on the basis of the processes which are relevant for the detailed model and for the boundary conditions considered for a specific scenario. The model is valid only for certain conditions, and these conditions have to be defined. The second question is: how can effective parameters for the model be derived, based on the knowledge about the heterogeneous structure of the detailed small-scale model. This question is related to the third question: How can the effective parameters be predicted on the basis of local data and a simplified concept about the heterogeneous structure? How can heterogeneity be quantified? A further important question is: How uncertain are the parameters, based on the uncertainty of the knowledge of the real parameter field?
The development of upscaled models and of methods to derive effective or equivalent parameters for them is very important in order to improve our capacities to handle the complex flow and transport processes which we face in nowadays applications. We need models to make predictions of these processes and to analyze data measured on the relevant scales. Such models are for many problems not available, nor is it clear how they can be derived. Especially for non-linear problems, such as two-phase flow, there are many open questions and progress is urgently needed. This work makes a contribution to the

comparison and evaluation of different upscaling methods and provides upscaled models and parameters for several two-phase flow problems. It contributes also to the answer for the question, how heterogeneity can be quantified and how such quantifications can be incorporated into the models.

1.4 Flow and transport processes in the subsurface

In the following, the flow and transport processes investigated in this study and the models which describe them will be outlined. As the models are explained in books (e.g. Fetter (2001), Domenico and Schwartz (1990), Freeze and Cherry (1979), Fischer et al. (1979), de Marsily (1986) and Helmig (1997)), they will here not be explained in too much detail. The term "model" will appear often. In the following it is always used in the sense of an equation (usually a differential equation) which relates observable quantities (such as concentration, pressure or temperature) at a given time and a given location in space to medium parameters and the initial and boundary conditions applied. It is understood as a mathematical model that represents the processes in the medium. The units of several quantities will appear. **M** is a mass unit, **L** is a length unit and **T** is a time unit.
It should be mentioned that it is always assumed here that the pore space is rigid. The deformation of the porous structure during flow and transport is not taken into account. This excludes a variety of problems, such as swelling or shrinking material, the dissolution of solid material due to acid tracers, the clogging of pore space due to colloid transport or bacterial growth and many others.

1.4.1 The question of scales

The equations for modeling flow and transport in porous media are treated differently for different length scales. The smallest reasonable scale is the length scale where single pores and grains are resolved. The flow of a fluid inside the pore space is modelled. The transport of solute tracer dissolved in the fluid is modelled directly. This scale is called the **pore scale**. As it is not feasible for most applications to describe flow and transport on the pore scale, the averaged flux or mass flux of solute through a certain volume of porous material is considered. The pore space is then no longer resolved. The volume has to be large enough to cover many pores, so that the flux measured with the same boundary conditions in different samples of the same material would be the same. The scale where the pore space is no longer resolved is called the **Darcy scale**. If fluxes are considered for field applications, such as, for example, the exploitation of an oil reservoir, the Darcy-scale properties of the materials also vary in space. This scale is called the **field scale** or **macroscale**.
The transition from the pore to the Darcy scale raises the question of an appropriate averaging volume. This can be illustrated by considering the porosity of the pore space n_f [-] (see e.g. Bear (1972)). The porosity is the volume percentage of pore space of the total averaging volume. If one has an averaging volume which is much smaller than the typical

grain size and pore size and measures the porosity, one gets a value which is either close to one or close to zero, depending on whether the location is inside a grain or a pore. If one measures the porosity at different locations, one gets values either close to one or close to zero, so the fluctuations of the measured porosity at different locations is large. If the averaging volume is increased, the fluctuations become smaller and the measured porosity will become an almost constant value between zero and one. The averaging volume above which the fluctuations of the measured porosity are negligible defines a **representative elementary volume (REV)**. This concept is sketched in Figure 1.5.

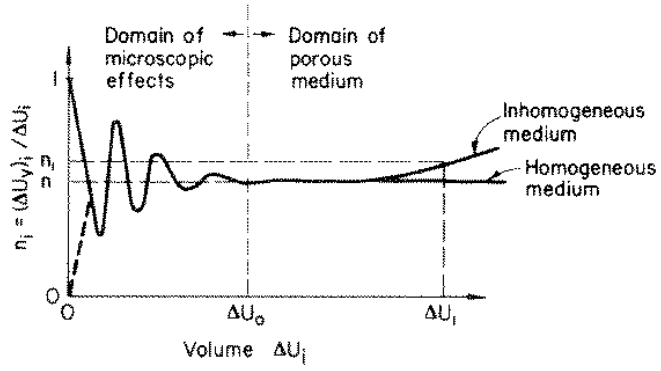

Figure 1.5: The concept of an REV. Taken from Bear (1972). ΔU_i is the averaging volume.

It is assumed here that the porosity of the medium shows no trends. A trend would mean that the averaged porosity does not fluctuate, but still changes with space. This would be the case if, for example, the averaged porosity on the left-hand side of the field is larger than on the right-hand side.

The Darcy scale comprises a large enough number of REVs so that the pore scale is no longer resolved, but the medium is described by properties which are averaged over the pore space.

If a medium is heterogeneous on a larger scale, the same concept can be applied. If a property is averaged over a small averaging volume, the averaged property measured at different locations fluctuates. If the medium has heterogeneous structures with a finite typical length scale and the averaging volume becomes larger than the typical length scale of the heterogeneity, the averaged property measured at different locations does not fluctuate any more. The averaging volume is then called a **macroscopic REV**, as it is in principle the same as an REV, but is used for the transition from the Darcy scale to the field scale instead of for the transition from the pore scale to the Darcy scale.

Several issues related to the REV concept should be mentioned. First, it is not necessarily an isotropic property. In a layered medium with horizontal layering, for example, the REV length in the horizontal direction is zero, as there is no heterogeneity in the horizontal direction. In the vertical direction, the REV length is the length defined above. Also, the REV for the porosity or the heterogeneous structure does not necessarily coincide

with the equivalent averaging scale for an observable quantity. This problem is especially important for unstable processes. This is discussed in detail in Chapter 4.

1.4.2 Flow of a single fluid

Pore-scale model

The flow of an incompressible fluid through a porous medium is described by a balance equation for the mass of the fluid and by a balance equation for the momentum of the fluid. The flow of water in the pore space is described in principle by the Navier-Stokes equations. The fluid flow in the empty pore space is, however, supposed to be slow so that inertia forces can be neglected. If the fluids are incompressible, it is described in the steady-state case by the Stokes equation (conservation of momentum)

$$\mu \Delta \vec{v} - \vec{\nabla} P + \rho g \vec{e}_z = \vec{0}. \tag{1.1}$$

μ [M / (L T)] is the viscosity of the fluid, ρ [M / L^3] is its density, $g = 9.81 m/s^2$ is the gravitational constant, $\vec{v}$ [L / T] is the flow velocity and P [M / (L T^2)] is the pressure. Also, the fluid is assumed to be incompressible, which leads to the mass balance equation

$$\vec{\nabla} \cdot \vec{v} = 0. \tag{1.2}$$

At the interface between pore space and soil material, there is a no-slip condition

$$\vec{v}|_\Gamma = 0. \tag{1.3}$$

Γ symbolizes the interface between pore space and grain.

Darcy-scale model

Darcy scale flow is mostly relevant for water. Therefore the flowing fluid is supposed to be water in the following. If the flow is described on the Darcy scale, the specific discharge or Darcy velocity $\vec{q}$ [L / T] is considered, which is the volumetric flux over an interface of porous material times the area of the interface (see Figure 1.6). As the pore space of the medium is not resolved, the Darcy velocity is related to the flow velocity $\vec{v}$ as

$$\vec{q} = n_f \vec{v}, \tag{1.4}$$

where n_f [-] is the porosity of the medium.

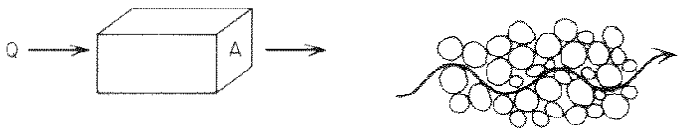

Figure 1.6: Relation between flow velocity and Darcy velocity. Taken from Freeze and Cherry (1979)

It has been shown by Whitaker (1986a), Levy (1987), Auriault (1983) and Sanchez-Palencia (1980) that the volume average of the equations describing the flow on the pore scale (1.1, 1.2 and 1.3) yield the Darcy equation

$$\vec{q} = -\frac{\mathbf{K}_{\text{int}}}{\mu}\vec{\nabla}(P + \rho g z) \tag{1.5}$$

This equation describing flow through porous material was used before its rigorous derivation from the Stokes equations. $\mathbf{K}_{\text{int}}$ [L^2] is the intrinsic permeability tensor of the medium, which is a material-specific property. If water as the single fluid is considered, it is often common to use an equivalent pressure head h [L] instead of the pressure,

$$h = \frac{P}{\rho g}. \tag{1.6}$$

h will always be used in this definition. It is, however, also used as the hydraulic head, which is the sum of h and the vertical elevation z. The reason for using a pressure head instead of the pressure is, that it is much easier to measure the sum of h and the elevation z in the field than to measure an absolute pressure. If water flow is considered, it is more common to use the hydraulic conductivity K [L / T] instead of the intrinsic permeability. It is defined as

$$\mathbf{K} = \frac{\mathbf{K}_{\text{int}}\rho_{\text{water}} g}{\mu_{\text{water}}}. \tag{1.7}$$

The Darcy equation then reads

$$\vec{q} = -\mathbf{K}\vec{\nabla}(h + z). \tag{1.8}$$

The mass continuity of water in the porous medium reads

$$S_f \frac{\partial h}{\partial t} + \vec{\nabla} \cdot \vec{q} = s, \tag{1.9}$$

where S_f [1 / L] is the storage coefficient, which accounts for storage of water due to compression of the water or of the porous material. s stands here for external sources and sinks. Very often, only the steady-state problem is considered.

Model on the field-scale

The most important parameter for modelling single phase-flow is the hydraulic conductivity K. This parameter shows a high range in earth materials. Typical values are listed in Table 1.1. The permeabilities of gravel and sandstone differ by several orders of magnitude. In natural soil and rock formations, the hydraulic conductivity is also highly heterogeneous. As an example, the Borden test site can be considered (Sudicky, 1986). The Borden aquifer is considered very homogeneous, compared to other known aquifers. Yet even there hydraulic conductivities measured in the field also differ over orders of magnitude.

Material	Hydaulic conductivity K [m / s]
Gravel	$3 \cdot 10^{-4} - 3 \cdot 10^{-2}$
Coarse sand	$9 \cdot 10^{-7} - 6 \cdot 10^{-3}$
Medium sand	$9 \cdot 10^{-7} - 5 \cdot 10^{-4}$
Silt, loess	$1 \cdot 10^{-9} - 2 \cdot 10^{-5}$
Till	$1 \cdot 10^{-12} - 2 \cdot 10^{-6}$
Clay	$1 \cdot 10^{-11} - 4.7 \cdot 10^{-9}$
Sandstone	$1 \cdot 10^{-11} - 1.4 \cdot 10^{-8}$
Shale	$1 \cdot 10^{-13} - 2 \cdot 10^{-9}$
Weathered granite	$3.3 \cdot 10^{-6} - 5.2 \cdot 10^{-5}$

Table 1.1: Typical values of hydraulic conductivities, after Domenico and Schwartz (1990)

For a single-phase flow problem on the field scale, the heterogeneity of the local (Darcy scale) hydraulic conductivity can therefore not be neglected. It has been shown by many authors (King (1987), Gelhar (1993), Dagan (1979) among many others) that the upscaled model for steady state single phase flow in a heterogeneous hydraulic conductivity field has the same shape as the steady state model on the Darcy scale (1.9) if the field is much larger than the typical length scale of the heterogeneity. For uniform flow in one direction, the effective permeability K_{eff} in an isotropic permeability field is

$$K_{\text{eff}} = K_g \exp\left(\sigma_f^2 \left(\frac{1}{2} - \frac{1}{d}\right)\right). \tag{1.10}$$

This result has not been derived exactly, but it has been confirmed by many independent analyses (e.g. King (1987), Dagan (1979), Gelhar (1993), Hristopulos (2003), Beckie et al. (1994) and Attinger (2003)). K_g is the geometric mean of the local permeability field, σ_f^2 is the variance of the logarithm of the local permeability and d is the spatial dimension. An overview of the effective permeability of the single phase flow problem on the field scale can be found in Renard and de Marsily (1997). The effective permeability has to have a value between the harmonic and the arithmetic mean of the local permeability field (see Renard and de Marsily (1997)).
As outlined above, two-phase flow processes play an important role for many applications. The equations which describe the flow of two fluids will be discussed in the following.

1.4.3 Flow of two immiscible fluids

Pore-scale model

If the flow of two fluids is described on the pore scale, the Stokes equation is considered separately for each fluid,

$$\begin{aligned} &\mu_i \Delta \vec{v}_i - \vec{\nabla} P_i + \rho_i g \vec{e}_z = \vec{0} \\ &\vec{\nabla} \cdot \vec{v}_i = 0, \qquad i = nw, w. \end{aligned} \tag{1.11}$$

The index i is used to indicate the two different fluids. w is an index for the wetting phase while nw is an index for the non-wetting phase. They are both assumed to be incompressible. The velocity at the grain-pore interface in each fluid is assumed to vanish, while the velocity of each fluid at the fluid-fluid interface has to be equal to each other.

$$\vec{v}_i|_\Gamma = \vec{0}, \quad \vec{v}_w|_{\Gamma_{w,nw}} = \vec{v}_{nw}|_{\Gamma_{w,nw}}. \tag{1.12}$$

$\Gamma_{w,nw}$ stands for the interface between the two fluids. The stress tensor at the interface between the fluids is

$$-P_w\vec{n}_{w,nw} + \tau_w \cdot \vec{n}_{w,nw} = -P_{nw}\vec{n}_{w,nw} + \tau_{nw} \cdot \vec{n}_{w,nw} + 2\sigma_{w,nw}H\vec{n}_{w,nw}. \tag{1.13}$$

$\vec{n}_{w,nw}$ is the vector normal to the interface $\Gamma_{w,nw}$, τ_i [M / (L T^2)] is the stress tensor in phase i, $\sigma_{w,nw}$ [M / T^2]is the surface tension between the fluids and H [1 / L] symbolizes the mean curvature of the interface.
In principle, we would have to distinguish between two immiscible phases, such as gas and liquid, and would also have to take the mass transfer of different components between these phases into account. As the mass transfer is neglected here, we can identify a phase by a fluid. Both words are used here as synonyms
Two dimensionless numbers are used to quantify the flow behaviour, as there are three driving forces: viscous forces, buoyancy forces and capillary forces. The definition of these numbers is discussed in Hilfer and Øren (1996). Capillary forces and viscous forces are compared by the **capillary number** Ca [-] for fluid i:

$$Ca_i = \frac{\mu_i v}{\sigma_{w,nw}}. \tag{1.14}$$

The **Bond number** Bo [-] compares buoyancy to capillary forces

$$Bo = \frac{(\rho_1 - \rho_2)gl^2}{\sigma_{w,nw}}. \tag{1.15}$$

l [L] is a typical length scale for a pore. An alternative to the Bond number is the **gravillary number** Gl [-] for fluid i as defined in Hilfer and Øren (1996), which uses the density of a fluid instead of the density difference.

$$Gl_i = \frac{\rho_i g l^2}{\sigma_{w,nw}}. \tag{1.16}$$

If the wetting fluid displaces the non-wetting one, the flow process is usually called **imbibition**. If the non-wetting fluid displaces the wetting one it is called **drainage**.
The pore scale model of two-phase flow will partly be used in Chapter 4.

Darcy-scale model

The derivation of the two-phase flow equations for the Darcy scale is not so well established as for the single-phase flow equations. In the steady-state case and if both fluids

are connected throughout the pore space, it has been shown by Whitaker (1986b) that the specific discharge for each fluid is given by a Darcy-type of equation

$$\vec{q}_i = -\frac{\mathbf{K}_{\text{int}} k_r}{\mu_i} \vec{\nabla}(P_i + \rho_i g z). \tag{1.17}$$

i is used here again as an index for the two fluids. k_r [-] is the relative permeability, which is a number between zero and one and accounts for the change of the permeability of the porous medium due to the presence of a second fluid which blocks part of the pore space for the first fluid. The relative permeability is assumed to be a function of the volume percentage of the fluid in the medium. The volume percentage is called the saturation S [-] of the fluid.
It is sometimes discussed whether relation (1.17) is complete. Whitaker (1986b) concludes that there might be a coupling between the Darcy velocity of one fluid to the Darcy velocity of the other fluid. In this case, the velocity of one fluid would also depend on the pressure gradient in the other fluid. However, as this effect is supposed to be of minor importance, it is neglected here.
For each fluid, there is a mass balance equation

$$n_f \frac{\partial S_i}{\partial t} - \vec{\nabla} \cdot \vec{q}_i = s_i, \qquad i = w, nw. \tag{1.18}$$

Combining equations (1.17) and (1.18) yields

$$n_f \frac{\partial S_i}{\partial t} + \vec{\nabla} \cdot \left(\frac{\mathbf{K}_{\text{int}} k_r}{\mu_i} \vec{\nabla}(P_i + \rho_i g z) \right) = s_i. \tag{1.19}$$

There is one equation for each fluid, so that there are two equations in all for four unknowns (the pressure and the saturation in both fluids). The system is closed by two relations. First, the sum of the saturation of both fluids has to equal one everywhere in the medium

$$S_1 + S_2 = 1. \tag{1.20}$$

It is therefore sufficient to consider only the saturation of one fluid, as the saturation of the other one is fixed once this is given. The second condition is an empirical relation, which is used in analogy to the processes on the pore scale. The difference between the phase pressure of the non-wetting phase and of the wetting phase at a location $\vec{x}$ is assumed to be a unique function of the saturation at this location. The pressure difference is the capillary pressure P_c,

$$P_{\text{nw}} - P_{\text{w}} = P_c(S). \tag{1.21}$$

The index w stands for the wetting phase, while the index nw stands for the non-wetting phase. The relation between capillary pressure and saturation is empirical and has to be determined for a given soil type experimentally.
In this simple form, relation (1.21) is not what is found in experiments. The difference between the pressure in the wetting and in the non-wetting phase is a hysteretic relation.

The shape of the capillary pressure - saturation curve depends on whether a drainage (displacement of wetting by non-wetting fluid) or an imbibition (displacement of non-wetting by wetting fluid) is considered. If a drainage process after an imbibition process is considered (or vice versa), the curves also look different. Although hysteresis is certainly important, it is not the focus of this work and will not be taken into account. Also, it is found that the pressure difference between the fluids measured during a drainage or imbibition process depends on the velocity of the displacement. It has been suggested by Hassanizadeh et al. (2002) that the capillary pressure be extended by a term that accounts for the rate of change of the saturation. These dynamic effects are also important, but will be neglected here.
Dimensionless numbers on the Darcy scale have to be defined differently than on the pore scale. Hilfer and Øren (1996) define the capillary number as

$$\mathbf{Ca}_i = \frac{\mu_i q L}{P_b} \mathbf{K}^{-1}. \tag{1.22}$$

P_b is a typical capillary pressure on the Darcy scale, such as the capillary pressure where the saturation of both fluids is $S_i = 0.5$. L [L] is a typical length scale on the Darcy scale. The gravillary number on the Darcy scale is defined as

$$\mathbf{Gl}_i = \frac{\rho_i g L}{P_b}. \tag{1.23}$$

The Bond number is accordingly

$$\mathbf{Bo} = \frac{(\rho_1 - \rho_2) g L}{P_b}. \tag{1.24}$$

The dimensionless numbers will in the following chapters sometimes be defined differently. This will be outlined and explained explicitly.
If water and air are considered, it is often more convenient to convert the capillary pressure into a capillary pressure head h_c,

$$h_c = \frac{P_c}{\rho_{\text{water}} g}. \tag{1.25}$$

In the literature, the capillary pressure head is also often denoted Ψ.
There are different models for the constitutive relationships $P_c(S)$ and $k_r(S)$. Very often, the models of Brooks and Corey (Brooks and Corey, 1966) or Mualem and van Genuchten (Mualem, 1976; van Genuchten, 1980) are used. The capillary pressure in the Brooks-Corey model is parameterized as

$$P_c(S) = P_{\text{entry}} S_e^{-\frac{1}{\lambda}} \quad \text{with} \quad S_e = \frac{S_w - S_{wr}}{1 - S_{wr}}. \tag{1.26}$$

P_{entry} is the entry pressure of the porous medium. It is related to the entry pressure of the largest pore on the pore scale. If the capillary pressure is below the entry pressure, the

medium is filled with the wetting phase only. If water and air are considered, it is often more convenient to convert the entry pressure into an entry pressure head h_{entry}

$$h_{\text{entry}} = \frac{P_{\text{entry}}}{\rho_{\text{water}} g}. \tag{1.27}$$

The effective saturation of the wetting phase S_e [-] is the saturation which is rescaled with the residual saturation of the wetting phase, S_{wr} [-]. The residual saturation is the saturation of wetting fluid, which is strongly bound to the porous material due inter-molecular forces, so that it cannot be removed from the porous material. The corresponding residual saturation of the non-wetting phase is denoted S_{nwr} [-]. The residual non-wetting phase is due to trapped non-wetting fluid, which cannot be mobilized and thus can not be removed from the porous material. λ [-] is the Brooks-Corey parameter, which reflects the grain size distribution. If λ is small, there is a wide range of grain sizes and the $P_c - S$ curve is steep; if it is large, the curve is sharp and there is mainly one grain size. The relative permeability of the wetting phase is parameterized as

$$k_{r,w} = \begin{cases} 0 & \text{if} \quad S_w < S_{wr} \\ S_e^{(2/\lambda+3)} & \text{if} \quad S_{wr} < S_w < 1 - S_{nwr} \\ 1 & \text{if} \quad S_w > 1 - S_{nwr} \end{cases}. \tag{1.28}$$

The relative permeability of the non-wetting phase is parameterized as

$$k_{r,nw} = \begin{cases} 0 & \text{if} \quad S_w > 1 - S_{nwr} \\ (1 - S_e)^2 \left(1 - S_e^{(2/\lambda+1)}\right) & \text{if} \quad S_{wr} < S_w < 1 - S_{nwr} \\ 1 & \text{if} \quad S_w < S_{wr} \end{cases}. \tag{1.29}$$

The Brooks-Corey model has four material dependent parameters, the parameter λ, the entry pressure P_{entry} and the two residual saturations S_{wr} and S_{nwr}. Typical capillary pressure - saturation and relative permeability - saturation curves are shown in Figure 1.7.

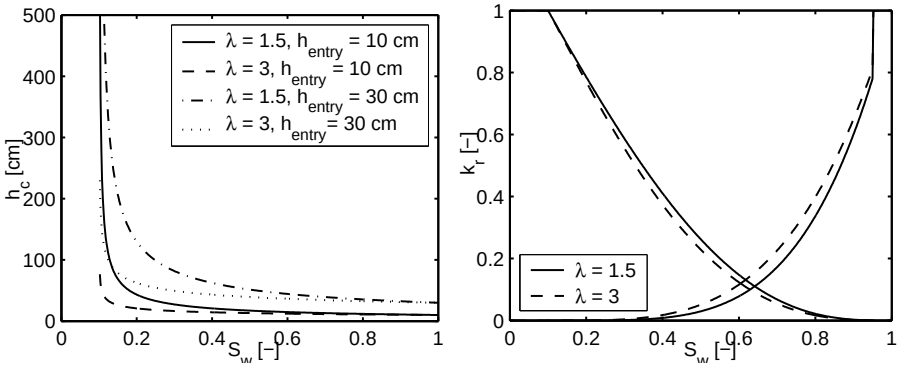

Figure 1.7: Capillary pressure - saturation and relative permeability - saturation curves for a Brooks-Corey model. The residual saturations are $S_{wr} = 0.9$, $S_{nwr} = 0.05$.

The Mualem-van Genuchten model is mostly used for gas-water systems so that the capillary pressure head h_c (1.25) is used instead of the capillary pressure. The model does not have an entry pressure, but the non-wetting phase can enter the medium as soon as the capillary pressure is non-zero. The $S - h_c$ relation is given by

$$S_e = (1 + (-\alpha h_c)^n)^{-m}. \tag{1.30}$$

The $h_c - S$ relation has to be obtained by inverting the relation. The effective water saturation is given here as

$$S_e = \frac{S_w - S_{wr}}{1 - S_{wr} - S_{nwr}}. \tag{1.31}$$

The parameter α [1 / L] has the dimension of an inverse pressure head and can be considered the inverse capillary-pressure head at an intermediate saturation. The parameters n [-] and m [-] are material-specific parameters. The relative permeability for the wetting phase is

$$k_{r,w} = S_e^{(1/2)} \left(1 - \left(1 - S_e^{(1/m)}\right)^m\right)^2 \tag{1.32}$$

and for the non-wetting phase

$$k_{r,nw} = (1 - S_e)^{(1/2)} \left(1 - S_e^{(1/m)}\right)^{2m}. \tag{1.33}$$

The Mualem van Genuchten model has five material-specific parameters, the parameters α, n and m and the two residual saturations S_{wr} and S_{nwr}. Typical curves are shown in Figure 1.8.

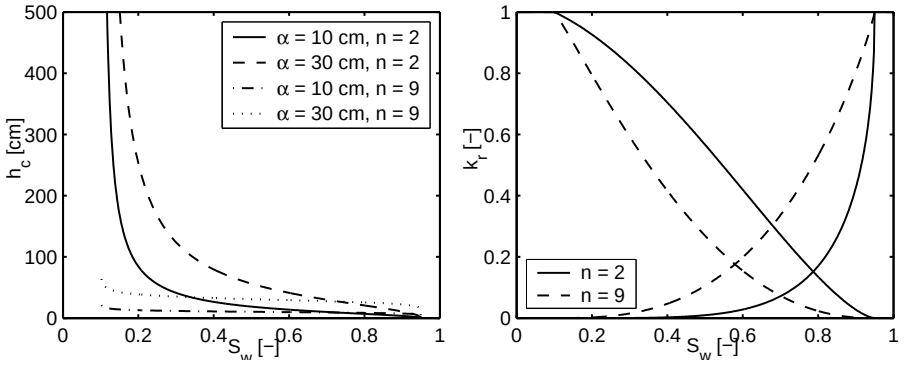

Figure 1.8: Capillary pressure - saturation and relative permeability - saturation curves for a Mualem - van Genuchten model. The residual saturations are $S_{wr} = 0.9$, $S_{nwr} = 0.05$. The parameters m and n are related via $m = (n-1)/n$.

The fully coupled system of two-phase flow equations ((1.19), (1.20) and (1.21)) will be considered for two different typical length scales in the Chapters 6 and 7.

1.4.4 Flow in the unsaturated zone: Richards equation

A special case of flow of two immiscible fluids on the Darcy scale is flow the soil zone inbetween the land surface and underlying aquifers, or the unsaturated zone. In this part there is air and water flowing at the same time. In principle it is described by the model outlined in the last sub-section. However, it is usually assumed that the air is always connected to the surface. It is also usually assumed, that as the viscosity of air is two orders of magnitude smaller than that of water ($\mu_{\text{air}} = 1.7\,10^{-5} kg/(ms)$, $\mu_{\text{water}} = 1.0\,10^{-3} kg/(ms)$), air can compared to water always assumed to be in equilibrium. The air pressure is thus considered to be constant. In principle the air is then at atmospheric pressure, however, atmospheric pressure is often set to zero for simplicity. This assumption simplifies the system of two-phase flow equations. As the air is considered as stagnant in the background, the flow of air does not have to be considered, and the only relevant fluid is the water. As the air pressure is set to zero, the water pressure head is identical to the negative capillary pressure head,

$$h = \frac{P_{\text{water}}}{\rho_{\text{water}} g} = \frac{P_{\text{air}} - P_c}{\rho_{\text{water}} g} = -\frac{P_c}{\rho_{\text{water}} g} = -h_c. \tag{1.34}$$

As the water saturation as well as the relative permeability is assumed to be uniquely related to the capillary pressure (and thus to the water pressure, see (1.17) and (1.21)), the continuity equation (1.19) reduces to one equation with one unknown, which is the water pressure head,

$$\frac{\partial n_f S(h)}{\partial t} + \vec{\nabla} \cdot \left[K k_r(h) \left(\vec{\nabla} h + \vec{e} \right) \right] = s. \tag{1.35}$$

The index is therefore dropped. The constitutive relations for this model are the relative permeability of the water k_r and the capillary pressure - saturation relation. Equation (1.35) is called Richards equation. As water in an aquifer has in steady state conditions a hydrostatic pressure distribution with a pressure of zero (corresponding to the atmospheric pressure), the water pressure in the unsaturated zone has negative values. It can be considered as a suction due to the capillary forces, which drive the wetting fluid water into the dry soil.
Richards equation (1.35) will be used in Chapter 5, where flow in the unsaturated zone is analyzed.

1.4.5 Transport of solute in single-phase flow

If substances are soluble in a fluid (usually water), they are transported with the flowing fluid through the porous medium. Such a scenario is important if a contaminant is released into groundwater. An example is the use of nitrate for agricultural purposes. The nitrate on the field is washed out with precipitation and infiltrates the underlying aquifer through the soil. In order to keep the nitrate concentration of drinking water at an acceptable level, the transport of the nitrate with the groundwater flow has to be understood.
It is often reasonable to assume that the solute does not change the properties of the water in which it is dissolved. This is no longer true, for example, for salt, which changes the

water density. Should the water properties remain unchanged, the concentration of solute is modelled by a mass conservation equation

$$\frac{\partial c}{\partial t} + \vec{\nabla} \cdot \vec{J} = s. \tag{1.36}$$

c [M / L^3] is the solute concentration and $\vec{J}$ [M / (L^2 T)] is the mass flux. s again stands for sinks and sources. The mass flux is caused by two mechanisms. Solute is transported advectively with the flow field of the water $\vec{v}$ (as defined in (1.4) and (1.5)). In addition to that, the solute diffuses in the water. The diffusive flux is proportional to the concentration gradient. The mass flux is thus

$$\vec{J} = \vec{v}c - D\vec{\nabla}c. \tag{1.37}$$

D [L^2 / T] is the diffusion coefficient. In water, it is typically of the order $D \propto 10^{-9} m^2/s$. The transport equation for the solute then reads (cf. (1.4)):

$$\frac{\partial c}{\partial t} + \frac{\vec{q}}{n_f} \cdot \vec{\nabla}c - \vec{\nabla} \cdot D\vec{\nabla}c = s. \tag{1.38}$$

In a heterogeneous flow field, the solute is mixed much more strongly than by diffusion. This is due to the fluctuations of the flow velocity field. The principle has been investigated by Taylor (1953) for the transport of solute in the flow field of a stream tube. The flow velocity inside the tube has a parabolic profile. A solute particle in the middle of the tube is thus transported faster than a solute particle close to the boundary. If a vertical tracer line is considered at an initial time, it will be at a different horizontal location at a later time. The particle in the middle of the tube will be ahead of the particle close to the boundary. Their distance will grow linearly with time. However, this is only true at early times. At later times, the two particles will have been transported vertically to different streamlines by diffusion. At early times, the travel distance due to diffusion is small but, if one waits long enough so that diffusion mixes the solute vertically over the whole width of the tube, the particles will have been transported advectively with different velocities. It has been shown by Taylor (1953) that the growth of the width of the solute line in the tube is proportional to the square root of time for long times.
The same principle holds for transport in a heterogeneous velocity field in the subsurface. The solute on different streamlines of the flow field is transported advectively with the streamlines. As the streamlines in a heterogeneous hydraulic conductivity field have different velocities and fluctuate in space, the solute plume is distorted. Due to diffusion the tracer is mixed after some time over many streamlines, so that one solute particle has been transported on an ensemble of streamlines. This leads to macrodispersion, which is much more efficient than diffusion. The transport equation for the solute in heterogeneous flow fields in the long-term limit then reads

$$\frac{\partial c}{\partial t} + \frac{\langle \vec{q} \rangle}{n_f} \cdot \vec{\nabla}c - \vec{\nabla} \cdot \mathbf{D}^\star \vec{\nabla}c = s. \tag{1.39}$$

$\langle \vec{q} \rangle$ is the spatially averaged flow-velocity field and $\mathbf{D}^\star$ is the macrodispersion tensor. It has been analyzed by many authors. For example, Gelhar and Axness (1983), Kitanidis

(1988) and Dagan (1984) have found that in a log-normally distributed permeability field (meaning the logarithm of the hydraulic conductivity is normally distributed), it is

$$\mathbf{D}_L^\star = D + \sigma_f^2 \ell \langle \vec{q} \rangle, \quad \mathbf{D}_T^\star = D. \tag{1.40}$$

The tensor $\mathbf{D}^\star$ is diagonal. L is the index for the entry in mean flow direction, while T is the index for the transversal direction. σ_f^2 is the variance of the logarithm of the hydraulic conductivity and ℓ is the integral scale of the field (see Chapter 3). As the macrodispersion tensor is proportional to the typical length scale of heterogeneity in the field, field measurements of the dispersion coefficient vary a lot. Experiments on a larger scale show a larger dispersion coefficient, as they capture larger scales of heterogeneity.
In the examples for upscaling which are discussed in this study, macrodispersion will not be taken into account. However, it is a very widely investigated effect and should therefore be mentioned. It could be considered the problem for which upscaling methods have been applied most successfully in the last decades. It involves many aspects that have not been addressed here. Some of them are:

- Solute is not only transported with the flow, but usually undergoes chemical reactions. The chemical properties of the porous material are usually also heterogeneously distributed. Such problems have been studied by Attinger et al. (1999), Bellin et al. (1993) or Miralles-Wilhelm and Gelhar (1986) among many others.

- The dispersive behaviour (1.39) is only valid in the long-term limit. In real applications, this limit is seldom reached. In the preasymptotic case, the macrodispersion coefficient is smaller than $\mathbf{D}^\star$. The preasymptotic behaviour has been investigated, for example, by Rajaram and Gelhar (1993), Fiori (1998), Dagan (1990), Dagan (1988), Cirpka and Kitanidis (2000) or Dentz et al. (2000).

- As outlined above, in most cases soil has heterogeneities on all length scales. The result (1.39) is valid for a field with a finite correlation length. The macrodispersion coefficient is much more complex if the structure of the field is complex (e.g. Kemblowski and Wen (1993)). The same is true of fields where boundaries have to be considered.

In the case of the flow of two immiscible fluids, where solute is dissolved in each fluid and transported with the flow field, the problem becomes much more complex. The models for this scenario are discussed in Helmig (1997) and will not be considered further here.

1.5 Outline of the study

This study deals with the question: How can information about a process be transferred from a smaller to a larger scale? The key questions for upscaling have been formulated by Leihnse (2005) as

- How do process descriptions change by transfer to a larger scale?

- How are new parameters and / or effective parameters defined in the upscaled process description?
- Which information on the underlying structure of the small-scale process must be known for the upscaling to be meaningful?

This study is guided by these three questions.
As information about the soil structure in the subsurface is always sparse, the third question is very important. It is addressed in Chapter 2, where various concepts for characterizing heterogeneity are discussed. In Chapter 3, various methods for deriving upscaled models and upscaled parameters are discussed. The methods which are then used in this study are described in more detail. In this way, the first two questions are addressed. Chapter 4 is dedicated to the problem of stability and upscaling. Upscaling methods are usually applied under the assumption that a heterogeneous structure is fixed and prescribed by the soil. If processes are unstable, however, this is not longer true. If and how unstable processes can be upscaled is discussed using the example of two-phase flow. Chapters 5 to 7 present applications of upscaling. The methods described in Chapter 3 are applied to three different two-phase flow scenarios. The three questions cited above are discussed for all three problems. In particular, the question of the characterization of heterogeneity is addressed in Chapters 5 and 6. In Chapter 5, flow in the unsaturated zone is analyzed. This is a two-phase flow process on a relatively small length scale, typically several meters. On this scale, gravity and capillary forces are the main driving forces. In Chapter 6, two-phase flow on the same length scale is discussed, but the fluids are considered here to have similar properties in terms of viscosity and density. The processes in Chapter 5 and 6 can be described as two different two-phase flow processes on the same length scale. The processes considered in Chapter 6 are more complex than those in chapter 5. Two-phase flow on a much larger scale is discussed in Chapter 7. In this chapter immiscible displacement on a scale of kilometers is discussed. On this scale, the driving forces are viscous forces and gravity, while capillary forces can be neglected. The whole work is summarized in Chapter 8, where the main conclusions, as well as the main open questions, are outlined.

Chapter 2

Characterization of heterogeneity

In upscaled models, the influence of soil heterogeneity is captured by effective processes and effective parameters. Depending on the field, different measures might be appropriate to characterize heterogeneity. This chapter provides a summary of the most common definitions and methods to quantify and characterize heterogeneity. As data for model parameters are mostly scarce, the heterogeneous parameter field is often described by a random field. The relevant properties and concepts needed for a stochastic description of the parameter field are given in Section 2.1. In Section 2.2 quantifications for connected paths are discussed, as connected paths of materials with parameters with either very high or very low values are important for flow and transport in the subsurface.

2.1 Random fields and their properties

In many methods of upscaling, the parameters describing the properties of heterogeneous materials are represented by spatial random variables (i.e., random fields) with given univariate or multivariate stochastic distributions. These distributions are often based on parameteric models of probability density functions equipped with parameters such as mean, variance and covariances. A general overview over stochastic processes can be found in books (e.g. van Kampen (1992), Issaks and Srivastava (1989), Davis (1986) and Kitanidis (1997)). In this chapter the basic terms and principles, which are used in the chapters 4 to 7, will be explained.

Mean and perturbations

When considering a parameter (such as the hydraulic conductivity K) to be a random field within stochastic approaches, the parameter is split into its stochastic mean $< K >$ and fluctuations $\tilde{K}$ about the mean. For example, the hydraulic conductivity K would be written as

$$K(\vec{x}) = \langle K(\vec{x}) \rangle + \tilde{K}(\vec{x}). \tag{2.1}$$

Variance and auto-covariance

For a parameter field denoted as $f(\vec{x})$, the autocovariance $C_{ff}(\vec{x},\vec{x}')$ between the parameter values at the locations $\vec{x}$ and $\vec{x}'$ is defined by

$$C_{ff}(\vec{x},\vec{x}') = \langle (f(\vec{x}) - \langle f(\vec{x}) \rangle) \left(f(\vec{x}') - \langle f(\vec{x}') \rangle \right) \rangle = \langle \tilde{f}(\vec{x}) \tilde{f}(\vec{x}') \rangle, \tag{2.2}$$

where the brackets stand for a stochastic average or a volume average, depending on the approach. The difference between the locations $\vec{x}$ and $\vec{x}'$ is called the separation vector $\vec{h}$, and the distance is the separation distance h. The autocovariance at $h = 0$, $\vec{x} = \vec{x}'$ is the variance σ_f^2.

Integral scales

In heterogeneous fields, the autocovariance typically decreases with the separation distance h. The decay or range of correlation over distance is one of the most important structural characteristics. A measure for this behaviour is the integral scale Λ of a random field. I is the integral of the autocovariance in one spatial direction normalized by the variance, while the coordinates in the other directions remain set to zero:

$$\Lambda_i = \int \frac{C_{ff}(\vec{h})_{h_{\neq i}=0}}{\sigma_f^2} dh_i \tag{2.3}$$

Second-order stationarity

The parameter fields are usually assumed to be second order stationary, which means that the variance is finite and that the mean and the autocovariance are invariant under translation (cf. 2.4):

$$C_{ff}(\vec{x},\vec{x}') = C_{ff}(\vec{x} - \vec{x}') = C_{ff}(\vec{h}). \tag{2.4}$$

In other words, the auto-covariance of a second order stationary field depends only on the difference vector of the locations, where the two parameters are measured.

Covariance models

The autocovariance of random fields can be defined using a parametric model. Among the most common ones is the Gaussian model, which implies that the autocovariance decays fast with distance. Other common model assumptions are an exponential decay with a longer range of correlation, the nugget effect for pure white noise and power functions or polynomials with a defined cutoff range for the maximum distance of correlation.
For the Gaussian autocovariance function, the integral scale is

$$\Lambda_i = \frac{1}{\sigma_f^2} \int_{-\infty}^{\infty} \sigma_f^2 \exp\left(-\frac{h_i^2}{\lambda^2} \right) dh_i = 2\sqrt{\pi}\sigma_f^2 \lambda. \tag{2.5}$$

However, if the autocovariance is modelled by a function which decays slowly, such as

$$C_{ff}(\vec{h}) = \sigma_f^2 \left(\frac{\lambda}{|\vec{h}| + \lambda} \right), \tag{2.6}$$

the same integral diverges. In this case, the field has long-range correlations. Two example fields are shown in Figure 2.1.

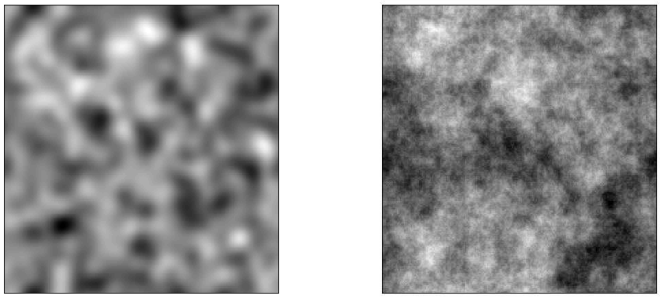

Figure 2.1: Field with (left) and without (right) finite integral scale (according to covariances (2.5) and (2.6)

Isotropy and anisotropy

Isotropic random space variables have the same covariance function for all $\vec{h}$ with the same norm, i.e., the covariance function depends only on separation distance but not on the direction of the separation vector.
Anisotropic media can be defined by using different norms of separation distance for different directions of the separation vector. This leads to different integral scales for different directions.
In three dimensions, for example, an anisotropic medium could be be described by a Gaussian covariance function such as

$$C_{ff}(\vec{h}) = \sigma_f^2 \exp\left(- \left(\frac{h_1^2}{\lambda_1^2} + \frac{h_2^2}{\lambda_2^2} + \frac{h_3^2}{\lambda_3^2} \right) \right). \tag{2.7}$$

Examples for an isotropic and an anisotropic field are shown in Figure 2.2.

Second order statistics

The second order properties of a stationary field are the the mean and the autocovariance function. The latter may be defined by a parametric model and integral scales Λ_i. The mean gives an order of magnitude for the parameter, the variance gives a measure how strong the fluctuations of the value around the mean are, and the integral scales provide estimates of the spatial scales of the fluctuations. The integral scale gives also an estimate

how large an averaging volume has to be so that the medium appears homogeneous. An averaging volume has to cover several integral scales.
Due to practical reasons only second order properties are taken into account in perturbation theory (see Chapter 3). Third or higher order moments are difficult to handle. Second order properties are good measures for heterogeneity if the fields obey multivariate Gaussian distributions. The moments of a Gaussian field $f(\vec{x})$ with mean zero $\langle f \rangle = 0$ are

$$\begin{aligned} \langle \Pi_{i=1}^{2n+1} f(\vec{x}_i) \rangle &= 0 \\ \langle \Pi_{i=1}^{2n} f(\vec{x}_i) \rangle &= \sum_{\text{all permutations}} \Pi_{i=1}^{n} \langle f(\vec{x}_i) f(\vec{x}_{n+i}) \rangle \end{aligned} \tag{2.8}$$

All multivariate random fields are completely described by their moments. As all moments of Gaussian fields are composed of the first and second moments only, they are completely determined by their second order statistics.

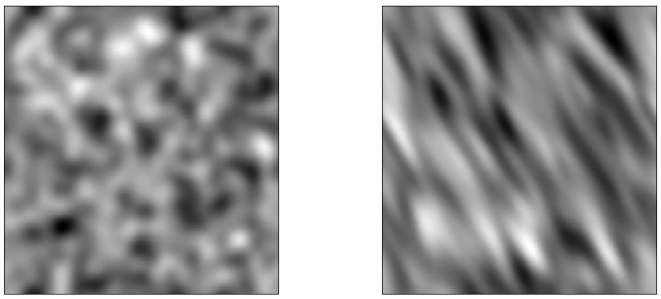

Figure 2.2: Isotropic field (left) and and anisotropic field (right)

Realizations and ensembles

One outcome of a random process, i.e., a specific random field with given values, is called a realization. The total of all possible realizations forms an ensemble. The ensemble represents the joint probability density. A set of realizations drawn from an ensemble is called a sample.
The interpretation of quantities like permeability as emsembles (by describing them as random fields) is not really an appropriate picture that meets nature: A specific soil or material at hand is not random. If the field parameters could be measured with non-invasive techniques everywhere, it would be a deterministic field. The randomness reflects the lack of knowledge about the exact distribution. Only sample means, sample variances and spatial covariances can be obtained by local measurements. The picture behind the stochastic interpretation of a parameter field as ensemble is that, in absence of better knowledge, there is an infinite amount of possible realizations satisfying the available data.

Spatial averages and ensemble averages

the stochastic average $< f >$ (or ensemble average) of a random process f is obtained by integrating the local value $f(x)$ over the local probability density function $p(f,x)$ of the ensemble (see Figure 2.12):

$$< f(x) >= \int_{-\infty}^{+\infty} f p(f,x) df. \tag{2.9}$$

A spatial average $\overline{f}$ of a parameter f over a finite length interval of length L is defined as

$$\overline{f} = \frac{1}{L} \int_0^L f(x) dx, \tag{2.10}$$

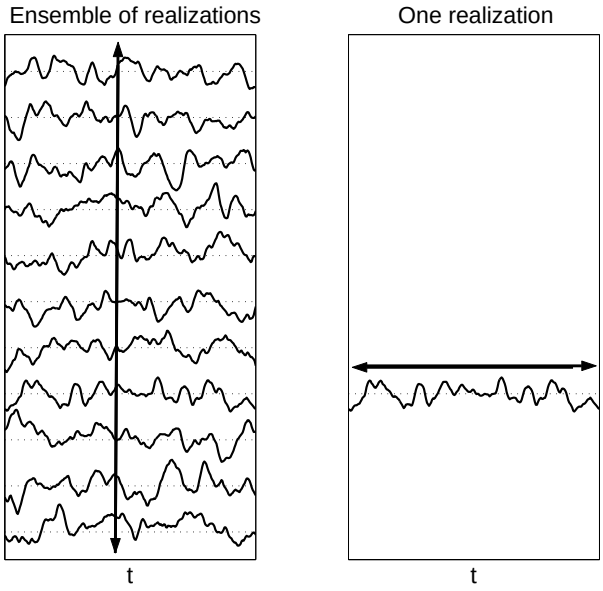

Figure 2.12: Ensemble averaging (left) and spatial averaging (right). Both averages are equivalent in ergodic media

Ergodicity

In reality, data on the spatial distribution are sparse and erroneous, so that spatial averages cannot be performed at sufficient precision. However, although ensembles of soil configurations do not physically exist, ensemble averages are often used instead. In order to use stochastic averaging approaches instead of spatial ones, the two averaging procedures have to be equivalent.
A process is ergodic if, at any given location, the ensemble average over the probability density is identical to the spatial average of the parameter in a single realization. Because this is valid for the spatial average in each single realization, the spatial average must be identical in each realization, making spatial averages independent of the individual

realization. Then, the ensemble variance and covariance of the spatially averaged process vanishes.
To be precise, this imples that the spatial averaging volume must be infinite. In practice this is not possible, but sufficiently large averaging volumes are held to be acceptable. This sufficiency is derived as follows. If a second order stationary process with finite integral scale Λ is considered, the variance of the spatial average is

$$\begin{aligned}\langle(\overline{f}-\langle\overline{f}\rangle)^2\rangle = \langle\frac{1}{L}\int_0^L(f(x)-\langle f\rangle)dx\frac{1}{L}\int_0^L(f(x')-\langle f\rangle)dx'\rangle = \\ \frac{1}{L^2}\int_0^L\int_0^L C_{ff}(x-x')dxdx' = \frac{\sigma_f^2}{L}\Lambda.\end{aligned} \tag{2.11}$$

The variance vanishes if the interval L is much larger than the integral scale of the process, so that the averaging interval is large enough to sample a large number of integral scales.

2.2 Higher order structures

Parameter fields of soil are mostly not well described as Gaussian fields. The characterization of the field by its second order properties might not capture the main characteristics of heterogeneity. Other measures of heterogeneity than moments of the parameters might be more appropriate to characterize such fields. This can be illustrated with the extreme example of the fields which have been discussed by Vogel (2002) and Zinn and Harvey (2003).
To illustrate the generation of such fields one can start off with an isotropic multi-Gaussian field $f(\vec{x})$ with a Gaussian autocovariance, such as (2.5), and a mean of zero. This field could be generated using a standard field generated (Deutsch and Journel, 1992). In such a field, the extremely high values and the extreme low values form isolated structures, while the fields in the intermediate range are well connected throughout the field. The univariate Gaussian probability density function of this field is

$$P(f) = \frac{1}{\sqrt{2\pi\sigma_f^2}}\exp\left(-\frac{f^2}{2\sigma_f^2}\right). \tag{2.12}$$

The field can be mapped to a field with a uniform distribution with values between -1 and 1 using the transformation

$$g(\vec{x}) = \mathrm{erf}\left(\frac{f(\vec{x})}{\sqrt{2}\sqrt{\sigma_f^2}}\right). \tag{2.13}$$

Here, the extreme values are also isolated, while the intermediate values around 0 are well connected throughout the field. By taking the absolute value or minus the absolute value of the field, it is transformed into a field, where either the high values or the low values

are connected, while the opposite extreme values are isolated. The distribution is then transformed back into a uniform distribution with values between -1 and 1 by stretching the distribution

$$h(\vec{x}) = 2\left(\pm|g(\vec{x})|\right) \mp 1. \tag{2.14}$$

By mapping the uniform distribution back to a Gaussian using

$$F(\vec{x}) = \sqrt{2}\sqrt{\sigma_f^2}\,\mathrm{erfinv}\left(h(\vec{x})\right), \tag{2.15}$$

a field is generated with has the same univariate Gaussian probability distribution as the first one. However, the shape of the covariance function has been changed, and either the extremely high or the extremely low values are well connected, while the values of the opposite extreme form isolated structures (see Figure 2.3).

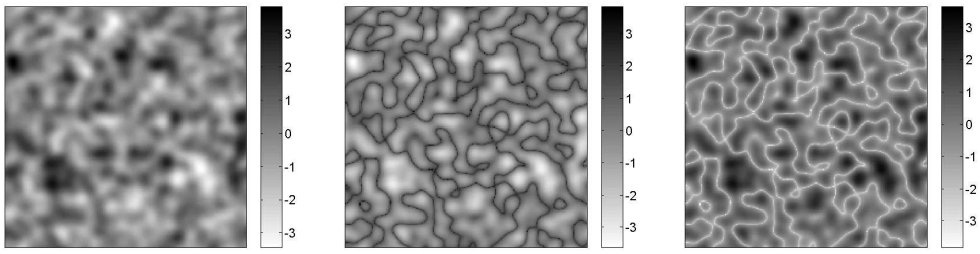

Figure 2.3: The starting field (left) is Gaussian with Gaussian autocovariance. The shifted fields have either high values connected (middle) or low values connected (right).

For direct comparisons in later chapters, fields with the same covariance function as the transformed fields will be required. For this purpose, the covariance function of the transformed fields is evaluated and used to generate another multi-Gaussian random field. Figure 2.4 shows the corresponding multi-Gaussian field that has the same covariance as the transformed fields together with their probability distributions histograms and covariance functions. It is obvious that the fields cannot be distinguished by their second order stochastic properties. Yet, they are clearly distinct in terms of connected paths. The differences of the parameter fields would only become noticable from their stochastic properties if moments of higher order than the second one would be taken into account.

In the following chapters, the three fields shown in Figure 2.4 will often be used in test cases, as they have identical second order moments, but they clearly have a different structure. As soil is often not well described as multi-Gaussian, it is important to analyze the impact of these features on upscaled models. The Gaussian field will be denoted as field 1, the field where high values are connected will be denoted as field 2, while the field where low values are connected will be denoted as field 3.

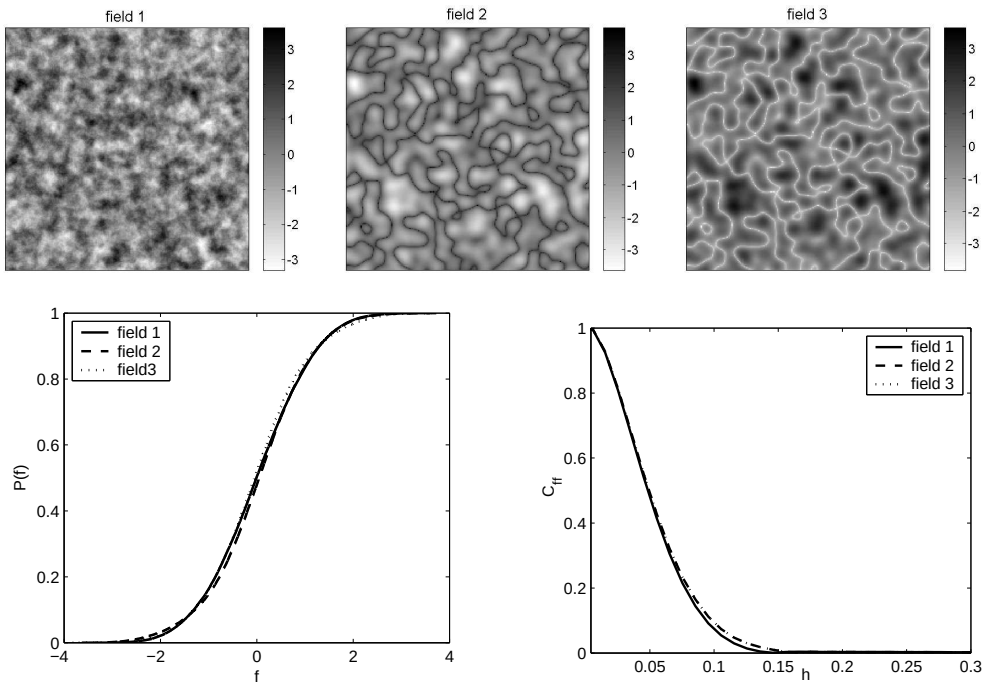

Figure 2.4: The three test fields and their cumulative probability density and autocovariance.

2.3 Connected paths of specific parameters

A different way to characterize heterogeneous fields is to quantify connected paths of certain parameter ranges. This is a useful approach if heterogeneous fields are clearly non-Gaussian (see Koltermann and Gorelick, 1996; Zinn and Harvey, 2003; Gomez-Hernandez and Wen, 1997). One way to do this is to use geometric measures for indicator fields (Knudby and Carrera, 2005). Indicator fields are generated by applying one or more threshold values to the fields. In general, an indicator field is generated by setting all values fulfilling a certain indicator property to one, while all other values are set to zero. For example, a one-cut indicator field $I(\vec{x})$ of a field $f(\vec{x})$ is obtained by setting all values below a certain thresholds to zero and all values above the threshold to one.

$$I_{thr}(\vec{x}) = \begin{cases} 1 & \text{if} \quad f(\vec{x}) \geq thr \\ 0 & \text{otherwise} \end{cases} \tag{2.16}$$

A two-cut indicator field $I(\vec{x})$ of a field $f(\vec{x})$ may be obtained by setting all values in-between two thresholds to one and all other values to zero.

$$I_{thr1,thr2}(\vec{x}) = \begin{cases} 1 & \text{if} \quad thr1 \leq f(\vec{x}) \leq thr2 \\ 0 & \text{otherwise} \end{cases} \tag{2.17}$$

In this way fields are generated which consist of zeros and ones. Indicator fields have similar features like pore scale models, where the parameter value at a site $\vec{x}$ is one if

there is a grain and zero if there is void space.
A variety of measures to quantify the structure of such binary fields exist. First of all, the same second order stochastic properties which have been discussed above for continuous fields can be applied to indicator fields. The mean gives the volume percentage Φ of material which fulfills the indicator property. The variance of a binary field $I(\vec{x})$ is directly related to the mean as

$$\sigma_I^2 = \langle I(\vec{x})^2 \rangle - \langle I(\vec{x}) \rangle^2 = \Phi(1-\Phi). \tag{2.18}$$

The correlation structure of the indicator fields gives information about the correlation of selected parameter values.
There are also measures for tortuosity, such as the surface-to-volume ratio of the indicator sets. An overview of such measures is, e.g., given in Adler (1992). In the following, we will focus on the quantification of connected paths of different material properties only, as this property has a large influence on the large scale flow and transport processes (see Gomez-Hernandez and Wen, 1997; Western et al., 2001; Zinn and Harvey, 2003). Because there is no unique measure for connectedness of the indicator fields, several possible quantifications will be discussed.

2.3.1 Bivariate distributions

Graphically spoken, the covariance or correlation discussed above (2.4) gives information about the probability to measure similar values at a given distance. Bivariate distributions contain detailed information about the probability to measure two specific values at a certain distance. If a parameter f is considered at two locations $\vec{x}$ and $\vec{x}'$, the bivariate probability density distribution $p(f(\vec{x}), f(\vec{x}'))$ is the probability density to measure the value f_1 at location $\vec{x}$ and, at the same time, f_2 at location $\vec{x}'$. For example, a Gaussian bivariate probability density for two variables with zero mean would read

$$p(f(\vec{x}), f(\vec{x}')) = \frac{1}{2\pi\sigma_f^2\sqrt{1-\rho^2}} \exp\left(-\frac{f(\vec{x})^2 - 2f(\vec{x})f(\vec{x}')\rho + f(\vec{x}')^2}{2\sigma_f^2(1-\rho^2)} \right), \tag{2.19}$$

where ρ is the correlation coefficient for the two locations $\vec{x}$ and $\vec{x}'$. If the correlation coefficient is zero, the bivariate distribution is just a product of the two Gaussian probability density distributions. If the two variables are totally correlated, the bivariate density is the product of one Gaussian probability density and a Dirac delta distribution for the two variables. Examples are shown in Figure 2.5.
The copula density is the bivariate density of the cumulative density function of the variables $f(\vec{x})$ and $f(\vec{x}')$. In this case the cumulative densities of the variables at both locations is the same

$$P(f) = \int_{-\infty}^{f} p(f')df'. \tag{2.20}$$

$p(f)$ is the probability density of f. As the cumulative density distribution is a monotonic function, it has a unique inverse $f = P^{-1}(P(f))$. The copula density c is thus

$$c(\Phi(\vec{x}), \Phi(\vec{x}')) = p(\Phi^{-1}(\Phi(\vec{x})), \Phi^{-1}(\Phi(\vec{x}'))). \tag{2.21}$$

It is independent of the probability distribution $p(f)$. In fact, a bivariate distribution can be constructed from the copula and the cumulative probability density. The information about connectedness of values is contained in the copula or copula density, while the information about the value distribution is contained in the cumulative probability density.

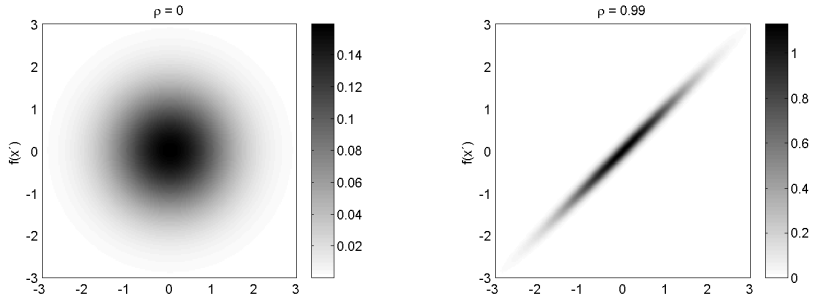

Figure 2.5: Gaussian bivariate distribution (2.19) with variance $\sigma_f^2 = 1$. Left: $\rho = 0$, right: $\rho = 0.99$.

The bivariate distribution or the copulas contain information about the spatial correlation of certain ranges of values. However, they do not necessarily provide information about the connected paths of material: they do not provide any information whether there is a connected path, which can be very tortuous, between those values at the two locations or not.

This is illustrated with the three test fields discussed above. As the univariate probability density for all three fields is identically Gaussian, the bivariate distribution can be used to compare the connectedness of the different value regimes.

In the field where high values are well connected (see Figure 2.4), the low values form isolated blobs. The isolated blobs can be observed in the bivariate distribution (see Figure 2.6). At low values, the density is stretched into a narrow band along the diagonal, which indicates high correlation, if the distance h is small. It becomes broader (meaning less correlated) for larger values. The opposite is true for the field where low values are well connected. Here, the high values form isolated blobs. This can be seen in the same way as described for the other field, just that high values show a strong correlation over some distance. However, the connected bands of high and low material in both fields are not reflected in the bivariate distribution. It is visible that these values are correlated over very small distances and after that they become less correlated. However, it cannot be assessed if the small correlated structures are connected or not.

The Gaussian field has just a usual Gaussian bivariate distribution as given in (2.19). The isolated structures with clearly visible correlation length are in the high and low parameter range.

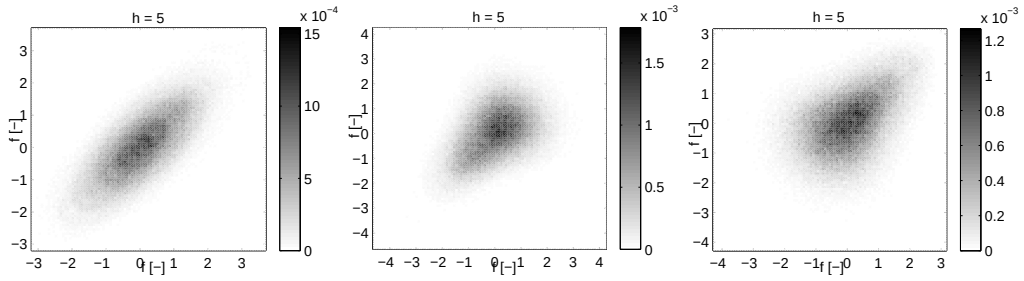

Figure 2.6: Bivariate distribution for the three test fields from Figure 2.4, left: intermediate values connected (multi-Gauss), middle: high values connected, right: low values connected.

2.3.2 Two-point cluster density

The two-point cluster density was introduced by Torquato et al. (1988). It is generated from an indicator field, or a two-cut indicator field. To indicate connectedness of certain ranges, it is more reasonable to consider two-cut indicator fields. First, these two-cut indicator fields $I(\vec{x})$ have to be generated from the full parameter fields. To calculate the two-point cluster density $C(\vec{x},\vec{x}')$, the single clusters of the indicator field have to be determined. The field with the cluster numbers is denoted $Cl(\vec{x})$. Examples are shown in Figure 2.7.

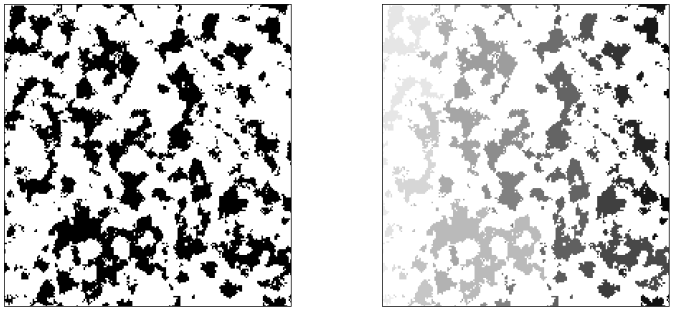

Figure 2.7: Example of an indicator field $I(\vec{x})$ (left) and the corresponding cluster field $Cl(\vec{x})$ (right), where different gray levels indicate different cluster numbers

From this field, the probability density of two points at location $\vec{x}$ and $\vec{x}'$ of the indicator field belonging to the same cluster can be calculated. If the field is stationary, this function depends only on the difference of the two locations $\vec{h} = \vec{x} - \vec{x}'$.

$$C(\vec{h}) = \frac{\langle I(\vec{x})P(\vec{x}',\vec{x})\rangle_{|\vec{x}-\vec{x}'|=h}}{\langle I(\vec{x})\rangle} \tag{2.22}$$

with

$$P(\vec{x}',\vec{x}) = \begin{cases} 1 & \text{if} \quad Cl(\vec{x}) = Cl(\vec{x}') \\ 0 & \text{otherwise} \end{cases} \tag{2.23}$$

Without the distinction of the different clusters, the two-point cluster function would be the correlation function of the indicator field.
The two-point cluster function quantifies exactly the information that is needed. Only if two points belong to the same cluster, there is a connected path in-between the two.
Applying the concept of the two-point cluster density function to the test fields introduced above illustrates that this concept quantifies the connectedness of the corresponding parameter ranges. If, e.g., three two-cut indicator fields are generated from each of the fields, one indicating the upper third of all values, one the lower third of all values and one the intermediate third of all values (see Figure 2.8), the two-point cluster density function of the fields allows for a distinction between the three fields.

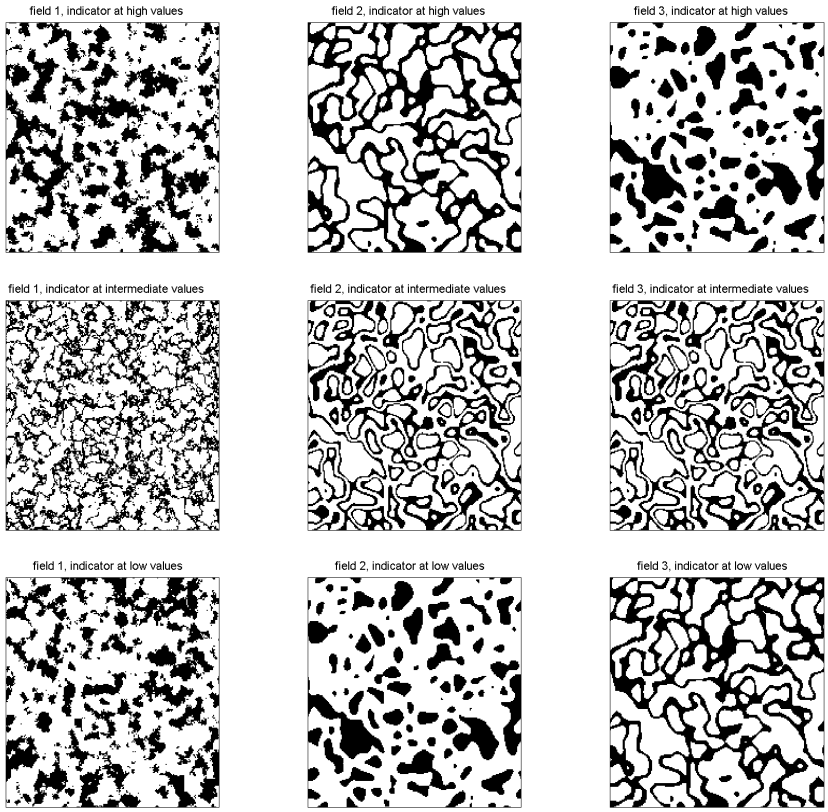

Figure 2.8: Two-cut indicator field for the three test-fields. Upper row: Indicator in the upper range, middle row: indicator in the intermediate range, lower row: indicator in the low range. Left column: field 1, middle column: field 2, right column: field 3 from Figure 2.4.

The two-point cluster density for the test fields are shown in Figure 2.9. The two-point cluster density of the field where high values are connected shows a long-range correlation

for indicators in the high parameter range, while it decays for the other two indicators. For the two-point cluster density of the field where low values are well connected, the correlation remains for indicators in the low range, while the correlations of the other indicators decay. For the Gaussian field where intermediate values are connected, the indicator for intermediate values remains connected over large distances, while the correlations of the other two indicators decay.

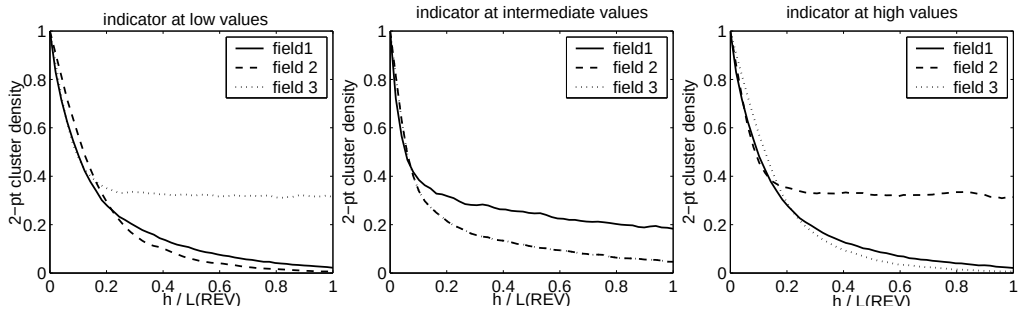

Figure 2.9: Two-point cluster density for the three test fields with indicators in the low range (left), intermediat range (middle) and in the high range (right)

The two-point cluster density is a very good measure for connectedness of specified parameter values. However, it is problematic to apply for field data, as a large amount of data is required to calculate it. For a limited amount of local data, it is strictly impossible to estimate the connectedness reasonably well this way.

2.3.3 Euler characteristic

Another measure for connected paths of certain parameter ranges is the Euler characteristic. The Euler characteristic is one of the Minkowski functionals (see Mecke and Wagner, 1991), which are geometric measures of structures. For a three-dimensional set, there are four Minkowski functionals: the volume, the surface, the integral mean curvature and the Euler characteristic. For a two-dimensional set, there are three Minkowski functionals: The surface, the boundary length and the Euler characteristic. In this work, only the Euler characteristic will be used, so that the other functionals will not be described any further. A good discussion of the Minkowski functionals is given in Mecke and Wagner (1991).
The Euler characteristic χ is a measure for the connectedness of a structure. In principle it is the integral curvature of the surface, integrated over the surface of the structure. In two dimensions, this is the number of isolated objects N minus the number of holes (equivalent to the number of redundant connections) C. In three dimensions, it is the number of isolated objects N plus the number of enclosed cavities H (surrounded by the object, so the object has the shape of a closed shell) minus the number of torus shaped holes C (so that the object has the shape of a ring).

$$\begin{aligned} \chi &= N - C \quad \text{in 2d} \\ \chi &= N - C + H \quad \text{in 3d} \end{aligned} \tag{2.24}$$

The nomenclature of Vogel (2002) is used here. With this definition, one could reason that a positive Euler characteristic indicates a disconnected structure with isolated objects, while a negative Euler characteristic indicates a connected structure which forms loops. The crossover, where values become connected, would be at Euler characteristic zero (see Figure 2.10).

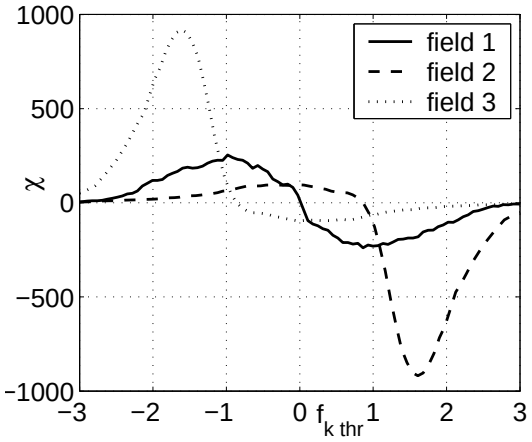

Figure 2.10: Euler characteristic for the three test fields with different indicator threshold values

The concept to use the Euler characteristic for a determination of connected material zones was introduced by Vogel (2002) for porous media on the pore scale, where the pore space is indicated with a one and the grains are indicated with a zero. Vogel (2002) outlined, that the same concept could also be applied to continuous fields, when indicator fields are considered.
The Euler characteristic applied to one-cut indicator fields generated from the fields discussed above, shows that the Euler characteristic can indicate the parameter range where values become connected. The second field has a crossover from positive to negative Euler characteristic for values in the range above $f_{thr} = 0.8$, while the third field has the crossover at $f_{thr} = -0.8$. The third field has the crossover at intermediate values at $f_{thr} = 0$.
The Euler characteristic does not yield the information about connected paths in such a direct way as the two-point cluster density does. However, it has the advantage that it can be calculated from local data and also from few data. It is clear that the quality of estimates will become questionable if data sets are small and the local extensions of the probes are small. But the Euler characteristic allows for an estimate, which is hardly possible with the two-point cluster function.
A drawback of the Euler characteristic is that it is not a comparable quantity. It does not matter whether a set consist of few large isolated structures or whether it consists of many small isolated structures when the structures are still isolated. So the resulting higher Euler number for the second case does not provide useful information. Only the sign of the Euler number matters, its value does not contain information. Therefore, the Euler

number has to be considered a “yes - no” information. Only if more information (such as other Minkowski functionals or the correlation structure) would be taken into account, the fields can be described more completely.
Another drawback of the Euler characteristic is, that the Euler characteristic does not reflect anisotropy of the field. Information about anisotropy has to be derived from additional measures, such as the auto-covariance of the field. It should also be mentioned that in three-dimensional fields (contrary to two-dimensional fields) it is possible, that extremely low values and extremely high values of a parameter field are connected at the same time. The analysis about connected paths with the Euler characteristic would have then to be performed with two-cut indicator fields for a variety of parameter ranges.

2.4 Percolation probability for an REV

The Euler characteristic is only a reasonable measure, if it is evaluated over a field, which is large enough to be representative for the whole parameter field. If this is not the case, if the field has e.g. long-range correlations, one would also be interested in the probability, that there exists a spanning cluster of a certain parameter range through an REV. Also, the Euler number has certain disadvantages, e.g., it cannot account for anisotropy. For several problems, measured from percolation theory (see Stauffer, 1992), such as the critical path for certain material properties, may be used to quantify the structure of the porous material. These methods are not applied in the following, however, they are of importance e.g. for fracture networks (see Berkowitz and Ewing, 1998; Sahimi, 1995). Hilfer (1992) used this kind of measure to derive effective permeabilities using percolation theory. If the fields are irregular, percolation methods are better suited to derive upcaled models than e.g. regular effective medium theory (see Hilfer, 1991; King et al., 2002; Hunt, 2005).

2.5 Summary

In this chapter, different approaches to characterize and quantify heterogeneous structure have been summarized and discussed. The stochastic approach is very important in the field of porous media. The parameters, considered to be correlated random fields, are often characterized by their stochastic properties. This approach is not only important for upscaling as will be discussed in the following chapter, but also opens the field of uncertainty analysis. For practical applications, the stochastic properties are mostly considered up to second moments.
There are examples of fields, where higher order moments have a high importance for the characterization of their structure. To characterize such fields, other measures than second order properties might be more suitable. In the second part of this chapter, measures for connected paths of certain material properties have been discussed. Such measures can be obtained, e.g., from indicator fields.

The different characterizations will be applied to the three two-phase flow problems discussed in the Chapters 5 to 7. In particular in Chapter 5 and Chapter 6 the measures for connected paths will be compared to the second order stochastic properties.
In the following chapter different methods to derive upscaled models and effective parameters will be discussed.

Chapter 3

Upscaling methods

Models for flow and transport in heterogeneous materials on large length scales, where detailed parameter distributionss are no longer resolved, have to be derived by averaging the respective processes while considering the heterogeneity of the materials. The models on the large scales are formulated for new variables, which are averages of the corresponding small-scale variables. The influence of the small-scale material structure, as described in the last chapter, on the large scale in the averaged models is reflected in the averaged parameters. It may also be the case that the averaged behaviour is best modelled with concepts that differ from the concepts of the small-scale models. In such cases, material structures do not only influence parameter values, but also the process descriptions on the large scale.
Different approaches are used to derive upscaled models. These approaches are not necessarily exclusive in the sense that the methods would contradict each other. They are rather formulated for a different characterization of heterogeneity. The methods considered here are

- Volume averaging,
- Homogenization,
- Effective medium theory,
- Perturbation approximation ,
- Coarse graining and
- Renormalization.

Some of these methods, which will be applied to different problems in the following chapters, will be outlined in detail in the following. This list of methods is not complete, important methods such as percolation theory are not mentioned. A thorough overview about percolation theory in porous media is given by Hunt (2005) or Berkowitz and Ewing (1998).

Deterministic Approaches

Some approaches, including volume averaging and homogenization, have the purpose to derive spatially averaged problems in heterogeneous media, where the medium structure is supposed to be known deterministically. The goal is to explicitly derive the equations for the spatially averaged variables, given a specific parameter field. In this way the approaches are considered deterministic. The effective parameters for the upscaled models can, however, also be derived using a stochastic description of the parameter field.
Volume averaging (e.g. Whitaker, 1999)) is applied to a composite of materials separated by sharp interfaces. The flow equation is averaged over a certain averaging volume, while considering the variables in the distinct material phases separately. Here, the volume average has to be considered a moving average, so that the spatial scale is not changed, which is a significant difference to homogenization theory. The upscaled models are strongly influenced by the conditions defined at the interfaces. The averaged problems can usually not be derived in a closed form. Therefore, closure problems have to be formulated and solved. Explicit results for the upscaled models are mostly obtained for periodic media and for the condition that the averaging volume covers a representative elementary volume (REV, see Section 1.4.1). The method does not make many "a priori" assumptions. Because it is not used for the two-phase flow problems considered in the following, this method will not be outlined further.
In **Homogenization theory** (e.g. Hornung, 1997; Sanchez-Palencia and Zaoui, 1987; Bensoussan et al., 1978; Cioranescu and Donato, 1999), contrary to volume averaging, there are some (quite strong) assumptions made about the relation of the scales. This is outlined in detail below. The parameter fields are assumed to have regular structures. They either have to be periodic or stationary in a stochastic sense. Fields with irregular structures, such as binary random fields at the percolation threshold, are not captured by the method. However, this is equivalent to requiring the existence of an REV, which is mostly assumed to hold when flow and transport processes in the subsurface are upscaled. Although homogenization is a method based on strong assumptions, it allows for a good estimation of the relevant processes, and it has a clearly defined regime of validity.

Non-Deterministic Approaches

For a given parameter field, the upscaled parameters can be calculated exactly with the method of volume averaging or homogenization theory. In practice, however, parameter fields are not explicitly known. Instead, heterogeneity is quantified by certain stochastic measures (see Chapter 2), which have to be derived from few and sparse data, often supported by rather point-like small measurement volumes only. Therefore, methods are required which allow to estimate the upscaled parameters without deterministic knowledge of the structure, instead relying on a more general quantification of heterogeneity.
Effective medium theory (e.g. Pozdniakov and Tsang, 2004) has often been used to derive effective conductivity for flow in soil with known background material and inclusions of unknown spatial distribution and unknown material properties. Although not derived rigorously from physical considerations, this theory often works quite well in practice.

The material properties of the inclusions are described by univariate parameter distributions only. The drawback of the method is that spatial correlation of the inclusion structure is not reflected.

Stochastic approaches allow for a more comprehensive description of soil structure (e.g. Gelhar, 1993; Dagan, 1989; Zhang, 2002; Rubin, 1997). Due to the lack of deterministic knowledge on the soil structure, it stands to reason to use stochastic approaches, where spatially heterogeneous parameter fields are represented by correlated random space variables. At each location, the parameter is conceptualized as a stochastic process and a multivariate probability distribution is assumed, fitting the stochastic properties of measured data. Typically, the distributions are assumed to be as simple as possible, e.g., it is assumed to be Gaussian or lognormal. As the parameters are stochastic processes, so are the state variables of the processes. Conclusions on the stochastic properties of the state variables are then drawn from the stochastic properties of the parameters. To derive the upscaled behaviour, models for the spatial mean values of the state variables have to be derived. However, it is mostly assumed that ergodicity is fulfilled, which means that spatial averages and stochastic averages are equivalent. Then, stochastically averaged (ensemble average) models can be employed to replace spatially averaged models. In general, the averages of the variables can not be calculated in a closed form. Usually results are derived using a **perturbation approximation**, where variables are decomposed into their mean values and perturbations, i.e., fluctuations about the mean. In most cases, perturbation expansions are truncated after the first or second order.

Averaged equations are usually obtained by averaging over a volume which is large enough to cover a representative elementary volume. **Coarse graining** is a method to average over arbitrary averaging volumes, which in cludes small ones (Attinger, 2003; McComb, 1996; Hristopulos, 2003; Rubin et al., 1999). Coarse graining is often applied in the context of grid coarsening in numerical models (e.g. Durlofsky (1992) and Durlofsky (1998)). If averaging is performed over small patches, the partly upscaled models can be considered to be the starting point for further upscaling steps over the next length scale. This step can be repeated with increasing patch size. **Renormalization** makes use of such successive steps to derive a relation between scale and averaged properties. Renormalization has also been used to average flow and transport problems in the subsurface (King, 1989; Hristopulos, 2003; Attinger, 2003; Jaekel et al., 1996). Mostly, the results for averages over REVs do not qualitatively differ from results obtained with conventional perturbation theory. Hence, coarse graining and renormalization are not discussed further in this work. However, it should be noted that renormalization has been applied for other problems in order to derive averaged models for irregular fields with long-range correlations.

All methods considered in this work require the media to be regular, meaning that they have a local REV (see Section 1.4.1), i.e., they are periodic or have a finite correlation length. This excludes a whole group of media, which are irregular and have long range correlations. Irregular media pose many open questions for future research. For such types of media, different approaches such as **percolation theory** or renormalization theory are said to be more appropriate to describe the averaged flow or transport behaviour.

While stressing that these types of media and upscaling techniques are relevant indeed, they will not be considered here in order to keep the work focussed. In the following, the methods applied in the next chapters will be explained in more detail.

3.1 Homogenization Theory

Homogenization theory is a method that allows to derive upscaled models for problems in heterogeneous media as their volume averages. Their parameter fields must be known deterministically in order to exactly derive the effective parameters for the upscaled models. Within the framework of homogenization theory, problems in heterogeneous media are described on larger scales by spatially averaging over length scales which is small compared to the total problem but large enough to average out the heterogeneities. The purpose is to derive models with effective parameters which are **intrinsic to the materials** and **independent of the large scale boundary conditions** of the problems. This implies that the parameters of the homogenized problems should not depend on the specific configurations of initial and boundary conditions, and they should also not depend on the fluid properties.
The following sections outline the procedure of homogenization. It should be noted that not all problems are homogenizable. It should also be noted, that in principle, the existence and uniqueness of the solutions upscaled by homogenization would have to be proved.

3.1.1 Basic ideas and assumptions

Periodicity of the parameter fields

In the following, the method of homogenization will be developed for periodic fields. In periodic fields, one periodic unit cell contains the entire range of heterogeneity. When such fields are averaged over their unit cells, they become perfectly homogeneous.
In principle, homogenization theory can be extended to non-periodic cases: The unit cell of a periodic field is, in a stochastic sense, similar to the REV of a stochastic field. Fields without finite integral scale have no REV and hence cannot be conceptualized by periodic fields.

Separation of scales

Periodic fields have two different length scales: the length scale of the periodic domains and the length scales of the unit cells. Assuming that the patterns within the unit cells are not too complex, these are the only lengths scales involved.
The two length scales of the medium must be distinct, i.e., the large length scale (in the following denoted by L) is much larger than the small length scale (in the following denoted by ℓ, cf. Figure 3.1). Their ratio is defined as:

$$\varepsilon = \frac{\ell}{L}, \quad \varepsilon \ll 1. \tag{3.1}$$

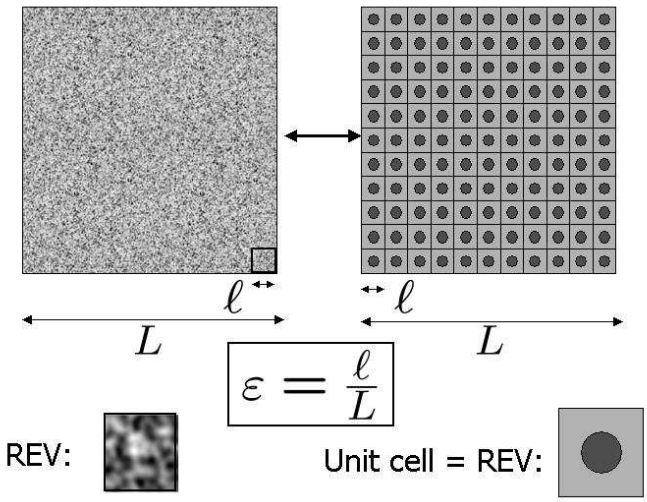

Figure 3.1: Heterogeneous fields with two distinct length scales. Left: Random field, right: periodic field. The unit cell in the random field has to be large enough to cover an REV, therefore the small scale structure appears smaller than in the periodic medium.

With decreasing ε, the heterogeneity becomes less and less "visible" (see Figure 3.2). At the limit of perfect separation of scales with $\varepsilon \to 0$, the medium appears to be homogeneous.

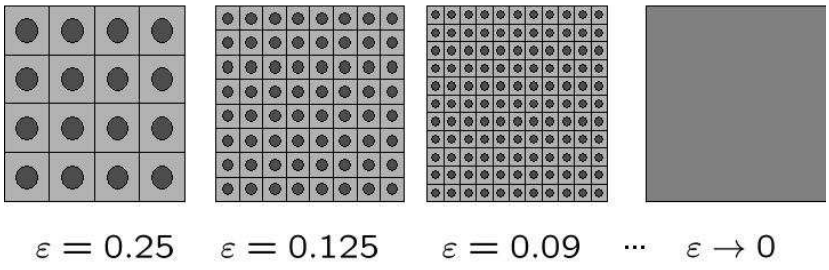

Figure 3.2: Periodic field in the limit $\varepsilon \to 0$, after Hornung (1997)

The separation of scales is a very important assumption made in homogenization theory. The parameter ε will be considered as an expansion parameter in the system. Also, the two length scales will be considered to be independent variables. This is a strong assumption which, in principle, holds only in the limit $\varepsilon \to 0$.

Local periodicity of the state variables

At a later stage, the equations of state will be solved for each order of ε independently, so the separation of scales is required not only for the parameters, but also for the state variables. The state variables (or the solution of the problem) must have fluctuations on the two length scales L and ℓ **only**: Fluctuations on the large length scale due to the boundary conditions applied on the large scale and fluctuations on the small scale due to the heterogeneity of the medium. For reasons of mathematical simplicity, this separation of scales in the state variables is implemented by assuming local periodicity. This assumption is not too far-fetched since the parameter field is also assumed to be periodic. Local periodicity can be compared to local stationarity, which would be the corresponding property in a random medium.
This is sketched in Figure 3.3. Here, the solution has the form of two superposed sine waves. The large wave is due to boundary conditions, while the small scale fluctuations are due to the heterogeneity of the parameter field. The fluctuations on the small scale are not affected by the fluctuations on the large scale: Their frequency is so much larger than that of the large scale fluctuations that the change within one fast fluctuation due to the superposed large scale fluctuation is negligible.

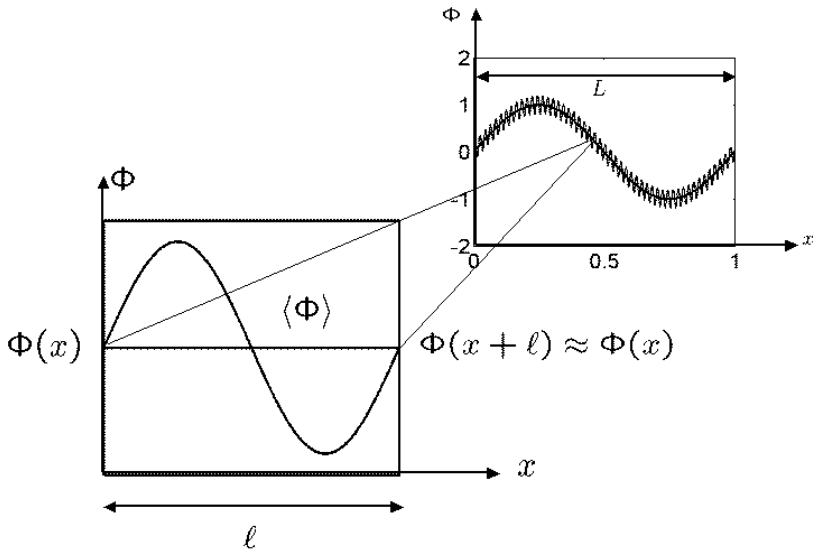

Figure 3.3: Local periodicity of the solution

The assumption of local periodicity for the state variables implies that homogenization theory cannot be applied to problems which generate unstable solutions. For example, a displacement front which is viscous unstable would generate fingers or patterns on all length scales and hence would contradict the assumption of local periodicity or local stationarity.

3.1.2 General procedure to derive the upscaled problem

Choice of time scales

If the problem considered is time dependent, the choice of a typical time scale is a crucial point. Often, a typical time scale which relates to the large length scale is chosen. With this choice, the system is restricted to slow processes. In principle, there could be different time scales in the system, and if it is expected that more than one time scale is important for the process, all of them have to be taken into account.

Scaling of dimensionless numbers and parameter ratios

Homogenization theory can be performed in the most straightforward way if the problem is considered in a dimensionless form, using the dimensionless numbers of the system (as explained in Section 1.4). In the remainder of the section, all variables and parameters are supposed to be dimensionless (except when stated differently).
As the state equations will be expanded in terms of the scale ratio ε, the order i in terms of the parameter ε has to be determined for each dimensionless number Q.

$$\varepsilon^{i+1} \ll Q \ll \varepsilon^{i-1}, \rightarrow Q = O(\varepsilon^i) \tag{3.2}$$

The upscaled problems are valid only for this specific flow regime. By quantifying the dimensionless numbers, the upscaled problems become restricted to certain scenarios. In this way, homogenization is less general than other methods: The homogenized problems can be derived only if the dimensionless numbers can clearly be defined with respect to an order of ε, such that the equation (3.2) holds.
Also, the ratio of parameters has to be set in relation to ε. If the medium consists, e.g., of two materials with conductivity k_1 and k_2, the order i with which the ratio appears has to be determined as

$$\varepsilon^{i+1} \ll k1/k2 \ll \varepsilon^{i-1}, \rightarrow k1/k2 = O(\varepsilon^i). \tag{3.3}$$

Again, the upscaled model is valid only for this specific range of parameter ratios. On the one hand, the determination of these ranges is crucial for the derivation of the upscaled model. On the other hand, the choice of the dimensionless numbers is somewhat arbitrary. For example, the typical pressure in the system can be defined from the soil parameters as a typical capillary pressure, or it can be defined from typical values of the pressure due to boundary conditions. Also, parameters can be functions of the state variables, which makes the dimensionless numbers dependent on state variables and thus the flow regime for which the upscaled model was derived might not be valid for the whole time. Thus, a good reasoning for the dimensionless numbers and parameter contrasts is very important when homogenization theory is applied.

Choice of the base length scale

The space variable can be made dimensionless with either the large length scale L or the small length scale ℓ. The results will not depend on the choice of this base scale. However, a decision has to be made whether the system is considered on the small scale and will be zoomed out in the end to the large scale, or whether the system should be considered on the large scale and the small scale processes are zoomed in. In the following, the second approach is followed.
As outlined before, the two length scales will be treated as independent variables. That means that any space dependency occuring on the large scale will be written in terms of the large length scale, while any space dependency occuring on the small scale will be written in terms of the small length scale. This approach introduces two dimensionless space coordinates treated independently, the first one made dimensionless with the small length scale ℓ and the second one made dimensionless with the large length scale L:

$$\hat{X} = \frac{\vec{x}}{L} \quad \hat{Y} = \frac{\vec{x}}{l} = \frac{1}{\varepsilon}\hat{X} \tag{3.4}$$

As one scale is chosen as the base scale, the other variable has to be scaled accordingly in terms of ε. In differential equations, the space coordinates explicitly appear in the gradients. If the large length scale is chosen as base system, the gradients are made dimensionless with the large length scale L. However, as the variables $\hat{X}$ and $\hat{Y}$ are treated independently, the gradient has to be split into a derivative with respect to $\hat{X}$ and into a derivative with respect to $\hat{Y}$. As the base variable chosen here is $\hat{X}$, the derivative with respect to $\hat{Y}$ has to be scaled to the same base system:

$$L\frac{\partial}{\partial x} \rightarrow \frac{\partial}{\partial \hat{X}} + \frac{1}{\varepsilon}\frac{\partial}{\partial \hat{Y}}. \tag{3.5}$$

in which x is the dimensional space coordinate. Vice versa, if the small scale had been chosen as base scale, the gradient would have to be made dimensionless with the small length scale.

Expansion of the solution in terms of ε

The homogenized solution is based on an expansion with respect to the ratio ε of the two length scales of the system. If e.g. the pressure equation explained in Section 1.4.2 (equation (1.9) for the steady state case)

$$\vec{\nabla} K(\vec{\nabla} P) = 0 \tag{3.6}$$

is considered, P would be expanded as

$$P(\hat{X},\hat{Y}) = P^{(0)}(\hat{X},\hat{Y}) + \varepsilon P^{(1)}(\hat{X},\hat{Y}) + \varepsilon^2 P^{(2)}(\hat{X},\hat{Y}) + \ldots. \tag{3.7}$$

Each order $P^{(i)}$ has to be $\hat{Y}$-periodic (the assumption of local periodicity has to be fulfilled for each order independently). Although this is just a formal expansion, it is based on the

assumption that $P^{(0)}$, $P^{(1)}$, $P^{(2)}$, ... all have a similar magnitude. If $\varepsilon \to 0$, the solution converges to $P^{(0)}$ and all higher order contributions vanish. Clearly, the convergence of all higher orders to zero is an assumption and, in principle, would have to be proved.
If non-linear equations are considered, all functions of the state variables are expanded in Taylor series around the zeroth order of the variables. A function of the pressure $\Psi(P)$, e.g., would read

$$\Psi(P) = \Psi^{(0)} + \varepsilon\Psi^{(1)} + \varepsilon^2\Psi^{(2)} + \dots \tag{3.8}$$

with

$$\begin{aligned} \Psi^{(1)} &= \left.\frac{d\Psi}{dP}\right|_{P=P^{(0)}} P^{(1)} \\ \Psi^{(2)} &= \left.\frac{d\Psi}{dP}\right|_{P=P^{(0)}} P^{(2)} + \frac{1}{2}\left.\frac{d^2\Psi}{dP^2}\right|_{P=P^{(0)}} \left(P^{(1)}\right)^2. \end{aligned} \tag{3.9}$$

Splitting in different orders of ε

The expansion (3.7) and the transformed gradient (3.5) are inserted into the respective state equations. Also, the scaling (3.2) and (3.3) is written explicitly. Now, terms of different orders of ε appear in the equations. When considering a very simple example:

$$\vec{\nabla} \cdot \vec{Q} = 0, \tag{3.10}$$

the expansion and the transformed gradient yield

$$\left(\vec{\nabla}_{\hat{X}} + \frac{1}{\varepsilon}\vec{\nabla}_{\hat{Y}}\right) \cdot \left(\vec{Q}^{(0)} + \varepsilon\vec{Q}^{(1)} + \varepsilon^2\vec{Q}^{(2)} + \dots\right) = 0. \tag{3.11}$$

In this simple example, there are no dimensionless numbers and parameters to be scaled. Due to the separation of scales, it can be assumed that the equation is met for each order of ε **independently**. Thus, the equation can be split into a system of coupled equations, where each equation stands for one order of ε. To this end, the equation is sorted for the different orders of ε. For the simple example above, we get equations of the type

$$\vec{\nabla}_{\hat{Y}} \cdot \vec{Q}^{(i+1)} + \vec{\nabla}_{\hat{X}} \cdot \vec{Q}^{(i)} = 0. \tag{3.12}$$

The boundary conditions for the single equations come from the requirement that each order of the solution is $\hat{Y}$-periodic, or from other explicitly stated conditions (such as e.g. continuity of flux). The equations have to be solved iteratively.

Limit $\varepsilon \to 0$

In principle, the resulting system has an infinite number of equations, which all have to be solved. However, we are only interested in the limiting case that ε is very small, where

only the orders ε^0, ε^{-1}, ε^{-2}, ... appear and all orders ε^1, ε^2, ... disappear. For the simple example above, we only have the equations

$$\begin{aligned} \varepsilon^{-1} &: \vec{\nabla}_y \cdot \vec{Q}^{(0)} = 0 \\ \varepsilon^{0} &: \vec{\nabla}_y \cdot \vec{Q}^{(1)} + \vec{\nabla}_x \cdot \vec{Q}^{(0)} = 0. \end{aligned} \tag{3.13}$$

The limit $\varepsilon \to 0$ is an ideal limit. In reality, any system has a small but finite ε. Therefore, higher orders will contribute. These contributions could explicitely be taken into account by considering higher orders (such as ε^1 or higher).

Upscaled problem

The upscaled problem is describe by the equation of the orders relevant for the large scale. This one equation is averaged over the unit cell. This way, the small-scale fluctuations, which are due to the heterogeneity, are averaged out. As the highest order problem is coupled to the lower order equations, the lower order equations have to be solved explicitly. For the simple example above, the upscaled problem is

$$\int_\Omega \vec{\nabla}_{\hat{Y}} \cdot \vec{Q}^{(1)} d^d\hat{Y} + \vec{\nabla}_{\hat{X}} \cdot \int_\Omega \vec{Q}^{(0)} d^d\hat{Y} = 0, \tag{3.14}$$

where Ω is the unit cell. By applying Gauss' theorem, the first term can be transformed into a surface integral. However, as each order $\vec{Q}^{(i)}$ is supposed to be $\hat{Y}$-periodic, the surface integral vanishes.

$$\int_\Omega \vec{\nabla}_{\hat{Y}} \cdot \vec{Q}^{(1)} d^d\hat{Y} = \int_{D\Omega} \vec{Q}^{(1)} \cdot \vec{n} d^d\hat{Y} = 0 \tag{3.15}$$

Therefore, the remaining upscaled problem simply is

$$\vec{\nabla}_{\hat{X}} \cdot \int_\Omega \vec{Q}^{(0)} d^d\hat{Y} = 0. \tag{3.16}$$

In general, for all terms F which are periodic on the small scale, integrals of the form

$$\int_\Omega \vec{\nabla}_{\hat{Y}} \cdot F d^d\hat{Y} = 0 \tag{3.17}$$

vanish.

3.2 Effective medium theory

In the field of flow and transport in the subsurface, effective medium theory is mainly applied to calculate the effective permeability for single phase flow through composite materials. Contrary to homogenization theory, it is not a method to derive an upscaled model.

In effective medium theory, the effective upscaled permeability of a heterogeneous medium is mostly derived by analyzing the inclusion of heterogeneous material or parts of it into homogeneous material. The exact parameter distribution of the fields is not required or taken into account. Depending on the setup, the univariate probability distribution of materials or the univariate probability distribution of inclusion materials in a connected background material with known permeability are the only information needed.
Conceptually, the problem in the composite material is simplified to problems that can be solved analytically. A solution for the effective properties can then be found in a closed form. This concept, however, is based on strong assumptions and is not derived in a rigorous way. Still, it works quite well in many practical applications. It has often been applied to model the flow porous media (e.g. Pozdniakov and Tsang, 2004) but also to model the flow in fractures and fracture networks (e.g. Jackson et al., 2000; Zimmerman and Bodvarsson, 1996; Zimmerman et al., 1992).

3.2.1 Flow field through a single spherical inclusion

Flow through a single spherical inclusion can be solved analytically. Therefore, the approximations made to calculate effective parameters in effective medium theory are mostly based on this setup, as shown in Figure 3.4 for a 2d problem. Extensions to 3d (or 1d) are straightforward. A spherical inclusion with radius R_0 of different material is placed into the center of a porous material. The permeabilities are K_1 and K_2 in the background material and inside the inclusion, respectively. Within both materials, the permeability is constant.

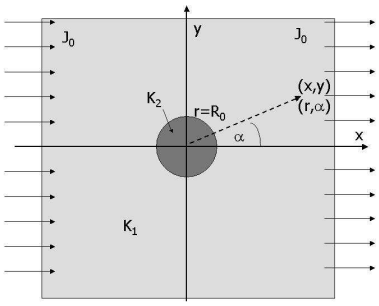

Figure 3.4: Sketch for the flow in a homogeneous medium with a spherical inclusion

The steady state single phase flow equation (1.9) in spherical coordinates is

$$\frac{1}{r}\frac{\partial}{\partial r}\left(rK\frac{\partial P}{\partial r}\right)+\frac{1}{r}\frac{\partial}{\partial \alpha}\left(K\frac{1}{r}\frac{\partial P}{\partial \alpha}\right)=0. \tag{3.18}$$

The flow equation is here used in the pressure formulation. K is thus not the hydraulic conductivity, but the intrinsic permeability K_{int}. In order to keep the notations short, the index int will not be used in the remainder of this chapter, as it is not of importance for the methods explained here.

Far away from the inclusion, a homogeneous flow field is imposed, which is aligned with the x-axis. The medium is large, so that boundary influences can be neglected:

$$\vec{q}_0 = v\vec{e}_x. \tag{3.19}$$

That means, the pressure decreases linearly in x-direction.

$$P_0 = -\frac{1}{K}vx = -\frac{1}{K}vr\cos(\alpha) \tag{3.20}$$

At the interface between inclusion and background, both pressure and fluxes have to be continuous.

$$P_i(\vec{r}|r = R_0) = P_e(\vec{r}|r = R_0), \quad \vec{q}_i(\vec{r}|r = R_0) = \vec{q}_e(\vec{r}|r = R_0). \tag{3.21}$$

and pressure has to be finite at $(x = 0, y = 0)$.
The problem can be solved by separating the variables

$$P(r,\alpha) = P_r(r)P_\alpha(\alpha). \tag{3.22}$$

The α-part of the problem is

$$\begin{aligned} &\frac{\partial^2 P_\alpha}{\partial \alpha^2} = -P_\alpha \\ &\text{General solution:} \quad P_\alpha = A_\alpha\cos(\alpha) + B_\alpha\sin(\alpha). \end{aligned} \tag{3.23}$$

The pressure at the far away boundary is a field linearly increasing in x-direction. This leads to

$$A_\alpha = 1, B_\alpha = 0, \quad P_\alpha = \cos(\alpha). \tag{3.24}$$

The radial part of the problem is

$$\begin{aligned} &\frac{\partial^2 P_r}{\partial r^2} + \frac{1}{r}\frac{\partial P_r}{\partial r} = \frac{1}{r^2}P_r \\ &\text{General solution:} \quad P_r = \left(Ar + B\frac{1}{r}\right) \end{aligned} \tag{3.25}$$

The pressure is split into an inner part of the sphere and an outer part of the sphere:

$$P_{\text{int}} = \cos(\alpha)\left(A_i r + B_i\frac{1}{r}\right), \quad P_{\text{ext}} = \cos(\alpha)\left(A_e r + B_e\frac{1}{r}\right). \tag{3.26}$$

The constants have to be determined from the interface and boundary conditions.

$$\begin{aligned} &A_e = -\frac{v}{K_1}, \quad B_e = \frac{vR_0^2\left(\frac{K_2}{K_1} - 1\right)}{K_1 + K_2} \\ &B_i = 0, \quad A_i = \frac{-2v}{(K_1 + K_2)}. \end{aligned} \tag{3.27}$$

The pressure field has the solution

$$
\begin{aligned}
P_{\text{ext}} &= P_0 \left(1 + \left(\frac{R_0}{r} \right)^2 \frac{K_1 - K_2}{K_1 + K_2} \right) \\
P_{\text{int}} &= P_0 \left(1 + \frac{K_1 - K_2}{K_1 + K_2} \right).
\end{aligned}
\tag{3.28}
$$

3.2.2 Maxwell approach

The concept behind the Maxwell approach is, that the heterogeneous medium is composed of connected background material and inclusion materials (see e.g. Landauer (1952)). A sphere with radius R_0 of this heterogeneous material is embedded in a homogeneous surrounding medium with the same permeability as the connected background material and then compared to an embedded sphere with the same radius composed of homogeneous material with (unknown) effective permeability K_{eff}. In the simplest case, the background material has a permeability K_1 and there are inclusions of one material only with permeability K_2 (see Figure 3.5).

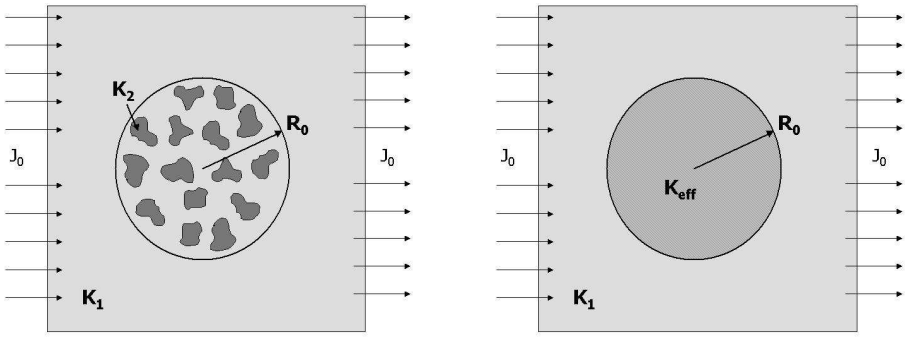

Figure 3.5: Sketch for the Maxwell approach

The effective permeability is derived from the requirement that the perturbations ΔP caused to the pressure and the pressure gradient field outside of the embedded spheres have to be equal for both scenarios.
The effective permeability is obtained by the requirement that the embedded heterogeneous sphere produces the same perturbation ΔP in the external pressure field as the embedded homogeneous sphere with effective permeability K_{eff}.
The perturbation due to the homogeneous effective permeability inclusion is (cf. 3.28)

$$
\Delta P_{\text{hom}} = P_0 \left(\frac{R_0}{r} \right)^2 \frac{K_1 - K_{\text{eff}}}{K_1 + K_{\text{eff}}} \tag{3.29}
$$

The perturbation field due to the inclusions in the heterogeneous material cannot be calculated, but is approximated as the sum of the perturbations due to N identical spheres of

inclusion material, which are all placed in the center of the sphere. The number N of inclusions and their radius r_0 is chosen in the way that the volume percentage of inclusions $\Phi_2 = N r_0^2 / R_0^2$ is met:

$$\Delta P_{\text{het}} = N \frac{r_0^2}{r^2} \frac{K_1 - K_2}{K_1 + K_2} = \Phi_2 \frac{R_0^2}{r^2} \frac{K_1 - K_2}{K_1 + K_2} \tag{3.30}$$

As only the sum of the perturbation of the inclusions is considered, the result does not depend on the chosen size and number of the spheres. In this approximation, the interactions of the inclusions within the pressure field are neglected. Clearly, this is a strong assumption which becomes questionable when the volume percentage of the inclusion becomes large.
Combining these equations yields:

$$\frac{K_1 - K_{\text{eff}}}{K_1 + K_{\text{eff}}} = \Phi_2 \frac{K_1 - K_2}{K_1 + K_2}. \tag{3.31}$$

The result can easily be extended to a composite material of one background material with permeability K_1 and $M-1$ inclusion materials with different permeabilities. The equation for the effective permeability is then:

$$\frac{K_1 - K_{\text{eff}}}{K_1 + K_{\text{eff}}} = \sum_{i=2}^{M} \Phi_i \frac{K_1 - K_i}{K_1 + K_i}. \tag{3.32}$$

The general result for d dimensions and M inclusion materials is:

$$\frac{K_1 - K_{\text{eff}}}{(d-1)K_1 + K_{\text{eff}}} = \sum_{i=1}^{M} \Phi_i \frac{K_1 - K_i}{(d-1)K_1 + K_i}. \tag{3.33}$$

For a continuous range of inclusions the sum is replaced by an integral:

$$\frac{K_1 - K_{\text{eff}}}{(d-1)K_1 + K_{\text{eff}}} = \int \Phi(K) \frac{K_1 - K}{(d-1)K_1 + K} dK. \tag{3.34}$$

In a stochastic framework, the volume percentage of the material $\Phi(K)$ has to be interpreted as a probability distribution. In this case, only the inclusions are supposed to have a distribution, while there is still one distinct background material.
The Maxwell approach yields an explicit scheme to calculate effective permeabilities. Equation (3.33) can be solved directly. The information about the heterogeneous structure of the material taken into account can be summarized as:

- The materials are not treated symmetrically. One material is the background material, while all other materials are treated as inclusions. The background material is connected throughout the whole medium, while all inclusion materials are isolated. Compared to a real porous medium, this picture is seldomly found. In fact, for most materials, the background material has a too strong influence on the effective permeability when using the Maxwell approach.

- All inclusion materials are described by their volume percentage only. No information about the geometry of the heterogeneous structure, such as tortuosity is taken into account. Stochastic information is limited to univariate distributions of the volume percentages or permeabilities, so that no multivariate stochastic information such as correlation is taken into account.

3.2.3 Self - consistent approach

This approach is often also called the Bruggeman Landauer approach (Landauer, 1978). It comceptualizes heterogeneous materials with inclusions in a different manner than the Maxwell approach. The different concepts of the composite structure for the Maxwell approach and the self-consistent approach are sketched in Figure 3.6. In the self-consistent approach, both materials are taken into account symmetrically: depending on the volume percentage, the roles of inclusion material and background material are exchanged in the self-consistent approach, whereas they are maintained for all volume percentages in the Maxwell approach.

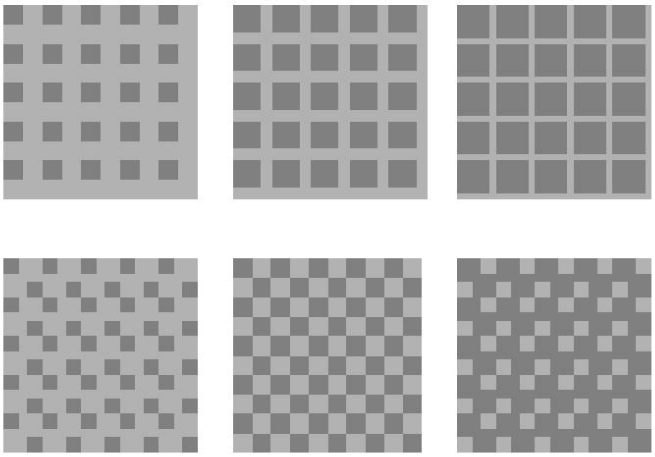

Figure 3.6: Sketch for the different concepts of the composite materials for the Maxwell and the self consistent approach. In the upper row, a composite for the Maxwell approach is shown. In the lower row, a composite for the self-consistent approach is shown. The volume percentage of inclusions in the left column is $\Phi_2 = 0.25$*, in the middle column it is* $\Phi_2 = 0.5$ *and in the last column it is* $\Phi_2 = 0.75$*.*

The self-consistent approach is best illustrated on a two-composite material with permeabilities K_1 and K_2. The medium is made of different patches of both materials. It is compared to a homogeneous medium with effective permeability. Each patch of the heterogeneous material is successively placed into the effective homogeneous material, causing a perturbation in the pressure field (see Figure 3.7). The effective permeability is

obtained by the requirement that the perturbations caused by all the included patches into the effective material have to cancel, leading to an implicit approach.
Like in the Maxwell approach, approximations are necessary in order to calculate the perturbations. The average of the fluctuations of all patches is approximated as the sum of the fluctuations caused by identical spheres, which are shifted to the center of the coordinate system. Again, all interactions between the single inclusions are neglected.

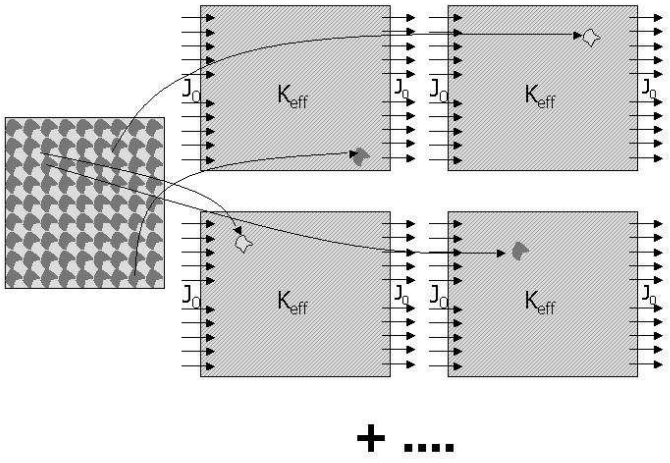

Figure 3.7: Sketch for the self-consistent approach

In the effective homogeneous material, the pressure field is

$$P = P_0. \tag{3.35}$$

The total volume percentage of patches of material one is Φ_1 and that of material two is Φ_2. The averaged perturbation of the external pressure field due to all the patches implanted into the effective homogeneous is

$$\Delta P = \left(\frac{R_0}{r}\right)^2 \left(\Phi_1 \frac{K_{\text{eff}} - K_1}{K_{\text{eff}} + K_1} + \Phi_2 \frac{K_{\text{eff}} - K_2}{K_{\text{eff}} + K_2}\right) \tag{3.36}$$

Since the averaged fluctuations due to all inclusions in the effective homogeneous material have to vanish, one obtains

$$\Phi_1 \frac{K_{\text{eff}} - K_1}{K_{\text{eff}} + K_1} + \Phi_2 \frac{K_{\text{eff}} - K_2}{K_{\text{eff}} + K_2} = 0. \tag{3.37}$$

The general implicit equation for the effective permeability for the d-dimensional problem, where a medium is composed of M phases, is

$$\sum_{n=1}^{M} \Phi_n \frac{K_{\text{eff}} - K_n}{(d-1)K_{\text{eff}} + K_n} = 0. \tag{3.38}$$

In a medium with continuous parameter distribution or in a stochastic framework, the sum over the volume percentages has to be exchanged by an integral over the parameter distribution $\Phi(K)$ or probability distribution respectively.

$$\begin{aligned} \int \frac{K_{\text{eff}} - K}{(d-1)K_{\text{eff}} + K} \Phi(K) dK = 0 \\ \int \left(-1 + \frac{dK_{\text{eff}}}{(d-1)K_{\text{eff}} + K} \right) \Phi(K) dK = 0 \\ K_{\text{eff}} = \left[\int \frac{d}{(d-1)K_{\text{eff}} + K} \Phi(K) dK \right]^{-1}. \end{aligned} \tag{3.39}$$

The effective permeability K_{eff} is thus defined implicitly. The information about the heterogeneous structure of the material taken into account in the self-consistent approach can be summarized as:

- All materials are treated symmetrically. No material is specified as the connected phase.

- Like in the Maxwell approach, the structure of the heterogeneity (such as tortuosity or correlation structure) is not taken into account.

3.2.4 Differential effective medium theory

The differential effective medium theory is based on the same principles as the Maxwell approach. Again, the procedure is explained for a two-composite medium in 2d, but it can be extended to multi-composite materials and higher dimensions.

One material of the composites is assigned to be the background material and is connected everywhere. The other material is treated as inclusion material forming isolated structures. Consequently, like for the Maxwell approach, it has been discussed that the background material is over-emphasized. The differential effective medium theory partly overcomes this problem by incrementally increasing the volume percentage of inclusion material.

Based on the incremental change of volume percentage of inclusion material, the incremental change of effective permeability is derived. The new effective permeability is the starting point for the next incremental step. At each incremental step, the background material is exchanged with the old effective material (see Figure 3.8).

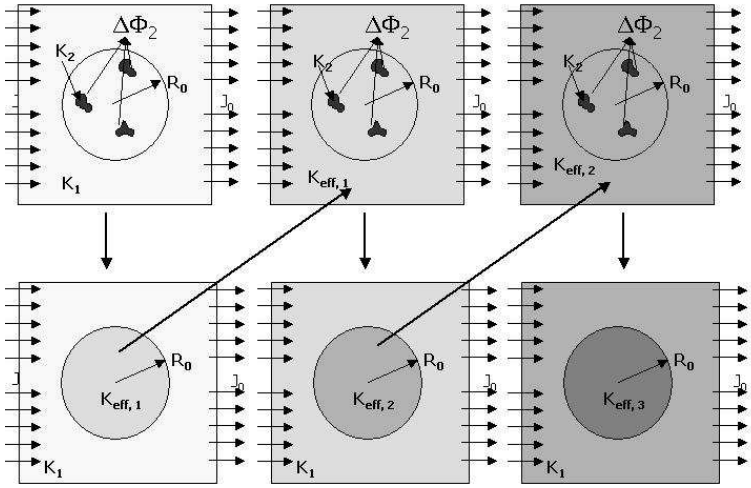

Figure 3.8: Sketch for the differential effective medium theory approach

If the volume percentage of inclusion material in the composite is Φ_2, a percentage of

$$\Delta\Phi_{\text{exch}} = \frac{\Delta\Phi_2}{1-\Phi_2} \tag{3.40}$$

needs to be exchanged in order to obtain a volume percentage of $\Phi_2 + \Delta\Phi_2$ of inclusion material. The effective permeability before the exchange is supposed to be known. The composite with effective properties is treated as the background material. The Maxwell approach method (eq. (3.31)) can be applied to derive the effective permeability after the exchange if it is expanded (eq. (3.31)) to first order in Φ_2.

$$K_{\text{eff}} = K_1 \left(1 - 2\Phi_2 \frac{K_1 - K_2}{K_1 + K_2} + O(\Phi_2^2)\right) \tag{3.41}$$

In the case considered here, the background permeability is the effective permeability before the exchange step, $K_{\text{eff}}(\Phi_2)$. The inclusion material is still K_2 and the effective permeability after the inclusion step is $K_{\text{eff}}(\Phi_2 + \Delta\Phi_2)$. The new volume percentage of inclusions is $\Phi_2 + \Delta\Phi_2$. This yields

$$K_{\text{eff}}(\Phi_2 + \Delta\Phi_2) - K_{\text{eff}}(\Phi_2) = 2K_{\text{eff}}(\Phi_2) \left(\frac{K_2 - K_{\text{eff}}(\Phi_2)}{K_2 + K_{\text{eff}}(\Phi_2)}\right) \frac{\Delta\Phi_2}{1-\Phi_2}. \tag{3.42}$$

If the incremental step is considered infinitesimally small, this yields a differential equation

$$(1-\Phi_2)\frac{dK_{\text{eff}}}{d\Phi_2} = K_{\text{eff}} \left(\frac{K_2 - K_{\text{eff}}(\Phi_2)}{K_2 + K_{\text{eff}}(\Phi_2)}\right). \tag{3.43}$$

A simplistic choice for the initial condition is a zero volume percentage of inclusion material Φ_2 and an effective permeability equal to the permeability of the background material, so that $K_{\text{eff}}(\Phi_2 = 0) = K_1$. Equation (3.43) can be integrated analytically

$$\left(\frac{K_2 - K_{\text{eff}}}{K_2 - K_1}\right)\left(\frac{K_1}{K_{\text{eff}}}\right)^{(1/2)} = 1 - \Phi_2. \tag{3.44}$$

The general result for two composites in d dimension is

$$\left(\frac{K_2 - K_{\text{eff}}}{K_2 - K_1}\right)\left(\frac{K_1}{K_{\text{eff}}}\right)^{(1/d)} = 1 - \Phi_2. \tag{3.45}$$

In the presence of more than one inclusion material, the procedure becomes much more complex. In principle, the incremental change of the permeability depends on the path, on which the final configuration of inclusion materials has been reached. Also, a partly unconnected background can be reproduced by using the background material also as one of the inclusion materials.
When choosing a path where the volume percentages of all inclusions are increased simultaneously at the same rates, the incemental change of effective permeability is:

$$\kappa_{\text{eff}}(\Phi + \Delta\Phi) - \kappa_{\text{eff}}(\Phi) = 2\kappa_{\text{eff}}(\Phi)\left[\sum_{i=2}^{N} \rho_i \frac{\kappa_i - \kappa_{\text{eff}}(\Phi)}{\kappa_i + \kappa_{\text{eff}}(\Phi)}\right]\frac{\Delta\Phi}{1-\Phi}. \tag{3.46}$$

Again, a differential equation for the effective permeability can be derived

$$\frac{d\Phi}{(1-\Phi)} = \frac{1}{2}\frac{d\kappa_{\text{eff}}}{\kappa_{\text{eff}}}\left[\sum_{i=2}^{N} \rho_i \frac{\kappa_i - \kappa_{\text{eff}}(\Phi)}{\kappa_i + \kappa_{\text{eff}}(\Phi)}\right]^{-1}. \tag{3.47}$$

A solution procedure for this problem is shown in Norris et al. (1985). Equation (3.47) is integrated from $\Phi = 0$ (with $\kappa_{\text{eff}}(\Phi = 0) = \kappa_1$) to Φ. This yields an equation, which then has to be solved for κ_{eff}:

$$\frac{F(\kappa_{\text{eff}}, \kappa_1, \ldots, \kappa_N, \rho_2, \ldots, \rho_N)}{F(\kappa_0, \kappa_1, \ldots, \kappa_N, \rho_2, \ldots, \rho_N)} = \frac{1-\Phi}{1}, \tag{3.48}$$

where F is defined as

$$F(\kappa, \kappa_1, \ldots, \kappa_N, p_1, \ldots, p_{N-1}) = \Pi_{i=1}^{N}(\kappa - \tilde{\kappa}_i)^{R_i}. \tag{3.49}$$

$\tilde{\kappa}_i$ are the roots of a function $G(\kappa)$ and R_i are the residues of $1/G(\kappa)$. G is given as

$$G(\kappa) = \sum_{i=1}^{N} \rho_i \frac{2\kappa(\kappa - \kappa_i)}{\kappa + \kappa_i}. \tag{3.50}$$

The information about the heterogeneous structure of the material taken into account in differential effective medium theory can be summarized as:

- Because the Maxwell approach is applied differentially, all materials are again treated symmetrically; no material is specified as the connected phase.
- Again, the structure of the heterogeneity (such as tortuosity or correlation structure) is not taken into account.

3.2.5 Superconductive and unconductive material

One of the drawbacks of the effective medium theory approaches can be illustrated by considering the effective properties in the limit of unconductive or superconductive inclusions. These are important limiting cases that are relevant for media with very high parameter contrasts, such as fractured media.

Maxwell approach

In the Maxwell approach, the case of unconductive inclusions with $K_2/K_1 \to 0$ yields (cf. equation (3.31))

$$K_{\text{eff}} = K_1 \frac{1-\Phi_2}{1+\frac{1}{d-1}\Phi_2}. \tag{3.51}$$

The case of superconductive inclusions with $K_2/K_1 \to \infty$ leads to

$$K_{\text{eff}} = K_1 \frac{1+(d-1)\Phi_2}{1-\Phi_2} \tag{3.52}$$

The corresponding curves are plotted in Figure 3.9.

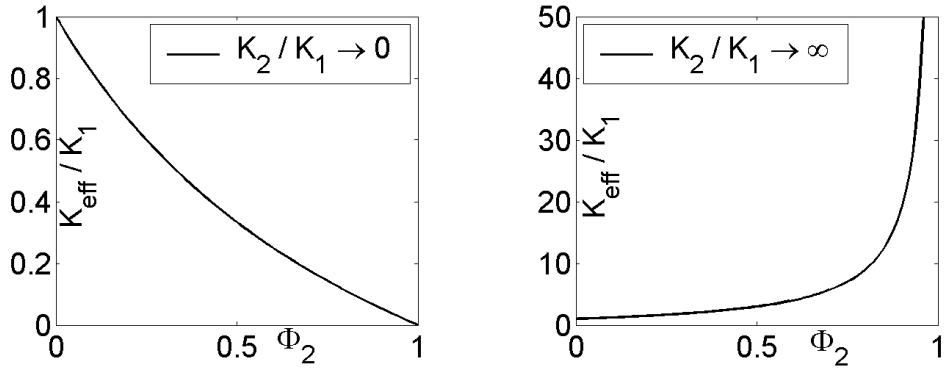

Figure 3.9: 2d effective permeability for undconductive and superconductive inclusions with the Maxwell approach

For unconductive inclusions in the Maxwell aproach, the effective permeability vanishes only when the inclusions fill the whole medium. For most realistic structures, this will happen much earlier: the inclusions will block the medium for flow as soon as there is a connecting path of material 2 through the medium. The same is true for superconductive inclusions. In the Maxwell approach, the effective permeability becomes infinite only when the inclusions occupy the entire volume, whereas most realistic composites will become superconductive as soon as there is a connecting path of the inclusions. This problem occurs here independently of the spatial dimension.

Differential effective medium approach

The same problem occurs for the differential effective medium approach. If the inclusion material becomes unconductive ($K_2 \to 0$) the effective permeability is

$$K_{\text{eff}} = K_1 \left(1 - \Phi_2\right)^{d/(d-1)}. \tag{3.53}$$

The effective permeability vanishes only if the volume percentage of the inclusion material is unity. However, at the point where Φ_2 is close to one, the differential effective medium approach gives better results as the Maxwell approach due to the successive updating of the embedding material surrounding the sphere, and the resulting effective permeability is much smaller.
The same holds for the opposite case, i.e., for superconductive inclusion material with $K_2/K_1 \to \infty$. Here, the percolation threshold is also not reflected in the differential effective medium approach. In this limit, the effective permeability is

$$K_{\text{eff}} = K_1 \frac{1}{\left(1 - \Phi_2\right)^d}. \tag{3.54}$$

However, the excessive emphasis of the background material is again less pronounced than in the Maxwell approach. The corresponding curves are shown and compared to the curves from the Maxwell approach in Figure 3.10.

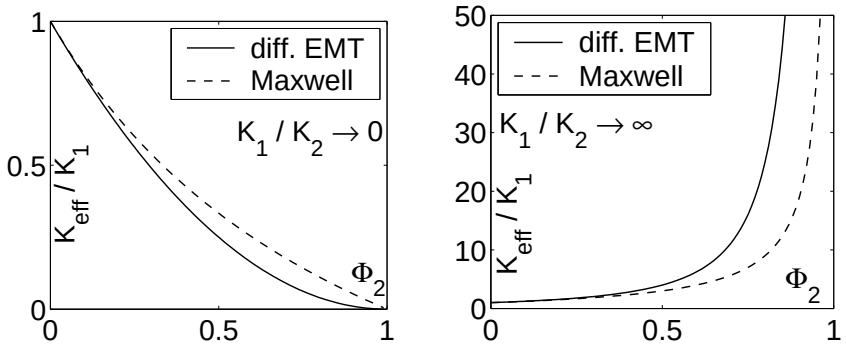

Figure 3.10: 2d effective permeability for undconductive and superconductive inclusions with the Maxwell approach and the differential effective medium theory approach

Self-consistent approach

The behaviour of the percolation threshold is reproduced much better by the self-consistent approach. If one material is much more (or less) conductive than the other, the limiting values are in 2d (cf. equation (3.37))

$$K_{\text{eff}} = K_1 \left(\Phi_1 - \frac{1}{d-1}\Phi_2\right) = K_1 \left(1 - \frac{d}{d-1}\Phi_2\right) \quad \text{for} \quad \frac{K_2}{K_1} \to 0 \tag{3.55}$$

and

$$K_{\text{eff}} = K_1 \frac{1}{\Phi_1 - (d-1)\Phi_2} = K_1 \frac{1}{1 - d\Phi_2} \quad \text{for} \quad \frac{K_2}{K_1} \to \infty. \tag{3.56}$$

The corresponding curves are shown in Figure 3.11.

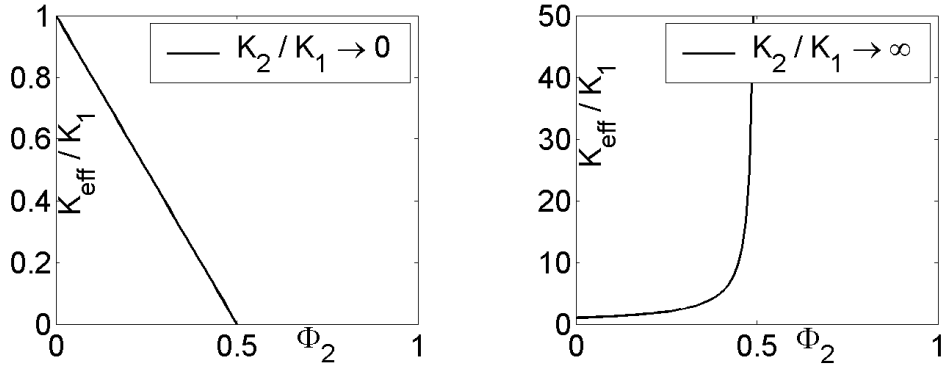

Figure 3.11: 2d effective permeability for undconductive and superconductive inclusions with the self-consistent approach

A finite percolation threshold can be reproduced with this method. However, it is not necessarily a reasonable approximation for the actual value of the threshold. In 2d, a threshold of $\Phi_{2,thr} = 0.5$ is obtained. In reality, the percolation threshold for a two-dimensional medium depends strongly on the microstructure of the medium. In the three-dimensional case, we get thresholds of $\Phi_{2,thr} = 2/3$ for unconductive inclusions and $\Phi_{2,thr} = 1/3$ for superconductive inclusions. Again, these values are not necessarily good estimates for the percolation threshold.

3.3 Perturbation approximations in a stochastic framework

Effective medium theory often is a good method to approximate effective conductivities of heterogeneous materials. However, they do not reflect correlated spatial structures of materials.

Including correlation structures in stochastic models at least requires information about stochastic second moments of the fields. The parameter fields are represented by spatial random variables (i.e., random fields) with a given multivariate stochastic distribution, as discussed in the previous chapter. Usually, only first and second order properties are considered. The stochastic framework has excessively been used to derive upscaled models for flow and transport in the subsurface. The concept is described in a number of books and articles (e.g. Gelhar, 1993; Dagan, 1989; Zhang, 2002; Rubin, 1997). Therefore, it will not be repeated here in detail, but the general concepts will be outlined.

The purpose of stochastic approaches is not only to derive upscaled models for parameter fields, but also to derive stochastic properties of dependent state variables such as their

variances. Measures such as variances are important for error estimates, quantification of uncertainty and risk assessment. Also, they are important to estimate the applicability of upscaled models. The variance of variables provides information about their fluctuations between realizations in an ensemble. Only if these fluctuations become small does the averaged problem represent the problem in single realizations.
In spite of their importance, the derivation of stochastic properties will not be treated here for the sake of conciseness. The detailed derivations can be found in the publications listed above.

3.3.1 Stochastic equations

In a second order stationary field, the averaged parameters are constant in space. As the parameters in the flow- or transport equation are stochastic, so is the variable of the equation. The differential equation becomes a stochastic differential equation. For example, in the flow equation where the permeability K is split into mean and fluctuations ($K(\vec{x}) = \langle K \rangle + \tilde{K}(\vec{x})$)

$$\vec{\nabla} \cdot \left(\langle K \rangle + \tilde{K}(\vec{x}) \right) \vec{\nabla} P = 0, \tag{3.57}$$

the pressure P is a random variable. It can therefore also be split into its mean and fluctuations:

$$P(\vec{x}) = \langle P(\vec{x}) \rangle + \tilde{P}(\vec{x}). \tag{3.58}$$

As stochastic averages and spatial averages are interchangable when ergodicity holds, upscaled variables can be defined by their stochastic average (in this case $\langle P \rangle$). The goal for deriving the upscaled problem is therefore to derive an equation for the stochastically averaged variable.

Upscaling and dilution

It should be stressed that the choice and character of the averaged variable depends very much on the actual questions posed. How to upscale specific quantities for specific problem setups must be considered carefully.
If, for example, the transport of a solute plume is considered at early travel times, spatially averaged solute concentrations, ensemble averages and the distribution in single realizations differ significantly. Ensemble average and volume average differ per definition, because the solute plume has not covered a distance sufficient to install ergodic conditions. Also, the spatially averaged concentration is a smoothed function, while the solute plume in each of the single realizations is distorted but has a sharp transition at the plume outline.
Only if the transport time is very long so that the solute has covered a sufficient distance to be ergodic, the spatial average and the stochastic average become equivalent. Also, only if it has been distributed over different streamlines due to transverse diffusive/dispersive exchange and thus has been mixed, the process is said to be self-averaging, so that the distribution within a single realization is equivalent to the two averaged distributions.

Hence, a spatially or stochastically averaged solute plume, for example, does not provide a good measure for dilution at early travel times. The ensemble average plume is smooth due to the uncertainty in predicition the center of mass of the plumes in each single realization. Interpreting this smoothness as a measure for dilution leads to drastic overpredictions. An adequate measure of dilution is the width of the plume in each single realization, which can then be averaged. These issues are discussed in great detail in the publications of Attinger et al. (1999), Dentz et al. (2000), Rajaram and Gelhar (1993) and Fiori (1998).

3.3.2 Expansion around the averaged solution

For flow problems, the desired upscaled quantity usually is the volume average of the quantity. Furtunately, under ergodic conditions, one can use the stochastic average instead and, therefore, it stands to reason to proceed from an expansion around the stochastic average of the variables. This can be illustrated on the example of single phase flow, where the pressure is expanded as (3.58). If this is inserted into the pressure equation (3.57) and the equation is averaged, one obtains an equation for the averaged pressure

$$\vec{\nabla} \cdot \langle K \rangle \vec{\nabla} \langle P \rangle + \vec{\nabla} \cdot \langle \tilde{K} \vec{\nabla} \tilde{P} \rangle = 0. \tag{3.59}$$

Because the average of the product of the fluctuations is unknown, a **closure problem** for the pressure fluctuations has to be formulated. This can be obtained by subtracting the averaged equation (3.59) from the original one (3.57), yielding an equation for the pressure fluctuations $\tilde{P}$

$$\vec{\nabla} \cdot \tilde{K} \vec{\nabla} \langle P \rangle + \vec{\nabla} \cdot \langle K \rangle \vec{\nabla} \tilde{P} + \vec{\nabla} \cdot \tilde{K} \vec{\nabla} \tilde{P} - \vec{\nabla} \cdot \langle \tilde{K} \vec{\nabla} \tilde{P} \rangle = 0. \tag{3.60}$$

This equation is coupled to the equation for the averaged pressure. It cannot be solved in a closed form, but the solution is approximated to some certain order of the fluctuation $\tilde{K}$, usually the first order. All terms of higher order in the fluctuations are neglected. This approximation does only make sense for small fluctuations, where the variance is much smaller than the square of the mean permeability and the truncated terms are indeed negligible.

3.3.3 Expansion around the homogeneous solution

Instead of expanding variables around their average, such as the expansion of the pressure (3.58) in the single phase flow equation, they can also be expanded around the solution of the respective homogeneous problem in orders of their fluctuations. In the example of single-phase flow, both pressure and permeability would be expanded as

$$\begin{aligned} P &= P^{(0)} + P^{(1)} + P^{(2)} + \dots \\ K &= K^{(0)} + K^{(1)} + K^{(2)} + \dots \end{aligned} \tag{3.61}$$

In some sense, this expansion is similar to that used in homogenization with the variance used as expansion parameter instead of the scale ratio. In the simple case that permeability is distributed Gaussian, its expansion can be truncated after the first order with $K^0 =< K >$ and $K^1 = K'$.

The expansion is inserted into the differential equation, so that terms of different orders in the fluctuations appear. As the terms are proportional to polynomials of different orders in the fluctuations, they are independent, so that each order has to be fulfilled independently. In this way the equation is decoupled into a system of equations for the different orders, coupled in the direction of rising orders, and the zeroth order term is given by the solution of the homogeneous problem. Again using the example of single-phase flow:

$$\begin{aligned}
&\vec{\nabla} \cdot K^{(0)} \vec{\nabla} P^{(0)} = 0 \\
&\vec{\nabla} \cdot K^{(0)} \vec{\nabla} P^{(1)} + \vec{\nabla} \cdot K^{(1)} \vec{\nabla} P^{(0)} = 0 \\
&\vec{\nabla} \cdot K^{(0)} \vec{\nabla} P^{(2)} + \vec{\nabla} \cdot K^{(1)} \vec{\nabla} P^{(1)} + \vec{\nabla} \cdot K^{(2)} \vec{\nabla} P^{(0)} = 0 \\
&\vdots
\end{aligned} \tag{3.62}$$

By averaging all single equations and adding them, an equation for the averaged variable (here the pressure) can be derived.

Expanding non-linear differential equations

The expansion around the homogeneous solution has the advantage that the orders of the variables are solved for directly. This is useful if, e.g., variances or other higher order properties of variables are considered. It also has the advantage that non-linear systems can be treated more easily. To stick to the example of pressure, let's assume that permeability is a function of the pressure like it is the case in the unsaturated zone. Then, permeability can be expressed as the product of the fully saturated permeability and the relative permeability. The latter is a function of the pressure with values between zero and one. In ths case, $K = K(\vec{x}) k_r(P) = (\langle K \rangle + \tilde{K}(\vec{x})) k_r(P)$. The relative permeability can be expanded into a Taylor series around the homogeneous solution of the pressure $P^{(0)}$

$$k_r = k_r(P^{(0)}) + \left.\frac{dk_r}{dP}\right|_{P=P^{(0)}} (P^{(1)} + P^{(2)} + \ldots) + \frac{1}{2} \left.\frac{d^2 k_r}{dP^2}\right|_{P=P^{(0)}} (P^{(1)} + P^{(2)} + \ldots)^2 + \ldots. \tag{3.63}$$

an then sorted for the different orders of the fluctuations

$$k_r = k_r^{(0)} + k_r^{(1)} + k_r^{(2)} + \ldots \tag{3.64}$$

with

$$\begin{aligned} k_r^{(0)} &= k_r(P^{(0)}) \\ k_r^{(1)} &= \left.\frac{dk_r}{dP}\right|_{P=P^{(0)}} P^{(1)} \\ k_r^{(2)} &= \left.\frac{dk_r}{dP}\right|_{P=P^{(0)}} P^{(2)} + \frac{1}{2}\left.\frac{d^2k_r}{dP^2}\right|_{P=P^{(0)}} (P^{(1)})^2 \\ &\vdots \end{aligned} \tag{3.65}$$

Now, the different orders of the flow equation read

$$\begin{aligned} &\vec{\nabla}\cdot K^{(0)} k_r(P^{(0)})\vec{\nabla}P^{(0)} = 0 \\ &\vec{\nabla}\cdot K^{(0)} k_r(P^{(0)})\vec{\nabla}P^{(1)} + \vec{\nabla}\cdot K^{(0)} \left.\frac{dk_r}{dP}\right|_{P=P^{(0)}} P^{(1)}\vec{\nabla}P^{(0)} + \vec{\nabla}\cdot K^{(1)}\vec{\nabla}P^{(0)} = 0 \\ &\vdots \end{aligned} \tag{3.66}$$

The zeroth order equation is again the homogeneous (nonlinear) equation. All higher orders are linear. That allows for solution approaches such as the method of Green's functions. Once the zeroth order equation is solved, the first order could be written as

$$P^{(1)} = -\int G(\vec{x},\vec{x}')\vec{\nabla}_{x'}\cdot K^{(1)}(\vec{x}')\vec{\nabla}_{x'}P^{(0)}(\vec{x}')d^dx'. \tag{3.67}$$

where G is the Green's function which solves

$$\vec{\nabla}\cdot K^{(0)}\left(k_r(P^{(0)})\vec{\nabla}G(\vec{x}) + \left.\frac{dk_r}{dP}\right|_{P=P^{(0)}} G(\vec{x})\vec{\nabla}P^{(0)}\right) = \delta^d(\vec{x}-\vec{x}'). \tag{3.68}$$

3.3.4 Transformation into a Neuman series

In the case of linear problems only, the stochastic differential equations can directly be transformed into an integral equations using the method of Green's functions, without the procedure of formal expansion and sorting according to orders. This will again be demonstrated for the problem of single-phase flow. Equation (3.57) can formally be solved as

$$P(\vec{x}) = P^{\text{hom}}(\vec{x}) + \int G(\vec{x},\vec{x}')\vec{\nabla}_{x'}\cdot\tilde{K}(\vec{x}')\vec{\nabla}_{x'}P(\vec{x}')d^dx'. \tag{3.69}$$

The Green's function solves

$$\vec{\nabla}\cdot\langle K\rangle\vec{\nabla}G(\vec{x}) = \delta^d(\vec{x}-\vec{x}'). \tag{3.70}$$

P^{hom} is the solution of the homogeneous problem. The Green's function for the Laplace equation in different dimension can be found in books, such as e.g. Arfken and Weber (2001).

In this approach, the solution depends on the solution itself. To solve the problem, the solution can be inserted back into the term under the integral, yielding an infinite sum of integrals with increasing order in the fluctuations of the parameter. For pressure:

$$P(\vec{x}) = P^{\text{hom}}(\vec{x}) - \int G(\vec{x},\vec{x}')\vec{\nabla}_{x'} \cdot \tilde{K}(\vec{x}')\vec{\nabla}_{x'} P^{\text{hom}}(\vec{x}')d^d x' + \int\int G(\vec{x},\vec{x}')\vec{\nabla}_{x'} \cdot \tilde{K}(\vec{x}')\vec{\nabla}_{x'} G(\vec{x}',\vec{x}'')\vec{\nabla}_{x''} \cdot \tilde{K}(\vec{x}'')\vec{\nabla}_{x''} P^{\text{hom}}(\vec{x}'')d^d x' d^d x'' + \ldots \tag{3.71}$$

The solution can again be approximated by taking into account terms up to a certain order of the fluctuations only. When only the terms denoted in (3.71) are considered, this would yield a second order approximation for pressure.
To obtain the upscaled problem, one can either insert the approximate solution back into the initial problem and average the equation. One could also have an approach for the shape of the upscaled problem and compare the (undetermined) parameters of the solution of the upscaled problem to the effective parameters, which come out of the averaged solution. If the effective parameters have the same form in terms of time- and space dependency, this can be considered a confirmation of the form of the upscaled problem. To illustrate this, the flux in a homogeneous medium with a uniform pressure gradient can be written as

$$\vec{q} = -K\vec{\nabla}P, \tag{3.72}$$

with K being a constant in an isotropic medium. If the (approximate) averaged flux has the shape

$$\langle\vec{q}\rangle = -\mathbf{K}_{\text{eff}}\vec{\nabla}\langle P\rangle, \tag{3.73}$$

this confirms that the upscaled problem has the same shape as the problem in a homogeneous medium with the effective permeability $\mathbf{K}_{\text{eff}}$.

3.4 Summary

Some upscaling methods for flow and transport problems in the subsurface have been outlined in this chapter. These methods will be applied to several example problems in the following chapters, in order to study the influence of the soil structure on the upscaled models.
Homogenization theory is a quite rigorous method to derive an upscaled model. It is, however, based on fairly strong assumptions. First, the medium has to have a clear separation of scales, which also has to hold for the solution of the problem. Second, the upscaled problem is valid for a very specific range of parameter contrasts only, and for a specific range of the dimensionless numbers of the problem. Third, it is usually assumed that the processes happen very slowly, so that the problem on the small scale can be considered to be in steady state. For a given parameter field, homogenization theory directly provides the effective parameters for the upscaled model.
Parameter fields for soil are mostly not known explicitly. Therefore, methods to derive effective parameters based on a general quantification of heterogeneity are considered.

Effective medium theory is a simple and often useful method to derive effective parameters for flow problems. The methods are not derived rigorously, but often work quite well in practice. They are derived for composite materials. In some methods, a background-inclusion structure is assumed, while other methods (also stochastic methods) are mostly set up for media where the materials are treated symmetrically.
Heterogeneity of soil can also be described using stochastic approaches. Here, upscaled models and effective parameters are mostly derived using perturbation theory up to a certain order in the fluctuations of the parameters. This implies, that the fluctuations have to be small. Otherwise the perturbation approximation is not reasonable. In most cases, results are derived to second order of the fluctuations of the parameters. The heterogeneity of the field is thus captured by its second order properties, which are the mean, the variance and an autocovariance model.
In Chapter 5 to 7 upscaled flow problems will be derived with homogenization theory. Effective parameters are calculated from different stochastic averages. For non-Gaussian fields effective medium theory is applied to calculate effective parameters.

Chapter 4

Stability and upscaling

The upscaling methods described in Chapter 3 can be applied to analyze the influence of soil structure on flow and transport processes in the subsurface. The influence of the structure is captured in the effective models and parameters. However, there are processes, which generate a spatially fluctuating fluid distribution that is not related to the structure of the soil. This effect relates to unstable processes. Several mechanisms can cause e.g. unstable flow in displacement problems of one fluid by another immiscible fluid. If an perturbation is introduced into a homogeneous system, such as a perturbation of the fluid-fluid interface or an irregularity of the fluid properties, the perturbation of the fluid distribution can become self-enforcing and grow with time in a way that the growth is not related to the structure of the porous material. In order to predict averaged properties it is then less important to characterize the soil structure, but rather to understand of the stability criteria and their relation to the characteristics of the flow pattern. In immiscible displacement processes irregular flow patterns can be due to viscous or gravity instabilities or to entry pressure effects, which result in channelling along preferential flow paths. These different mechanisms lead to different characteristics of the flow patterns. They will therefore be discussed separately below. Viscous instabilities will be addressed in Section 4.1. This topic will be discussed again in Chapter 7. Channeling due to capillary entry pressure effects will be addressed in Section 4.2. The possibilities of upscaling of unstable flow problems is then discussed in Section 4.3.

4.1 Viscous and gravity instability

Viscous and gravity fingering can occur when viscous or gravity forces drive the flow and capillary forces are weak in comparison. The comparison of the forces is quantified by dimensionless numbers. On the pore scale this is here the Bond number and the Capillary number (1.14) and (1.15). On the Darcy and field scale the equivalent dimensionless numbers (1.22) and (1.24) are used. For a detailed discussion of the topic see Homsy (1987) or Kueper and Frind (1988). The principle of viscous instability can best be explained by the horizontal displacement of one fluid by another one with equal density in a Hele Shaw cell. A Hele Shaw cell is made of two parallel glass plates at a narrow distance compared

to the length scale of the plates. The cell is initially filled with one fluid, which is then displaced by another, immiscible fluid. If the flow is slow and the gap between the two fluids is narrow compared to the extension of the sheets, the average flow velocity in the gap for a single fluid can be described by a Darcy type of equation (Homsy, 1987)

$$\vec{v} = -\frac{b^2}{12\mu}\vec{\nabla}P. \tag{4.1}$$

b [L] is the length of the gap between the glass sheets an P, v and μ are the pressure, the flow velocity and the fluid viscosity as defined in Chapter 1, (1.1). The capillary forces at the interface are here neglected, so that the pressure is independent of the fluid type. The viscosity is an averaged viscosity for both fluids, which is discussed below. The interface between the fluids is planar and moves with a constant velocity. If the interface is disturbed, the interface at two vertical positions will be at different horizontal locations, as sketched in Figure 4.1. If the pressure is approximated as linearly increasing everywhere in the cell, the total permeability over a horizontal section at a certain vertical position y is

$$K(y) = \frac{b^2}{12}\left(\frac{X(y)}{L\mu_1} + \frac{L - X(y)}{L\mu_2}\right), \tag{4.2}$$

where L is the length of the Hele Shaw cell and X is the position of the front. The displacing fluid is labelled with 1, while the displaced fluid is labelled with 2. The ratio of the viscosities between the fluids is denoted as M [-], $M = \mu_1/\mu_2$.

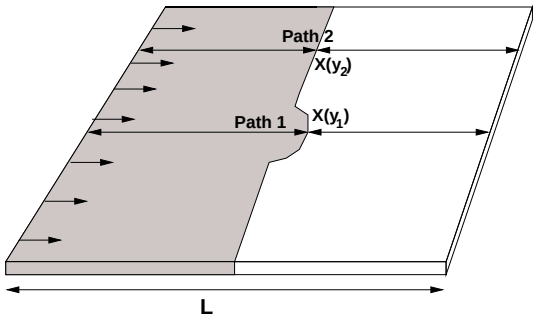

Figure 4.1: Sketch of a perturbation of the fluid interface in a Hele Shaw cell

If the displacing fluid has a lower viscosity than the displaced fluid ($M < 1$), the averaged permeability over a section perpendicular to the fluid interface will be higher, if the location of the front is ahead, than if it is behind the mean front position. That means, the velocity on the section where the front is ahead the mean front position is larger than at a location where the front is behind it. The perturbation of the front is increased. An example of an unstable front in a radial displacement in a Hele Shaw cell is shown in Figure 4.2. The front becomes unstable and forms fingering patterns. If the displacing fluid has a higher viscosity than the displaced fluid ($M > 1$), the opposite is true and the velocity on a section where the front is ahead of the mean front position is lower than on a section where the front is behind it (see Figure 4.1). The perturbation is damped out and the front is stabilizing.

This explanation is of course simplified, especially as the pressure field was here assumed to be undisturbed by the perturbation. A better understanding of the development of the solution can be obtained by a stability analysis of the flow problem, such as performed by Saffman and Taylor (1958), Paterson (1981) or Saffman (1986). The growth of the irregularities of the front is studied there by analysing the time behaviour of a periodic disturbance of the fluid - fluid interface. To solve the problem a linearization of the time dependence has to be introduced. The growth rate of the fingers depends on their width, so that for certain parameters there is a finger width which grows fastest and dominates the pattern. In the process of growing, the fingers split, and may shield the growth of other fingers in parts of the medium. If the capillary number is small (meaning capillary forces are strong, cf. eq. (1.14)) the front is stabilized, as capillary forces try to minimize the interface between the two fluids.

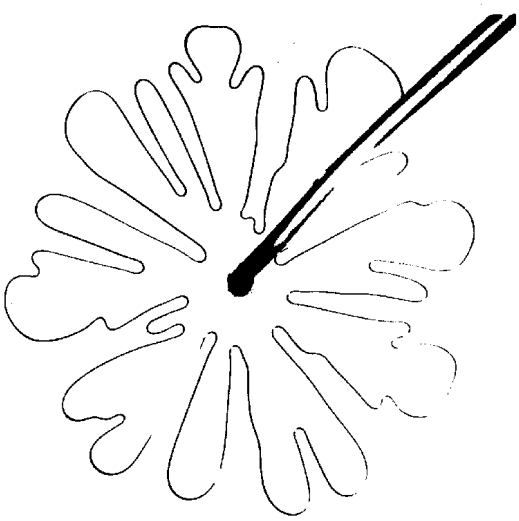

Figure 4.2: Viscous fingering for radial flow in a Hele Shaw cell. From Paterson (1981).

The mechanisms of viscous fingering in a Hele Shaw cell can be transferred to flow in a porous medium (see Figure 4.3). Stability analysis of the homogeneous solution has also be performed for that case (e.g. Yortsos, 1987, 1990; Chikhliwala et al., 1988; Yortsos and Huang, 1986). The solution of the fluid saturation is analyzed and regimes where the solution becomes unstable and grows in fingers can be determined.
Gravity instability can be sketched with the example of a closed vertical Hele Shaw cell, which is filled with two layers of fluids, the heavier one being on top of the lighter one. If the interface between the two fluids is undisturbed, there is hydrostatic pressure in both fluids

$$P(z) = -\begin{cases} \rho_1 g z & \text{if} \quad z < \text{interface} \\ \rho_2 g z & \text{if} \quad z > \text{interface} \end{cases} . \tag{4.3}$$

Once the interface is disturbed, there is a higher pressure at one horizontal direction where the interface is disturbed downwards than at a location where it is disturbed upwards. This

drives fluid towards that location and enforces a finger to grow. To compensate, lighter fluid is driven upwards. If the denser fluid is underneath the lighter fluid, the configuration is stable.

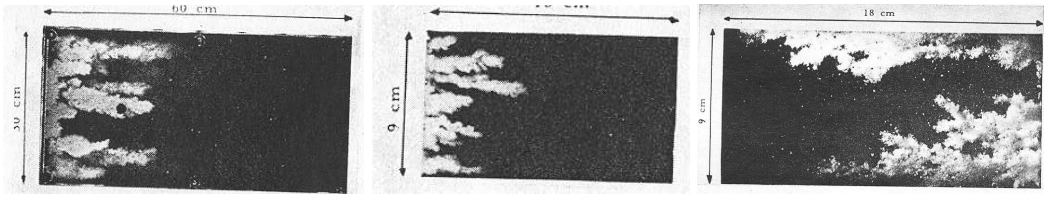

Figure 4.3: Viscous fingering in a porous medium for displacement of oil by water. From Chouke et al. (1959).

The influence of heterogeneous structure of the porous medium on viscous unstable flow behaviour is an yet unresolved problem. However a qualitative argumentation can be made. If

- the variance of the soil parameters is small and
- the field has a finite correlation length (meaning no connected pathways through the field) and
- the correlation length is small compared to the characteristic fingerwidth,

the flow is not influenced by the heterogeneous structure and fingers develop similar to the fingers in the corresponding homogeneous medium. If the variance of the field is high and the field has large scale structures, the tansition zone between high and low saturation of the displacing fluid will be driven by the structure of the soil. As a consequence no viscous fingering will occur. If the flow is viscously (or gravitionally) unstable, and the characteristic finger width as well as the characteristic finger velocity is known, the averaged behaviour can in principle be predicted. A saturation isoline taken in the transition zone between high and low saturation of the displacing fluid has a roughness, the roughness being due to the fingers. The roughness grows with the finger growth velocity. If the solution of the saturation distribution is averaged, the roughness will appear as a spread transition zone between the displacing and displaced fluid. The characteristic length of the transition zone increases with the finger growth velocity. The growth of a viscous unstable front and the averaged saturation are shown for an example case in Figure 4.4.
As the characteristic length of the interface grows with time, the interface behaves superdiffusive. A model which reproduces the averaged fluid distribution with the transition zone between the fluids can be considered an upscaled model, although the scale of soil heterogeneity is not involved. Such a model has been introduced by Blunt et al. (1994). It should however be mentioned, that the finger growth in time is also unclear. The behaviour of a Hele Shaw cell is well understood and has been investigated experimentally (e.g. Saffman and Taylor, 1958; Saffman, 1986; Paterson, 1981; Park et al., 1984). For

flow in porous media this is not the case. Stability analyses have been performed by linearizing the problem and there are only few experimental investigations of the topic (Chouke et al., 1959).

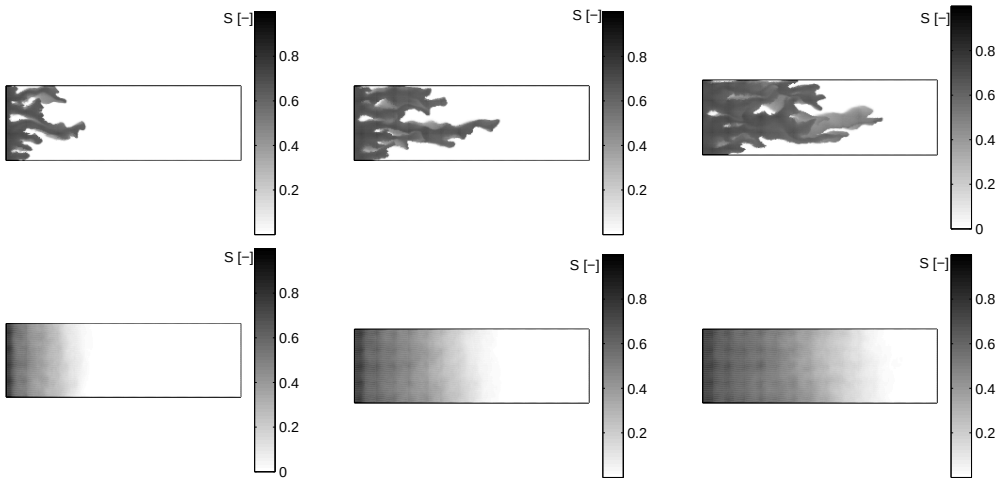

Figure 4.4: Viscous unstable displacement in a heterogeneous medium (top) and averaged saturation distribution (bottom)

4.2 Channelling in capillary driven flow

A different kind of irregular growth of the transition zone between displacing and displaced fluid occurs in the case of capillary dominated flow, if the displacement process is a drainage (see Chapter 1 and cf. Shaw (1986)) and the entry pressure distribution of the porous material is spatially heterogeneous. The irregularity of the transition zone is also not determined by the structure of the heterogeneous field, or rather is related to the structure only if there are channelling paths in the soil structure. This flow will in the following be called **capillary channeling**.
Although the mechanisms which lead to capillary channeling are known, the phenomenon is not well quantified. The slow drainage in an open fracture will therefore here be used as a simplified, qualitative analogy for the drainage in a porous medium. This problem is well understood and has been investigated theoretically and experimentally.
The outline to explain capillary channeling is here the following. The analogy between slow drainage in an open rough-walled fracture and drainage in a heterogeneous porous medium is explained in Section 4.2.1. An important effect which leads to irregular flow patterns is the trapping of wetting fluid by surrounding non-wetting fluid. To justify the analogy between fracture and porous medium, it is shown in Section 4.2.1 with a laboratory experiment that trapping effects occur not only in an open fracture, but also in heterogeneous porous media. In Section 4.2.2 a model is introduced to model drainage in an open rough walled fracture. In Section 4.2.3 the influence of structure of the aperture field of the fracture on the structure of the fluid distribution during the drainage process is analyzed. The fluid distribution was generated with the model introduced in Section

4.2.2. In Section 4.2.4 a laboratory experiment is described, where the fluid distribution during drainage in an open rough walled fracture was measured. The results support the results of Section 4.2.3.

4.2.1 Displacement in an open fracture as model for capillary dominated flow in porous media

The driving mechanism of this type of irregularity is also best explained by a simplified model of the process, e.g. a two-dimensional displacement in a horizontal rough walled fracture. Such a fracture can be described as a Hele-Shaw cell with rough surfaces of the glass plates (see Figure 4.5).

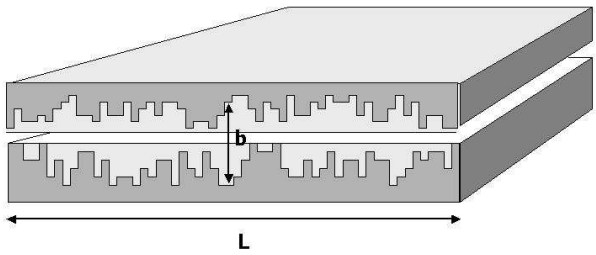

Figure 4.5: Open rough walled fracture

The entry pressure of one cell is obtained from the inverse aperture according to the Laplace-Young equation

$$P_{\text{entr}} = \sigma \cos(\Theta) \left(\frac{1}{R_1} + \frac{1}{R_2} \right), \tag{4.4}$$

where σ [N / m] denotes the surface tension and Θ [-] is the contact angle. R_1 [L] is the interface radius of curvature perpendicular to the fracture plane and R_2 [L] is the interface radius of curvature in the fracture plane (see Figure 4.6).
The radius of curvature perpendicular to the plane, R_1, can be identified to half of the aperture of the fracture b [L]. The mean aperture of this fracture is small compared to the horizontal length scale L [L] of the aperture field. Thus the capillary forces due to the in-plane radius of curvature of the interface R_2 can be neglected. The capillary entry pressure of one aperture b can then be approximated as

$$P_{\text{entry}}(b) = \frac{2\sigma \cos \Theta}{b}, \tag{4.5}$$

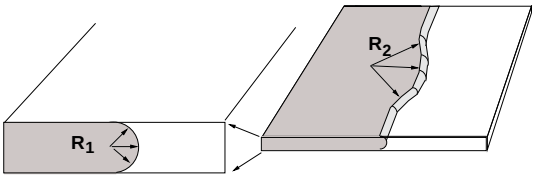

Figure 4.6: In - plane radius of curvature R_2 and radius of curvature perpendicular to the plane R_1

The two incompressible fluids have a sharp interface that moves through the medium as one fluid displaces the other one. The displacement process starts with a straight interface between the fluids. The pressure in the displacing fluid builds up until it exceeds the lowest entry pressure of the apertures connected to the interface. According to equation (4.5) this process takes place at the location with the highest aperture. After this cell has been incaded, all cells with high apertures connected to the invaded location, are invaded by the displacing fluid. At the same time the pressure in the fluid is decreased. As the flow is extremely slow the pressure can be considered to be constant in each fluid phase. The interface between the fluids is changed and the procedure is repeated until the displacing fluid reaches the outlet.
Due to trapping of the displaced fluid the interface between the two fluids has a specific structure. Once the interface between displacing and displaced fluid builds a closed ring with the displacing fluid at the outside, the displaced fluid which is inside of the ring cannot move. Although the entry pressure inside of the ring might be small enough to be overcome by the displacing fluid, it will not be invaded as the displaced fluid is trapped. The resulting patterns are then highly irregular.
Flow in an open rough walled fracture is a simplified picture for a flow process in a porous medium. Even for flow in an open fracture this picture is not correct. If the displaced fluid is the wetting phase it may span a film in-between the fracture surface and the displacing fluid when a location is invaded by non-wetting fluid. It is thus always connected and not really trapped. The trapping rather relates to a given scale. The flow through thin films is extremely slow and has an influence on the whole flow process only on a large time scale. Nevertheless, the underlying principle of the model can be compared to the displacement of a wetting fluid by a non-wetting fluid in a heterogeneous porous medium. The flow process needs to be capillary dominated (quantified by a small capillary number as defined in Hilfer and Øren (1996)). Also, the spatial entry pressure distribution has to have a high variance and the heterogeneous medium should be composed of different materials which have P_c-S distribution with a small slope. The kind of porous media which fulfills these requirements is a medium composed of diffeent composites. Inside of one composite the properties have to be homogeneous. The capillary pressure - saturation relation of one composite has to have a clear entry pressure, that differs clearly for the different composites ($P_{\text{entry},1}/P_{\text{entry},2} \ll 1$ where 1 is the index of the medium with the lower entry pressure), and a flat slope at saturations $S < 1$ (see Figure 4.7). In this way the saturation of the displacing fluid remains zero until the entry pressure is reached and increases then quickly with increasing pressure.

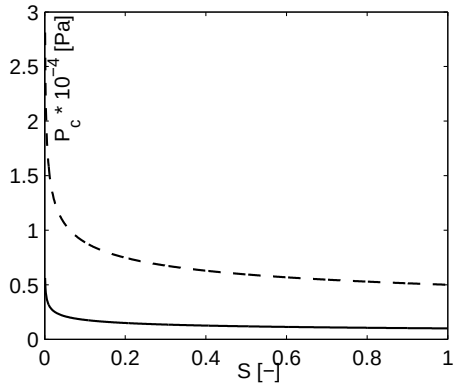

Figure 4.7: Example of two discinct P_c-S curves for two materials

For slow processes, the pressure in the displacing and the displaced fluid can be considered to be in equilibrium. This implies that the parts of the material with low entry pressure will have a higher water saturation than the parts of material with high entry pressure. As in a porous medium described on the Darcy scale both fluids are present in one block of material, both fluids are always connected. As outlined above, this is also true for the wetting phase in a fracture which is connected via films. But as the flow through the film is slow, it can be neglected on intermediate time scales. The same mechanism can occur in a porous medium described on the Darcy scale. The analogy between capillary driven displacement in an open rough walled fracture and in a porous medium is sketched in Figure 4.8.

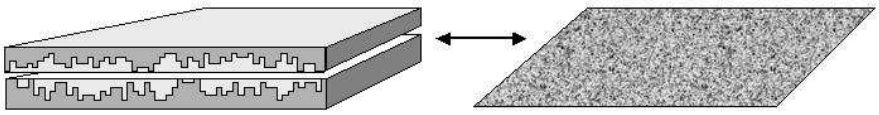

Figure 4.8: Open rough walled gracture as an analogy for a porous medium. The lengths are given in [m].

The phenomenon of trapping is here best explained by considering one cell of a certain material, which is surrounded by a different material. If a cell of material with higher entry pressure is surrounded by material with lower entry pressure, the non-wetting fluid will invade the material with the low entry pressure first up to a given (low) saturation of wetting phase.
Although the wetting fluid is still present at a given saturation in the surrounding material with lower entry pressure, the saturation there is according to the assumptions low.
The relative permeability for the wetting fluid becomes small. Although the entry pressure might at some stage be exceeded, non-wetting phase will not invade at intermediate times,

as the wetting fluid can only be displaced slowly due to its low relative permeability in the surrounding material.

Experimental evidence for trapping in heterogeneous media

The trapping of wetting fluid during the displacement of wetting fluid by non-wetting fluid (here: air) in a heterogeneous structure was analyzed in a laboratory experiment at the Paul Scherrer Institute in Villingen, Switzerland. A column of 0.05 x 0.05 m^2 area and a height of 0.12 m was filled with cubes of 0.01 x 0.01 x 0.01 m^3. The column was filled with heavy water (wetting phase) and drained with air (non-wetting phase). The cubes were made up of either a fine or a coarse sand. The parameters of the sands are given in Table 3.1. For the unsaturated parameter functions a Mualem - van Genuchten parametrization (van Genuchten, 1980) was used. The paramters are partly taken as the parameters from Ursino and Gimmi (2004). Heavy water has a density of $\rho_{D_2O} = 1.1 \cdot 10^3 kg/m^3$ and a viscosity of $\mu_{D_2O} = 1.01 \cdot 10^{-3} Nm/s$.

	$K_s[m/s]$	$n_f[-]$	$\alpha[1/m]$	$n[-]$
Coarse material	$1.3 \cdot 10^{-4}$	0.43	7.6	9.2
Fine material	$3.0 \cdot 10^{-5}$	0.43	4.7	6.6

	$\Theta_r[-]$	$\Theta_s[-]$	Grain size $[10^{-3}m]$
Coarse material	0.02	0.42	0.08-0.2
Fine material	0.0	0.42	0.1- 0.5

The parameter are chosen accordingly to Ursino and Gimmi (2004) as van Genuchten parameters (see 1.30). The parameter α can be considered to be proportional to the inverse entry pressure.
The column was packed with two inclusions of 3 x 3 x 3 subcubes of fine material surrounded by coarse material (see Figure 4.9).
At the bottom and at the top of the cube a layer of 5 x 5 cubes of coarse material was installed. At the bottom of the column a porous ceramic plate with a membrane on top prevented air from entering the porous plate. The saturated permeability of the combination of porous plate and membrane was measured as $K_s = 6.7\,10^{-7} m/s$. The bottom was connected to a water outlet tube, which was connected to a reservoir of water at a fixed height. The water reservoir was placed on a table with an externally adjustable height (see Figure 4.9). The corresponding boundary conditions are thus no-flow boundaries at the side boundaries and at the top boundary and a Dirichlet boundary at the bottom boundary. At the beginning of the experiment the column was water saturated, so that the initial condition is $S = 1$. It was then slowly drained by decreasing the water level of the reservoir.
The three-dimensional water distribution during the drainage process was monitored with neutron tomography in the facilities of the Paul Scherrer Institute (PSI) in Villingen, Switzerland. The facility is described in detail in Lehmann et al. (2001). The experimental setup was placed in the chamber of the neutron beam at the spallation source

of the PSI. The column was placed in-between the beam and a scintillator screen which measured the beam intensity. The column was placed on a rotating table, it could thus be rotated over 180 degrees. By measuring the two-dimensional neutron intensity of the beam at the scintillator plate at 180 different equidistant angles over 180 degrees of the column position, the three-dimensional neutron intensity in the column could be reconstructed (Lehmann et al., 2001). From the intensity the attenuation Σ [1 / L] of the beam in one measured voxel can be derived. The beam intensity decreases exponentially while the beam penetrates the material

$$I \propto \exp(-\Sigma L) + N \tag{4.6}$$

where I is the beam intensity and L is the length that has been passed. The attenuation coefficient measures the attenuation per voxel volume times the cross-section of the voxel. L is the voxel length for the attenuation in one voxel. A tomography consists of a three-dimensional field of the attenuation coefficients with, in our case, a xresolution of 410 x 410 x 751 voxels.

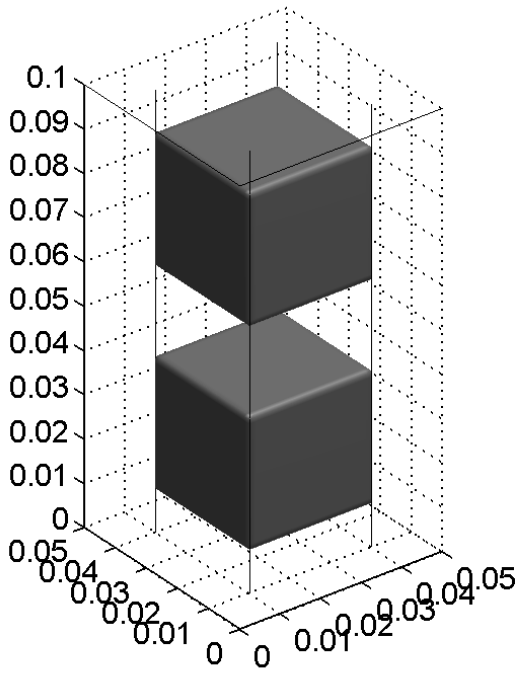

Figure 4.9: Structure of the column

Due to the scattering of neutrons and noise there is an additional term N which contributes to the beam intensity. This term needs to be subtracted in order to derive the material dependent attenuation. The scattering term N was here calculated by Monte Carlo simulations of the measurement setup by Hassanein et al. (2005).
The attenuation coefficient Σ can be written as the sum of attenuation coefficients of the different materials. In the materials used here the attenuation is due to the aluminium of

the column walls, the sand and the water in the column. The attenuation due to the air can be neglected in comparison to the attenuation due to the other materials. At a given averaged water saturation S in the whole column the attenuation in one voxel Σ_S is

$$\Sigma_S = \Sigma_{\text{aluminium}} + \Sigma_{\text{sand}} + \Sigma_{D_2O}. \tag{4.7}$$

At the beginning a tomography of the dry column is made. The attenuation in the dry material is

$$\Sigma_{\text{dry}} = \Sigma_{\text{aluminium}} + \Sigma_{\text{sand}} \tag{4.8}$$

Assuming that the column has not been shifted intbetween the tomogrophies of the wet and the dry column, the attenuation due to water in one voxel is

$$\Sigma_{D_2O} = \Sigma_S - \Sigma_{\text{dry}}. \tag{4.9}$$

The attenuation coefficient for pure heavy water is $\alpha_{D_2O} = 49.3m^{-1}$ (Hassanein et al., 2005). The water content at the location of a given voxel is therefore

$$\Theta = \frac{\Sigma_{D_2O}}{\alpha_{D_2O}}. \tag{4.10}$$

A voxel is much smaller than a reasonable REV. Moreover, it is not possible to place the dry and the saturated columns at exactly the same position during one tomography. As a consequence the pictures for the three-dimensional water saturation distribution need to be filtered.

The drainage experiment was performed in order to investigate trapping. The column was initially saturated with heavy water, after it had been flushed with several pore volumes of CO_2. As the CO_2 dissolves in the water, a high initial water saturation ($S_{\text{initial}} = 0.97$) in the column was obtained. The water table at the bottom of the column was adjusted at $0.13\,m$ below the bottom level. At equilibrium hydrostatic pressure distribution prevails in the column, thus the pressure head at the top equals $h = -0.25\,m$ (setting atmospheric pressure to zero). The entry pressure of the materials is not yet exceeded and no outflow of water occurs. The water level at the bottom was then slowly decreased with a constant speed of $4.17 \cdot 10^{-5} m/s$ via the remote control of the turning table. The setup of the experiment is shown in Figure 4.10.

The turning table was stopped at a height of $0.32\,m$ below the bottom level of the column. Only the entry pressure of the coarse material is at that point exceeded everywhere in the column. The height of the water table of the outflow reservoir was then lowered in one step to $0.45\,m$ below the bottom level of the column. At this bottom pressure head the entry pressure of the fine material was exceeded everywhere.

The pressure was held for 30 minutes. During this time no outflow of water occured. The water in the fine material was trapped, as it was surrounded by coarse material which was almost completely drained. This can be observed in the saturation distribution of a cross-section through the column in the middle of the column at different times and levels of the water level of the outflow reservoir (Figure 4.11). The coarse material has been drained, while the inclusion cells do not change in saturation.

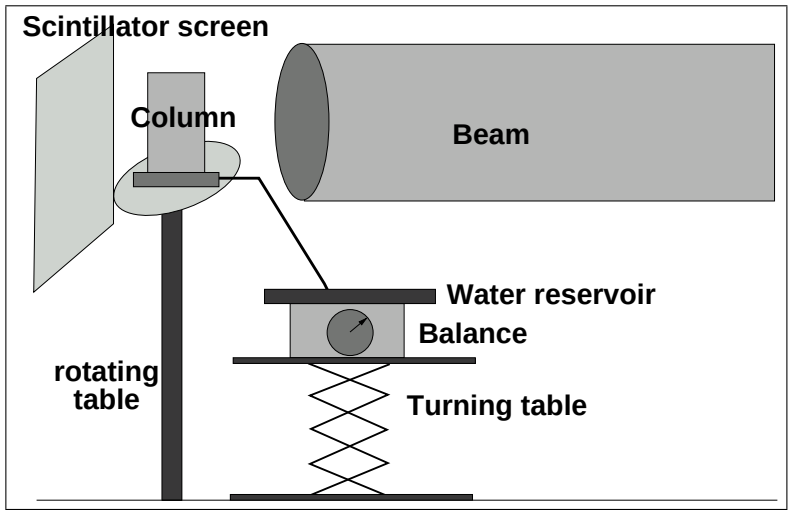

Figure 4.10: Setup of the experiment

These experiments are an illustration of trapping occuring during drainage in heterogeneous porous media. The difference between the entry pressures was in this experiment not high. The crucial point is that the materials were both well sorted, thus there is a sharp decrease in saturation once the entry pressure is exceeded. If slow drainage processes in such materials are considered, the drainage process in an open rough walled fracture can be considered an analogy for flow in porous media.

4.2.2 Modelling of the flow with invasion percolation

The slow drainage processes described above are equivalent to invasion percolation with trapping (TIP). The model has been introduced by Wilkinson and Willemsen (1983) and Dias and Wilkinson (1986). Invasion percolation with trapping on a regular grid can therefore be applied as a model for the basic mechanisms of the displacement process and with this to analyze the patterns generated by this flow process. TIP has been described in detail by various authors (e.g. Stauffer (1992)). In previous studies it has been found that TIP models capillary dominated drainage in porous media and fractures very well (e.g. Lenormand and Zarcone, 1989; Maloy et al., 1992; Amundsen et al., 1999; Knackstedt et al., 2001).
TIP can be applied for capillary dominated flow (quantified by small capillary numbers, cf. equation (1.14) and (1.22)). Other flow regimes have been studied with more sophisticated pore network models than TIP. These models account for the actual pressure drops in the pores and the configuration of the neighboring pores (cf. e.g. Blunt and Scher (1995)). Xu et al. (1998) and Aker et al. (2000) used network models to investigate the crossover between viscous and capillary dominated flow regimes, concluding that the cluster could be stabilized or destabilized, similar to TIP clusters in a gravity field investigated by Glass and Yarrington (1996). This intermediate regimes will here not be discussed further.

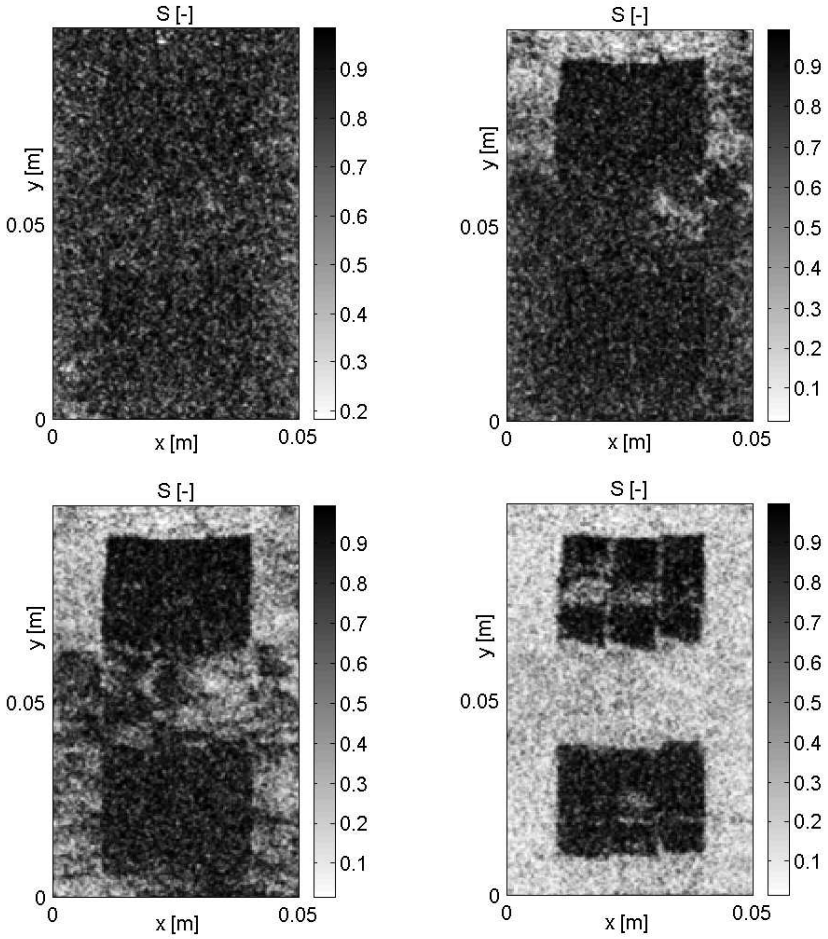

Figure 4.11: Saturation in the column during drainage at four different time steps

As an example for TIP a site percolation model with coordination number 4 is considered to describe drainage in an open rough walled fracture.
As described above (4.5) the entry pressure at the interface at a location where the aperture is b can in the fracture be approximated as

$$P_{\text{entr}} = \frac{2\sigma\cos(\Theta)}{b}. \tag{4.11}$$

at the interface width of the fracture. At the beginning of the percolation process, all sites of the lattice are occupied by the wetting fluid. The sites at the inlet are connected to a source line. When the percolation begins, the invading non-wetting fluid invades the site with the lowest entry pressure out of the set of sites that are connected to the source. Its neighboring sites then become connected to the source (cf. Figure 4.12). This procedure is repeated until a cell connected to the outlet line is invaded by the invading fluid. The invading fluid has then broken through the outlet of the fracture. In an invasion percolation process with trapping, clusters of displaced fluid, which are cut off from the outlet line,

are 'trapped', and can no longer be invaded. Trapping reflects the incompressibility of the displaced fluid.

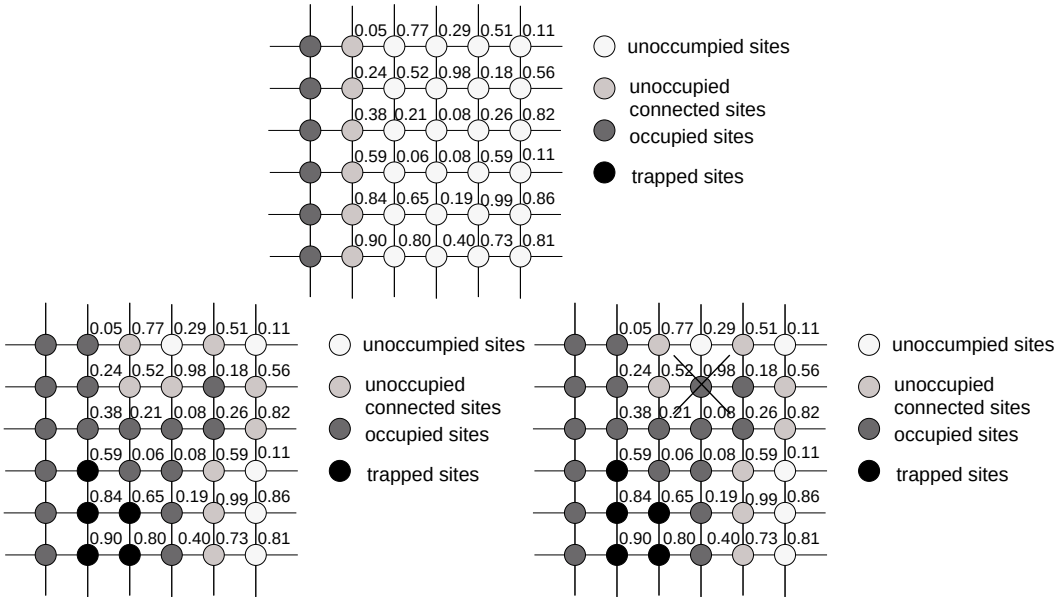

Figure 4.12: Sketch of TIP. First picture: Initial state. Second picture: Stage during the TIP, third picture: Next step after the second picture. The cell to be invaded in the following step is marked with a cross. The numbers are the apertures [mm] at the locations marked by the circle.

4.2.3 Influence of the soil structure on the flow pattern

The properties of TIP clusters generated on uncorrelated fields have been investigated (Wagner et al., 1997). Meakin (1988) and Wagner et al. (1997) investigated the impact of the spatial correlation of the random fields on IP and TIP clusters by analyzing the TIP clusters generated on random fields with a fractal variogram with different Hurst coefficients. The Hurst coefficient is a quantification of a fractal field. It is explained below (cf. 4.13). For small Hurst coefficients they found that the clusters are hardly influenced by the correlation structure. For large Hurst coefficients, the clusters become more segmented into blobs, connected by thin threads. For large Hurst coefficients, the structure of the aperture field also changes the fractal dimension of the clusters.

The influence of the correlation structure of the aperture field (or rather the entry pressure field) on the flow process can be illustrated with two aperture fields with different spatial correlation structures. Both have a Gaussian aperture distribution where negative values have been cut off. The fields have a size of 513 x 513 pixels. The mean aperture is $\overline{b} = 0.52mm$ and the standard deviation is $\sigma_b = 0.23mm$. These values compare well with the measurements of undisturbed fault-zone samples of Fischer et al. (1998). The first

aperture distribution has a Gaussian variogram γ (see e.g. Kitanidis (1997)) of the form

$$\begin{aligned}\gamma(\Delta x) &= \tfrac{1}{2}\overline{(b(\vec{x})-b(\vec{x}'))^2} = \sigma_b^2\left(1-\exp\left(-\tfrac{|\vec{x}-\vec{x}'|^2}{\lambda^2}\right)\right)\\ &= \sigma_b^2\left(1-\exp\left(-\tfrac{(\Delta x)^2}{\lambda^2}\right)\right),\end{aligned} \tag{4.12}$$

where x and x' are two different locations, separated by a vector of the length Δx, λ is the correlation length of the field, b is the aperture and the overbar denotes averaging over the aperture field. This distribution was generated with the code fgen (Robin et al., 1993a), which is based on the fast Fourier transformation method. This field will be referred to as the *Gaussian feld.* The variogram has a finite correlation length, defined by λ. The correlation length in the Gaussian fracture is $\lambda = 3.10mm$ (4 cells), thus the fracture contains 121 x 121 correlation lengths. Macroscopically it can be considered homogeneous and has no predefined channelling paths. The aperture distribution of the second field has been generated with a fractional Brownian motion process (c.f. Voss, 1985; Mandelbrot and Ness, 1968; Kemblowski and Wen, 1993). It has a variogram of the form

$$\gamma(\Delta x) = \frac{1}{2}\overline{(b(\vec{x})-b(\vec{x}'))^2} = A\left|\vec{x}-\vec{x}'\right|^{2H} = A(\Delta x)^{2H}, \tag{4.13}$$

in which A is a proportionality factor and H is the Hurst coefficient here chosen as $H = 0.2$. Theoretically, infinitely large fields generated with fractional Brownian motions have no finite variance. Only a field with finite size has a finite variance and the variance is related to the size of the field. This variogram has no finite correlation length scale and is typical for self-similar structures (such as fractals). This field will be referred to as *fractal fracture.* It does not possess a specific length scale. Structures can be found on all scales. There is a connected path of high apertures at the lower part of the field. Both fields are shown in Figure 4.13.

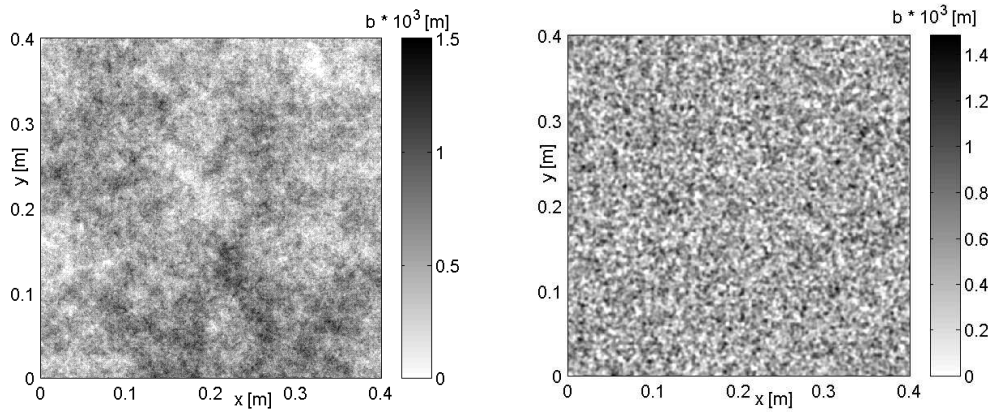

Figure 4.13: Aperture field of the fractal (left) and the Gaussian fracture (right)

The results of the invasion percolation model applied to the two fields is shown in Figure 4.14. for different time steps.

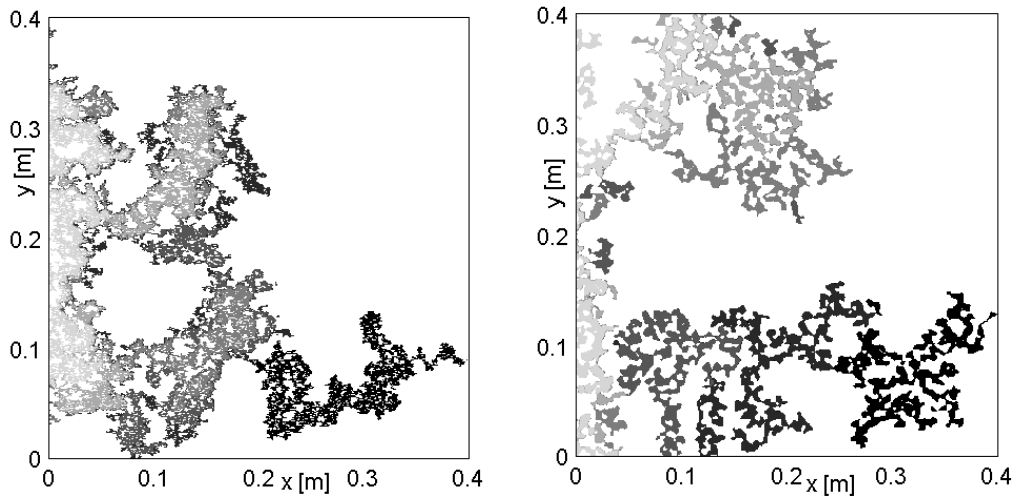

Figure 4.14: Displacement cluster obtained at different time steps in the the fractal (left) and the Gaussian fracture (right) using TIP. A darker shade indicates later time.

The cluster of the displacing fluid appear denser in the fractal fracture than in the Gaussian fracture. The density of the cluster is characterized by the cluster two-point density correlation function $\rho(\Delta x)$ (see e.g. Wagner et al. (1997)). It is defined as the spatial covariance of cells occupied by the invading fluid,

$$\rho(\Delta x) = \frac{\int I(x)I(x+h)dx}{\int (I(x))^2 dx}, \tag{4.14}$$

where the indicator variable $I(x)$ is 0 if the cell is occupied by the displaced fluid and 1 if the cell is occupied by the invading fluid. $\rho(\Delta x)$ is plotted for the clusters of the displacing fluid in both fractures in Figure 4.15. For intermediate distances Δx the density ρ in the cluster of the fractal fracture is larger than in the cluster in the Gaussian fracture. In the fractal fracture connected parts with high apertures with length scales larger than the correlation length of the field of the Gaussian fracture are available, and they are invaded completely by the invading fluid.

The difference of the density on small scales is the only obvious impact of the correlation structure of the aperture fields of the fractures. The density correlation function has no finite correlation length for the cluster in both aperture fields. The clusters are thus irregular, independent of the correlation structure of the aperture field.

The irregularity of clusters generated with invasion percolation on uncorrelated fields are well known. TIP clusters in uncorrelated fields are fractals. Fractals have no defined length scale by definition. According to the simulations shown above, this property does not change if correlation is introduced to the fields. The fact that the fluid clusters generated by capillary channelling flow are fractals, makes the concept of upscaled models questionable. The aperture field (or the entry pressure field) might have an REV (such as the Gaussian fracture described above). However, for the saturation field generated by

the flow process an REV cannot be identified. There are structures on all scales up to the large scale of the whole medium. If the fluid cluster is averaged spatially over patches of the fluid distribution field, the pattern remains irregular, even if the averaging volume is increased to the size of half of the field. A stochastic average of the fluid distribution results in a homogeneous saturation distribution. However, the stochastically averaged field does not represent the field in the single realization. It only represents the stochastic average of the measurement of fluid saturation. An upscaled model which models the averaged saturation field is therefore not useful for questions such as the breakthrough time of the displacing fluid at a certain location. Percolation models are better suited to predict these kind of informations.

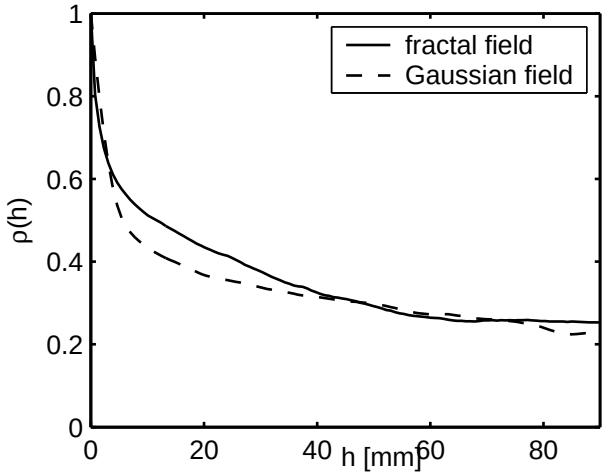

Figure 4.15: Densities of the TIP cluster in the fractal (left) and the Gaussian fracture (right)

A difference in the influence of the structure of the aperture field between the displacement process in the two fractures can be stated in terms of the predictability of the flow patterns. In the fractal fracture the preferential channel at the bottom is clearly visible. It could have been predicted from the aperture field of the fracture, that the displacing fluid would flow along this path. That means, **if** the large scale structures of a field are known, the flow could probably be predicted. In the Gaussian fracture however, no large scale structure is visible in the aperture field. The flow pattern could not have been predicted in advance, it is due to the irregularity of the flow process itself. To summarize: If a flow process is capillary dominated and in a field which matches the criteria described above, its averaged properties are unrelated to the field properties, but have to be derived from the properties of the irregular fluid clusters generated by the displacement mechanism (such as e.g. the fractal dimensions of the clusters).

4.2.4 Experimental test of the applicability of the TIP model as concept for capillary dominated flow

The applicability of the TIP model for channelling when the flow is dirven mainly by capillary forces (leading to the result that the process generates irregular patterns and is therefore not upscalable) has been tested by comparing the model to an experiment. In the experiment, capillary dominated displacement in artificial plexiglass fractures with a heterogeneous aperture field was performed and compared to results of TIP models. The fracture properties were the same as described above. The size of one fracture is $0.4m$ x $0.4m$, which is divided into 513 x 513 square shaped pixels. As a result the horizontal length of one pixel is in the range of the mean aperture. It was found that the in-plane curvature could in this case not be neglected for the calculation of the local capillary pressure. Therefore an extended TIP model which takes in-plane curvature into account was used to compare the experiments.

Extended TIP model

A model to include in-plane curvature was proposed by Hughes and Blunt (2001) and Glass et al. (1998) and investigated further by Neuweiler et al. (2004b). The latter model is simpler as the model of Glass et al. (1998) and has been shown in Neuweiler et al. (2004b) to be sufficient to reproduce the flow. It will therefore be used in the following.
In the extended TIP model of Neuweiler et al. (2004b), the in-plane radius r_2 at the fluid interface (see (4.4)) is recalculated after each invasion step. First, all invadable cells are marked. Then the cluster resulting from the invasion of an invadable cell is determined. After that, the nearest neighbors of the invaded site on both sides of the cluster surface are determined, where neighboring cells in the diagonal direction are also taken into account. The range of possible angles Γ between the two connecting lines of the cell and its nearest neighbors is here only $0, 1/4\pi, 1/2\pi, 3/4\pi$ and π (cf. Figure 4.16). The in-plane curvature radius is then calculated as

$$r_2 = R\tan\left(\frac{\Gamma}{2}\right) \tag{4.15}$$

(cf. Glass et al., 1998). The length scale R is a specific length scale for the in-plane curvature. Glass et al. (1998) suggest to apply half of the correlation length of the aperture field. In Neuweiler et al. (2004b) it is discussed that it should rather be considered the mean aperture of the field. In the experiment described here this corresponds to the size of the grid Δx. In the following, the typical radius R is assumed to be the grid length, $R = \Delta x$.
The local capillary entry pressure field is then recalculated for all cells adjacent to the front as

$$P_c = \sigma\cos\Theta\left(\frac{2}{b} + \frac{1}{\Delta x\tan(\Gamma/2)}\right). \tag{4.16}$$

Then a TIP step is performed using the recalculated local capillary entry pressure field to determine the cell with the lowest entry pressure.

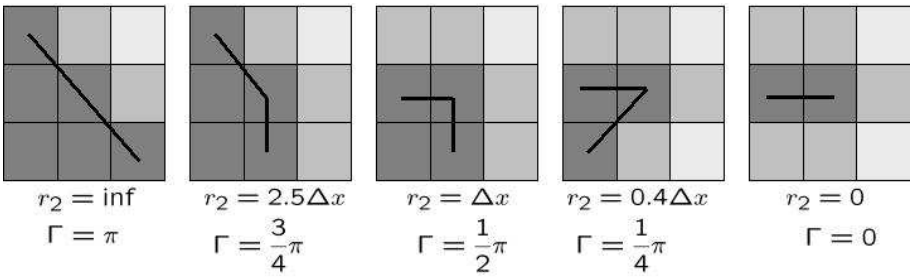

Figure 4.16: All possible configurations of the radius of in-plane curvature in the extendet TIP model

Taking into account in-plane curvature results in a smoothing of the front. However, as the typical range of the in-plane curvature is only important if it is in the range of the aperture, it is smoothing only up to that length scale. Below this length scale, the clusters of displacing fluid appear denser than those generated with the usual TIP. Above this scale, the in-plane curvature does not have an influence any more and the displacing fluid patterns appear the same as the TIP clusters. The clusters generated with the modified TIP are shown in Figure 4.17.

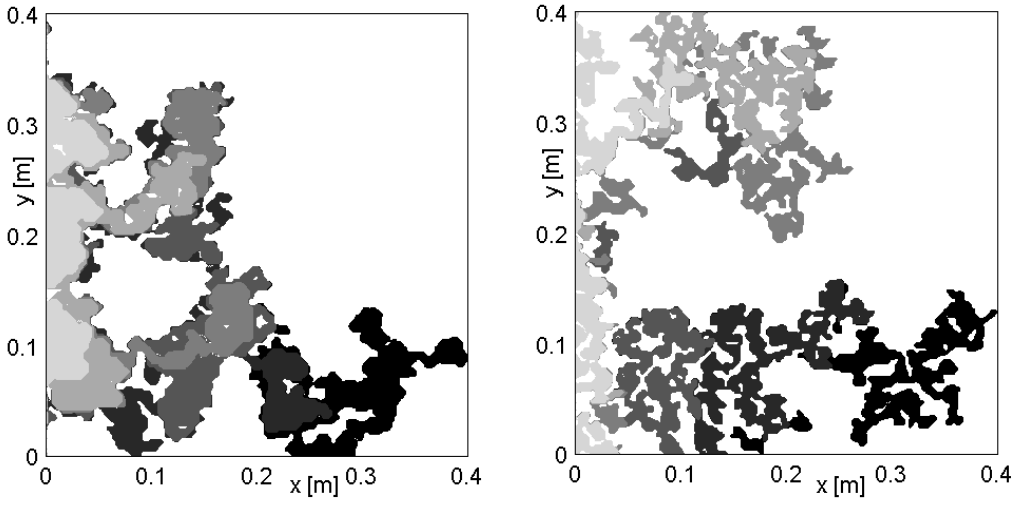

Figure 4.17: Displacement cluster in the fractal (left) and the Gaussian fracture (right) generated with the modified TIP model at different time steps. A darker shade indicates later time.

The clusters generated with the modified TIP model are also irregular. The cluster of the field generated with a power law variogram is denser than the cluster of the field with an exponential covariance. Both fields have a larger density at small distances than the clusters generated with TIP without the in-plane curvature. However, both fields are here

also irregular and have no finite integral scale, as the two-point density functions of the fields indicate (see Figure 4.18).

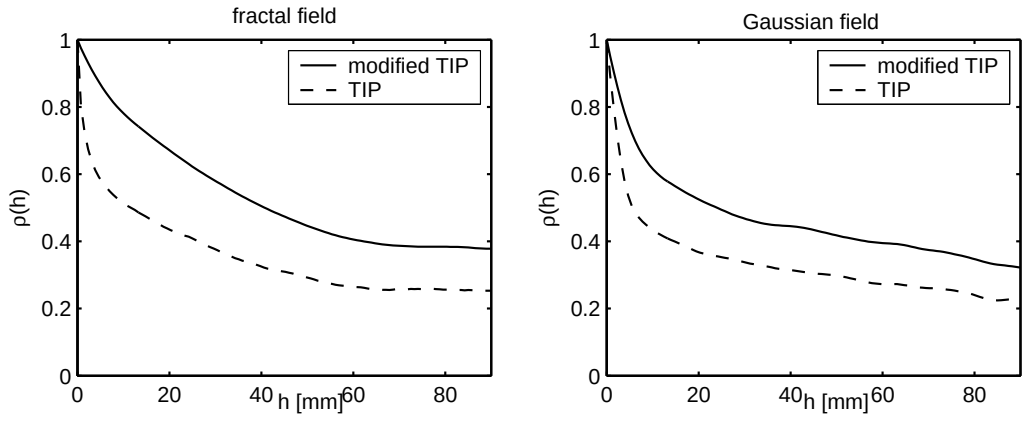

Figure 4.18: Densities of the cluster in the fractal (left) and the Gaussian fracture (right) generated with the original and with the modified TIP model

The findings from the simulations with the TIP models were also tested with laboratory experiments. In the following, these experiments will be described.

Experimental setup

Two quadratic Plexiglas plates were placed on top of each other and bolted together on the sides (see Figure 4.19). One of the Plexiglas plates has a pixel-shaped aperture field milled into the surface (For a more detailed description of the experiments see Neuweiler et al. (2004b)). Two surfaces were used, one with the properties of the fractal fracture (4.13), and one with the properties of the Gaussian fracture (4.12). The plates were sealed at two opposite sides. The other two sides were left unsealed as inlet and outlet lines. The outlet line of each artificial fracture was connected to a sealed Plexiglas reservoir, which was filled with water. A peristaltic pump was connected to the reservoir. Thus, the outflow of water was distributed evenly over the outlet line.
At the beginning, both fractures were saturated with water. In order to displace water by air, water is pumped out of the fracture from the sealed outlet reservoir with a constant flow rate. Air can flow into the fracture via the inlet line. The volumetric flow rate in the experiment was chosen as $Q = 8.33 \cdot 10^{-10} m^3/s$. Using the mean aperture as a typical aperture value, a capillary number (1.14) of $Ca_{\text{air}} = (v\mu_{air})/\sigma = 9 \cdot 10^{-10}$ is obtained for the Gaussian fracture and $Ca_{\text{air}} = 8 \cdot 10^{-10}$ for the fractal fracture. These magnitudes of the capillary number characterize capillary dominated flow (cf. Lenormand et al., 1988). We can assume that the pressures in the air phase as well as in the water phase are spatially constant at the time of the displacement and local pressure gradients in the fluids can be neglected.

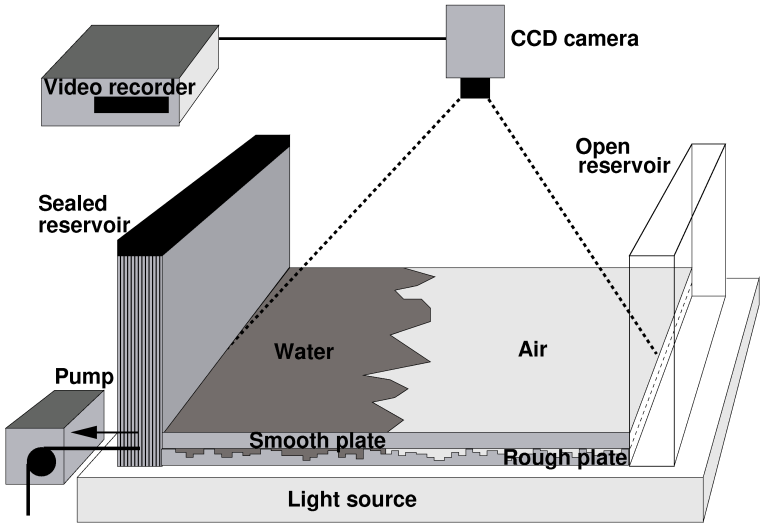

Figure 4.19: Experimental setup

The air distribution in the fracture was measured with light transmission technique, as explained in Detwiler et al. (1999) and Tidwell and Glass (1994). The fractures were placed on a planar cold light source, providing a uniform illumination from below. The resulting air-water cluster in the fracture was filmed with a CCD camera. The digitized pictures of such an experiment had a spatial resolution of 475 x 475 pixels (Gaussian fracture) and 464 x 464 pixels (fractal fracture). A picture of the water filled fracture was taken at the beginning of the experiment and subtracted from the pictures taken during the drainage of the fracture. Binary pictures of the air-water cluster are then obtained by assigning a cut-off grey value, above which the cell is assumed to be filled with air and below which the cell is assumed to be filled with water. The cut-off value was chosen in a way that all cluster features visible in the pictures were recovered while minimizing the background noise in the picture. The processing of the pictures is shown in Figure 4.20.

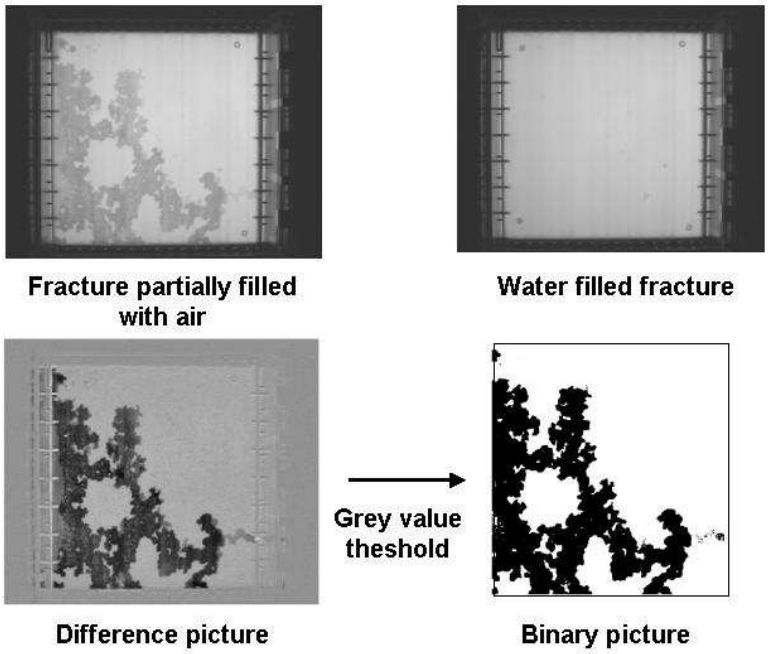

Figure 4.20: Processing of the pictures

Results of the experiments

The processed pictures at different time steps until breakthrough are shown in Figure 4.21.

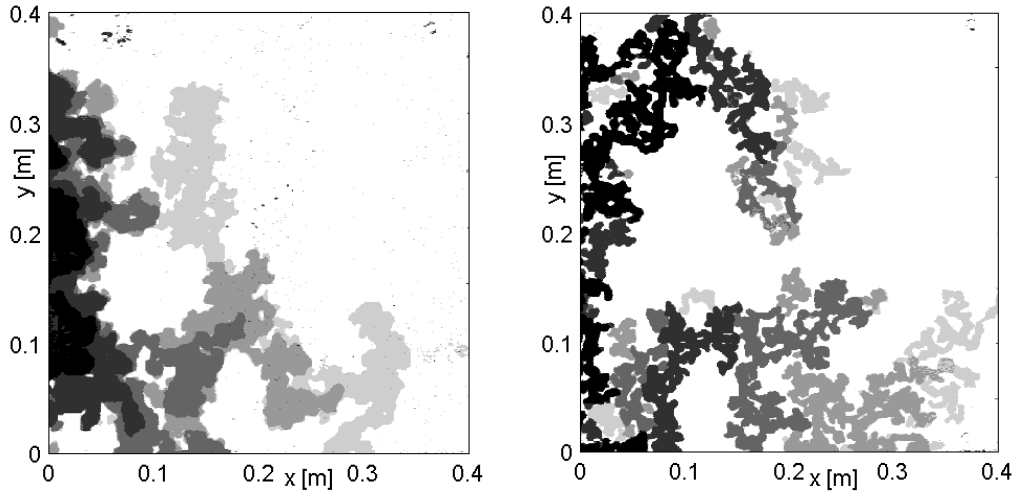

Figure 4.21: Displacement cluster in the fractal (left) and the Gaussian fracture (right) measured in the experiment at different times. A darker shade indicates later time.

In both models, the air clusters are irregular. Thus, in both fractures the displacement is unstable. In both cases, the clusters contain regions of trapped water, which have different length scales. The air cluster obtained in the fractal fracture covers the path of large apertures in the lower part of the fracture. The air cluster in the Gaussian fracture cannot be determined by the aperture structure of the fracture in an obvious way.
When comparing the experimentally obtained clusters to the clusters generated with the modified TIP model it is observed that the correspondence is good. The percentage of matching cells is 93.4 per cent for the fractal fracture and 74.8 per cent for the Gaussian fracture. The densities of the clusters and those of the numerically generated clusters (with modified TIP) are shown in Figure 4.22.

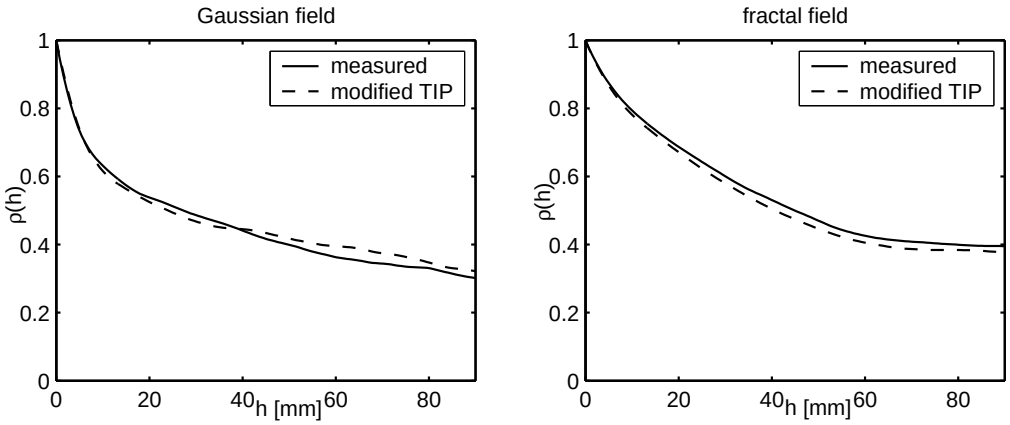

Figure 4.22: Densities of the displacement cluster in the fractal (left) and the Gaussian fracture (right) measured in the experiment and generated with the modified TIP model. The densities generated with the simple TIP model are shown in Figure 4.18.

The densities generated with the modified TIP model match the experimentally determined ones well. That suggests the conclusion that the modified TIP model captures the main flow mechanisms of the displacement process.
The concept of in-plane curvature has no counterpart on the large scale and therefore the modified TIP model is not transferable to flow in porous media on a continuum scale. However, the simple TIP model is a useful model for flow in fractures, where the in-plane curvature can be neglected. This model, as a general concept, is transferrable to flow in porous media. The application of the TIP model is thus useful to get understanding about the expected irregularity of the flow pattern.
Naturally, the details for displacement in porous media are different from those for displacement in open fractures. When air displaces water at one location in a fracture, there is only the water film at the fracture walls left at this location, which is very thin. The trapping mechanism is thus very efficient. If air displaces water at one location in a porous medium, there is more water remaining at this location. The permeability of the water is at this location reduced, however, the reduction is not to the same extend as in a fracture. The trapping mechanism is thus only relevant for an intermediate time scale,

while on a larger time scale the saturation of the air will be much more evenly distributed than that one in a fracture. For a quantitative comparison, comprehensive experimental investigations of immiscible displacement are required.

4.3 Upscaling for unstable flow scenarios

When unstable flow occurs in a medium which is macroscopically homogeneous one should not derive an upscaled model from the flow equation for a heterogeneous medium. In both cases considered here (viscous or gravity unstable flow or unstable flow due to capillary channelling), the irregularity or fluctuations of the solution are not related to the soil structure.
Relevant information about the averaged distribution, such as estimates of breakthrough times or probabilities to measure a given saturation at a given location at a given time, could however be derived if the instable pattern can be estimated. For viscous fingering the fastest finger growth rate can be determined on the basis of a linear stability analysis. If capillary channelling is expected to take place and the fracture analogon is expected to be applicable, TIP models of the flow may predict averaged quantities. However, classical upscaling approaches, which relate structural information of the soil to effective parameters can not be applied here in a reasonable way.

4.4 Summary

Two types of flow problems were discussed in this chapter. Both generate heterogeneous structures which are not necessarily related to the structure of the soil. The first type are viscous or gravity unstable displacement problems. The instability of the interface between displacing and displaced fluid can occur in homogeneous media and can be triggered by a small disturbance. The characteristic of the flow pattern can be analyzed with stability analysis.
The second type of flow is capillary dominated displacement in a heterogeneous medium. The patterns of the interface between displacing and displaced fluid are here also highly irregular, but have different properties compared to the viscous unstable patterns. The trapping of fluid is the crucial mechanism here, leading to irregular patterns. The properties were here analyzed in more detail by using the analogy between capillary dominated displacement and displacement in an open rough-walled fracture. The influence of soil structure on the flow patterns was analyzed. The irregularity of the displacement is only determined by the soil structure if there are large scale patterns in the parameter field.
Flow processes which are unstable in this way cannot be upscaled in the usual way. The irregular structure of the fluid distribution is not predictable in a deterministic way. To model such flow processes numerically is a high challenge and requires very fine resolution and a very good understanding of the characteristics of the instabilities. When, for example, the flooding of a reservoir is planned, unstable flow behaviour poses a big problem. Mostly, the large structures of a reservoir are well known from seismic tests

and other measurements. It is then assumed, that the flow is driven mainly by the large scale structure, so that instabilities do not evolve. For many other applications, such as remediation of contaminated soil by air sparging or prediction of two-phase flow in fractured rock, unstable flow causes big problems. If the time-dependency of the growth of the transition zone between the two phases is known, the spatial averaged fluid distribution could be predicted. It has then however to be considered, that the predictions are not predictions for the real flow process in the single porous medium at hand. They might be useful for risk assessment, but do not allow, for example, for the prediction of the time of breakthrough of the displacing fluid at a given location.
The growth of the transition zone between the fluids could be estimated from linear stability analysis for viscous and gravity unstable flow and from TIP simulations (or simulations with other adequat models, such as the diffusion limited aggregation model of Witten and Sander (1983) for fast processes) for capillary driven channeling flow. The problem is here, that stability analysis can be performed for homogeneous porous media. The influence of structure of the porous media on the characteristic properties of the unstable flow behaviour is a topic which has not been investigated much. It is a challenge for future research to get a better understanding of this topic. Especially experiments are needed, which address this question.
In the follwing chapters upscaling of different two-phase flow processes will be discussed. The problem of unstable flow will be addressed again in Chapter 7.

Chapter 5

Flow on an intermediate scale: Richards equation

Flow processes in the unsaturated zone are mostly two-phase flow processes (air and water), which is usually considered on a meter to 100 meter scale. It is described by Richards equation (see Chapter 1.4.4). Flow processes in the unsaturated zone are infiltration of water into the partly saturated soil towards underlying aquifers, but also evapotranspiration of water over the soil surface. The unsaturated zone is very important for estimation of transport times of contaminants from the land surface to underlying aquifers. On a larger length scale, it is a crucial part for modelling of water balances and energy fluxes. It is thus important for climate research. The flow processes in the unsaturated zone control the partitioning of all hydrologic fluxes. The unsaturated zone can thus be considered as the coupling element between the surface and subsurface compartment in the terrestrial part of the hydrologic cycle.

The flow is usually driven by capillary and gravity forces. It is modelled by the two-phase flow equation, where capillary forces, viscous forces and gravity forces have to be taken into account. However, the air is assumed to be stagnant and always at atmospheric pressure. Therefore the flow equations are simplified, as outlined in Section 1.4.4.

Using homogenization theory to derive an upscaled model for flow in the unsaturated zone implies, that we assume that the scales are separated (cf. Section 3.1). If we would average the equation using a stochastic approach, this assumption would not have to be made. The stochastically averaged problem has been investigated by many authors. The steady-state unsaturated flow equation has been analyzed in a stochastic framework by Yeh et al. (1985), Russo (1992),Russo (1998), Russo (2003), and Indelman et al. (1993), among others, the transient case by Mantoglou and Gelhar (1987b), Zhang (1999), and others. Yeh et al. (1985) derived an upscaled model which has the same shape as the original Richards equation. The effective unsaturated conductivity depends on the averaged head gradient and shows a stronger anisotropy than the saturated conductivity field. The parameters are given in terms of the second order stochastic properties of the saturated conductivity and the entry pressure head. Mantoglou and Gelhar (1987a) extended the work of Yeh et al. (1985) for the transient case and obtained a hysteretic dependence

of the effective unsaturated conductivity. Moreover, the conductivity has again different anisotropy properties than the saturated conductivity and depends on the mean head gradient. A detailed review on unsaturated flow with stochastic parameters can be found in Zhang (2002).

Due to the nonlinearity of the flow equations, the results underly restrictions. A typical assumption is that the mean flow is exclusively driven by gravity, so that the mean capillary head is uniform. Another typical assumption is that the relationship between the capillary pressure and the saturation follows an exponential function (Gardner, 1958; Russo, 1988). This model does not include entry pressure effects. Although entry-pressure effects are less important for water in the unsaturated zone than for non-wetting fluids in multi-fluid flow, a model without entry pressure does not reflect the variability of saturation and thus relative permeability at low pressure values (cf. Zhang et al. (1998)). As explicit results are only possible for simplified models, comparisons of stochastic results to Monte Carlo simulations ar needed (Unlu et al., 1990).

It is not necessarily the case that an upscaled model can be derived with stochastic theory. Depending on the flow and the medium structure, it might be that the equivalent equations for the averaged unknowns do not have the same form as the original equation and parameters can become non-local (e.g. Tartakovsky et al. (1999)).

In the following upscaled models for flow in the unsaturated zone in heterogeneous media will be derived with homogenization theory. The influence of the soil structure is then analyzed by comparing the effective parameters for the upscaled models using parameter fields with different structure. The resulting upscaled model is restricted to the assumption of scale separation and to a certain flow and parameter regime. In this way the results less general than the results of stochastic averaging, which are described above. This drawback of the method has however at the same time the advantage, that the upscaled equation is derived directly and for these fixed flow regimes the effective parameters can often be derived explicitly. As results from stochastic theory are usually extremely complex to interpret, and therefore have to be considered for very simplified cases, homogenization theory is here chosen as the method to analyse upscaled models.

The influence of soil structure on the effective parameters will then be analyzed by calculating the parameters with stochastic theory. The results will be compared to the numerically calculated parameters for the test fields introduced in Chapter 2 (Figure 2.4). Effective medium theory will then be applied as an alternative method to calculate the effective permeability function, in order to capture to account for the case that the parameter fields has connected paths of the extremely high or low values.

With regards to the last chapter it should be mentioned, that flow in the unsaturated zone can be unstable. Fast infiltration of water into dry soil is highly unstable. These instabilities are a topic which is investigated intensly (e.g. Nieber et al. (2005)). These unstable flow processes are neglected here. The flow processes which are considered here are slow flow processes which are stable, such as slow drainage.

5.1 Flow Equations

As described in Section 1.4.4, flow in the unsaturated zone is a two-phase flow problem, which is mostly considered in a simplified way. The air is assumed to be always connected to the atmosphere and to equilibrate quasi-instantaneously. That is, the air does not move and is always at constant pressure. It has merely the role of a background fluid. The atmospheric pressure is set to zero, so that the water pressure is equal to the negative capillary pressure.

5.1.1 Richards equation

As flow in the unsaturated zone is mostly considered in relation to groundwater flow, it is more common to use a pressure head instead of the pressure (cf. (1.25)).

$$h = \frac{P_{\text{water}}}{\rho_{\text{water}} g} = \frac{P_{\text{air}} - P_c}{\rho_{\text{water}} g} = -\frac{P_c}{\rho_{\text{water}} g} = -h_c. \tag{5.1}$$

As the air is considered to be always at equilibrium, the system is reduced to a single-phase system. The transient water flow in the unsaturated zone is then described by a mass-balance equation (Richards equation, see equation (1.35)):

$$\frac{\partial \Theta}{\partial t} + \vec{\nabla} \cdot \vec{q} = \mathscr{C}(h) \frac{\partial h}{\partial t} + \vec{\nabla} \cdot \vec{q} = s \tag{5.2}$$

in which h [L] is the pressure head, having negative values in unsaturated systems, $\vec{q}$ [L/T] is the specific discharge of soil water, s [1/T] stands for volumetric sources and sinks and $\mathscr{C}(h) = d\Theta/dh$ [1/L] is the moisture capacity, or the derivative of the water retention function, where Θ [-] is the volumetric water content. The water content is the product of the porosity n_f [-] and the saturation S [-], $\Theta = n_f S$. The specific discharge follows Darcy's law (cf. 1.17)), where the relative permeability is related to the pressure head

$$\vec{q} = -\mathbf{K} k_r(h) \left(\vec{\nabla} h + \vec{e}_z \right). \tag{5.3}$$

in which $\vec{e}_z$ [-] denotes the vertical unit vector pointing upward, K [L/T] is the hydraulic conductivity at full water saturation, and k_r [-] is the relative permeability of the water at unsaturated conditions. The hydraulic conductivity K is in the following assumed to be isotropic and the tensor notation is dropped.

5.1.2 Space dependency of the parameters

In order to derive the upscaled model for Richards equation, the heterogeneous problem has to be defined. All parameters could be space dependent, but only some of them will be taken into account here. The hydraulic conductivity is written as a typical value times a dimensionless space dependent function. In general this is

$$K(\vec{x}) = K_0 \kappa^\star(\vec{x}). \tag{5.4}$$

In a 2d problem it would make sense to use the geometric mean K_g as the typical value and consider the logarithm of the hydraulic conductivity f_k as a space dependent parameter

$$K(\vec{x}) = K_g \exp(f_k(\vec{x})). \tag{5.5}$$

If the conductivity is log-normally distributed, f_k would be a normally distributed random field.
The entry pressure head h_{entry} ((1.27),or an equivalent parameter, depending on the model for the constitutive relationships) is also usually heterogeneously distributed. The entry pressure head can also be written as a typical value times a dimensionless heterogeneous function

$$h_{\text{enty}}(\vec{x}) = Hh^\star(\vec{x}). \tag{5.6}$$

For a two-dimensional problem it might also be reasonable to use the geometric mean as the typical value and the logarithm of the dimensionless field as the heterogeneous parameter

$$h_{\text{entry}}(\vec{x}) = h_g \exp\left(f_h(\vec{x})\right). \tag{5.7}$$

In principle the constitutive relationships (here the relation between k_r and h and the relation between S and h) can have a number of parameters, which could all be space dependent. Also the porosity can be heterogeneously distributed. However, in the test examples considered here all parameters except for the hydraulic conductivity and the entry pressure head are assumed to be constant. Thus, the shape of the water retention function and the shape of the relative permeability function is the same in all materials. This is certainly not realistic. However, as the shape of these curves is usually described by parameters, which appear as powers, it is difficult to analyze them systematically. A discussion of the influence of the shape of constitutive relation functions on the averaged flow behaviour is beyond the scope of this study and needs to be investigated in the future.

5.1.3 Dimensionless Richards equation

The Richards equation can be made dimensionless by introducing characteristic values for all parameters and variables. The characteristic values for time and space are denoted T and L. We choose K_g and h_g as the characteristic value of the hydraulic conductivity and of the pressure head respectively. We thus express the dimensional quantities by:

$$h = h_g h^\star, \quad \vec{x} = L\vec{x}^\star, \quad t = Tt^\star, \quad \mathscr{C} = \frac{\mathscr{C}^\star}{h_g}, \quad \vec{q} = K_g \vec{q}^\star \tag{5.8}$$

in which symbols with stars are dimensionless. The typical time scale T is here chosen as a large scale time scale:

$$T = \frac{L}{K_g}. \tag{5.9}$$

A small scale time scale is not taken into account. By this choice of characteristic variables the upscaled models are all restricted to slow flow processes. If fast flow processes

are important, the typical time scale would be smaller than T of equation (5.9), and an additional typical time scale would have to be taken into account. The choice of a slow time scale is important, as upscaled dynamic effects, such as discussed e.g. by Hassanizadeh and Gray (1993), Hassanizadeh et al. (2002) or Bourgeat and Panfilov (1998) are with this choice not to be expected in the upscaled models.
Substituting eq. (5.3) into eq. (5.2), and applying the above mentioned choice of typical values (5.8), the dimensionless Richards equation becomes:

$$\mathscr{C}^\star(h^\star)\frac{\partial h^\star}{\partial t^\star} + \vec{\nabla}^\star \cdot \left(\exp(f_k) k_r(h^\star, f_h) \left(\frac{h_g}{L} \vec{\nabla}^\star h^\star + \vec{e}_z \right) \right) = qT \tag{5.10}$$

in which $\vec{\nabla}^\star$ denotes the vector of derivatives with respect to the dimensionless coordinates $\vec{x}^\star$. The dimensionless group which appears in this equation could be assigned to the Bond number, according to (1.24).

$$Bo = \frac{L}{h_g}. \tag{5.11}$$

The dimensionless number should quantify the relation between gravity and capillary forces. However, the Bond number as defined in (5.11) is not necessarily a good estimate for the balance of forces, if homogenization theory is performed. The Bond number (5.11) comes from the dimensionless grouping of the parameters. The forces, however, are rather compared by setting a typical gradient of the capillary pressure head in relation to one (dimensionless pressure head gradient due to gravity). That is, to balance the forces a Bond number as

$$Bo = \frac{L}{h_g \Delta h^\star} \tag{5.12}$$

should rather be used, instead of (5.11). $\Delta h^\star$ is a typical value for the dimensionless head difference. In case that the difference between the bottom and the top boundary pressure head is larger than the length scale of the heterogeneity ℓ in the parameter field, $h_g \Delta h^\star$ could be chosen as $h_g \Delta h^\star = H_b - H_t$ where H_t and H_b are estimates for the pressure head at the top and the bottom boundary. If this difference is small, the typical head difference in a heterogeneous system would reasonably be chosen as the typical length scale of the heterogeneities $h_g \Delta h^\star = \ell$, as the pressure head is expected to fluctuate on that scale. In case that the bottom and top pressure head are equal and the system is homogeneous (which is not considered here), the choice of the typical pressure head should be set to a non-zero value which is smaller than the length scale of the medium.
As the important point is here the large scale behaviour, it is reasonable to use typical quantities on the large scale for this. The time scale has to be chosen accordingly. All other dimensionless parameters are not affected by this scaling.
The star index is not used any more in the following. Unless it is stated explicitely, all quantities are considered dimensionless in the remainder of this chapter.

5.2 Homogenization of Richards equation

To obtain the homogenized equations, a scale expansion of the pressure head h in terms of ε is done, as explained in Chapter 3.1.

$$h(\hat{X},\hat{Y},t) = h^{(0)}(\hat{X},\hat{Y},t) + \varepsilon h^{(1)}(\hat{X},\hat{Y},t) + \varepsilon^2 h^{(2)}(\hat{X},\hat{Y},t) + \dots \tag{5.13}$$

$\hat{X}$ and $\hat{Y}$ are the dimensionless space variables which have been made dimensionless with the large length L and the small length ℓ respectively. Functions of the head, such as the moisture capacity $\mathscr{C}(h)$ and the relative permeability $k_r(h)$ are also expanded by Taylor series about $h^{(0)}$ (cf. (3.8) and (3.9)). All orders of the pressure head as well as all orders of the flux must be continuous on all scales. Considering a periodic field, all variables have to be $\hat{Y}$-periodic. The gradient is scaled according to equation (3.5).
The Bond number has to be set into relation of the scaling parameter ε in order to derive the upscaled equation. Two cases are here considered. The Bond number is assumed to be in the range of ε^0. This assumption leads to the **capillary equilibrium condition** (Pickup and Stephen, 2000; Dale et al., 1997). Capillary equilibrium allows for a quite easy method to obtain the effective parameter functions, as the effective parameters of the model are not related to the flow process on the large scale. Therefore, local capillary equilibrium is an often made as an assumption (e.g. Kueper and Worther, 1992; Pickup and Stephen, 2000; Pickup and Sorbie, 1996; Smith, 1991). It has also been compared to experiments (e.g. Desbarats, 1995; Braun et al., 2004).
However, the assumption that the typical pressure head difference is of the order of the large length scale is often not realistic. If the pressure head difference is small compared to the large scale, capillary forces and gravity forces balance each other on the small scale. Therefore the range of the order ε^{-1} is also considered. A Bond number equal or larger than ε^{-2} leads to gravity driven flow only. This case will also be shortly discussed. A Bond number smaller than ε^0 is first not realistic and second would lead to the same model as for the Bond number ε^0, however, without a gravity term.
A second prerequisite for splitting eq. (5.10) into separate equations of different orders in ε is that we restrict the functions k_r, $\mathscr{C}$ and the parameters describing the spatial variability. The flow has to be in a regime, where these parameters do not contribute orders ε^m with m different from zero to eq. (5.10). In such a case, the expansion of the dimensionless Richards equation would look different. It has been shown by Lewandowska et al. (2004) that a contrast in the hydraulic diffusivity of order ε^2 leads to a double continuum model for the upscaled Richards equation. It is assumed in the following that parameter contrasts are moderate.

5.2.1 Capillary equilibrium

The upscaled model for a small Bond number ($Bo \propto \varepsilon^0$) is equivalent to a model derived under the assumption of capillary equilibrium. The lowest-order equation obtained from eq. (5.10) is of order ε^{-2}:

$$\vec{\nabla}_{\hat{Y}} \cdot \left(\exp(f_k) k_r^{(0)}(f_h, h^{(0)}) \vec{\nabla}_{\hat{Y}} h^{(0)} \right) = 0. \tag{5.14}$$

This equation can only have the solution (see e.g. VanDuijn et al. (2002) and Lewandowska and Laurent (2001)):

$$h^{(0)} = h^{(0)}(\hat{X}, t). \tag{5.15}$$

Eq. (5.15) states that the system on the small scale is in capillary equilibrium, as the capillary pressure head is constant on the small scale $\hat{Y}$. A uniform distribution of the pressure head on the small scale does not imply other hydraulic quantities to be uniform because soil parameters still vary on the small scale. However, the capillary equilibrium makes the relationship between small-scale hydraulic parameters and large-scale pressure head unique. The capillary pressure head $h^{(0)}$ is constant over the unit cell and the saturation $S^{(0)}$ and all other functions of the capillary pressure head can be derived from the local (space dependent) parameter functions.
Considering eq. (5.15), the terms of order ε^{-1} in eq. (5.10) become:

$$\vec{\nabla}_{\hat{Y}} \cdot \left[\exp(f_k) k_r^{(0)}(f_h, h^{(0)}) \left(\frac{h_g}{L} \vec{\nabla}_{\hat{X}} h^{(0)} + Bo^{-1} \vec{\nabla}_{\hat{Y}} h^{(1)} + \vec{e}_z \right) \right] = 0. \tag{5.16}$$

As explained in Section 3.1, the homogenized equation is obtained by averaging the equation of order ε^0 spatially over the unit cell. In Chapter 2 volume averages were denoted by an overbar, while stochastic averages were denoted by angular brackets. The average over the unit cell will in the following be denoted by angular brackets in order to keep the notation simple.
Finally, the averaged equation of order ε^0 yields the homogenized large-scale flow equation. Considering eq. (5.15), the small-scale averaged zeroth-order equation is:

$$\langle \mathscr{C}^{(0)} \rangle \frac{\partial h^{(0)}}{\partial t} + \vec{\nabla}_{\hat{X}} \langle \exp(f_k) k_r^{(0)}(f_h, h^{(0)}) \left(Bo^{-1} (\vec{\nabla}_{\hat{X}} h^{(0)} + \vec{\nabla}_{\hat{Y}} h^{(1)}) + \vec{e}_z \right) \rangle = \langle sT \rangle \tag{5.17}$$

In order to obtain the upscaled equation for $h^{(0)}$, eq. (5.16) has to be solved for $h^{(1)}$ and the solution has to be substituted into eq. (5.17).
The first-order term $h^{(1)}$ of the head can be expressed as a product of a vector of auxiliary variables $\vec{\chi}$, depending only on the small-scale coordinates $\hat{Y}$ times the large-scale driving force $\vec{J}$ appearing in Eq. (5.16) (cf. Hornung, 1997):

$$h^{(1)} = \vec{\chi}(\hat{Y}) \cdot \vec{J}(\hat{X}, t) \tag{5.18}$$

with

$$\vec{J} = Bo^{-1} \nabla_{\hat{X}} h^{(0)} + \vec{e}_z \tag{5.19}$$

Due to local capillary equilibrium, $\vec{J}$ does not depend on the small-scale coordinates $\hat{Y}$. Now, eq. (5.16) becomes:

$$\vec{\nabla}_{\hat{Y}} \cdot \left(\exp(f_k) k_r^{(0)}(f_h) \left(\vec{J} + \vec{\nabla}_{\hat{Y}} \left(\vec{\chi} \cdot \vec{J} \right) \right) \right) = 0 \tag{5.20}$$

$\vec{\chi}$ as well as the resulting flux are periodic and continuous. Equation (5.20) has to be solved for the parameter field in the specific unit cell considered. The solution of $\vec{\chi}$ is

independent on the driving gradient $\vec{J}$. The zeroth-order equation (5.17) is obtained by inserting eqs. (5.18 & 5.19) into eq. (5.17):

$$\mathscr{C}_a^{(0)} \frac{\partial h^{(0)}}{\partial t} + \vec{\nabla}_{\hat{X}} \cdot \left(\mathbf{K}_e \left(Bo^{-1} (\vec{\nabla}_{\hat{X}} h^{(0)}) + \vec{e}_z \right) \right) = s_a T \tag{5.21}$$

with the arithmetic means $\mathscr{C}_a^{(0)}$ and s_a:

$$\mathscr{C}_a^{(0)}(h^{(0)}) = \langle \mathscr{C}^{(0)} \rangle \tag{5.22}$$

$$s_a = \langle s \rangle \tag{5.23}$$

and the effective dimensionless conductivity tensor K_e

$$\mathbf{K}_e(h^{(0)}) = \langle \exp(f_k) k_r^{(0)}(f_h) \left(\mathbf{I} + \vec{\nabla}_{\hat{\mathbf{Y}}} \otimes \vec{\chi} \right) \rangle \tag{5.24}$$

in which $\otimes$ is the dyadic-product operator.
The components of the $\vec{\chi}$-vector can be obtained by subsequently choosing $\vec{J}$ in (5.20) as a unit vector in each principal direction. This leads to the following procedure to determine the functional relationship $\mathbf{K}_e(h^{(0)})$:

- Choose a value for the mean pressure head $h^{(0)}$ within the unit cell.
- Calculate the corresponding distribution of the hydraulic conductivity field $\exp(f_k) k_r^{(0)}(h^{(0)}, f_h)$ throughout the unit cell.
- Choose a unit hydraulic gradient in direction i and apply periodic boundary conditions for the steady-state head equation within the unit cell. This results in the field of $\chi_i + \hat{Y}_i$.
- Calculate the mean flux vector for $\chi_i + \hat{Y}_i$. This yields the i-th column of the effective conductivity tensor $\mathbf{K}_e$.
- Repeat steps 3 and 4 with the other principal direction(s).

5.2.2 Gravity dominated flow

If gravity forces are comparingly strong, two time scales have to be estimated (cf. e.g. Mauri (2003) or Lunati et al. (2002)). The first time scale is due to gravity forces on the large length scale $T_1 = L/K_h$. In case that the Bond number is small, $Bo \propto \varepsilon^0$, the typical time scale due to capillary forces on the large scale $T_2 = L^2/(K_h H)$ is of the same order as T_1. However, if the Bond number is large, $Bo \approx \varepsilon^{-1}$, capillary forces and gravity forces on the large scale attain different time scales, which have both to be taken into account, if capillary and gravity forces are also considered in the upscaled problem. In this case we have

$$\frac{\partial}{\partial t^\star} = \frac{\partial}{\partial t_1} + \varepsilon \frac{\partial}{\partial t_2}. \tag{5.25}$$

The first term comes from scaling due to gravity forces, $t_1 = t/T_1$, while the second one results from scaling due to capillary forces, $t_2 = t/T_2$. t is here the time with dimensions, therefore the dimensionless time is marked with a star in equation (5.25). For the leading order term it is sufficient to consider the faster time scale of the two, t_1, only. Therefore, the differentiation of the time scales between t_1 and t_2 will here be neglected.
For the case that the Bond number is of order ε^{-1}, it is convenient to introduce a rescaled Bond number

$$Bo \propto \varepsilon^{-1}, \quad Bo = Bo' \frac{L}{\ell} \varepsilon, \quad Bo' \propto \varepsilon^0. \tag{5.26}$$

The highest order terms in the dimensionless Richards equation (5.10) are of the order ε^{-1}. Collecting all terms of this order yields

$$\vec{\nabla}_{\hat{Y}} \cdot \vec{q}^{(0)} = \vec{\nabla}_{\hat{Y}} \cdot \left(\kappa k_r^{(0)} \left(Bo'^{-1} \vec{\nabla}_{\hat{Y}} h^{(0)} + \vec{e}_z \right) \right) = 0, \tag{5.27}$$

where $h^{(0)}$ has again to be $\hat{Y}$-periodic. This equation has no simple solution and has in general to be solved numerically. Depending on the model, it might be that no solution can be found. The leading order pressure head $h^{(0)}$ is here not constant in $\hat{Y}$.
The next order in the dimensionless Richards equation (5.10) is that of order ε^0. We obtain

$$\mathscr{C}^{(0)} \frac{\partial h^{(0)}}{\partial t} - Bo'^{-1} \left(\vec{\nabla}_{\hat{X}} \cdot \vec{q}^{(0)} + \vec{\nabla}_{\hat{Y}} \cdot \vec{q}^{(1)} \right) = 0. \tag{5.28}$$

The leading order term of the upscaled Richards equation is now obtained by averaging the equation (5.28) over the unit cell. This gives

$$\langle \mathscr{C}^{(0)} \frac{\partial h^{(0)}}{\partial t} \rangle - \vec{\nabla}_{\hat{X}} \cdot \langle \vec{q}^{(0)} \rangle = \frac{\partial \langle \Theta^{(0)} \rangle}{\partial t} - \vec{\nabla}_{\hat{X}} \cdot \langle \vec{q}^{(0)} \rangle = 0. \tag{5.29}$$

If the parameter field is isotropic and the influx is uniformly distributed over the top boundary, the driving force is gravity only. The averaged zeroth order flux is then in vertical direction only. The equation can in this case be interpreted as the Richards equation with a gravity term only. The resulting effective unsaturated conductivity K_{eff} is equal to the constant flux

$$K_{\text{eff}}(\langle h^{(0)} \rangle) = \langle q^{(0)} \rangle (\langle h^{(0)} \rangle). \tag{5.30}$$

Although the capillary forces are not dominant on the large scale, the capillary term influences the result as it appears in the equation for $q^{(0)}$, (5.27). That means, capillary forces are important on the small scale, but no longer on the large scale.
As the original Richards equation has for the case of large Bond numbers a term of order ε, the same order has in principle to be kept in the upscaled equation. This is important if the Bond number is large but smaller than ε^{-1}. To obtain explicit results for the next order is, however, only possible for layered media. In the following, only the leading order will therefore be considered.
The upscaled Richards equation is in leading order

$$\frac{\partial \langle \Theta^{(0)} \rangle}{\partial t} - \vec{\nabla}_{\hat{X}} \cdot K_{\text{eff}}(\langle h^{(0)} \rangle) \vec{e}_z = 0. \tag{5.31}$$

The effective parameter functions can be obtained in the same way as for the case with strong capillary forces, albeit the procedure is more complex. It is as follows.

- Eq. (5.27) is solved for $h^{(0)}$, applying periodic boundary conditions. One value is kept fix at one location. The solution for $h^{(0)}$ is then averaged over the unit cell.
- The flux $\vec{q}^{(0)}$ is calculated according to (5.27) and is also averaged over the unit cell.
- From the local solution $h^{(0)}(\hat{Y})$ the water content $\Theta^{(0)}(\hat{Y})$ can be calculated and also averaged over the unit cell. In this way a $\langle h^{(0)} \rangle - \langle \Theta^{(0)} \rangle$ - curve can be obtained, and from this curve an effective moisture capacity function can be derived.
- The effective relative permeability function for the gravity term is obtained from the $\langle q^{(0)} \rangle - \langle h^{(0)} \rangle$ - curve.

5.2.3 Vertical flow in layered media

Vertical flow in a layered medium may be considered a quasi one-dimensional problem, as the flow does not depend on the horizontal coordinates. It is a simplified form of the general Richards equation problem and is therefore often analysed (e.g. Lu and Zhang, 2004; Neuweiler and Eichel, 2007). It allows for anlaytical solutions of simple problems (Romano et al., 1998; Srivastava and Yeh, 1991). The one-dimensional problem allows for an analysis of the case with intermediate Bond numbers. For a layered medium the first order corrections to the gravity dominated case can be derived. These terms should be taken into account when the Bond number is large, but smaller than ε^{-1}. By comparing the results it can also be assessed, how large the error would be, if the assumption of local capillary equilibrium would be made even if the Bond number is large.
The layered medium problem will therefore be discussed in the following.
The parameters are here made dimensionless with their harmonic mean instead of their geometric mean, as the flow is perpendicular to the layers.

$$h = h_h h^\star, \quad K(z) = K_h \kappa^\star, \quad \mathscr{C} = \frac{1}{h_h}\mathscr{C}^\star, \quad \vec{q} = K_h \vec{q}^\star, \tag{5.32}$$

in which symbols with stars are dimensionless. K_h is the harmonic mean of the hydraulic conductivity. The reference value h_h is the value of the entry pressure head, which is related to the harmonic mean of the conductivity. Such a relation is obtained by the appropriate scaling condition for the entry pressure head h_{entry} and the conductivity in Miller similar media (Miller and Miller, 1956; Sposito and Jury, 1990),

$$h_{\text{entry}} = \frac{C}{\sqrt{K}} \;\rightarrow\; h_h = \frac{C}{\sqrt{K_h}}, \tag{5.33}$$

where C is a constant. The proportionality comes from an analogy consideration on the pore scale. The hydraulic conductivity is related to the square of a typical pore diameter,

while the entry pressure head is related to the inverse of a typical pore diameter (see e.g. Fetter (2001)).
The upscaled model for the case of small Bond numbers will be repeated first. Then the case or large Bond numbers with first order corrections will be considered for the steady state case. The results will be extended to the transient case. In the end the results will be compared for a test case in order to assess the assumption of capillary equilibrium.

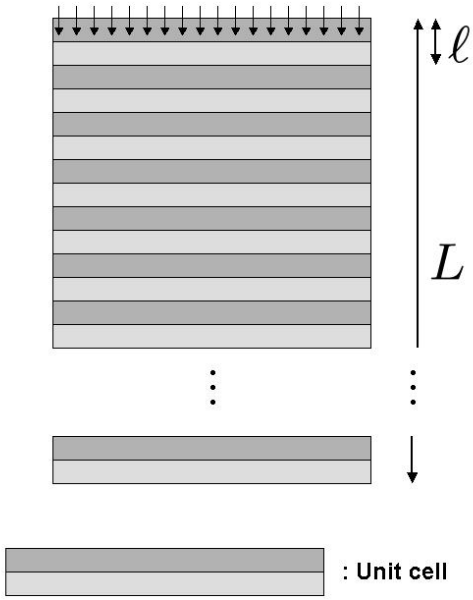

Figure 5.1: Sketch of vertical flow in a layered medium

Small Bond number

The case of small Bond numbers has in principle been discussed in the last section. In case that the Bond number is of order $Bo \propto \varepsilon^0$, the pressure head gradient term and the gravity term balance each other on the large scale. The capillary term and the gravity term in the dimensionless Richards equation (5.10) are then of the same order. The highest order terms in the dimensionless Richards equation (5.10) are of the order ε^{-2}. Collecting all terms of this order yields

$$\frac{\partial}{\partial \hat{Y}} q^{(-1)} = \frac{\partial}{\partial \hat{Y}} \left(\kappa k_r^{(0)} Bo^{-1} \frac{\partial}{\partial \hat{Y}} h^{(0)} \right) = 0. \tag{5.34}$$

Space gradients are here meant in vertical direction. This equation can therefore only be fulfilled if the zeroth order $h^{(0)}$ does not depend on the small scale $\hat{Y}$ and the leading order flux $q^{(-1)}$ vanishes,

$$h^{(0)} = h^{(0)}(\hat{X}, t), \qquad q^{(-1)} = 0. \tag{5.35}$$

For a finite value of $q^{(-1)}$ the pressure head $h^{(0)}$ could only be $\hat{Y}$-periodic if there was a pressure head gradient with positive sign in the first part of the unit cell and a pressure head gradient with a negative sign in the other part. This would lead to a change of sign of the flux $q^{(-1)}$, which is a contradiction to (5.34).
The next higher order of ε in the dimensionless Richards equation (5.10) is the order ε^{-1}. Collecting all terms of this order yields

$$\frac{\partial}{\partial \hat{Y}} q^{(0)} + \frac{\partial}{\partial \hat{X}} q^{(-1)} = \frac{\partial}{\partial \hat{Y}} q^{(0)} = -\frac{\partial}{\partial \hat{Y}} \kappa k_r^{(0)} \left[Bo^{-1} \left(\frac{\partial}{\partial \hat{X}} h^{(0)} + \frac{\partial}{\partial \hat{Y}} h^{(1)} \right) + 1 \right] = 0. \tag{5.36}$$

Considering that $h^{(1)}$ is continuous and $\hat{Y}$-periodic, this equation is solved by (assuming a unit cell from $\hat{Y} = 0$ to $\hat{Y} = 1$)

$$h^{(1)} = Bo^{-1} \left(\frac{\int_0^{\hat{Y}} \left(\kappa k_r^{(0)} \right)^{-1} d\hat{Y}'}{\int_0^1 \left(\kappa k_r^{(0)} \right)^{-1} d\hat{Y}'} - \hat{Y} \right) \left(Bo^{-1} \frac{\partial}{\partial \hat{X}} h^{(0)} + 1 \right) + C, \tag{5.37}$$

C being an arbitrary constant of integration. The flux $q^{(0)}$ is then

$$q^{(0)}(\hat{X}, t) = -\left(\int_0^1 \left(\kappa k_r^{(0)} \right)^{-1} d\hat{Y} \right)^{-1} \left(Bo^{-1} \frac{\partial}{\partial \hat{X}} h^{(0)} + 1 \right) \tag{5.38}$$

The upscaled Richards equation is now obtained by spatially averaging the terms of order ε^0 in the dimensionless Richards equation (5.10) over the unit cell.

$$\langle \mathscr{C}^{(0)} \rangle \frac{\partial h^{(0)}}{\partial t} - \frac{\partial}{\partial \hat{X}} \langle \left(\kappa k_r^{(0)} \right)^{-1} \rangle^{-1} \left(Bo^{-1} \frac{\partial}{\partial \hat{X}} h^{(0)} + 1 \right) = 0. \tag{5.39}$$

The effective unsaturated conductivity function for a specified value of $h^{(0)}$ is the harmonic mean of the local unsaturated conductivity function, $\kappa k_r^{(0)}$. By calculating these functions for a range of pressure head values, an effective moisture capacity and an effective relative permeability function can be determined.
For the vertical flow case no anisotropic conductivity tensor as Yeh et al. (1985) or Mantoglou and Gelhar (1987a) is obtained. However, if a general flow scenario for a two-dimensional layered medium would be considered, an anisotropic unsaturated conductivity would be obtained, namely the harmonic and the arithmetic mean of the local values for the vertical and horizontal entry. To compare the results to results of stochastic theory we could also assume that the parameter values are uncertain and lognormally distributed. The volume average over the unit cell is then replaced by an average over the ensemble. The local periodicity of the variables and parameters would be replaced by requiring local stationarity for the averaged quantities. Assuming e.g. a Russo-Gardener model (Gardner, 1958; Russo, 1988), as often done in stochastic theory, the relative permeability would be given as

$$k_r^{(0)} = k_r(h^{(0)}) = \exp\left(\alpha h^{(0)} \right). \tag{5.40}$$

α is a heterogeneous parameter. The arithmetic mean of the total unsaturated conductivity would then be

$$\langle \kappa k_r^{(0)} \rangle_{\text{arith}} = \int\int \kappa \exp\left(\alpha h^{(0)}\right) \mathscr{P}(\alpha,\kappa) d\alpha d\kappa. \tag{5.41}$$

$\mathscr{P}(\alpha,\kappa)$ is the bivariate probability distribution of α and κ. Depending on whether these parameters are assumed to be uncorrelated or perfectly correlated the result would differ. The harmonic mean would be

$$\langle \kappa k_r^{(0)} \rangle_{\text{harm}} = \left[\int\int \kappa^{-1} \exp\left(-\alpha h^{(0)}\right) \mathscr{P}(\alpha,\kappa) d\alpha d\kappa\right]^{-1}. \tag{5.42}$$

The conductivity would clearly be anisotropic, with a different anisotropy ratio as that of the saturated conductivity field. The results (5.41) and (5.42) for lognormal distribution of the parameters can to the best of our knowledge not be calculated analytically. If α is assumed to be normally distributed and α and κ are treated as independent parameters, (5.41) and (5.42) yield the same result as that of Yeh et al. (1985) (see eq. 4.5.22 in the book of Gelhar (1993)) if all large scale gradients in their result are neglected.
Contrary to the results of Yeh et al. (1985) we do not obtain a dependence of the effective parameters on the large scale head gradients. This is due to the demand of scale separation and capillary equilibrium, which leads to a total decoupling of large scale and small scale. If capillary forces do not dominate on the small scale this would be different. Here, it becomes clear that by restricting the problem to a certain flow regime with the dimensionless numbers and by the demand of scale separation, the results are not as general as the results obtained with stochastic theory. However, their validity is clearly defined and in this range the results can be calculated in an easier way.

Strongly gravity dominated flow

If pressure head differences are very low, it may be that the Bond number scales as ε^{-2}. However, as capillary forces are here neglected completely, the pressure head is no longer continuous on the small scale. This is questionable from a physical point of view.
The possibility of a discontinuous pressure head in the solution can be seen from the highest order equation. Using again a rescaled Bond number

$$Bo \propto \varepsilon^2, \quad Bo = Bo'\varepsilon^2, \quad Bo' \propto \varepsilon^0, \tag{5.43}$$

the highest order of ε in the dimensionless Richards equation (5.10) is the order $\varepsilon = -1$. Collecting all terms of this order yields

$$\frac{\partial}{\partial \hat{Y}} q^{(0)} = \frac{\partial}{\partial \hat{Y}} \left(\kappa k_r^{(0)}\right) = 0. \tag{5.44}$$

Here, capillary forces have in leading order no influence on the flow at all. The flow is directed only vertically, as it is also on the small scale dominated by gravity forces. The

solution for the local problem (5.44) can be determined for a given model straight away. The solution is simply

$$\vec{q}^{(0)} = \vec{q}^{(0)}(\hat{(}X),t)\vec{e}_z = \kappa k_r^{(0)}\vec{e}_z. \tag{5.45}$$

For a given model $k_r(h)$ this equation can with a given value for the flux $q^{(0)}$ be solved for $h^{(0)}$:

$$h^{(0)} = \mathrm{inv}k_r\left(\frac{q^{(0)}}{\kappa(\hat{Y})}\right), \tag{5.46}$$

where $\mathrm{inv}k_r$ is the inverse of the relative permeability. As the parameter field is periodic, the solution for $h^{(0)}$ is also periodic. However, if the hydraulic conductivity κ and the entry pressure head h_{entry} are piecewise constant, so is the solution $h^{(0)}$. This is not possible, as the pressure head has to be continuous. From the solution $h^{(0)}$ the saturation $S^{(0)}$ can be derived directly.
The leading order upscaled equation would be again

$$\frac{\partial\langle\Theta^{(0)}\rangle}{\partial t} - \frac{\partial}{\partial\hat{X}}K_{\mathrm{eff}}(\langle h^{(0)}\rangle) = 0, \tag{5.47}$$

where K_{eff} is identical to the constant flux $q^{(0)}$.

Large Bond number - steady state flow

If the Bond number is large, $Bo \propto \varepsilon^{-1}$, the flow is mainly gravity driven. The leading order problem is gravity dominated flow and corresponds to the case with no macroscopic head gradient. In the intermediate case with a small macroscopic head gradient, the Bond number will still be large, but smaller than ε^{-1}. To capture these effects first order corrections of the leading order problem have to be taken into account. The correction terms are of order ε and therefore supposed to be negligible. But for the case of intermediate Bond numbers correction terms which scale with the inverse Bond number will be larger than ε and can be kept. The first order correction leads to (small) corrections, which yields a (small) contribution of the averaged pressure head gradient.
The steady state case will be analyzed first. The results will then be extended to the transient case. The upscaled results will for the steady state case always be compared to those for saturated flow, in order to demonstrate their consistency.
In case of vertical steady state flow, the flux has to be constant in order to fulfill the mass balance equation. The (dimensionless) flow equation is then

$$\kappa k_r(h)\left(Bo^{-1}\frac{\partial}{\partial z}h + 1\right) = -q. \tag{5.48}$$

q was made dimensionless with the harmonic mean of the hydraulic conductivity K_h. In principle it should here rather be compared to the product of K_h and a typical value for the relative permeability.

For the case that the Bond number is of order $Bo \approx \varepsilon^{-1}$, it is convenient to introduce a rescaled Bond number

$$Bo \approx \varepsilon^{-1}, \quad Bo' = \varepsilon^1 Bo, \quad Bo' \approx \varepsilon^0. \tag{5.49}$$

The multiscale expansion for the head and all its functions are performed as explained in (5.13) and (3.8). The space variable is again split into small scale and large scale space variables $\hat{Y}$ and $\hat{X}$, and the space derivative is scaled accordingly (3.5).
If the dimensionless flux q would be small (order ε^n with $n > 0$), this would be a contradiction to the assumption of a large Bond number. The total flux with dimensions is then much smaller than the typical hydraulic conductivity. This requires a large pressure head on the large scale. This case would therefore lead to the capillary equilibrium condition and would be homogenized under these conditions.
The case that the dimensionless flux is very high (order ε^{-n} with $n > 0$), there is also no solution to the problem, as gravity and the typical pressure head gradient on the large scale are not sufficient to drive the flow through the porous medium.

Leading order problem

The only case that is compatible with a Bond number of the order $Bo \propto \varepsilon^{-1}$ is that the flux is of the same order as the typical hydraulic conductivity of the medium ($q = O(\varepsilon^0)$). In this case we get the following equation, collecting all terms of order ε^0,

$$\kappa(z) k_r^{(0)}(h_e, h^{(0)}) \left(Bo'^{-1} \frac{\partial}{\partial \hat{Y}} h^{(0)} + 1 \right) = -q. \tag{5.50}$$

This equation has to be solved numerically. The leading order pressure head $h^{(0)}$ is $\hat{Y}$-periodic and has to be continuous at interfaces. An example for a solution in a unit cell consisting of two layers is shown in Figure 5.2 for three different values of the flux q.

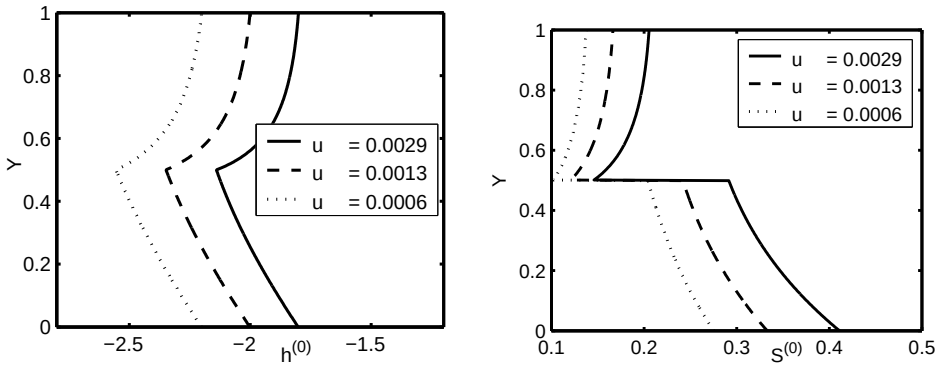

Figure 5.2: Local $h^{(0)}$ and $S^{(0)}$ curve for different values of q. $h^{(0)}$ is made dimensionless with h_h.

The average over (5.50) yields the leading order homogenized equation

$$\langle \frac{1}{\kappa k_r^{(0)}} \rangle^{-1} (\langle h^{(0)} \rangle) = -q. \tag{5.51}$$

This is the gravity dominated flow equation with the harmonic mean of the local hydraulic conductivity as effective conductivity. It is different from the effective conductivity obtained with capillary equilibrium, as $h^{(0)}$ is not locally constant. For a layered medium described with a stochastic approach the upscaled problem would be identical to the gravity dominated limit for the steady state case discussed by many authors (Yeh et al. (1985); Russo (2003); Lu and Zhang (2004) if only vertical gradients are considered or Tartakovsky et al. (1999) among others).

In case of flow under saturated conditions the relative permeability would be one $k_r^{(0)} = 1$. The flux is then completely determined by the harmonic mean of the hydraulic conductivity. The non-averaged zeroth order solution $h^{(0)}$ in a layered medium has then a saw tooth shape.

First order corrections

For the case that the Bond number is in a range $\varepsilon^0 < Bo < \varepsilon^{-1}$, the next order has to be taken into account. In this case the total flux has to be considered as split into

$$q = q^{(0)} + \varepsilon q^{(1)}. \tag{5.52}$$

The equation of order ε reads (taking the leading order equation (5.51) into account)

$$\begin{aligned} \kappa(z) k_r^{(1)} \left(Bo'^{-1} \frac{\partial}{\partial \hat{Y}} h^{(0)} + 1 \right) + Bo'^{-1} \kappa(z) k_r^{(0)} \left(\frac{\partial}{\partial \hat{Y}} h^{(1)} + \frac{\partial}{\partial \hat{X}} h^{(0)} \right) &= -q^{(1)}. \\ \frac{k_r^{(1)}}{k_r^{(0)}} \langle \frac{1}{\kappa k_r^{(0)}} \rangle^{-1} + Bo'^{-1} \kappa(z) k_r^{(0)} \left(\frac{\partial}{\partial \hat{Y}} h^{(1)} + \frac{\partial}{\partial \hat{X}} h^{(0)} \right) &= -q^{(1)}. \end{aligned} \tag{5.53}$$

The first order equation (5.53) has to be solved for $h^{(1)}$.

General solution of $h^{(1)}$

To solve the equation we proceed from the assumption that the solution $h^{(0)}$ depends locally on its average $\langle h^{(0)} \rangle$ (cf. Figure 5.2). This is clearly an assumption, which holds only for layered media. Equation (5.53) can be written as

$$A(\hat{Y}) h^{(1)} + \frac{\partial}{\partial \hat{Y}} h^{(1)} + B(\hat{Y}) = 0, \tag{5.54}$$

with the parameters

$$A(\hat{Y}) = Bo' \frac{1}{\kappa k_r^{(0)}} \langle \frac{1}{\kappa k_r^{(0)}} \rangle^{-1} \left. \frac{d \ln k_r^{(0)}}{dh} \right|_{h=h^{(0)}}$$
$$B(\hat{Y}) = \frac{dh^{(0)}}{d\langle h^{(0)} \rangle} \frac{\partial \langle h^{(0)} \rangle}{\partial \hat{X}} + Bo' \frac{1}{\kappa k_r^{(0)}} \frac{q^{(1)}}{K_0}. \tag{5.55}$$

The first order equation (5.54) is an equation for the first order corrections $h^{(1)}$, which has a decay term. This term is due to the change of the relative permeability $k_r^{(0)}$ if the first order correction of the pressure head is taken into account. As the change of the hydraulic conductivity will cause a change of the leading order head $h^{(0)}$, the first order correction of the head $h^{(1)}$ is dampened. The leading order head gradient on the large scale acts as a source term for small scale gradients of the first order corrections of the head.
For a the single phase flow problem the parameter A would be zero $A = 0$, the relative permeability would be constant $k_r^{(0)} = 1$ and the averaged first order (5.54) equation would reduce to

$$\langle B \rangle = 0 \quad \rightarrow Bo'^{-1} \langle \frac{1}{\kappa} \rangle^{-1} \frac{\partial \langle h^{(0)} \rangle}{\partial \hat{X}} = -q^{(1)}. \tag{5.56}$$

Adding the leading order (5.51) and the first order equation (5.56) would yield

$$\langle \frac{1}{\kappa} \rangle^{-1} \left(Bo^{-1} \frac{\partial \langle h^{(0)} \rangle}{\partial \hat{X}} + 1 \right) = -q^{(0)} - \varepsilon q^{(1)} = -q. \tag{5.57}$$

The flux is mainly driven by gravity with the gradient of the averaged zeroth order pressure head contributing a little. The effective conductivity for both terms is the harmonic mean of the local hydraulic conductivity.
The general solution for equation (5.54) is

$$h^{(1)} = \exp\left(-\int_0^{\hat{Y}} A(\hat{Y}') d\hat{Y}' \right) \left[C - \left[\int_0^{\hat{Y}} \exp\left(\int_0^{\hat{Y}'} A(\hat{Y}'') d\hat{Y}'' \right) B(\hat{Y}') d\hat{Y}' \right] \right]. \tag{5.58}$$

C is a constant of integration. The first order solution $h^{(1)}$ has to be periodic at the boundaries of the unit cell and at the interfaces of layers. Inserting the parameter B into this continuity condition yields an equation for the first order of the flux, which has an undetermined constant of integration C. By averaging equation (5.58), the constant of integration C can be related to the averaged first order pressure head $\langle h^{(1)} \rangle$.

Contribution of higher order terms to the averaged solution

In the expansion of the pressure head (5.13) there is a certain degree of arbitrariness concerning the average of the different orders. The upscaled solution is $\langle h \rangle = \langle h^{(0)} \rangle + \varepsilon \langle h^{(1)} \rangle + \ldots$. It depends on the large scale boundary conditions of the problem, whether

averaged higher order terms contribute to the averaged solution or not. Similar to Mauri (1991) and Mauri (2003) we assume here that the averaged orders higher than the zeroth order do not contribute to the solution. The boundary conditions of the large scale problem should be captured by the averaged zeroth order solution. Therefore, the averaged higher order terms have to vanish at the bottom and at the top boundary. For the special case that the flow is saturated, the averaged higher order terms have then to vanish everywhere, as the solution of (5.57) is correctly obtained by $\langle h^{(0)} \rangle$. A contribution of higher order terms would lead to a wrong result. It would also be possible to set the averaged first order $\langle h^{(1)} \rangle$ to a value non equal to zero. But then the boundary conditions would have to be captured in parts by $\langle h^{(0)} \rangle$ and $\langle h^{(1)} \rangle$, which is not a reasonable approach.
As the single phase flow problem should be contained as a limiting case in the unsaturated flow problem, the same requirement should be applied for the general unsaturated flow problem. This is only one possibility. It could e.g. also be required that the first order saturation vanishes in average, if the boundary conditions are given as saturations. The upscaled problem would then be different. However, the upscaled problem is then not sufficiently described by a model for the leading order $\langle h^{(0)} \rangle$, but an additional model for the first order $\langle h^{(1)} \rangle$ would be needed. It would then make more sense to proceed from a solution for the saturation S instead of a solution for the head h. From requiring that $\langle h^{(1)} \rangle = 0$, the constant of integration C can be derived.

First order terms in the homogenized equation

The procedure to derive the first order equation from the periodicity condition for $h^{(1)}$ and the requirement that the averaged first order term $h^{(1)}$ does not contribute to the solution is lengthy but straightforward.
The periodicity condition for $h^{(1)}$, given by (5.58), leads to

$$C = \frac{\langle \exp\left(\int_0^{\hat{Y}} A(\hat{Y}')d\hat{Y}'\right) B \rangle}{1 - \exp(\langle A \rangle)}. \tag{5.59}$$

If layer boundaries are considered the expression is more complex but in principle similar. Inserting this into the first order solution for $h^{(1)}$ (5.58) and requiring that the average $\langle h^{(1)} \rangle$ vanishes yields

$$\begin{aligned} &\langle \exp\left(-\int_0^{\hat{Y}} A(\hat{Y}')d\hat{Y}'\right)\rangle C = \langle \int_0^{\hat{Y}} \exp\left(\int_0^{\hat{Y}'} A(\hat{Y}'')d\hat{Y}''\right) B(\hat{Y}')d\hat{Y}'\rangle \\ &C = \langle \exp\left(-\int_0^{\hat{Y}} A(\hat{Y}')d\hat{Y}'\right)\rangle^{-1} \langle \int_0^{\hat{Y}} \exp\left(\int_0^{\hat{Y}'} A(\hat{Y}'')d\hat{Y}''\right) B(\hat{Y}')d\hat{Y}'\rangle \end{aligned} \tag{5.60}$$

Inserting the constant of integration C back into (5.59) and inserting B explicitly yields the upscaled problem (5.61).
The resulting first order terms are

$$D_1 \frac{\partial \langle h^{(0)} \rangle}{\partial \hat{X}} = -D_2 q^{(1)} \tag{5.61}$$

with the parameters

$$
\begin{aligned}
D_1 =& (\exp(\langle A\rangle) - 1)\frac{\langle \int_0^{\hat{Y}} \exp\left(\int_0^{\hat{Y}'} A(\hat{Y}'')d\hat{Y}''\right)\frac{dh^{(0)}}{d\langle h^{(0)}\rangle}(\hat{Y}')d\hat{Y}'\rangle}{\langle \exp\left(-\int_0^{\hat{Y}} A(\hat{Y}')d\hat{Y}'\right)\rangle} + \\
& \langle \exp\left(\int_0^{\hat{Y}} A(\hat{Y}')d\hat{Y}'\right)\frac{dh^{(0)}}{d\langle h^{(0)}\rangle}\rangle \\
D_2 =& Bo'\left[(\exp(\langle A\rangle) - 1)\frac{\langle \int_0^{\hat{Y}} \exp\left(\int_0^{\hat{Y}'} A(\hat{Y}'')d\hat{Y}''\right)\frac{1}{\kappa k_r^{(0)}}d\hat{Y}'\rangle}{\langle \exp\left(-\int_0^{\hat{Y}} A(\hat{Y}')d\hat{Y}'\right)\rangle} + \right. \\
& \left. \langle \exp\left(\int_0^{\hat{Y}} A(\hat{Y}')d\hat{Y}'\right)\frac{1}{\kappa k_r^{(0)}}\rangle\right]
\end{aligned}
\tag{5.62}
$$

For the case of single phase flow ($A = 0$ and $k_r^{(0)} = 1$) the parameters simplify to $D_1 = 1$ and $D_2 = Bo'\langle 1/(\kappa)\rangle$. The single phase flow case is thus completely contained in the general unsaturated flow case. The parameters D_1 and D_2 are tedious to calculate, however, the procedure is straightforward once the solution for the zeroth order equation $h^{(0)}$ has been calculated from the leading order problem.
The sum of zeroth order equation and first order equation can therefore be written as

$$
\left[Bo^{-1}\mathscr{K}_c\frac{\partial\langle h^{(0)}\rangle}{\partial\hat{X}} + \mathscr{K}_g\right] = -q^{(0)} - \varepsilon q^{(1)} = -q, \tag{5.63}
$$

with the parameters

$$
\mathscr{K}_g = \langle\frac{1}{\kappa k_r^{(0)}}\rangle^{-1}, \quad \mathscr{K}_c = \frac{D_1}{D_2}Bo'. \tag{5.64}
$$

It has the same shape as the original Richards equation, but with a different gravity and capillary effective conductivity. The conductivity of the capillary term is similar the harmonic mean of the local conductivities, but it is modified due to the coupling between the relative permeability and the first order correction of the pressure head. As the Bond number is still assumed to be large, the capillary contribution in the upscaled equation (5.63) is small.
This analysis was performed for the case that the flow is mainly gravity driven, but has a small correction to the gravity driven part. The transition between this flow regime and the capillary dominated flow regime are in principle not captured with homogenization theory. The results are valid for a strict scaling of the Bond number with the scaling parameter ε. However, the parameters obtained here for the gravity dominated case will in the limit that the Bond number becomes small tend to the capillary dominated results. Equation (5.50) is then dominated by the gradient of the zeroth order pressure head, while the gravity term and the right hand side become small. The zeroth order pressure head becomes thus

locally constant as in the capillary dominated regime. On the other hand the parameter A becomes very small and $dh^{(0)}/d\langle h^{(0)}\rangle \approx 1$ in B. Therefore the deviation between $\mathscr{K}_c$ and $\mathscr{K}_g$ become small. The gravity dominated case contains therefore the capillary dominated case as a limit. This upscaled model can be considered a model which covers both flow regimes, similar to the model discussed in Szymkiewicz and Lewandowska (2006). This is illustrated in Figure 5.3, where the effective conductivity curve for the gravity term and the capillary term for different Bond numbers are shown for an example of a layered medium, parameterized by a Brooks-Corey model (Brooks and Corey, 1966). The local parameters of the different materials are explained in the test case discussed below. The ratios of the conductivities $\mathscr{K}_c$ and $\mathscr{K}_g$ and the effective hydraulic conductivity obtained with capillary equilibrium are shown. With decreasing Bond number the ratio gets close to unity.

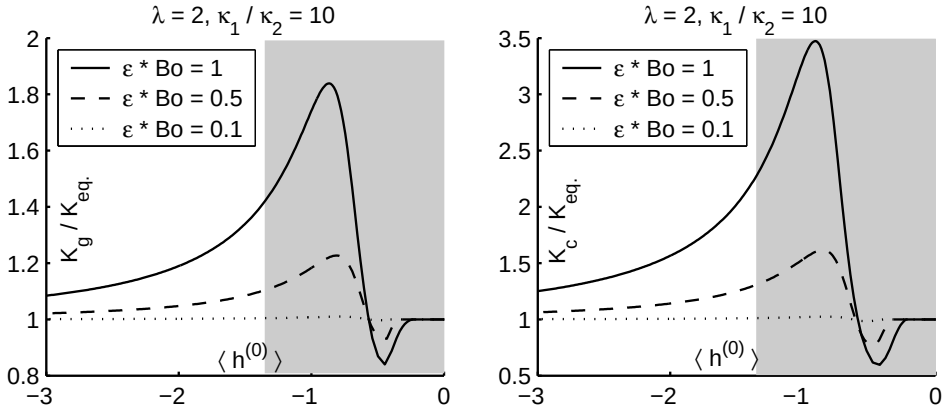

Figure 5.3: Ratio of effective conductivity for large Bond numbers and conductivity obtained with capillary equilibrium. Left: gravity term, right: capillary term. $h^{(0)}$ is made dimensionless with h_h.

First order terms of the effective retention function

It should be mentioned that if the first order in ε is taken into account, the effective retention function will not only depend on the averaged pressure head, but also on its gradient. The averaged water content $\langle\Theta\rangle$ to first order is $\langle\Theta^{(0)}\rangle + \varepsilon\langle\Theta^{(1)}\rangle$

$$\langle\Theta^{(0)}\rangle(\langle h^{(0)}\rangle) + \varepsilon\langle\frac{d\Theta}{dh}\bigg|_{h=h^{(0)}} h^{(1)}\rangle. \tag{5.65}$$

The first order pressure head $h^{(1)}$ depends on the gradient of the averaged zeroth order pressure head $\partial h^{(0)}/\partial\hat{X}$, and therefore the retention function will to first order also depend on the averaged hydraulic gradient.

Large Bond number - Transient flow

The transient case is slightly more complex than the steady state case. The leading order problems are equivalent. The contributions of the next order can be treated similarly as for the steady state case, however, the flux is here not locally constant.
In the transient case the time has to be scaled. As written above, fast processes or small time scales will here not be taken into account and there are two processes which define the two different time scales (cf. (5.25)). The dimensionless equation with all terms to order ε reads

$$\begin{aligned}
&\frac{\partial}{\partial t_1}\left(\Theta^{(0)}+\varepsilon\Theta^{(1)}\right)+\left(\frac{\partial}{\partial \hat{X}}+\frac{1}{\varepsilon}\frac{\partial}{\partial \hat{Y}}\right)\left(q^{(0)}+\varepsilon q^{(1)}\right)=0\\
&q^{(0)}=-\kappa k_r^{(0)}\left(Bo'^{-1}\frac{\partial}{\partial \hat{Y}}h^{(0)}+1\right)\\
&q^{(1)}=-\kappa k_r^{(1)}\left(Bo'^{-1}\frac{\partial}{\partial \hat{Y}}h^{(0)}+1\right)-\kappa k_r^{(0)}Bo'^{-1}\left(\frac{\partial}{\partial \hat{X}}h^{(0)}+\frac{\partial}{\partial \hat{Y}}h^{(1)}\right)
\end{aligned} \tag{5.66}$$

Leading order problem

The highest order equation is of order ε^{-1},

$$\frac{\partial}{\partial \hat{Y}}q^{(0)}=0 \quad \rightarrow q^{(0)}=q^{(0)}(\hat{X},t_1,t_2). \tag{5.67}$$

This problem is identical to the steady state problem (5.50). The problem has in general to be solved for $h^{(0)}$ numerically. The flux $q^{(0)}$ is solved by (5.51). The highest order upscaled problem is the average over the terms of order ε^0

$$\frac{\partial\langle\Theta^{(0)}\rangle}{\partial t_1}+\frac{\partial}{\partial \hat{X}}q^{(0)}=\frac{\partial\langle\Theta^{(0)}\rangle}{\partial t_1}-\langle\frac{1}{\kappa k_r^{(0)}}\rangle^{-1}(\langle h^{(0)}\rangle)=0. \tag{5.68}$$

This is in principle the same leading order problem as obtained for the steady state. The leading order term of the effective retention function $\langle\Theta^{(0)}\rangle$ is obtained by calculating the local retention function $\Theta(h^{(0)})$ from the solution $h^{(0)}(\hat{Y})$ for a given $\langle h^{(0)}\rangle$ and averaging it over the unit cell.

First order corrections

If the Bond number is large, but smaller than ε^{-1}, the first order corrections have to be taken into account. The upscaled problem is derived by adding to (5.68) the average over the next order, ε^1. This yields

$$\frac{\partial\langle\Theta^{(0)}\rangle}{\partial t_2}+\frac{\partial\langle\Theta^{(1)}\rangle}{\partial t_1}+\frac{\partial}{\partial \hat{X}}\langle q^{(1)}\rangle=0 \tag{5.69}$$

A solution for the flux $\langle q^{(1)} \rangle$ can be obtained by subtracting the averaged zeroth order equation (5.69) from the non-averaged zeroth order equation.

$$\frac{\partial(\Theta^{(0)} - \langle \Theta^{(0)} \rangle)}{\partial t_1} + \frac{\partial}{\partial \hat{Y}} q^{(1)} = \frac{\partial \tilde{\Theta}^{(0)}}{\partial t_1} + \frac{\partial}{\partial \hat{Y}} q^{(1)} = 0. \tag{5.70}$$

There is a local variability of the first order flux due to the local change of the water content with time. In this way the problem differs from the steady state problem. In a layered medium it is a reasonable assumption that $\tilde{\Theta}^{(0)}$ (the deviation of $\Theta^{(0)}$ from the mean $\langle \Theta^{(0)} \rangle$) depends at each location $\hat{Y}$ uniquely on the mean $\langle \Theta^{(0)} \rangle$ (see also the example shown in Figure 5.2). The problem can then be solved in almost the same way as the steady state case.
The equation (5.70) can be written as

$$\frac{d\tilde{\Theta}^{(0)}}{d\langle \Theta^{(0)} \rangle} \frac{\partial \langle \Theta^{(0)} \rangle}{\partial t_1} + \frac{\partial}{\partial \hat{Y}} u^{(1)} = 0. \tag{5.71}$$

Integrating the equation yields

$$\int_0^{\hat{Y}} \frac{d\tilde{\Theta}^{(0)}}{d\langle \Theta^{(0)} \rangle}(\hat{Y}') d\hat{Y}' \frac{\partial \langle \Theta^{(0)} \rangle}{\partial t_1} = u^{(1)}(\hat{Y}) - u^{(1)}(\hat{Y} = 0). \tag{5.72}$$

The averaged flux $\langle u^{(1)} \rangle$ is thus

$$\langle u^{(1)} \rangle = u^{(1)}(\hat{Y} = 0) + \langle \int_0^{\hat{Y}} \frac{d\tilde{\Theta}^{(0)}}{d\langle \Theta^{(0)} \rangle}(\hat{Y}') d\hat{Y}' \rangle \frac{\partial \langle \Theta^{(0)} \rangle}{\partial t_1} \tag{5.73}$$

The constant of integration $u^{(1)}(\hat{Y} = 0)$ has to be obtained by solving (5.70). By inserting the first order flux (5.66) this equation has the same shape as the steady state problem (5.54). The variable B has an additional term compared to the steady state problem, which is due to the coupling of the saturation change with time to the flux. The parameter B reads then

$$B(\hat{Y}) = \frac{dh^{(0)}}{d\langle h^{(0)} \rangle} \frac{\partial \langle h^{(0)} \rangle}{\partial \hat{X}} + Bo' \frac{1}{\kappa k_r^{(0)}} u^{(1)}(\hat{Y} = 0) + Bo' \frac{1}{\kappa k_r^{(0)}} \int_0^{\hat{Y}} \frac{d\tilde{\Theta}^{(0)}}{d\langle \Theta^{(0)} \rangle}(\hat{Y}') d\hat{Y}' \frac{\partial \langle \Theta^{(0)} \rangle}{\partial t_1} \tag{5.74}$$

To solve the constant of integration $u^{(1)}(\hat{Y} = 0)$, the same procedure as for the steady state flow problem can be applied, using the changed B value. The same condition $\langle h^{(1)} \rangle = 0$ will be used as the boundary conditions for the large scale problem are supposed to be captured in the zeroth order $\langle h^{(0)} \rangle$.
Going through all steps as in the steady state problem we end up again with a system such as (5.61), just in this case it reads

$$D_1 \frac{\partial \langle h^{(0)} \rangle}{\partial \hat{X}} + D_3 \frac{\partial \langle \Theta^{(0)} \rangle}{\partial t_1} = -D_2 u^{(1)}(\hat{Y} = 0). \tag{5.75}$$

The parameters D_1 and D_2 are the same as for the steady state case (5.62). The parameter D_3 is given by (5.78).
This leads to the following expression for $\langle q^{(1)} \rangle$

$$\langle q^{(1)} \rangle = -\mathscr{K}_c \frac{\partial \langle h^{(0)} \rangle}{\partial \hat{X}} - \mathscr{R} \frac{\partial \langle \Theta^{(0)} \rangle}{\partial t_1}. \tag{5.76}$$

with

$$\mathscr{K}_c = \frac{D_1}{D_2}, \mathscr{R} = \frac{D_3}{D_2} - \langle \int_0^{\hat{Y}} \frac{d\tilde{\Theta}^{(0)}}{d\langle \Theta^{(0)} \rangle}(\hat{Y}') d\hat{Y}' \rangle. \tag{5.77}$$

The parameters D_2 and D_1 are the same as for steady state flow (5.62), while D_3 is

$$\begin{aligned} D_3 = Bo' \Bigg[(\exp(\langle A \rangle) - 1) \frac{\langle \int_0^{\hat{Y}} \exp\left(\int_0^{\hat{Y}'} A(\hat{Y}'') d\hat{Y}'' \right) \int_0^{\hat{Y}'} \frac{d\tilde{\Theta}^{(0)}(\hat{Y}'')}{d\langle \Theta^{(0)} \rangle} d\hat{Y}'' d\hat{Y}' \rangle}{\langle \exp\left(- \int_0^{\hat{Y}} A(\hat{Y}') d\hat{Y}' \right) \rangle} + \\ \langle \exp\left(\int_0^{\hat{Y}} A(\hat{Y}') d\hat{Y}' \right) \int_0^{\hat{Y}} \frac{d\tilde{\Theta}^{(0)}}{d\langle \Theta^{(0)} \rangle} d\hat{Y}' \rangle \Bigg] \end{aligned} \tag{5.78}$$

The effective conductivity is the same as for the steady state case. The averaged first order flux has a coupling term for the pressure head gradient and the time derivative of the mean water content. Inserting the averaged flux into the first order equation, the upscaled Richards equation is

$$\frac{\partial \langle \Theta^{(0)} \rangle + \varepsilon \langle \Theta^{(1)} \rangle}{\partial t} + \varepsilon \frac{\partial}{\partial \hat{X}} \mathscr{R} \frac{\partial \langle \Theta^{(0)} \rangle}{\partial t_1} - \frac{\partial}{\partial \hat{X}} \left[Bo^{-1} \mathscr{K}_c(\langle h^{(0)} \rangle) \frac{\partial}{\partial \hat{X}} \langle h^{(0)} \rangle + \mathscr{K}_g(\langle h^{(0)} \rangle) \right] = 0. \tag{5.79}$$

The coupling between gradient and time derivative is not only due to the upscaled flux, but also due to the time derivative of the first order of the water content. As in the steady state case, the first order $\langle \Theta^{(1)} \rangle$ in ε depends not only on the averaged pressure head, but also on its gradient. This will also lead to a mixed time and space derivative term.
The mixed terms are however not crucial if the scales are well separated (meaning that $\varepsilon << 1$), as they appear explicitly as proportional to ε. The parameter ε is still supposed to be small and therefore negligible. However, it becomes also visible that in case that the scales are not so well separated and ε becomes larger, the upscaled model has no longer the form of Richards equation.
The point of considering the first order terms was that the capillary term scales with ε, but it is proportional to the inverse Bond number. If the Bond number decreases these terms get large and therefore only the capillary term should be kept. Neglecting the first order terms in the time derivative of the water content but keeping the capillary term leads to an equation which has the same shape as the Richards equation, but it has different conductivity functions for the capillary and the gravity term. These functions are identical to the curves for the steady state case.

Test case

As the local problem in the gravity dominated case is nonlinear, analytic results cannot be obtained or approximated in a useful way. In order to assess the differences between the upscaled parameters for the gravity and capillary dominated regimes, the effective conductivity and retention functions are compared with numerical simulations.
In the following the results obtained for a simple Brooks-Corey model (cf. Brooks and Corey, 1966) will be shown. The medium is assumed to be composed of two different soil types, each of which has a volume percentage $\phi_1 = \phi_2 = 0.5$ and an conductivity κ_i. We assume that the entry head h_{entr} is related to the saturated conductivity via a scaling condition for Miller similar media (Miller and Miller, 1956; Sposito and Jury, 1990)

$$h_{\text{entry}} = \frac{C}{\sqrt{\kappa}} \tag{5.80}$$

where C is a constant, which will here for convenience be chosen as $C = 1$. The local unsaturated hydraulic conductivity is described as

$$\kappa k_r = \begin{cases} \kappa \left(\dfrac{h_{\text{entr}}}{h}\right)^{(3\lambda+2)} = \left(\dfrac{1}{h}\right)^{(3\lambda+2)} \left(\dfrac{1}{\kappa}\right)^{(3/2\lambda)} & \text{if} \quad |h| > |h_{\text{entr}}| \\ 1 & \text{otherwise} \end{cases} \tag{5.81}$$

λ is the Brooks-Corey coefficient. The water saturation is

$$S = \begin{cases} \left(\dfrac{h_{\text{entr}}}{h}\right)^{\lambda} = \left(\dfrac{1}{h}\right)^{\lambda} \left(\dfrac{1}{\kappa}\right)^{1/2\lambda} & \text{if} \quad |h| > |h_{\text{entr}}| \\ 1 & \text{otherwise} \end{cases} \tag{5.82}$$

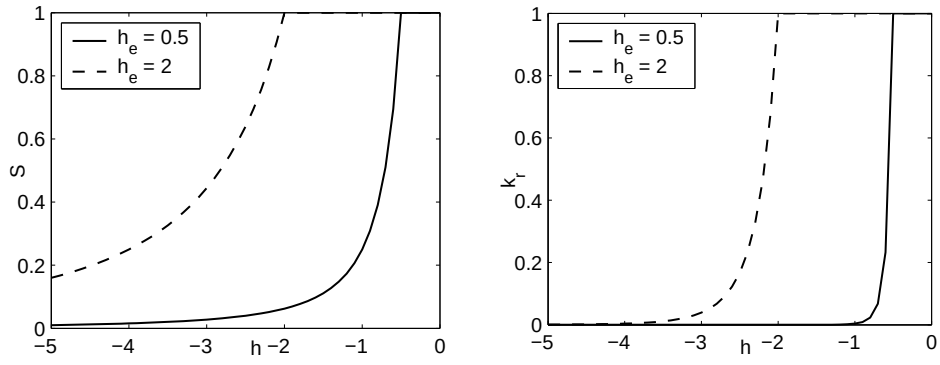

Figure 5.4: Examples for a saturation - head and relative permeability - head relation with the Brooks-Corey model (in both cases the parameter λ equals $\lambda = 2$).

Small Bond number

For the case that the Bond number is of order ε^0 the effective curves can be determined straight away. The parameter κ_1 is used here as the smaller hydraulic conductivity ($\kappa_1 <$

κ_2). The effective water content is the average of the local water content curves at a given pressure head $h^{(0)}$,

$$\Theta_{\text{eff}} = n_f \langle S^{(0)} \rangle =$$
$$n_f \begin{cases} \frac{1}{2}\left[\left(\frac{1}{h^{(0)}}\right)^{\lambda_1}\left(\frac{1}{\kappa_1}\right)^{1/2\lambda_1} + \left(\frac{1}{h^{(0)}}\right)^{\lambda_2}\left(\frac{1}{\kappa_2}\right)^{1/2\lambda_2}\right] & \text{if } \left|h^{(0)}\right| > \frac{1}{\kappa_1} \\ \left[\frac{1}{2} + \left(\frac{1}{h^{(0)}}\right)^{\lambda_2}\frac{1}{2}\left(\frac{1}{\kappa_2}\right)^{1/2\lambda_2}\right] & \text{if } \frac{1}{\kappa_1} > \left|h^{(0)}\right| > \frac{1}{\kappa_2} \\ 1 & \text{otherwise} \end{cases} \tag{5.83}$$

The effective conductivity is the harmonic average of the local unsaturated conductivities at a given pressure head $h^{(0)}$,

$$k_{\text{eff}} = \langle \frac{1}{\kappa k_r^{(0)}} \rangle^{-1} =$$
$$\begin{cases} 2\left[\left(h^{(0)}\right)^{(3\lambda_1+2)}(\kappa_1)^{(3/2\lambda_1)} + \left(h^{(0)}\right)^{(3\lambda_2+2)}(\kappa_2)^{(3/2\lambda_2)}\right]^{-1} & \text{if } \left|h^{(0)}\right| > \frac{1}{\kappa_1} \\ 2\left[\kappa_1^{-1} + \left(h^{(0)}\right)^{(3\lambda_2+2)}\kappa_2^{(3/2\lambda_2)}\right]^{-1} & \text{if } \frac{1}{\kappa_1} > \left|h^{(0)}\right| > \frac{1}{\kappa_2} \\ 2\left[\kappa_1^{-1} + \kappa_2^{-1}\right]^{-1} & \text{otherwise.} \end{cases} \tag{5.84}$$

As in Richards equation the air is always assumed to be mobile, the situation can occur that some cells are completely water saturated while other cells inbetween are partly drained. This is physically not possible, as the air cannot move into the cells which are inbetween completely saturated cells. The intermediate situation in (5.83) and (5.84) can in reality not occur and should be omitted.

Large Bond number

For the case that the Bond number scales as ε^{-1}, the effective parameter functions cannot be obtained analytically, but have to be calculated numerically. We used here the same two-layer medium as described above, with the same λ-value for both layers. The auxiliary equation (5.50) is solved on a grid, where the unit cell is discretized into 600 grid cells. The equation (5.69) with periodic boundary conditions is solved using Newton-Raphson iterations (as described in Press et al. (1988)) until a relative accuracy of 10^{-10} for the pressure head $h^{(0)}$ is obtained. The Jacobian matrix of the discretized auxiliary equation (5.69) is calculated analytically, where the conductivity for the flow over the interface between two grid cells is assumed to be the harmonic mean. The equation is solved using a biconjugate gradient solver. Note that as the equation is dimensionless, no dimensions for the grid length etc. are required.

Comparison of effective curves

To compare two extreme cases for the effective parameter functions we compared the effective unsaturated hydraulic conductivity curves and pressure head-saturation curves for the case that the material in the two layers is very well and not so well sorted, so that the λ-parameter in the Brooks-Corey model is high or moderate. We chose here a parameter $\lambda = 4$ and $\lambda = 2$. We then considered for these two values the case that the contrast of the conductivities is small, represented by a ratio $\kappa_1/\kappa_2 = 2$. As the other extreme we considered a ratio $\kappa_1/\kappa_2 = 10$. The Bond number Bo is chosen as $Bo = 1$ and $Bo = \varepsilon^{-1}$. The effective conductivity curves for the four resulting cases are shown in Figure 5.5. The plots show five effective conductivity curves. Two of them are the capillary and the gravity term for the case of large Bond numbers, one is the hydraulic conductivity for the case of small Bond numbers and two are the hydraulic conductivity curves of the single layers.

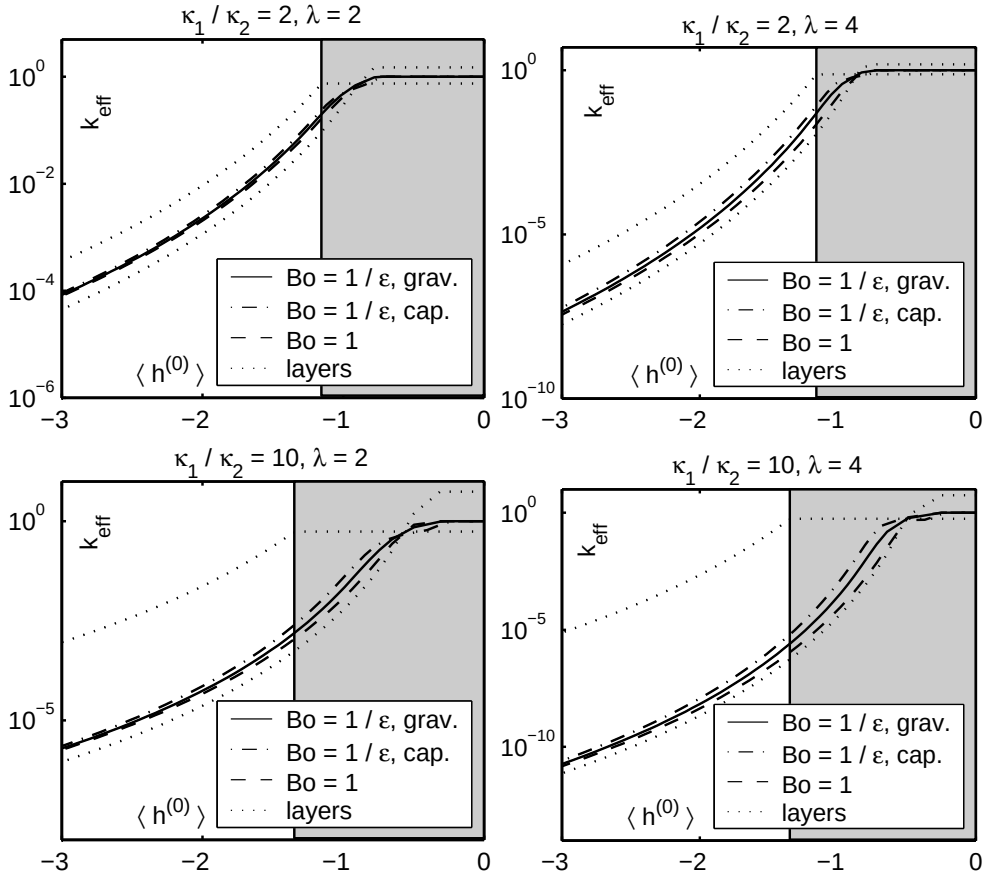

Figure 5.5: Effective conductivity curve for different soil parameters. $h^{(0)}$ is made dimensionless with h_h and K is made dimensionless with K_h. For all four cases two different Bond numbers are considered, $Bo = 1$ and $Bo = \varepsilon^{-1}$.

The domain with the gray background in the plots corresponds to the situation that parts of

material are drained, which are inbetween completely saturated material. This is unrealistic as the air has no access to these cells. The values in the area with the gray background should therefore rather be equal to the totally saturated values.

For the moderately sorted materials ($\lambda = 2$) we find that the effective conductivity curves for the case of small and large Bond number are not that different. It should also be mentioned here that $\lambda = 2$ is not a small value, but would probably already be considered quite high. The curves lie inbetween the effective permeability curves of the single layers and are closer to the smaller values. This is reasonable, as due to the layering we get an harmonic average, which gets a stronger weighted contribution from smaller values. For well sorted materials ($\lambda = 4$) we find that the effective curves for the different Bond numbers differ more than in the former case ($\lambda = 2$). However, $\lambda = 4$ can be considered very high. The highest deviation between K_{eff} for $Bo \propto \varepsilon^0$ and $\mathscr{K}_G$ for $Bo \propto \varepsilon^{-1}$ is found at high hydraulic pressure heads (that is small absolute value of the pressure heads). For $\lambda = 2$ the largest deviation, defined as

$$\Delta_{\mathscr{K}} = \frac{2\sqrt{(\mathscr{K}_1 - \mathscr{K}_2)^2}}{\mathscr{K}_1 + \mathscr{K}_2}, \tag{5.85}$$

is $\Delta_{\mathscr{K}} = 0.2$ for $\kappa_1/\kappa_2 = 2$ and $\Delta_{\mathscr{K}} = 0.6$ for $\kappa_1/\kappa_2 = 10$. For $\lambda = 4$ the largest deviation is $\Delta_{\mathscr{K}} = 0.7$ for $\kappa_1/\kappa_2 = 2$ and $\Delta_{\mathscr{K}} = 1.4$ for $\kappa_1/\kappa_2 = 10$.

The effective parameter curves can be obtained without much computational effort for the capillary dominated case, while in the case that gravity forces have an impact on the small scale the effective curves need to be calculated numerically. As the differences between the effective curves are not that big for small values of λ, the result of the capillary equilibrium approach is a good estimate for the effective parameter curves, also for the case of large Bond numbers. If the materials are well sorted, the results will show larger differences. However, also here the deviations between the effective parameters are moderate.

If large Bond numbers are considered, the effective conductivity curve for the capillary term differs from that for the gravity term. The difference is more pronounced if the parameter contrast is high. However, for large Bond numbers the capillary term is only a term of order ε in the equation and will therefore not have a large impact on the whole equation.

The effective saturation-capillary head curves are shown in Figure 5.6.

The plots show the curves for small and large Bond numbers. Differences between the two curves are only significant in case that the λ-parameter and the parameter contrast are high at the same time. It is clear that the water content is not so sensitive to the different head configurations ($h^{(0)}$ constant for small Bond numbers and $h^{(0)}$ $\hat{Y}$-dependent for large Bond numbers), as the water content is calculated as the arithmetic mean of the local water content distribution. The effective conductivity is more sensitive, as it can be considered an harmonic mean of the local values, which is much more influenced by extreme values.

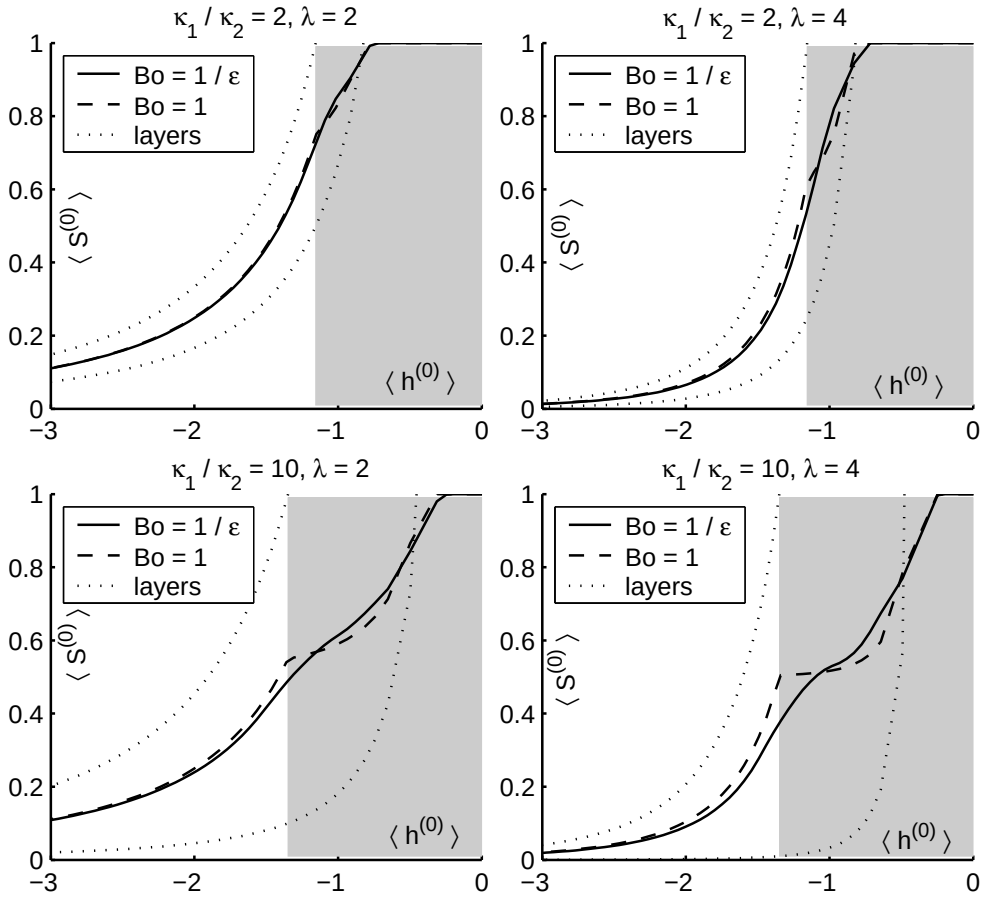

Figure 5.6: Effective capillary pressure head curve for different soil parameters. $h^{(0)}$ is made dimensionless with h_h.

5.2.4 Summary of the upscaled models

The upscaled models obtained for both small and large Bond numbers have the same shape as the original Richards equation. For vertical flow in a layered medium intermediate Bond numbers can also be considered. If the Bond number is high, but significantly smaller than ε^{-1}, the problem is treated as gravity dominated, but first order correction terms are taken into account. The point of considering the first order terms was that the capillary term scales with ε, but it is proportional to the inverse Bond number. If the Bond number decreases these terms get large and therefore only the capillary term should be kept. For the steady state case that leads to an upscaled problem, which has the same shape as Richards equation, but has different hydraulic conductivity curves for the gravity and the capillary term. The effective retention function to first order does not only depend on the mean head, but also on the mean head gradient. For the transient problem the homogenized problem has an additional term to the Richards equation, which couples time derivatives and head gradients. However, if only higher order correction terms are kept

which scale with the inverse Bond number, these coupling terms disappear. The gravity and capillary term have the same effective conductivity curves as in the steady state problem. It has however been demonstrated that the upscaled problem for small Bond numbers is obtained as a limit from the problem for large Bond numbers.

It has to be made clear that the equations are only valid for slow flow processes. This assumption is inherently made by the choice of the typical time scales. We considered here only large time scales, associated with the large length scale. Therefore, effects related to the small scale dynamics of the flow are not to be expected to have an effect on the upscaled equations. That is, the upscaled models might be applied to flow problems such as e.g. multistep outflow experimens with small pressure head steps or flow in the unsaturated zone with a slow change of inflow over time. However, flow problems such as e.g. single step outflow experiments with a high pressure head step cannot be expected to be described well with the upscaled models derived here, as dynamic effects, which are not taken into account here, will become important.

The effective parameter curves for the case of strong capillary forces can be derived in a simple procedure. The pressure head can be considered locally constant. This is equivalent to the capillary equilibrium condition, which is often applied in practice. The moisture capacity derived with this condition is an arithmetic mean of local moisture capacity functions while the effective relative permeability is obtained from the local problem based on the local conductivities. The local functions are obtained straightforward from the small scale constitutive relationships. For the case of weaker capillary forces the effective parameter functions are no longer that simple. First, the effective conductivity curve for the capillary term is not the same as that for the gravity term in the upscaled Richards equation. Second, the local parameters are solutions of nonlinear equations that have to be solved numerically.

Comparing the results of four test cases in layered media lead to the conclusion that the difference between the results for the two flow regimes becomes significant only if the materials of the layers are well sorted (meaning the capillary pressure head-water content relation has to have a small slope at intermediate water contents), and even then they are moderate. The heterogeneity of the material properties overrules the local fluctuations of the pressure head due to the balance of gravity and capillary forces at large Bond numbers. The layered medium flow can here be considered to be the extreme case, as the heterogeneity is in the direction of gravity. This implies that the effective curves obtained with a capillary equilibrium assumption are often good approximations.

If, for example, a slow flow process in the unsaturated zone is considered, where a slowly changing constant flux is applied to the soil surface and the water content at a given depth is fixed by the groundwater table, the effective model for this process could be derived using the capillary equilibrium model. It might be that the influx is quite high, in which case the typical pressure head gradient would be small compared to the length scale of the thickness of the unsaturated zone. The finding of this section is, that the error made by assuming capillary equilibrium conditions (although the prerequisits are not fulfilled) would be small.

5.3 Prediction of effective parameters and influence of structure

The influence of the soil structure on the upscaled model is discussed in this section. The upscaled model for the capillary equilibrium case is considered only, as it allows to derive results analytically and it has been discussed in Section 5.2.4 that capillary equilibrium is also a good approximation for the case of large Bond numbers.

Once the small scale parameter distribution in the medium is known, the effective parameters for the upscaled models derived in the last section can be determined. However, the detailed parameter distribution is mostly not known. It is therefore important to characterize heterogeneity in an efficient way. The next point is then to incorporate the characterization of heterogeneity into the upscaled models.

In Chapter 2 it was discussed that different concepts are applied to characterize heterogeneity. The fields can be assumed to be random with a Gaussian distribution, which is described by its second order stochastic properties. For the capillary equilibrium approach effective parameters can be calculated in a stochastic framework quite well. However, if the fields are non-Gaussian, a characterization of heterogeneity which uses information about connected phases could be more efficient to determine the upscaled model. The question of non-Gaussian fields is very important, as channeling of flow along preferential flow paths is a phenomenon often observed in the field (Forrer et al., 1999; Roth et al., 1991). Channeling can occur in Gaussian fields for certain saturation distributions, as has been shown by Birkhoelzer and Tsang (1997). However, evidence from field data is rather that channels are alreday present in the structure of the soil parameters.

The first part of this section is dedicated to the stochastic description of the heterogeneous field, as presented in Neuweiler and Cirpka (2005). The second part addresses the question how effective parameter curves can be derived if the fields are clearly non-Gaussian and have connected structures at extreme values, as presented in Neuweiler and Vogel (2007).

5.3.1 Stochastic averages for Gaussian fields

The parameters for the upscaled model derived in the last section (5.2) for small Bond numbers will now be calculated, assuming that the parameters are unknown and described by correlated random fields. As outlined in Section 2, homogenization theory is usually formulated for parameter fields with distinct parts of material, where the properties inside of one part are constant. However, this is not a necessary requirement and we can also consider the parameter fields to be continuous. In a stochastic framework, we consider these fields as outcome of a random process with known statistical parameters. For a sufficiently large unit cell, the ergodicity assumption holds and we may replace volume averages by ensemble averages. For a smaller unit cell, the ensemble-averaged quantities are only the expected values of the volume-averaged ones; the deviation of the volume average of an actual realization from the ensemble average could still be large.

Heterogeneous parameter field

The upscaled model for the flow is given by (5.21), with the effective moisture capacity function (5.22), the effective source term (5.23) and the effective conductivity (5.24). A heterogeneous medium is considered, where the hydraulic conductivity and the entry pressure head are heterogeneously distributed, while all other parameters are constant. The hydraulic conductivity is parametrized as (5.5) and the entry pressure head as (5.7). The heterogeneous parameters in the system are thus f_k, which is normally distributed and f_h, which will later be related to the parameter f_k. The parameter f_k appears in the hydraulic conductivity, while the parameter f_h appears in the constitutive relations $k_r = k_r(f_h, h), \mathscr{C} = \mathscr{C}(f_h, h)$. The total conductivity depends thus on both parameters.
The field of the log-hydraulic conductivity fluctuations f_k is assumed to be isotropic. The ensemble-averaged effective parameter functions and stochastic properties of the fields can be calculated using perturbation approximations. As the perturbation expansions have to be truncated, this approach is only reasonable if both parameter f_k and f_h have small variances.

Perturbation expansion

For stochastic averaging, it is more practical to derive the upscaled model considering eq. (5.16) for the first-order head $h^{(1)}$ directly, rather than to introduce the auxiliary variable $\vec{\chi}$. Equation (5.16) has two spatial parameters varying on the small scale, the log-hydraulic conductivity f_k and the log-scaling factor of the entry pressure head f_h. The hydraulic conductivity and the relative permeability are expanded as

$$Kk_r = K_g \exp(f_k) k_r(f_h, h^{(0)}) = K_g \left[1 + f_k + \frac{1}{2} f_k^2 + \dots\right] \left[k_r^{(0)}\Big|_{f_h=0} + \frac{dk_r^{(0)}}{df_h}\Big|_{f_h=0} f_h + \dots\right]. \tag{5.86}$$

Substituting the perturbation expansion for the spatially variable parameters into the equation of order ε^{-1}, eq. (5.16), yields:

$$\vec{\nabla}_{\hat{Y}} \cdot \left(k_r^{(0)}\Big|_{f_h=0} \mathscr{P}\left(\hat{X}, \hat{Y}\right) \left(\vec{J} + \vec{\nabla}_{\hat{Y}} h^{(1)}\right)\right) + k_r^{(0)}\Big|_{f_h=0} \nabla_{\hat{Y}}^2 h^{(1)} = 0 \tag{5.87}$$

in which $\mathscr{P}$ denotes the fluctuating terms:

$$\mathscr{P} = \left(f_k + \frac{1}{2} f_k^2 + \dots\right) + \left(k_r^{(0)}\Big|_{f_h=0}\right)^{-1} \left(\frac{dk_r^{(0)}}{df_h}\Big|_{f_h=0} f_h + \dots\right) \left(1 + f_k + \frac{1}{2} f_k^2 + \dots\right) \tag{5.88}$$

Eq. (5.87) can be transformed into the corresponding integral equation as explained in Chapter 3.3.5:

$$h^{(1)}(\hat{\mathbf{X}}, \hat{\mathbf{Y}}) = \int_\Omega G(\hat{\mathbf{Y}}, \hat{\mathbf{Y}}') \vec{\nabla}_{\hat{\mathbf{Y}}'} \cdot \left(\mathscr{P}(\hat{Y}') \left(\vec{J} + \vec{\nabla}_{\hat{Y}'} h^{(1)}(\hat{X}, \hat{Y}')\right)\right) d\hat{Y}' \tag{5.89}$$

which is recursive. G is the Green's function solving $\vec{\nabla}^2_{\hat{Y}} G = \delta(\hat{Y} - \hat{Y}')$. In a two-dimensional, infinite domain it is given by $G = 1/(2\pi)\ln(|\hat{Y} - \hat{Y}'|)$. Assuming periodicity of the field may cause slight deviations.
The zeroth order-equation, eq. (5.17), reads now:

$$\langle \mathscr{C}^{(0)} \rangle \frac{\partial h^{(0)}}{\partial t} + \vec{\nabla}_{\hat{X}} \cdot \left(\langle \exp(f_k) k_r^{(0)}(f_h) \rangle \left(Bo^{-1} \vec{\nabla}_{\hat{X}} h^{(0)} + \vec{e}_z \right) \right)$$
$$+ \vec{\nabla}_{\hat{X}} \cdot \left(\langle \exp(f_k) k_r^{(0)}(f_h) Bo^{-1} \vec{\nabla}_{\hat{Y}} h^{(1)} \rangle \right) = sT \tag{5.90}$$

The brackets stand now for ensemble averaged quantities. With this framework, the ensemble-averaged equation can for given constitutive relationships be evaluated to a given order of the parameter f_k and f_h.

Example Brooks-Corey Model

A Brooks-Corey model for a two-dimensional medium is analyzed in the following as a test example to calculate the averaged equation (5.90) and stochastic parameters. The constitutive relations read

$$S(h) = \begin{cases} \left(\dfrac{h_{\text{entry}}}{h} \right)^{\lambda} & \text{if} \quad |h| > \left| h_{\text{entry}} \right| \\ 1 & \text{otherwise} \end{cases}, \tag{5.91}$$

$$k_r(S) = \begin{cases} (S)^{2/\lambda+3} = \left(\dfrac{h_{\text{entry}}}{h} \right)^{2+3\lambda} & \text{if} \quad \left| h_{\text{entry}} \right| \geq |h| \\ 1 & \text{otherwise} \end{cases}, \tag{5.92}$$

with the entry-pressure head h_{entry} and the Brooks-Corey parameter n. S is the water saturation. Here, the residual saturation is assumed zero. The moisture capacity is :

$$\mathscr{C}(h) = n_f \frac{dS}{dh} = \begin{cases} -\dfrac{\lambda\, n_f}{h_{\text{entry}}} \left(\dfrac{h_{\text{entry}}}{h} \right)^{\lambda+1} & \text{if} \quad |h| > \left| h_{\text{entry}} \right| \\ 0 & \text{otherwise} \end{cases}. \tag{5.93}$$

h is negative under unsaturated conditions. n_f is the porosity of the medium. It is assumed that the entry pressure head is related to the hydraulic conductivity via Leverett scaling (Leverett, 1941) or Miller-Miller similarity (Miller and Miller, 1956; Sposito and Jury, 1990):

$$h_{\text{entry}} \propto \frac{1}{\sqrt{K}}. \tag{5.94}$$

Under these conditions, the geometric mean of the entry-pressure head h_g is the entry-pressure head which corresponds to the geometric mean of the hydraulic conductivity,

and the fluctuations are fully correlated:

$$f_h = -\frac{1}{2} f_k \tag{5.95}$$

$$\frac{h_{\text{entry}}}{h_g} = \exp\left(-\frac{1}{2} f_k\right). \tag{5.96}$$

The parameters in the constitutive relationships (5.91), (5.92), (5.93) and (5.94) are given with dimensions.

Effective Moisture Capacity Curve

Accounting for eq. (5.93), the moisture capacity-curve field for a fixed pressure head (here $h^{(0)}$) is given by substituting the dimensionless pressure head $h^\star$ according to eq. (5.8) and the random field according to eq. (5.96) into the definition of eq. (5.93):

$$\mathscr{C}(f_k, h^{(0)}) = \begin{cases} -\lambda n_f \exp\left(\dfrac{\lambda+1}{2}\mathscr{A} - \dfrac{\lambda}{2} f_k\right) & \text{if } f_k > \mathscr{A} \\ 0 & \text{otherwise} \end{cases}, \tag{5.97}$$

with $\mathscr{A} = -2\ln\left(h^{(0)}\right)$. The ensemble-averaged effective moisture capacity $\langle \mathscr{C}(h^{(0)}) \rangle$ can be computed by integrating the product of $\mathscr{C}(f_k, h^{(0)})$, given by eq. (5.97), and the Gaussian probability density function $p(f_k)$ of f_k over all values of f_k:

$$\begin{aligned} \langle \mathscr{C}(h^{(0)}) \rangle &= \int_\infty \mathscr{C}(f_k, h^{(0)}) p(f_k) df_k = \int_\infty \mathscr{C}(f_k, h^{(0)}) \frac{1}{\sqrt{2\pi\sigma_{f_k}^2}} \exp\left(-\frac{f_k^2}{2\sigma_{f_k}^2}\right) df_k \\ &= n_f \frac{-n}{2} \exp\left(\frac{n+1}{2}\mathscr{A}\right) \exp\left(\frac{n^2}{8}\sigma_{f_k}^2\right) \cdot \left(1 - \operatorname{erf}\left(\frac{n\sigma_{f_k}^2}{2\sqrt{2}} + \frac{\mathscr{A}}{\sigma_{f_k}^2\sqrt{2}}\right)\right). \end{aligned} \tag{5.98}$$

Ensemble-averaged moisture capacitiess $\langle \mathscr{C}(h^{(0)}) \rangle$ are plotted in Figure 5.7 for different values of log-hydraulic conductivity variance $\sigma_{f_k}^2$. The curves get wider with increasing variance. Also, the effect of a definite entry pressure head gets lost because the entry pressure head h_e has a distribution with a non-zero probability for all positive values.

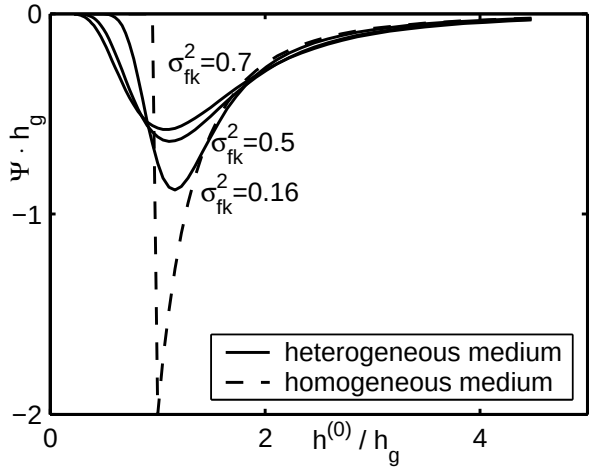

Figure 5.7: Effective dimensionless moisture capacity, $\mathscr{C} h_g$ as function of $h^{(0)}/h_g$.

Statistical Properties of the Total Hydraulic Conductivity Field

In the previous part, the total conductivity $K_{tot} = K_0 k_r$ was expanded about the zeroth-order term $K_g \, k_r^{(0)}\Big|_{f_h=0,h^{(0)}}$. In the following, however, we will expand the total conductivity about its geometric mean. In a two-dimensional problem this is a reasonable approach from a physical point of view. The effective conductivity in a two-dimensional field is the geometric mean if the permeability distribution is lognormally distributed (e.g. King (1987)). Although the probability distribution for the total conductivity is not lognormal, the geometric mean of the total conductivity is the most reasonable value for an expansion. In order to do so, we determine the statistical properties of the total conductivity. Subsequently, we will substitute the expansion about the geometric mean of the total conductivity into eq. (5.87).

Applying the Brooks-Corey parameterization, the dimensionless total conductivity is:

$$K_{tot} = K_0 k_r = \exp(f_k) S^{2/\lambda+3} = \begin{cases} \exp(f_k) & \text{if} \quad f_k \leq \mathscr{A} \\ \exp\left(\left(1+\frac{3}{2}\lambda\right)\mathscr{A} - \frac{3}{2}\lambda f_k\right) & \text{if} \quad f_k > \mathscr{A} \end{cases} . \quad (5.99)$$

The expected value, or arithmetic mean of K_{tot}, denoted $\langle K_{tot} \rangle_a$, can be obtained by multiplying $K_{tot}(f_k)$ with the probability density function (*pdf*) of f_k and integrating over all

possible values of f_k:

$$\langle K_{tot}\rangle_a = \int_\infty K_{tot}(f_k)\frac{1}{\sqrt{2\pi\sigma_{f_k}^2}}\exp\left(-\frac{f_k^2}{2\sigma_{f_k}^2}\right)df_k \tag{5.100}$$
$$= \frac{1}{2}\left[\exp\left(\frac{\sigma_{f_k}^2}{2}\right)\left(1+\operatorname{erf}\left(\frac{\mathscr{A}-\sigma_{f_k}^2}{\sigma_{f_k}\sqrt{2}}\right)\right)+\exp\left(\left(1+\frac{3}{2}\lambda\right)\mathscr{A}+\frac{9\lambda^2\sigma_{f_k}^2}{8}\right)\cdot\right.$$
$$\left.\left(1-\operatorname{erf}\left(\frac{\mathscr{A}+3/2\lambda\sigma_{f_k}^2}{\sigma_{f_k}\sqrt{2}}\right)\right)\right].$$

The geometric mean of the total conductivity, denoted $\langle K_{tot}\rangle_g$, is the exponential of the expected value of the log-total hydraulic conductivity, $\langle K_{tot}\rangle_g = \exp(\langle\ln(K_{tot})\rangle)$

$$\langle K_{tot}\rangle_g = \exp\left(\int_\infty \frac{\ln\left(K_{tot}(f_k)\right)}{\sqrt{2\pi\sigma_{f_k}^2}}\exp\left(-\frac{f_k^2}{2\sigma_{f_k}^2}\right)df_k\right)$$
$$= \exp\left((1+\frac{3\lambda}{2})\left(\frac{\mathscr{A}}{2}-\frac{\sigma_{f_k}}{\sqrt{2\pi}}\exp\left(-\frac{\mathscr{A}^2}{2\sigma_{f_k}^2}\right)\right)\right.$$
$$\left.-\frac{\mathscr{A}}{2}\operatorname{erf}\left(\frac{\mathscr{A}}{\sigma_{f_k}\sqrt{2}}\right)-\frac{3|\mathscr{A}|\lambda}{4}\operatorname{erf}\left(\frac{|\mathscr{A}|}{\sigma_{f_k}\sqrt{2}}\right)\right). \tag{5.101}$$

The variance of the total conductivity $\sigma_{K_{tot}}^2$ can be obtained with the same method:

$$\sigma_{K_{tot}}^2 = -\langle K_{tot}\rangle_a^2+\frac{1}{2}\left[\exp\left(2\sigma_f^2\right)\left(1+\operatorname{erf}\left(\frac{\mathscr{A}-\sigma_{f_k}^2}{\sigma_{f_k}\sqrt{2}}\right)\right)\right. \tag{5.102}$$
$$\left.+\exp\left((2+3\lambda)\mathscr{A}+\frac{9\lambda^2\sigma_{f_k}^2}{2}\right)\left(1-\operatorname{erf}\left(\frac{\mathscr{A}+3\lambda\sigma_{f_k}^2}{\sigma_{f_k}\sqrt{2}}\right)\right)\right],$$

while the variance of the log-total hydraulic conductivity is

$$\sigma_{\ln(K_{tot})}^2 = \frac{1}{8}\left[4\mathscr{A}^2\left(1+\frac{3}{2}\lambda\right)^2+4\sigma_{f_k}^2+9\lambda^2\sigma_{f_k}^2-8\mathscr{A}\exp\left(-\frac{\mathscr{A}^2}{2\sigma_{f_k}^2}\right)\sqrt{\frac{\sigma_{f_k}^2}{2\pi}}\left(1+\frac{3}{2}\lambda\right)^2\right.$$
$$-3\lambda\frac{\sqrt{\mathscr{A}^2}}{\mathscr{A}}\left(\mathscr{A}^2(4+3\lambda)+3\lambda\sigma_{f_k}^2\right)\operatorname{erf}\left(\frac{\sqrt{\mathscr{A}^2}}{\sqrt{2\sigma_{f_k}^2}}\right)+$$
$$\left.4\left(\sigma_{f_k}^2-\mathscr{A}^2\right)\operatorname{erf}\left(\frac{\mathscr{A}}{\sqrt{2\sigma_{f_k}^2}}\right)\right]-\ln(\langle K_{tot}\rangle_g)^2. \tag{5.103}$$

The coefficients of variation of the effective total conductivity, $\sigma_{K_{tot}}/\langle K_{tot}\rangle$ depend via $\mathscr{A} = -2\ln\left(h^{(0)}\right)$ strongly on the large-scale head $h^{(0)}$.
The averaged total conductivities according to eqs. (5.100 & 5.101) and the variances according to eqs. (5.102 & 5.103) do not show the effects of a definite entry pressure, since is has been averaged out. In this respect, both results differ from first-order results for the averaged log-total hydraulic conductivity that have been obtained by Zhang et al. (1998). The first order result is the total conductivity of a homogeneous medium parameterized by the expected values of the parameters:

$$\langle K_{tot}\rangle_{ord.1} = \begin{cases} \exp\left(\frac{1}{h^{(0)}}\right)^{(2+3\lambda)} & \text{if } h^{(0)} > 1 \\ 1 & \text{otherwise} \end{cases}, \tag{5.104}$$

and the first-order variance of log hydraulic conductivity is:

$$\sigma^2_{\ln(K_{tot})\,ord.1} = \sigma^2_{f_k} \begin{cases} 1-(2+3\lambda)+\frac{1}{4}(2+3\lambda)^2 & \text{if } h^{(0)} > 1 \\ 1 & \text{otherwise} \end{cases}. \tag{5.105}$$

Figure 5.8 shows plots of the averaged total conductivities according to eqs. (5.101 & 5.104) and the variances according to eqs. (5.103 & 5.105) for $\sigma^2_{f_k} = 1.0$ and $\sigma^2_{f_k} = 0.01$. The differences are pronounced most at pressure head values in the range of the entry pressure head h_g, where the geometric mean is much lower than the first-order mean. With decreasing variance $\sigma^2_{f_k}$ the averages converge to the same zeroth-order curve. The first-order approximation over-estimates the total conductivity at low capillary pressure heads. The variance $\sigma^2_{\ln(K_{tot})}$ has a minimum at pressure heads below h_g, with a smaller value than the variance of the log hydraulic conductivity $\sigma^2_{f_k}$. If the pressure head equals zero, the medium is water saturated and $\sigma^2_{\ln(K_{tot})}$ equals $\sigma^2_{f_k}$. As the pressure increases, the hydraulic conductivity of coarse material (high hydraulic conductivity and low entry pressure head) decreases. For small values of the pressure head $h^{(0)}$, the decrease of the total hydraulic conductivity with increasing head is still rather small, so that the total conductivities within zones of high hydraulic conductivity are in an intermediate range. With more values of the total conductivity in the intermediate range, the variance of the log-total hydraulic conductivity decreases with increasing pressure heads in the range of capillary pressure heads below the entry pressure head. The latter effect is not captured by first-order theory. For high capillary pressure heads, the total conductivities in the zones of high hydraulic conductivity get very small, thus increasing the variance of log-total hydraulic conductivity.
The geometric mean $\langle K_{tot}\rangle_g$ according to eq. (5.101) and variance $\sigma^2_{\ln(K_{tot})}$ according to eq. (5.103) depend on the variance of log hydraulic conductivity $\sigma^2_{f_k}$ and the large scale pressure head in a complex way. Figure 5.9 shows a plot of the expected value $\langle K_{tot}\rangle_g$ as a function of the variance of log hydraulic conductivity $\sigma^2_{f_k}$ for three different values of $\mathscr{A}$ ($\mathscr{A} = 3$, $\mathscr{A} = 0$ and $\mathscr{A} = -3$). The first value corresponds to $h^{(0)} = 0.2$, the second one to $h^{(0)} = 1$, and the third one to $h^{(0)} = 5$. Figure 5.9 shows also the variances $\sigma^2_{\ln(K_{tot})}$ according to eq. (5.103) as function of $\sigma^2_{f_k}$ for the same values of $\mathscr{A}$.

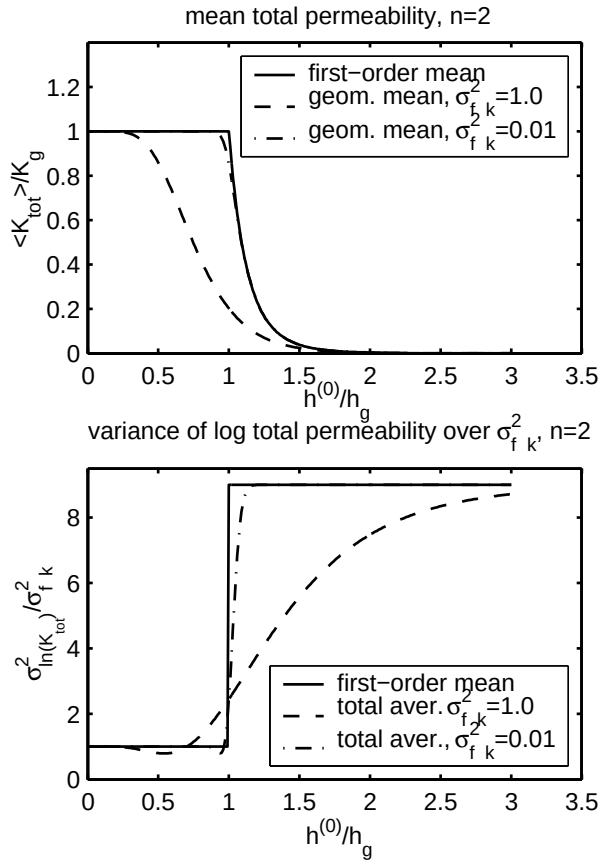

Figure 5.8: Mean $\langle K_{tot} \rangle$ of the total conductivity, and variance $\sigma^2_{ln(K_{tot})}$ of the log-total hydraulic conductivity normalized with $\sigma^2_{f_k}$. First-order mean and averages according to eqs. (5.101 & 5.103 - 5.105).

If the non-dimensionless entry pressure head is high or low compared to h_g, the geometric mean of K_{tot} is almost constant, at least for the value range of $\sigma^2_{f_k}$ considered here. If $h^{(0)}$ is very low, the medium is saturated and the hydraulic conductivity determines K_{tot}. In this case, the geometric mean equals the geometric mean of the hydraulic conductivity, independently of $\sigma^2_{f_k}$. This is consistent with the linear increase of the variance of $\ln(K_{tot})$ with a slope of 1 for $h^{(0)} = 0.2$. If $h^{(0)}$ is large compared to h_g there is hardly any water in the medium. The geometric mean of the total conductivity is therefore very low, and the value does not depend on $\sigma^2_{f_k}$. Due to the low water content the variance $\sigma^2_{\ln(K_{tot})}$ is much larger than in the case of small pressure head $h^{(0)}$, and it increases also linearly with $\sigma^2_{f_k}$. In the case that the pressure head $h^{(0)}$ equals h_g, we are in an intermediate regime. At $\sigma^2_{f_k} = 0$, the pressure head equals the entry pressure head in a homogeneous medium and the geometric mean of total conductivity equals the geometric mean of the intrinsic one. As $\sigma^2_{f_k}$ increases, more parts of the material have a lower entry pressure head than h_g and thus have a water saturation $S < 1$. Their total conductivity is smaller. Due to the step-

wise shape of the capillary pressure-saturation curve, the parts in the medium with higher entry pressure head do not counterbalance this effect. As a result, the geometric mean $\langle K_{tot} \rangle_g$ decreases with $\sigma^2_{f_k}$. The variance $\sigma^2_{\ln(K_{tot})}$ also grows with $\sigma^2_{f_k}$, but with a slope larger than unity, because the medium becomes less saturated with larger $\sigma^2_{f_k}$, leading to a higher variance than in the water-saturated case.

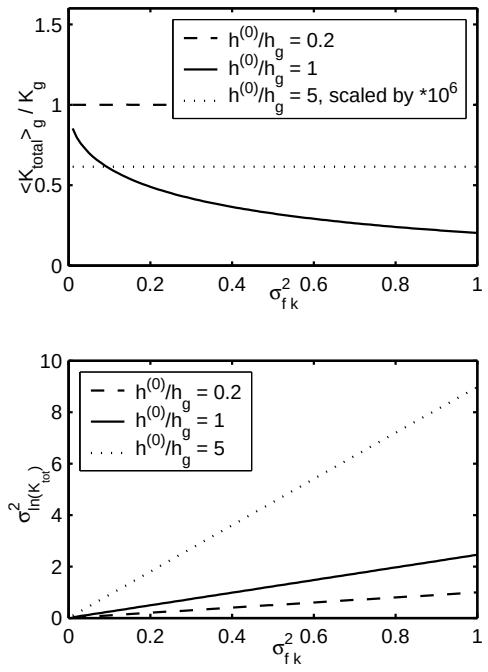

Figure 5.9: Expected value of total hydraulic conductivity $\langle K_{tot} \rangle_g / K_g$ and variance $\sigma^2_{\ln(K_{tot})}$ as function of the variance $\sigma^2_{f_k}$ for different values of mean pressure head $h^{(0)}$. Note the factore of 10^{-6} in the dotted line in the upper plot.

In order to evaluate the ensemble averaged unsaturated flow equation, eq. (5.90), the correlation structure of log-total hydraulic conductivity is important. In this context, it is worth noting that the two-point auto-covariance function cannot fully determine the statistics of the total conductivity since the latter is, due to the non-linear relative permeability, not a multi-Gaussian field. Nonetheless, higher moments are neglected. The log- hydraulic conductivity at location $\vec{x}_1$ is denoted by f_1 and at location $\vec{x}_2$ by f_2. The two-point auto-covariance can then be computed by:

$$\langle \ln(K'_{tot}(\vec{x}_1)) \ln(K'_{tot}(\vec{x}_2)) \rangle - (\ln(\langle K_{tot} \rangle_g))^2 = \tag{5.106}$$
$$\int_{\infty}^{} \int_{\infty}^{} \left(\frac{\ln(K_{tot}(f_1)) \ln(K_{tot}(f_2))}{2\pi\sigma^2_{f_k}\sqrt{1-\rho^2}} \right.$$
$$\left. \exp\left(-\frac{f_1^2 - 2f_1 f_2 \rho + f_2^2}{2\sigma^2_{f_k}} \right) \right) df_1 df_2 - (\ln(\langle K_{tot} \rangle_g))^2,$$

in which ρ is the correlation function of the log- hydraulic conductivity fluctuations, which may be parameterized by standard models such as the Gaussian and the exponential ones. To the best of my knowledge, the second integration of eq. (5.106) cannot be performed in closed form. Instead, a numerical integration is performed for the three examples discussed above ($\mathscr{A} = -3$, $\mathscr{A} = 0$ and $\mathscr{A} = 3$) using the numerical integration tool of Mathematica (Wolfram, 1991).

Figure 5.10 shows the correlation coefficient of the log total conductivity as function of ρ for the given values of $\mathscr{A}$ and a variance of the hydraulic conductivity of $\sigma^2_{f_k} = 1.0$ and $n = 2$. For non-dimensionless entry pressure heads $h^{(0)}$ much higher or lower than h_g, the correlation function is the same as the correlation function for f_k. If $h^{(0)}$ is in the range of h_g, the correlation function decreases faster than the correlation function of f_k. As high permeable zones are drained easier and thus have smaller total conductivities, parts with high hydraulic conductivity are flipped into the low end of the total conductivity range, leading to a smaller correlation length of the field.

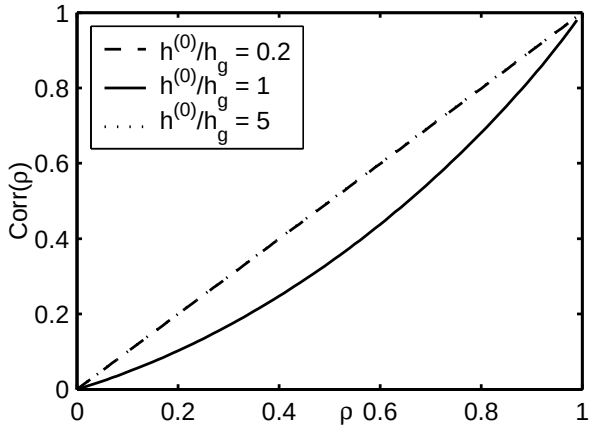

Figure 5.10: Auto-correlation of the log of the total hydraulic conductivity, $\sigma^2_{f_k} = 1.0$, $n = 2$, $Corr(\rho) = (\langle \ln(K_{tot}(f_1)) \ln(K_{tot}(f_2)) \rangle - (\ln(\langle K_{tot} \rangle_g))^2)/(\sigma^2_{\ln(K_{tot})})$.

The effective total hydraulic conductivity (5.90) can be calculated using the stochastic properties discussed above. As outlined, the expansion is performed about $\langle K_{tot}\rangle_g$, computed by eq. (5.101), with the expansion parameter $\sigma^2_{\ln(K_{tot})}$. The second term in eq. (5.90) to the second order of this expansion reads:

$$\vec{\nabla}_{\hat{X}} \cdot \left(\langle K_{tot}\rangle_g \left(1 + \frac{1}{2}\sigma^2_{\ln(K_{tot})} \right) \vec{J} \right).$$

In order to calculate $h^{(1)}$ the order ε^{-1} of the Richard's equation, equation (5.87), has to be solved. It reads with the expansion in terms of $\sigma^2_{\ln(K_{tot})}$

$$\vec{\nabla}_{\hat{Y}} \cdot \left(\left(\ln(K_{tot}) + \frac{1}{2}\ln(K_{tot})^2 + \ldots \right) \left(\vec{J} + \vec{\nabla}_{\hat{Y}} h^{(1)} \right) \right) + \nabla^2_{\hat{Y}} h^{(1)} = 0. \tag{5.107}$$

The Green's function is:

$$G = \frac{1}{2\pi} \sum_{i=-\infty}^{+\infty} \sum_{j=-\infty}^{+\infty} \ln\left(\left| \hat{Y} + i\varepsilon^{-1}\vec{e}_1 + j\varepsilon^{-1}\vec{e}_2 - \hat{Y}' \right| \right) \approx \frac{1}{2\pi} \ln\left(\left| \hat{Y} - \hat{Y}' \right| \right), \tag{5.108}$$

in which the approximation denotes the two-dimensional solution for an infinite rather than a periodic domain. $\vec{e}_1$ and $\vec{e}_2$ are unit vectors in both spatial directions.
With this expansion the third term in eq. (5.90) can be determined to second order by:

$$\begin{aligned} &\vec{\nabla}_{\hat{X}} \cdot \left(\langle \langle K_{tot}\rangle_g \exp(\ln(K_{tot})) \vec{\nabla}_{\hat{Y}} h^{(1)} \rangle \right) = \\ &\frac{1}{2\pi} \vec{\nabla}_{\hat{X}} \cdot \left[\langle K_{tot}\rangle_g \int_\Omega \left(\nabla^2_{\hat{Y}} \ln\left(\left| \hat{Y} - \hat{Y}' \right| \right) \quad \left\langle \left(\ln(K'_{tot}(\hat{Y})) \ln(K'_{tot}(\hat{Y}')) \right) \right\rangle \vec{J} d\hat{Y}' \right) \right]. \end{aligned} \tag{5.109}$$

This type of integral has been evaluated before by Dagan (1993) for single-phase flow in a macroscopically uniform flow field, using covariance functions with finite integral scale. In the scale expansion framework of homogenization theory, the constraint of a uniform flow field on the large scale is relaxed: Here, large-scale trends may exist but must be negligible on the small scale. For isotropic media, the effective single-phase conductivity does not depend on the correlation scale of the medium. As the covariance of the total hydraulic conductivity decays at least as fast as the covariance of the log-hydraulic conductivity f_k, we assume that here the integral does not depend on the integral scale either and the covariance of $\ln(K_{tot})$ can be approximated as a Gaussian one. We furthermore assume that the mean flow can be assumed uniform on the small scale. The result becomes thus:

$$\vec{\nabla}_{\hat{X}} \cdot \left(\langle \exp(f_k) k_r^{(0)} \vec{\nabla}_{\hat{Y}} h^{(1)} \rangle \right) \approx -\frac{1}{2} \nabla_{\hat{X}} \cdot \left(\langle K_{tot}\rangle_g \sigma^2_{\ln(K_{tot})} \vec{J} \right). \tag{5.110}$$

Finally, the ensemble-averaged homogenized equation (5.90) is:

$$\langle \mathscr{C}^{(0)} \rangle \frac{\partial h^{(0)}}{\partial t} + \nabla_{\hat{X}} \cdot \left(\langle K_{tot} \rangle_g \left(Bo^{-1} \nabla_{\hat{X}} h^{(0)} + e_z \right) \right) = qT \tag{5.111}$$

with the effective parameter functions $\langle \mathscr{C}^{(0)} \rangle$ and $\langle K_{tot} \rangle_g$.
As the distribution of the total conductivity is not multi-Gaussian, the next order with non-zero contribution to the effective parameters is the third one. It is quite expectable that higher-order contributions are more important in unsaturated flow than in single-phase flow.
Figure 5.11 shows an example for the effective curve $K_{tot}\left(h^{(0)}\right)$ using the parameters $n = 2$, $\sigma^2_{f_k} = 0.25$ and $\sigma^2_{f_k} = 1.0$. The averaging of the entry-pressure effect is clearly visible. In comparison to the homogeneous case, the effective total conductivity $\langle K_{tot} \rangle_g$ is always smaller.

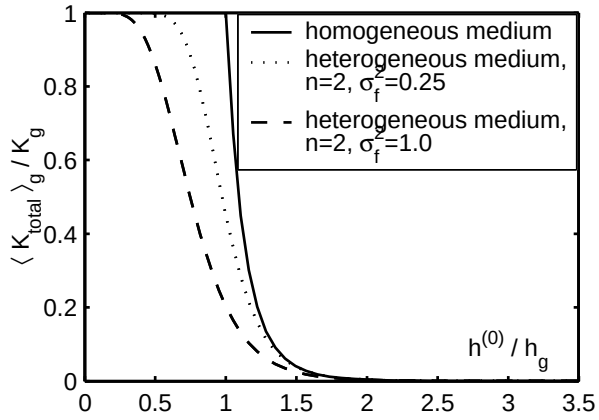

Figure 5.11: $\langle K_{tot} \rangle_g / K_g$ in relation to $h^{(0)}/h_g$ for different variances $\sigma^2_{f_k}$.

5.3.2 Models for non-Gaussian media with connected extreme values

If the parameter fields are not Gaussian but have connected parts of materials with extreme parameter values, second-order ensemble averaged properties might not capture the main influence of the heterogeneous structure. Well connected zones of low conductivity may significantly reduce flow through the domain, whereas well connected zones of high conductivity lead to channeling flow. When a water-saturated medium is drained, the zones of coarse material are the first to drain. In this process, the zones of highest hydraulic conductivity become the least permeable ones. Therefore, the impact of the connected parts can change qualitatively during the flow process.

Comparison of Gaussian and non-Gaussian test fields

To illustrate the influence of the non-Gaussian feature, the effective conductivity is calculated for the three test fields introduced in Chapter 2 (cf. Figure 2.4). The second and

third field are characterized by well connected bands with parameters which are highly or poorly conductive under saturated conditions. The first field is a Gaussian field with connected material of intermediate saturated hydraulic conductivity.

The effective parameter functions (effective moisture capacity according to eq. (5.22) and effective total conductivity according eq. (5.24)) for all three types of fields were calculated. For the effective functions, we used fields with the same parameters as the example fields of Figure 2.4, however the fields were 512 x 512 cells large. An ensemble averaging was not necessary in order to calculate the effective parameter functions, as the size was already larger than an REV. The deviations between curves obtained from different fields were negligible.

The effective moisture capacity is obtained by calculating the arithmetic mean of the saturation fields for different values of $h^{(0)}$ and calculating the derivative with respect to the pressure head $h^{(0)}$ numerically. The moisture capacity curves for all types of fields are almost identical because they are the arithmetic means of the local values. Since the *pdf* of the f_k fields does not differ with connectivity type, identical moisture capacity curves are to be expected. The curves are not shown here.

The hydraulic conductivity curves are obtained by numerical simulation of the small-scale problem in a field for each type of the test fields fields, as outlined in Section 5.2.1. These curves are compared to the geometric mean $\langle K_{tot} \rangle_g$ of the total conductivity, evaluated by eq. (5.101). The small-scale problem is solved by a cell-centered Finite Volume scheme applying periodic boundary conditions (see Cirpka and Kitanidis, 2002). The resulting system of linear equations is solved by a conjugate gradient method with algebraic multigrid preconditioning Ruge and Stüben (1987). Due to the periodic boundary conditions, the system of equations for the pressure is singular. However, the total conductivity is calculated from the averaged flux and thus only from the pressure gradients. The singularity can therefore be overcome by fixing the pressure at one node to an arbitrary value, without changing the result for the effective total conductivity.

The resulting effective relative permeability curves are shown in Figure 5.12. In all three cases, the effective relative permeability curve evaluated numerically differs from the geometric mean. Considering relative errors (given by the dotted lines in the plots), however, large errors occurred only in the fields where either high or low conductivitiesties are well connected. In the first case, the stochastic theory overestimates the relative permeability, while in the second case it underestimates the relative permeability. This behavior is counterintuitive, but can be explained by the statistical properties of the total conductivity.

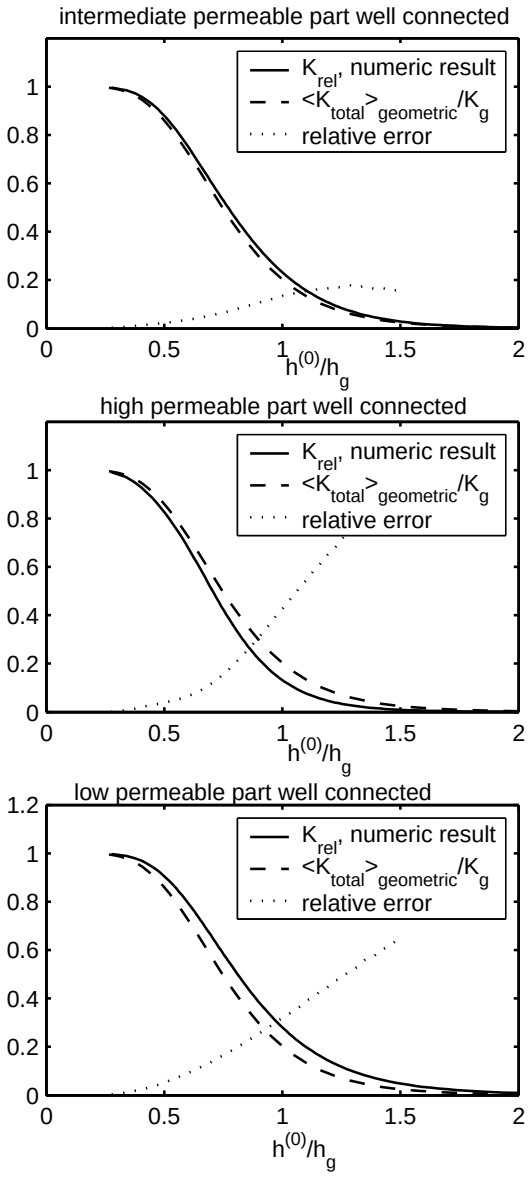

Figure 5.12: Effective relative permeability curves for the test fields shown in Chapter 2. Comparison between numerical up-scaling and approximation by the geometric mean. Permeabilities were normalized by the effective saturated permeabilities. Deviations between the saturated permeabilities for the three fields were by a factor of 1.1.

For the field of type 3, the explanation is the most straightforward. The parameter distribution of the total conductivity is given by eq. (5.99). The function monotonically increases with f_k for $f_k < \mathscr{A}$, while it decreases for $f_k > \mathscr{A}$, thus exhibiting a maximum at $f_k = \mathscr{A}$.
At capillary pressure heads where the maximum total conductivity is in a well connected regime, the high total conductivities (defined by the corresponding $\mathscr{A}$) are well connected.

This does not necessarily lead to channeling behavior. Channeling occurs only when, additionally to the connectedness of the high hydraulic conductivity zones, the variance of the total hydraulic conductivity field is high. In the three examples given above, this happens in the third case. Here, low values of f_k are highly connected. At heads, where these values are similar to $\mathscr{A}$, the high total conductivity zones are well connected and the variance of the total conductivity is high (see eq. (5.102)). As stated above, the combined effects result in channeling. Obviously, channeling leads to a higher effective conductivity than estimated by the geometric mean of the total conductivity (see also the single-phase results of Zinn and Harvey (2003)). In the field of type 1, the well connected values of f_k correspond to higher values of $\mathscr{A}$, where the variance of the total conductivity is smaller so that the channeling is less pronounced. In the field of type 2 we have the opposite effect to the third field. For the values of $\mathscr{A}$ corresponding to the values of $h^{(0)}$ shown here, the low permeable parts are well connected. At the same time the variance of the total conductivity is high. We thus get an anti-channeling effect. The well-connected low permeable material blocks the flow, leading to a lower relative permeability than predicted by stochastic theory.

Including information about connectivity

From the example it becomes clear that second order stochastic averages might not be the best approach to estimate the unsaturated hydraulic conductivity, if material with either very high or very low saturated conductivity forms connected bands while the rest of the material is isolated. This means, the non-Gaussian features have a significant impact on the upscaled model. To estimate the unsaturated hydraulic conductivity it may here be more useful to apply upscaling methods which allow to take information about connectivity into account.
The methods introduced in Chapter 3.2 can be employed for this purpose. Effective medium theory is mostly derived for media made of different composites. The Maxwell approach and the differential effctive medium approach are derived for media with background and inclusions. This approach can be profitable here, as the connected material can be assigend to the background, while the rest is assigned to the inclusion material. The Maxwell approach allows for continuous fields, while differential effective medium theory does require fields with distinct composites. A continuous field would therefore have to be mapped to a field with different classes, where the differentiation of the classes has to be done in a reasonable manner. The most important point is that one class is defined for the parameter range where material is connected. A classification for this can be done using the Euler number for the indicator field or a two-point cluster density (cf. Chapter 2.2), if enough data are available.
As the effective medium theory approaches in Chapter 3.2 are all mean field results, the effective conductivity curves are calculated from the parameter distributions of the fields only. Different capillary pressure head values $h^{(0)}$ are chosen and the resulting dimensionless total conductivity values, $k_{\text{total}} = \kappa k_r(h^{(0)})$, corresponding to a capillary pressure head value are calculated for each field. Including the information about the connected

material, the effective conductivity is then calculated for both approaches using (3.33) and (3.48).

Effective curves for test fields

The three test fields from Chapter 2 (Figure 2.4) are used to compare different parameter functions. As effective medium theory is applied to approximate the effective parameter functions, the values of the fields are divided into five classes and the values of the field are set to the values of the classes. In order to see the differences due to the structure of the fields clearly, the variance was set very high to $\sigma_f^2 = 10$. The fields are shown in Figure 5.13.

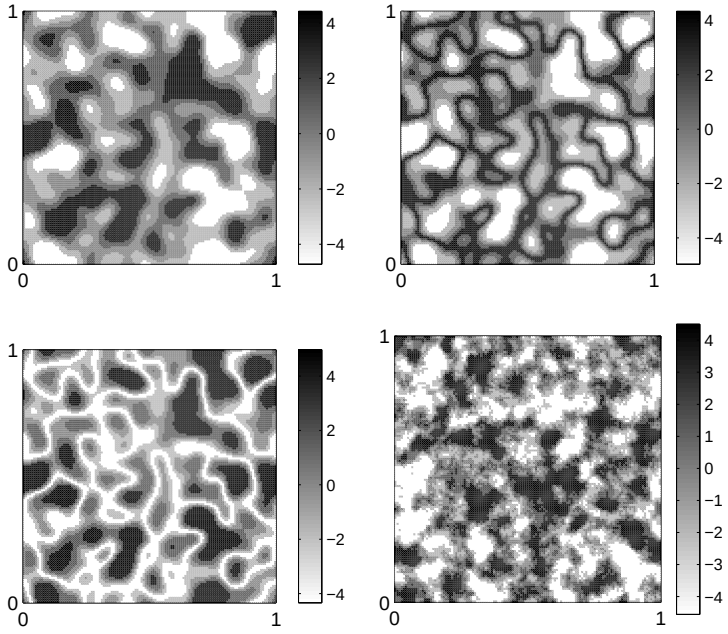

Figure 5.13: Test fields showing $f = \ln(\kappa)$. Upper left: Generated from a field with Gaussian covariance, $\lambda = 8.0$. Upper right: Generated from field with Gaussian covariance, which has been transformed so that high values are connected, $\lambda = 5.0$. Lower left: Generated from field with Gaussian covariance, which has been transformed so that low values are connected, $\lambda = 5.0$. Lower right: Generated from a Gaussian field with the same mean, variance and autocovariance as upper right and lower left, $\lambda = 5.0$.

The Euler number introduced in Section 3.2.3 for the indicator fields of the classes is calculated in order to determine the connected material. The Euler number for the different indicators and the three test fields is shown in Figure 5.14. According to Figure 5.14 the intermediate phase is connected in fields 1 and 4, in field 2 the phase with the highest saturated hydraulic conductivity is connected, while for field 3 the phase with the lowest saturated hydraulic conductivity is connected. The effective conductivity functions are then calculated for a range of zero order pressure heads $h^{(0)}$ using the Maxwell approach

and the differential effective medium theory approach. For field 1 and 4 the third phase, for field 2 the first phase and or field 3 the fifth phase are assigned to the background material.

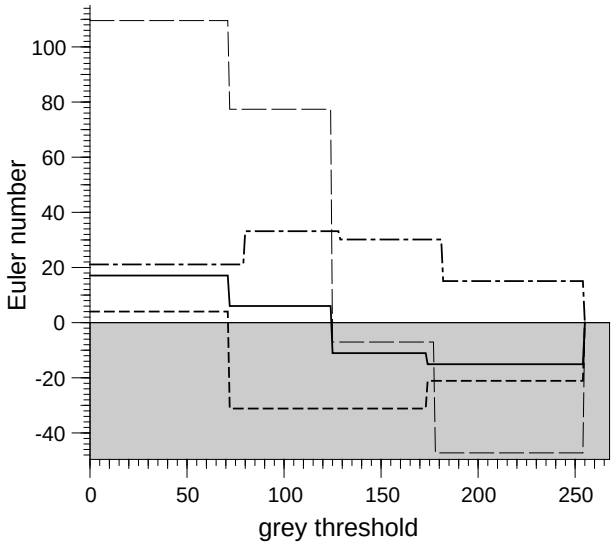

Figure 5.14: Euler function of the four fields shown in Figure 5.13. Solid line: field 1 large dashed line: field 4, small dashed line: field 3, dashed-dotted line: field 2.

In order to compare the different effective medium theory approaches, the effective conductivity function is also calculated using the self-consistent approach.
The effective curves for the three fields are shown in a semi-log plot in Figure 5.15 for the three effective medium theory approaches together with the second order result (5.101) and the result from the numerically calculated results of homogenization theory as explained in Section 5.2.1. The capillary pressure head values are chosen between $h^{(0)} = 0$ and $h^{(0)} = -3$. For smaller capillary pressure head values no principal changes of the results occure.
The curves calculated using the geometric mean are quite similar for all four fields. This is to be expected, as the parameter distributions are more or less the same for all four materials. This hydraulic conductivity curve fits the homogenization result only well for field 1 and field 4, where the intermediate values are connected. This is to be expected, as these two fields are closer to Gaussian fields than field 2 and field 3. However, for field 1 and field 4 the other two approaches (Maxwell and differential effective medium) are also not so far away from the homogenization result. The slight overprediction of the hydraulic conductivity of these methods is due to the fact that the intermediate hydraulic conductivity is higher than the averaged hydraulic conductivity.
For the non-Gaussian fields (fields 2 and 3) the situation is different. In the effective curves of fields 2 and 3 it can clearly be seen that the connectivity has an influence on the effective conductivities. In field 2, where the high saturated hydraulic conductivity values are connected, the hydraulic conductivity curve calculated with homogenization theory lies for high pressure heads far above the curve for field 1, although mean and variance of

the fields are equal. In this case, the self-consistent approach underestimates the hydraulic conductivity, as the connectivity of the high saturated hydraulic conductivity values is not considered. At full saturation the (dimensionless) hydraulic conductivity is $K = 3.9$, while the self-consistent approach would predict it to be $K = 1.2$. On the other hand, the Maxwell approach overestimates the hydraulic conductivity at high pressure heads. For full saturation it would predict a hydraulic conductivity of $K = 12.5$. The influence of the background material is here too stong. The high permeable phase is connected in field 2, however, the tortuousity of this pattern formed by this phase is very high. Also, not all parts are connected throughout the material. All these aspects are neglected in the Maxwell approach. The differential effective medium approach also overpredicts the effective conductivity, but not to such a high degree as the Maxwell approach. At full saturation it would predict a hydraulic conductivity of $K = 6.5$. It is the best estimate for the effective curve.

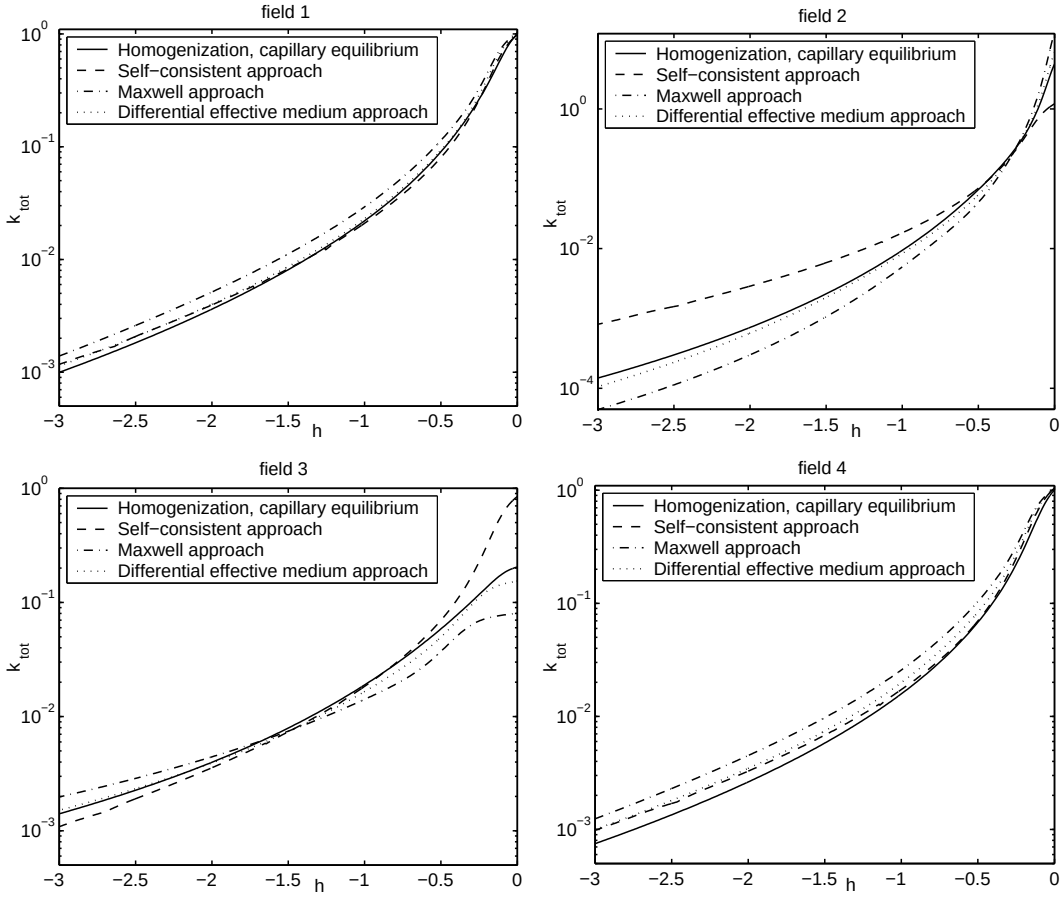

Figure 5.15: Total effective conductivity curves using the three different self-consistent approaches and the capillary equilibrium results obtained with homogenization theory. Upper left: field 1. Upper right: field 2. Lower left: field 3. Lower right: field 4.

At low pressure heads, where the connected part in field 2 has a very low water saturation and becomes very poorly conductive, the self-consistent approach overestimates

the hydraulic conductivity, while the Maxwell approach underestimates it. Again, the differential effective medium approach yields the best result.
The discussion for field 2 can be transferred to field 3 straight away, only that now the zones with low saturated hydraulic conductivity are connected, so that the self-consistent approach overpredicts the effective curve at high pressure heads, while the Maxwell approach and the differential effective medium approach underpredict the curves. The saturated (dimensionless) hydraulic conductivity values are $K = 0.19$ with homogenization theory, $K = 0.85$ with the self-consistent approach, $K = 0.08$ with the Maxwell approach and $K = 0.15$ with the differential effective medium theory approach. Again, the differential effective medium approach gives the best estimates.
The relative deviations ($\sqrt{(K_{\text{effmed.}} - K_{\text{hom.}})^2 / K_{\text{hom.}}^2}$ for the relative deviation between a effective medium conductivity $K_{\text{effmed.}}$ and $K_{\text{hom.}}$, if $K_{\text{hom.}}$ is supposed to be the "real" value) for high and low pressure heads are for field 2 and 3 in the same range for the pressure heads considered here. Inbetween there is a range of pressure heads, where the deviations for all three effective medium approaches become very small. This is the range where the variance of the unsaturated hydraulic conductivity field decreases compared to that of the saturated hydraulic conductivity. It should be noted that the relative deviations of the effective medium theory conductivities and the real ones are in general moderate compared to the very high variance of the log hydraulic conductivity. The relative deviations are (with some exceptions) almost all below 1.
It should be noted that the effective conductivity curves shown here were derived with an approach for media with a connected background material and isolated inclusions. This is in an isotropic two-dimensional medium clearly always the case. However, if a three-dimensional isotropic medium is considered, the topology of the material field can become more complex. In a three-dimensional medium more than one phase can be connected through the material. In this case the Maxwell approach or the differential effective medium theory approach can only be applied in a simplified way. The effective properties for all connected materials have to be approximated first, for example by taking the geometric mean, and all connected materials have to be considered to be one connected phase. All other phases are considered to be inclusions.
It should also be noted that the test fields considered here are all isotropic. However, an extension of the results to non-isotropic media would be straightforward, for the stochastic theory results as well as for the effective medium theory results.

5.4 Summary

In this chapter an upscaled model for flow processes modelled by Richards equation has been derived. The flow process described by Richards equation is usually flow in the unsaturated soil zone. Assuming the prerequisites for homogenization theory are given, the upscaled models for different Bond numbers were considered. The Bond number quantifies the ratio between gravity and capillary forces in a two-phase flow system. Analysing the case of vertical flow in a layered system, it has been demonstrated that the assumption

of capillary equilibrium is a good assumption, even when the Bond number is high. The upscaled models derived here are valid for slow flow processes only, as the typical time scale is assumed to be large.
The effective parameters for the upscaled model were then analyzed with a stochastic approach. Explicit results were obtained in a perturbation approximation. The effective parameters for some test examples showed that entry pressure effects disappear in the upscaled model and that the effective conductivity is especially at high saturations underpredicted if the effective conductivity is approximated by the mean of the local values only.
For the non-Gaussian fields introduced in Chapter 2, effective medium theory was used to derive the effective conductivity. It has been shown that in case that extreme parameter values in the field are connected, the effective conductivity can be predicted quite well with differential effective theory, while predictions made with the stochastic second order results are poor.

Chapter 6

Flow on an intermediate scale: Gravity driven two-phase flow

In this chapter the influence of soil structure on upscaled models for a two-phase flow problem will be discussed, where the simplifications made for Richards equation can no longer be used. That means, the pressure gradients in both phases have to be taken into account. It is thus described by the fully coupled system of equations for two-phase flow, as outlined in Section 1.4.3 (see also Eichel et al. (2005)). As in the last chapter, the flow process is considered for a length scale, where capillary forces are non-negligible. However, contrary to the last chapter, the non-wetting fluid is here important and it will be shown, that the parameters assigned to the non-wetting fluid are very sensitive to heterogeneous soil parameters. As the general case of the fully coupled two-phase flow problem is very complex, the special flow scenario of gravity driven counterflow of DNAPL and water is considered. The setup is sketched in Figure 6.1.
Gravity driven counterflow is important when a fluid with a higher density is on top of fluid which has a lower density in a system with closed boundaries. Such processes play a role for CO_2 sequestration or for the upward flow of gas in a waste deposit, which builds up from corroding material. It gravity driven counterflow might also occur during leakage of light non-aquous phase liquids (LNAPLs) from a waste deposit. It is however clear

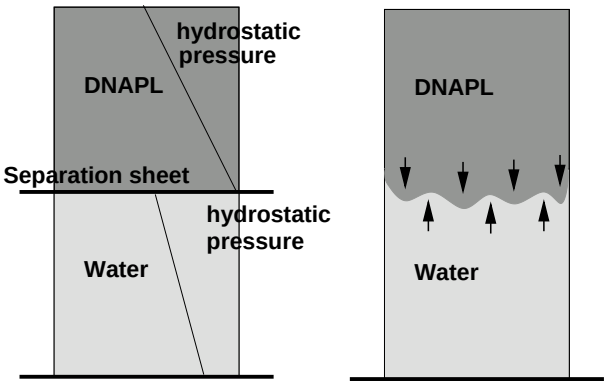

Figure 6.1: Sketch for the example flow scenario for countercurrent flow

The example could be illustrated with an experiment. A flume filled with heterogeneous porous material is considered. At initial time, the lower part of a porous medium is filled with water and the upper part is filled with DNAPL (as a fluid with a higher density than water, which is immiscible to water). All boundaries of the box are closed. The setup has to be considered in the way that at the beginning there is a separating sheet inbetween the fluids, for simpliciy it is assumed to be at half of the height of the box. The sheet carries the load of the DNAPL. With the sheet in place both fluids have a hydrostatic pressure distribution. The DNAPL-pressure at the top of the box and at the water pressure at the separation sheet are zero. Then the sheet is removed, so that the bottom of the box carries the full load of both fluids. At initial time the pressure distribution of the DNAPL is not changed, while the pressure distribution of the water is shifted by the amount of the load of the DANPL. As DNAPL is denser than water, gravity drives the DNAPL downwards, while the water is driven upwards, so that the total flux vanishes when averaged horizontally over the flume. In a homogeneous medium the steady state would then be a saturation distribution of the DNAPL, which corresponds to the P_c-S curve, so that everywhere we have $P_c = \Delta\rho gz$ if L is the height of the flume. The section on the P_c axis with length $\Delta\rho gL$ is the section which yields a total saturation of $S = 0.5$ for both fluids in the box. If the $P_c - S$ relationship is sharp, or the porous material is well sorted, the final configuration will be that both fluids are segregated.

In a heterogeneous medium the stable steady state condition is more complex, however the same criterion as described for the homogeneous medium holds. The saturation distribution will be heterogeneous. In principle this flow process, which leads to the steady state is unstable. As the porous medium is heterogeneous, we assume that the fluctuations of the invading DNAPL front are dominated by the structure of the heterogeneity and not the finger characteristics for the flow instabilities in the homogeneous flow scenario. This is clearly an assumption, which would have to be tested experimentally. It is however clear that if the parameter constrast in the medium is large and the structures are not much larger than the typical finger width, the flow will be guided by the heterogeneous structure.

In the following the flow problem will be explained in detail. The upscaled problem will then be derived using homogenization theory. Stochastis averaging has also been used in order to upscale the two-phase flow problem (e.g. Abdin et al., 1995), however, the results are extremely complex and underly many simlifications. They are therefore difficult to interpret. The effective parameters for the upscaled problem derived with homogenization theory will be calculated using stochastic methods. The results will be compared to the results calculated numerically for the test fields introduced in Chapter 2 (Figure 2.4). The effective permeability will then be compared to the effective permeability estimated with effective medium theory. In this way the parameter curves are reproduced for the case that the parameter fields have connected paths of extremely high or low values.

6.1 Flow equations

As the viscosity contrast between the two fluids is small, the fully coupled two-phase flow equations (1.17) and (1.18) have to be considered. As in two-phase flow the fluid phases have different densities, it is more common to use the pressure instead of the pressure head. Therefore, in the following the pressure will be used as primary variable, instead of the head which was used in the Richards equation.

$$\begin{aligned} & n_f \frac{\partial S_i}{\partial t} - \vec{\nabla} \cdot \vec{q}_i = n_f \frac{\partial S_i}{\partial t} + \vec{\nabla} \cdot \frac{\mathbf{K}_{\text{int}}}{\mu_i} k_{\text{rel,i}} \left(\vec{\nabla} P_i + \rho_i g \vec{e}_z \right) = 0 \\ & S_w + S_{nw} = 1 \\ & P_{nw} - P_w = P_c(S), \end{aligned} \tag{6.1}$$

where P_i [M / (LT^2)] is the phase pressure of fluid i, P_c [M / (LT)] is the capillary pressure, S_i [-] is the saturation of fluid i, μ_i [M / (L T)] and ρ_i [M / L^3] are its viscosity and density. K_{int} [L^2] is the intrinsic permeability of the medium and $g = 9.81 m/s^2$ is the constant of gravitation. The intrinsic permeability is in the following assumed to be isotropic and the tensor notation is dropped. $\vec{e}_z$ is the unit vector in vertical direction and n_f [-] is the porosity.
We use here the coupled equations as well as a formulation which is based on the total flow velocity. The two formulations are discussed in Binning and Celia (1999). The derivation of this formulation is explained in detail in Marle (1981).
The total flow veolcity $\vec{q}_{\text{total}}$ [L / T] is defined as

$$\vec{q}_{\text{total}} = \vec{q}_{nw} + \vec{q}_w. \tag{6.2}$$

By using this expression as

$$\vec{q}_{\text{total}} = -\frac{K_{\text{int}} k_{\text{rel,nw}}}{\mu_{\text{nw}}} (\vec{\nabla} P_{\text{nw}} + \rho_{\text{nw}} g \vec{e}_z) - \frac{K_{\text{int}} k_{\text{rel,w}}}{\mu_{\text{w}}} (\vec{\nabla} (P_{\text{nw}} - P_{\text{c}}) + \rho_{\text{w}} g \vec{e}_z) \tag{6.3}$$

solving for $\vec{\nabla} P_{\text{nw}}$ and inserting it into the continuity equation for the non-wetting fluid, this continuity equation would be

$$n_f \frac{\partial S_{nw}}{\partial t} + \vec{\nabla} \cdot \left[\vec{q}_{\text{total}} f_{nw}(S) + \frac{K_{\text{int}} \Delta\rho g}{\mu_w} \Lambda_{nw}(S) \vec{e}_z + \frac{K_{\text{int}} \Delta\rho g}{\mu_w} \Lambda_{nw}(S) \vec{\nabla} P_c(S) \right] = 0. \tag{6.4}$$

$\Delta\rho = \rho_w - \rho_{nw}$ is the density difference between the fluids. f_{nw} is the fractional flow function for the non-wetting fluid

$$f_{nw}(S) = \frac{k_{\text{rel,nw}}(S)/\mu_{nw}}{k_{\text{rel,nw}}(S)/\mu_{nw} + k_{\text{rel,w}}(S)/\mu_w} \tag{6.5}$$

and Λ is

$$\Lambda_{nw}(S) = f_{nw}(S) k_{\text{rel,w}}(S). \tag{6.6}$$

The fractional flow function f and Λ can be defined for the wetting fluid accordingly.

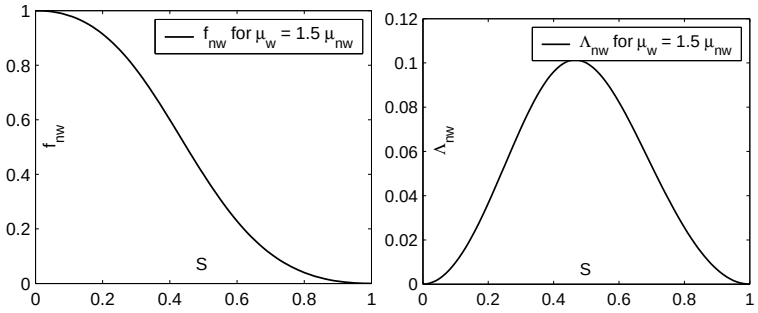

Figure 6.2: Examples for the fractional flow function f_{nw} and for the function Λ_{nw}

6.1.1 Space dependent parameters

In general, all soil properties in a heterogeneous medium have to be considered heterogeneous. Here, only the entry pressure P_{entry} (or an equivalent typical capillary pressure value, see equation (1.26)) and the intrinsic permeability are assumed to be heterogeneous. We assume further that the entry pressure and the saturated permeability are coupled via Leverett scaling (Leverett, 1941) or equivalently Miller-Miller similarity

$$P_{\text{entry}} \propto \frac{1}{\sqrt{K_{\text{int}}}}. \tag{6.7}$$

We write the heterogeneous saturated permeability distribution as

$$K_{\text{int}} = K_{\text{int,g}} \exp(f_k) \tag{6.8}$$

and the entry pressure is then (due to Leverett scaling)

$$P_{\text{entry}} = P_g \exp\left(-\frac{1}{2} f_k\right), \tag{6.9}$$

similar to the scaling which was used for the Richards equation. $K_{\text{int,g}}$ is the geometric mean of the saturated permeability and P_g the geometric mean of the entry pressures. The only heterogeneous parameter considered here is thus again the log permeability f_k. The field is assumed to be periodic in order for homogenization to be applicable. However, as outlined already in Chapter 3, the field does not have to be periodic, the main point is that the field is regular in the way that it does not have any long-range correlations.

6.1.2 Dimensionless variables

In order to make the equations dimensionless we adapt the formulation of Hilfer and Øren (1996), defining the typical time scale with buoyancy forces instead of their formulation using the flow velocity. The total velocity is here not a suitable quantity, as the mean total flow velocity is zero and therefore the local phase velocities will show large fluctuations.

Hilfer and Øren (1996) use a typical capillary pressure (such as the geometric mean of the entry pressure field), P_g, as a scaling for the capillary forces. However, as capillary forces and gravity forces are compared via a capillary pressure gradient, we use here a typical capillary pressure difference ΔP_g to scale the capillary pressure. As typical length scale the scale of the domain is used, as we are interested in the large scale processes. The permeability is scaled by the geometric mean of the saturated permeability, $K_{\text{int,g}}$, according to (6.8). The total flow velocity $\vec{q}_{\text{total}}$ is scaled with a typical flow velocity U. This variable is problematic. In average it vanishes, but locally it will be non-negligible. The variables read then

$$\mathbf{x} = L\mathbf{x}^\star, \quad t = \frac{L\mu_w}{K_{\text{int,g}}\Delta\rho g}t^\star, \quad P_c = \Delta P_g p_c^\star, \quad K_{\text{int,sat}} = K_{\text{int,g}}\exp(f_k), \quad \vec{q}_{\text{total}} = U\vec{q}^\star_{\text{total}}. \tag{6.10}$$

6.1.3 Dimensionless continuity equation: Total flux formulation

The dimensionless continuity equation for the non-wetting fluid can be written as

$$n_f\partial_{t^\star}S_{nw} + Gr\,\vec{q}^\star_{\text{total}}\cdot\vec{\nabla}^\star f_{nw}(S) - \vec{\nabla}^\star\exp(f_k)Bo\,\Lambda(S)\vec{\nabla}^\star p_c^\star + \vec{\nabla}^\star\exp(f_k)\Lambda_{nw}(S)\vec{e}_z = 0, \tag{6.11}$$

where Gr is the gravity number

$$Gr = \frac{U\mu_w}{K_{\text{int,g}}\Delta\rho g}. \tag{6.12}$$

The star marks dimensionless variables. f_{nw} and Λ_{nw} are the fractional flow functions defined in (6.5) and (6.6). They are dimensionless by definition. In a homogeneous medium with closed boundaries, the viscous term $\vec{q}_{\text{total}}\vec{\nabla}f(S)$ does not appear in the case that the flow process is viscous and gravity stable. Although the gravity number is therefore supposed to vanish for the averaged flow process, it will locally in the heterogeneous medium be non-negligible.
Bo is the Bond number, similar to the one defined in equation (1.24). A typical capillary pressure difference instead of a typical capillary pressure is used, for the same reason as explained in Chapter 5. It is similar to the Bond number defined for the Richards equation, but is here depending on the density difference between DNAPL and water,

$$Bo = \frac{\Delta\rho g L}{\Delta P_g}. \tag{6.13}$$

6.1.4 Dimensionless continuity equation: Pressure formulation

Due to the heterogeneity of the soil and the unstability of the flow, the flow scenario will rather be such that the two fluids will bypass each other, the DNAPL flowing in the coarser material and the water flowing in the finer material. This bypassing depends on the structure of the soil. In case that either the coarse or the fine part of the material forms

isolated structures, i.e. there are no connected paths of this material through the box, bypassing flow cannot take place. However, if there is bypassing of the fluids, the fluids will flow in separated parts of the material.

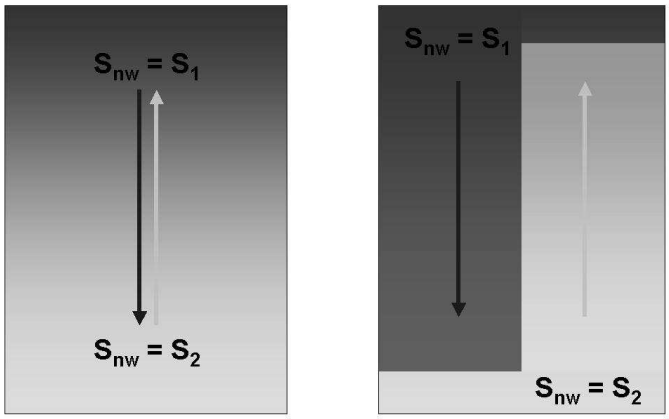

Figure 6.3: Homogeneous counterflow (left) and bypassing flow (right)

For such a model it will be necessary to consider the flow equations for each phase separately. As there is not much interference of the fluids (except for the blocking of certain parts of material), it is more reasonable to search for an averaged equation for both fluids separately and combine them afterwards to an upscaled equation in the form of (6.11) than to upscale this equation from the beginning. This will be explained in more detail in the next section.
The pressure of each phase has therefore also to be made dimensionless with a typical pressure. A typical pressure difference is chosen to scale the pressure

$$P_i = \Delta\mathscr{P}_i p_i^\star. \tag{6.14}$$

The dimensionless continuity equations for each phase read

$$n_f \frac{\partial}{\partial t^\star} S_i + \vec{\nabla}^\star \cdot \left[\frac{\mu_w}{\mu_i} \frac{\rho_i}{\Delta\rho} \exp(f_k) k_{r,i} \left(G_i \vec{\nabla}^\star p_i^\star + \vec{e}_z \right) \right] = 0. \tag{6.15}$$

G_i is a dimensionless number, which relates viscous and gravity forces in each fluid,

$$G_i = \frac{\Delta\mathscr{P}_i}{L\rho_i g}. \tag{6.16}$$

Unless stated explicitely otherwise, the variables will from now on be considered dimensionless. The star index is not used any more in order to keep the notation short.

6.2 Upscaled model

In order to derive an upscaled model for a system as described in the example, a scale expansion such as in homogenization theory can be used. The medium is thus assumed to have a clearly defined REV. It is also assumed that the length scale of an REV ℓ is much smaller than the length scale of the whole box. That is, the two length scales are assumed to be clearly separated. As the box is assumed to be of a laboratory scale, the heterogeneities are small scale.
The problem will finally be considered to be a continuity equation for the DNAPL. Therefore, the non-wetting phase saturation will be considered as primary variable and is expanded as

$$S_{nw} = S_{nw}^{(0)} + \varepsilon S_{nw}^{(1)} + \varepsilon^2 S_{nw}^{(2)} + \dots \tag{6.17}$$

Also the pressure in each phase is expanded as

$$p_i = p_i^{(0)} + \varepsilon p_i^{(1)} + \varepsilon^2 p_i^{(2)} + \dots \tag{6.18}$$

All other functions depending on any of these parameters can be derived from these expansions according to (3.9). Note that in principle there are only two primary variables required. However, if two primary variables are fixed, the other variables can be derived as (3.9). Therefore there is nothing wrong with using expansions for saturation and pressures separately.
In the total flux formulation of the equation (6.11) the saturation is the unknown variable. The total flow velocity is treated as a heterogeneous parameter. However, it is coupled to the pressure equation, so that there is also the pressure as a second unknown. In order to derive an upscaled equation it might however be useful to keep the total flow velocity as a parameter field, which is approximated in a sensible way. The problem has then only one unknown, which is the saturation. This formulation will be used here, as in the upscaled problem the total fluy will be zero.

6.2.1 Dimensionless numbers

The dimensionless numbers have to be set into relation to the expansion parameter ε. They are fixed for the following as

$$Bo = O(\varepsilon^0), \quad G_i = O(\varepsilon^0). \tag{6.19}$$

The gravity number is at this stage left undefined. This quantity is a bit problematic, as it would be assigned differently for the upscaled model and for the heterogeneous one. In the homogeneous model the total flow velocity is zero. Therefore there is no gravity number for the averaged system. However, when defined for the heterogeneous medium, it can become quite large.
The Bond number suggests that the typical capillary pressure difference over the box is in the same range as the density difference times gravitational constant. For a lab-scale setup this is a reasonable assumption. The saturation differences are high, so that

it is a reasonable assumption to proceed from a capillary pressure difference in the range of the entry pressure. This might well be comparable to the density difference times gravitational constant times the length of the box. For a scenario on a field scale this might not be reasonable any more.
The gravity numbers for the single fluids suggest that the pressure difference in each fluid is in the range of its density times the gravitational constant times the length of the box. As at the beginning both fluids have hydrostatic conditions and we assume that the fluids will bypass each other, this is also a reasonable assumption.
The typical time scale is determined by the less mobile fluid. Therefore it is estimated as

$$T = \frac{\mu_{\min} L}{K_{\text{int}}}. \tag{6.20}$$

$\mu_{\min}$ is the smaller viscosity of the two.

6.2.2 Averaging procedures

There are different procedures to derive an upscaled model. One approach would be to proceed from the total flow velocity formulation (6.11) in a heterogeneous medium and to average this equation. However, the unknown total flow velocity is problematic. It is difficult to scale in terms of an expansion parameter ε. In average it is small, while locally it can be high.
Also, the contributions of the different terms in the heterogeneous equation and in the upscaled equation will be different. Counterflow in a homogeneous medium is captured by the last term on the right hand side in (6.11). As outlined above we may proceed from the assumption that the two fluids bypass each other, so that DNAPL will flow downwards in some parts of the medium and water will flow upwards in other parts of the medium. This leads in average to countercurrent flow. However, in the heterogeneous medium this process is captured by the viscous term, which is the first term on the right hand side in (6.11). This term will be large in the heterogeneous model, but has to vanish in the averaged model. The bypassing means for the saturation of DNAPL that it will be either very high or very low in the medium. The parameter Λ in (6.11) will be very small in the heterogeneous model, as the saturation is very high or very low. In the averaged model this term has to be large. The procedure to upscale (6.11) is therefore not very useful for the type of flow considered here.
Instead the continuity equation for each phase will be considered separately. The averaged continuity equations will then be put together to a continuity equation based on a total flow formulation.

6.2.3 Local capillary equilibrium

Although the averaged equations will be derived from the continuity equations for each fluid separately, we will make use of the condition that the Bond number is of order ε^0.

The highest order term of the expanded continuity equation in the total flux formulation will be considered. This is the part which is of order ε^{-2}:

$$\vec{\nabla}_{\hat{Y}} \exp(f_k) Bo \Lambda(S) \vec{\nabla}_{\hat{Y}} p_c = 0. \tag{6.21}$$

As shown for the capillary equilibrium case for the Richards equation, the solution is that the capillary pressure does not depend on the small scale $p_c = p_c(\hat{X}, t)$. The reason for the dominance of the capillary forces on the small scale is that the capillary term has a second spatial derivative, while buoyancy forces have only a first spatial derivative. Small scale fluctuations of the capillary pressure will be equalized quasi-instantaneously, and other forces can on the small scale be neglected for the leading order terms.
As the capillary pressure does not depend on the small scale, the saturation distribution for a given averaged capillary pressure is fix. Also the local parameter functions, such as relative permeability, fractional flow function or Λ function are locally constant for a given value of a capillary pressure.

6.2.4 Continuity equations of the single fluids

Applying the scale expansion described in Section 3.1.2 to the saturation and the pressure in the continuity equation of each fluid (6.15), leads to a system of equation with different orders ε. The highest order terms are of order ε^{-2}. The equations (6.15) of order ε^{-2} read

$$\vec{\nabla}_{\hat{Y}} \exp(f_k(\hat{Y})) k_{r,i}(S_i^{(0)}) \vec{\nabla}_{\hat{Y}} {p_i}^{(0)}(\hat{X}, \hat{Y}, t) = 0. \tag{6.22}$$

The pressure p is $\hat{Y}$-periodic and there are no sources and sinks for the pressure on the small scale. Therefore, the only solution of (6.22) is that the pressure in each phase has to be independent of the small scale, ${p_i}^{(0)} = {p_i}^{(0)}(\hat{X}, t)$. This implies, not only the capillary pressure is locally constant, but also the pressure of each fluid is locally constant.
Provided that we have capillary equilibrium, the equations of order ε^{-1} read

$$\vec{\nabla}_{\hat{Y}} \left[\exp(f_k(\hat{Y})) k_{r,i}(S_i^{(0)}) \left(G_i \vec{\nabla}_{\hat{X}} {p_i}^{(0)} + G_i \vec{\nabla}_{\hat{Y}} {p_i}^{(1)} + \vec{e}_z \right) \right] = 0. \tag{6.23}$$

As $S_i^{(0)}(\hat{Y})$ is fixed by the constant capillary pressure, the only unknown is $p_i^{(1)}$ which has to be periodic over the unit cell.
This problem is completely similar to the first order problem of the Richards equation problem with capillary equilibrium. A solution can be obtained with the approach

$$p_i^{(1)}(\hat{X}, \hat{Y}) = \vec{\chi}_i(\hat{Y}) \cdot (G_i \vec{\nabla}_{\hat{X}} p_i^{(0)}(\hat{X}) + \vec{e}_z). \tag{6.24}$$

The result of a problem like (6.23) has been discussed for the Richard's equation problem. The analogy is here reasonable from a physical point of view. As discussed, the two fluids flow independently of each other and "see" the other fluid mainly due to its blocking of parts of the material. In Richards equation the air is also only seen as a background fluid that blocks parts of the material for water.
To obtain the upscaled flow equations, the equation of order ε^0 is averaged over the unit cell. All terms of the shape $\vec{\nabla}_{\hat{Y}} \cdot \vec{v}$ do vanish in average ($\langle \vec{\nabla}_{\hat{Y}} \cdot \vec{v} \rangle = 0$) due to the periodic boundary conditions at the boudary of the unit cell.

6.2.5 Averaged leading order equation for a single fluid

The averaged continuity equation to order ε^0 reads (considering that the pressure $p^{(0)}$ does not depend on the small scale $\hat{Y}$):

$$n_f \partial_t \langle S_i^{(0)} \rangle + \vec{\nabla}_{\hat{X}} \cdot \left[\frac{\mu_w}{\mu_i} \frac{\rho_i}{\Delta\rho} \langle \exp(f_k(\hat{Y})) k_{r,i}(S_i^{(0)}) \left(G_i \vec{\nabla}_{\hat{X}} p_i{}^{(0)} + G_i \vec{\nabla}_{\hat{Y}} p_i{}^{(1)} + \vec{e}_z \right) \rangle \right] =$$
$$n_f \partial_t S_{\text{eff}}(p_c^{(0)}) + \frac{\mu_w}{\mu_i} \frac{\rho_i}{\Delta\rho} \vec{\nabla}_{\hat{X}} \cdot \left[\mathbf{K}_{\text{eff}} \left(G_i \vec{\nabla}_{\hat{X}} p_i{}^{(0)} + \vec{e}_z \right) \right] = 0 \quad (6.25)$$

with

$$\mathbf{K}_{\text{eff,i}} = \langle \exp(f_k(\hat{Y})) k_{r,i}(S_i^{(0)}) \left(\mathbf{1} + \vec{\nabla}_{\hat{Y}} \otimes \vec{\chi}(\hat{Y}) \right) \rangle, \quad S_{\text{eff}} = \langle S_i^{(0)} \rangle, \quad (6.26)$$

where $\mathbf{K}_{\text{eff,i}}$ is the effective permeability tensor for phase i. $\vec{\chi}$ is the solution of (6.23), $\otimes$ is the dyadic tensor product and $\mathbf{1}$ is the unity matrix. The solution for $\vec{\chi}$ has in general to be found numerically, the same way as it was shown for the Richards equation problem. We summarize the practical steps to obtain the effective permeability tensor $\mathbf{K}_{\text{eff,i}}$.

1. Choose a value for the mean capillary pressure $p_c^{(0)}$ within the unit cell.
2. Calculate the corresponding distribution of the saturation field $S_i^{(0)}$ throughout the unit cell.
3. For the saturation field calculate the distribution of the permeability field $\exp(f_k) k_{r,i}^{(0)}$ throughout the unit cell.
4. Choose a unit hydraulic gradient in direction j and apply periodic boundary conditions for the steady-state head equation within the unit cell. This results in the field of $\chi_j + \hat{Y}_j$.
5. Calculate the mean flux vector for $\chi_j + \hat{Y}_j$. This yields the j-th column of the effective permeability tensor $\mathbf{K}_{\text{eff,i}}$.
6. Repeat steps 4 and 5 in the direction perpendicular to j.

Contrary to the Richards equation, the effective permeability is here calculated for both fluids. The effective capillary pressure - saturation curve is obtained in the same way (see also Braun et al. (2004)):

1. Choose a value for the mean capillary pressure $p_c^{(0)}$ within the unit cell.
2. Calculate the corresponding distribution of the saturation field $S_i^{(0)}$ throughout the unit cell.
3. Average the saturation distribution over the unit cell to obtain $S_{\text{i,eff}}$.

We obtain in the upscaled model the same type of equations as in the small scale one, but with an effective relative permeability function and an effective capillary pressure - saturation function.

6.2.6 Averaged continuity equation for the DNAPL with a total flux formulation

From the continuity equation for the two single fluids we can construct an effective continuity equation for the DNAPL in the formulation, which is based on the total flow (same form as (6.11)).

$$n_f \partial_t S_{\mathrm{nw,eff}}(p_c^{(0)}) - \vec{\nabla}_{\hat{X}} \Lambda_{\mathrm{eff}}(S_{\mathrm{nw,eff}}(p_c^{(0)})) \vec{\nabla}_{\hat{X}} p_c^{(0)} + \vec{\nabla}_{\hat{X}} \Lambda_{\mathrm{eff}}(S_{\mathrm{nw,eff}}(p_c^{(0)})) \vec{e}_z = 0, \quad (6.27)$$

with

$$\Lambda_{\mathrm{eff}}(S_{\mathrm{nw,eff}}) = \frac{K_{\mathrm{eff,nw}} K_{\mathrm{eff,w}}}{\mu_{nw}/\mu_w K_{\mathrm{eff,w}} + K_{\mathrm{eff,nw}}}. \quad (6.28)$$

The viscous term does not appear here, as the two averaged flow velocities have to counterbalance each other when they are averaged over the unit cell. The function Λ_{eff} contains the most important information for the flow process. It represents a measure for the mobility of the two fluids. The residual saturation, which is the averaged saturation at which the medium becomes conductive for the non-wetting fluid, also appears in Λ_{eff}.
The averaged model is qualitatively different from the model of the heterogeneous medium. In the averaged model there is in average no total flux. The counterflow is captured by the gravity term. In the heterogeneous model the viscous term is important.

6.3 Prediction of effective parameters and influence of structure

The influence of soil structure has for the full two-phase flow problem an additional aspect compared to the Richards equation, where only the water phase is considered. Besides the effective constitutive relationships the residual saturation is strongly affected by the soil structure. Residual saturation appears in the Richards equation model as a parameter in the capillary pressure saturation relation and relative permeability function. However, trapping of water or air due to entry pressure effects in a heterogeneous medium cannot occur in the Richards equation model. The air is by construction always considered to be connected to the surface and the water is the wetting phase and does therefore not have to overcome an entry pressure. In the two-phase problem the non-wetting fluid cannot infiltrate regions where it would infiltrate as its phase pressure exceeds the entry pressure, if these regions are blocked as they are fully saturated with wetting fluid. The trapping effect is very much influenced by the structure of the soil heterogeneities.

6.3.1 Accessibility criteria - residual saturation

The result (6.28) was obtained under the assumption of capillary equilibrium. That means, once a capillary pressure is fixed, the saturation on the small scale is determined by the local capillary pressure saturation relation. The question might however be asked, how

the DNAPL could access regions which are detached from the connected DNAPL phase and are surrounded by regions, in which the DNAPL cannot infiltrate as the entry pressure is not exceeded. Such regions are in principle not accessible for the DNAPL.

It has been observed in experiments that during DNAPL infiltration there appear patches filled with DNAPL, which seem to be completely detached from the connected DNAPL phase. The transport of the DNAPL to these regions happened on paths visible only on the pore scale, and the connected phase in these pores was snapped off after a while. The transport of the DNAPL into the patches was not observable on the large scale. The static percolation approach, where all soil patches are filled with DNAPL according to their entry pressure, regardless of their accessibility from the connected DNAPL phase, could therefore be considered a reasonable approach to model the static DNAPL saturation in the medium. However, the movement of DNAPL into detached patches happened only on very large time scales. For intermediate times it is not to be expected that DNAPL will infiltrate into detached zones. The problem of accessibility has therefore to be considered.

As outlined above, the accessibility aspect causes an inconsistency considering the macroscopic residual saturation. This can be illustrated by considering a medium which has no residual saturation in the local parameter functions. Proceeding from capillary equilibrium, the residual saturation of non-wetting fluid of the capillary pressure saturation relation is zero. Once the smallest entry pressure in the medium is exceeded, the total saturation of non-wetting fluid in the unit cell is non-zero. However, the effective residual saturation of non-wetting fluid in the relative permeability relationship can be non-zero. The saturation of non-wetting phase might increase, but it increases in zones which are detached and which it can in reality not enter. Therefore, the medium remains impermeable for the non-wetting fluid. To make the residual saturations consistent, it would be better to have no saturation of the non-wetting fluid in the medium, until the medium becomes conductive for the non-wetting fluid. This is also more reasonable from a physical point of view. The macroscopic residual saturation of the effective relative permeability function has thus consistently also to be chosen as the macroscopic residual saturation for the effective capillary pressure saturation relationship.

As the wetting fluid is always connected, there is no macroscopic residual saturation of wetting fluid.

An alternative routine to calculate effective parameters can be used, which takes accessibility criteria into account. For a given capillary pressure, in all regions, which have a lower entry pressure than the given capillary pressure, but which are surrounded by parts which have a higher entry pressure, the saturation of the non-wetting phase is set to zero. The averaged non-wetting saturation exceeds zero only at the pressure, where a connected path throughout the unit cell is established. This does not change the effective permeability of the non-wetting phase assigned to the given capillary pressure, as only connected paths contribute to the permeability. However, it slightly changes the effective permeability of the wetting phase.

The effective capillary saturation function with local capillary equilibrium is derived from the distribution of volume percentages of the different materials, or their parameters respectively. If the macroscopic residual saturation should be taken into account, the infor-

mation about connected or isolated structures of certain parameters has additionally to be available.
The change of the capillary pressure curve with or without connectivity properties makes a large difference if mass balances are considered.

6.3.2 Effective mobility

The routine to calculate the effective mobility function Λ_{eff} (6.28) is clear for a given parameter field. For practical purposes a parameter field is however mostly not known. Therefore the effective mobility function or permeability functions of the single fluids has to be derived based on a more general description of the heterogeneous parameters. A method that employs only information about the probability distribution of the parameters or about the volume percentage of the different materials is here not a very good approach. The material becomes conductive for the non-wetting phase only once the entry pressure of the material which is connected through the field is exceeded. Therefore the structure is here very important. Also, the usual approach to calculate effective permeability, such as using the geometric mean, are here not useful approaches. All parts in the material for which the entry pressure is not exceeded have a local permeability of zero. The geometric mean would therefore always be zero, although these patches might be small and the whole material is conductive for the non-wetting phase. As the fields have unconductive parts for the non-wetting fluid, any approach based on a log-normal permeability distribution is not useful. Effective medium theory could be more appropriate to calculate the effective permeability for the non-wetting fluid. The self-consistent approach has a fixed percolation threshold of $p_c = 0.5$ in 2d and $p_c = 0.33$ in 3d. Whenever a volume percentage of more than the percolation threshold of unconductive material is in the medium, the medium is unconductive, independently on the structure. A fixed percolation threshold is not useful here to derive upscaled models.
If connectivity criteria should be considered the most useful approach is the Maxwell approach or differential effective medium theory, where the connected material part is assigned to the background. The drawback is here that the material properties of the background have to be homogeneous, so that in case the connected material phase is again composed of different materials, an effective parameter has to be used separately for the connected part.

6.3.3 Example 1: Log-normally distributed test fields for a Brooks-Corey model

Similar to the Richards equation problem the heterogeneous parameters of the soil could be modeled as correlated random fields.
In the following a Brooks-Corey model with $\lambda = 2$ (see Section 1.4.3, equation (1.26)) will be used to model the capillary pressure saturation relation. The relative permeabilities will be modeled as quadratic functions for simplicity. As outlined above, we assume that the entry pressure is heterogeneously distributed and that it is coupled to the intrinsic

permeability (6.7), so that it is related to log permeability f_k via (6.9). All parameter functions will therefore be related to f_k. The water saturation reads

$$\begin{aligned} S_w^{(0)} &= \begin{cases} \left(\dfrac{P^\star_{\text{entry}}}{P^{(0)}}\right)^2 & \text{if } P^{(0)} > P_{\text{entry}} \\ 1 & \text{otherwise} \end{cases} \\ &= \begin{cases} \left(\dfrac{\exp\left(-\dfrac{1}{2}f_k\right)}{P^{(0)}}\right)^2 & \text{if } f_k > -2\ln(P^{(0)}) \\ 1 & \text{otherwise} \end{cases} \end{aligned} \tag{6.29}$$

The wetting permeability is $k_{r,w} = S_w^2$ and the non-wetting permeability is $k_{r,nw} = (1 - S_w)^2$, which reads as function depending on f_k:

$$k_{r,w}^{(0)} = \begin{cases} \left(\dfrac{\exp\left(-\dfrac{1}{2}f_k\right)}{P^{(0)}}\right)^4 & \text{if } f_k > -2\ln(P^{(0)}) \\ 1 & \text{otherwise} \end{cases}, \tag{6.30}$$

$$k_{r,nw}^{(0)} = \begin{cases} \left(1 - \left(\dfrac{\exp\left(-\dfrac{1}{2}f_k\right)}{P^{(0)}}\right)^2\right)^2 & \text{if } f_k > -2\ln(P^{(0)}) \\ 0 & \text{otherwise} \end{cases}. \tag{6.31}$$

The parameter f_k is assumed to be normally distributed with a variance σ_f^2. The average of a function of f_k, $\Phi(f_k)$ is then obtained by integration over the probability density

$$\langle \Phi \rangle = \int_{-\infty}^{\infty} \Phi(f_k) \frac{1}{\sqrt{2\pi\sigma_f^2}} \exp\left(-\frac{f_k^2}{2\sigma_f^2}\right) df_k. \tag{6.32}$$

Results without accessibility criteria

For the averaged capillary pressure saturation relation without accessibility criteria we get

$$\begin{aligned} \langle S_w \rangle = &\frac{1}{2}\left[\exp\left(-2\ln(P^{(0)}) + \frac{\sigma_f^2}{2}\right)\left(1 - \operatorname{erf}\left(\frac{-2\ln(P^{(0)}) + \sigma_f^2}{\sqrt{2}\sigma_f}\right)\right) + \right. \\ &\left.\left(1 - \operatorname{erf}\left(\frac{-\sqrt{2}\ln(P^{(0)})}{\sigma_f}\right)\right)\right]. \end{aligned} \tag{6.33}$$

The average wetting and non-wetting permeability can also be calculated, although the averaged permeabilities are certainly not good approximations for the effective permeabilities, but will overpredict them. A better estimate for the effective permeability would be the geometric mean of the local permeability. For the wetting fluid the geometric mean of the local permeability could be calculated according to (5.101) in the Richards equation problem. The geometric mean is however not a good approximation for the effective permeability of the non-wetting fluid, as the local permeability always vanishes at certain locations in a lognormally distributed f_k field. The geometric mean is therefore always equal to zero. As this problem does not occur with the arithmetic mean, is will be used here as an approximation for the effective permeability.

$$\begin{aligned}\langle K_{\text{int}} k_{r,w} \rangle_{\text{no acc.}} = &\frac{1}{2}\left[\exp\left(-4\ln(P^{(0)}) + \frac{\sigma_f^2}{2}\right)\left(1 - \text{erf}\left(\frac{-2\ln(P^{(0)}) + \sigma_f^2}{\sqrt{2}\sigma_f}\right)\right) + \right. \\ &\left. \exp\left(\frac{\sigma_f^2}{2}\right)\left(1 - \text{erf}\left(\frac{2\ln(P^{(0)}) + \sigma_f^2}{\sqrt{2}\sigma_f}\right)\right)\right].\end{aligned} \tag{6.34}$$

$$\begin{aligned}\langle K_{\text{int}} k_{r,nw} \rangle_{\text{no acc.}} = &\frac{1}{2}\left[\exp\left(\frac{\sigma_f^2}{2}\right)\left(1 + \text{erf}\left(\frac{2\ln(P^{(0)}) + \sigma_f^2}{\sqrt{2}\sigma_f}\right)\right) + \right. \\ &\exp\left(-4\ln(P^{(0)}) + \frac{\sigma_f^2}{2}\right)\left(1 + \text{erf}\left(\frac{2\ln(P^{(0)}) - \sigma_f^2}{\sqrt{2}\sigma_f}\right)\right) - \\ &\left. 2\exp\left(-2\ln(P^{(0)})\right)\left(1 + \text{erf}\left(\frac{2\ln(P^{(0)})}{\sqrt{2}\sigma_f}\right)\right)\right].\end{aligned} \tag{6.35}$$

Plots of the curves are shown in Figure 6.4 below, together with plots for the homogeneous parameter functions. The homogeneous curves were constructed for the parameter $f_k = 0$. It can be seen that the entry pressure effect vanishes, as there is a probability to find every entry pressure due to the log-normal distribution. The overprediction of the relative permeability curve for the nonlinearity is not realistic. The effect comes from the overweighting of high values with the arithmetic mean, which was used to calculate the effective permeabilities. The overprediction of the relative permeability of the non-wetting fluid leads to an overprediction of the effective Λ function.

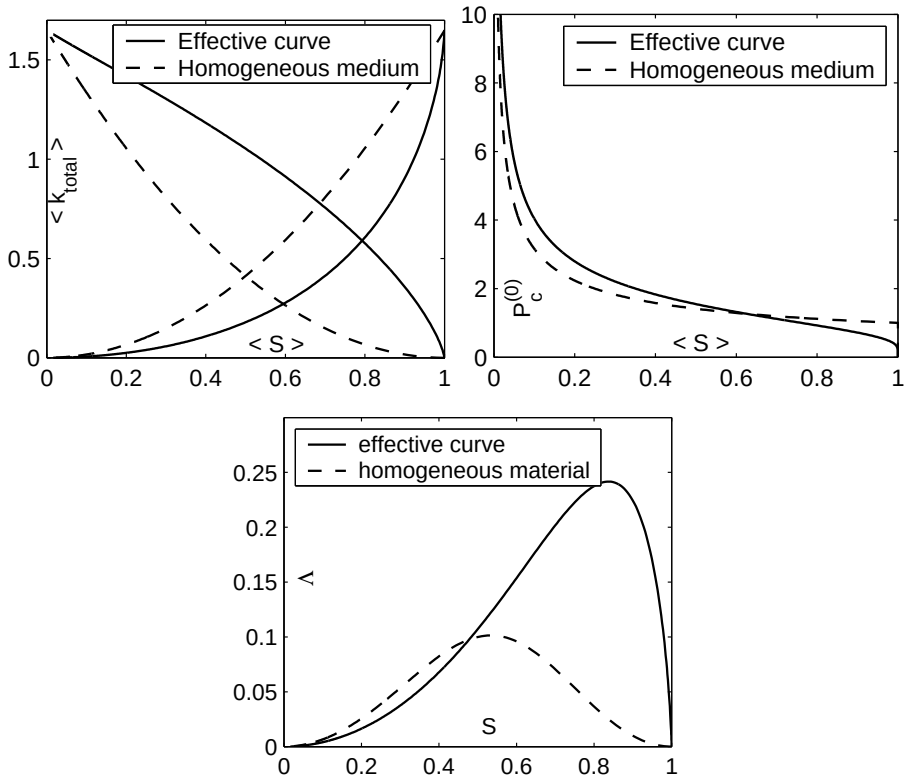

Figure 6.4: Effective capillary pressure - saturation function (left), effective permeability - saturation function (right) and effective Λ-function obtained with the model shown above, taking no accessibility criteria into account

Results with accessibility criteria

If accessibility criteria are taken into account, there is a threshold value $f_{k,thr}$, above which the parameters are conductive. The threshold value is assigned to material with a parameter value f_k, below which the materials form isolated structures. Only if this threshold is reached does DNPL enter the medium. This leads to a macroscopic entry pressure effect. The effective parameter functions read then

$$\langle S_w \rangle_{\text{acc.}} = \begin{cases} \langle S_w \rangle_{\text{no acc.}} & \text{if } P^{(0)} < \exp(-1/2 f_{kthr}) \\ 1 & \text{otherwise} \end{cases} , \tag{6.36}$$

$$\langle K_{\text{int}} k_{r,w} \rangle_{\text{acc.}} = \begin{cases} \langle K_{\text{int}} k_{r,w} \rangle_{\text{no acc.}} & \text{if } P^{(0)} < \exp(-1/2 f_{kthr}) \\ 1 & \text{otherwise} \end{cases} , \tag{6.37}$$

$$\langle K_{\text{int}} k_{r,nw} \rangle_{\text{acc.}} = \begin{cases} \langle K_{\text{int}} k_{r,nw} \rangle_{\text{no acc.}} & \text{if } P^{(0)} < \exp(-1/2 f_{kthr}) \\ 0 & \text{otherwise} \end{cases} . \tag{6.38}$$

For the test fields of chapter 2 the threshold values were $f_{k,thr} = 0$ for field 1, $f_{k,thr} = 1.23$ for field 2 and $f_{k,trh} = -1.23$ for field 3.

Plots for the effective capillary pressure - saturation curve, for the effective permeability curves and for the effective Λ curve with and without accessibility criteria are shown in Figure 6.5. The relative permeability of the wetting fluid is one for capillary pressure values lower than the value which is matched by the vertical line. The relative permeability of the non-wetting fluid and the Λ function is zero below the corresponding values.

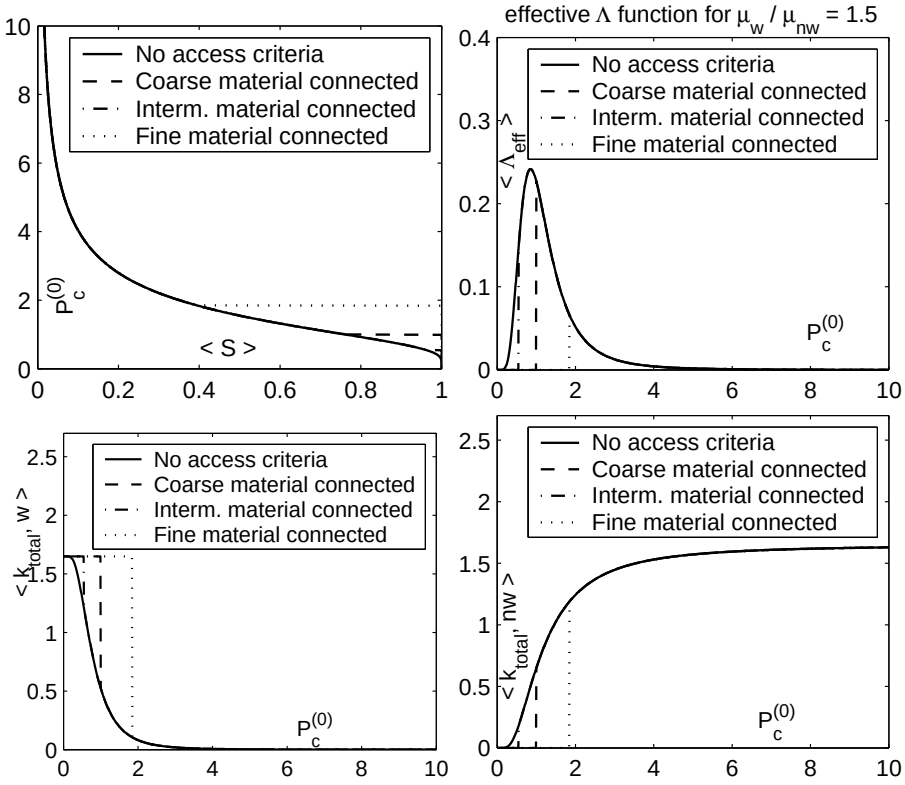

Figure 6.5: Effective capillary pressure - saturation function (upper left), effective Λ-function (upper right) and effective permeability - capillary pressure function (bottom left for wetting and bottom right for non-wetting) taking accessibility criteria into account

The effective capillary pressure saturation curve is influenced by the presence of connected and isolated parts, as for different threshold values a different macroscopic entry pressure appears in the model. The macroscopic entry pressure corresponds to the entry pressure of the material with the parameter, below which the material forms isolated structures. The mobility is very much affected by the isolated and connected structure of the medium, as due to the trapping of wetting fluid (or rather due to the accessibility criteria for the non-wetting fluid) the non-wetting phase remains immobile unless the entry pressure of the first connected structure is reached.

Comparison of the permeabilities to numerically obtained results

The effective saturation for the model without accessibility criteria is obtained by averaging over the static saturation distribution. As only the probability distribution of the parameters are needed, the results are not different for the three different test fields (see also Neuweiler et al. (2004a)). If accessibility is taken into account, the curves differ in terms of their macroscopic entry pressure. The mobility is however very much influenced. The important parameter function for the problem considered here is the effective function Λ_{eff}. This function is plotted for the three test fields in Figure 6.6. The effective curves were calculated following the outline in Section 6.2.5. The small-scale problem for the calculation of the effective permeability was solved by a cell-centered Finite Volume scheme applying periodic boundary conditions (see Cirpka and Kitanidis (2002)), as in the Richards equation problem. The resulting system of linear equations was solved by a conjugate gradient method with algebraic multigrid preconditioning Ruge and Stüben (1987).

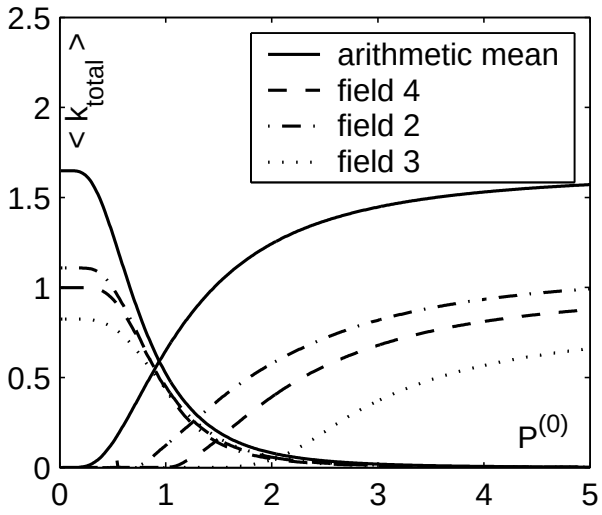

Figure 6.6: Effective permeability - capillary pressure function predicted with arithmetic averages and calculated numerically

The wetting phase is not too much affected by the accessibility criteria and are not so badly predicted with the arithmetic mean (although the saturated value is too high). The non-wetting phase is however very much overpredicted by the arithmetic mean, especially at pressure values where the non-wetting phase cannot enter into the medium. If accessibility criteria would be taken into account the non-wetting permeability could be matched better, however, the abrupt step from permeability zero to the arithmetic mean would not be realistic.

The numerically obtained results show that the large scale residual saturation is clearly influenced by the connectivity properties of the field. The residual saturation of the medium where high values of f_k are well connected is $S = 0.05$ ($P^{(0)} = 0.5$) that of the material where intermediate values are well connected is $S = 0.22$ ($P^{(0)} = 1$) and that of the

material where low values are well connected is $S = 0.55$ ($P^{(0)} = 2$) in Figure 6.6. The difference is very large and the residual saturation is expected to have a high impact on the large scale flow behaviour. Not only the residual saturation is affected, but also the maximum of the effective function Λ_{eff} differs by a factor of 5 between the material where high values are well connected and the material where low values are well connected. The fluids will therefore show a much larger mobility in the first material than in the second one.
Due to these differences between the effective functions Λ_{eff} of the three materials, one would expect the displacement to be much slower in the material where low parameter values are well connected than in the material where high values are well connected. The amount of DNAPL which remains trapped in the upper part of the medium will be much higher in the second material than in the first one.

6.3.4 Example 2: Three material composites for a Brooks-Corey model

From the last example it becomes clear that the arithmetic mean is not a good approach to calculate the effective permeability functions for the two fluids. Effective medium theory might in this case be a better approach. The self-consistent approach described in Section 3.2.3 could be applied, however, the permeability of the non-wetting fluid will vanish if half of the material is unconductive, independently on whether this material is isolated or has connected paths through the medium. If the field is normally distributed, such as the three test fields introduced in Chapter 2 (cf. Figure 2.4), the non-wetting phase will become conductive for $P_c^{(0)} < 1$ (corresponding to $f_{k,thr} = 0$) for all three fields. This is not realistic. The Maxwell approach described in Section 3.2.2 or the differential effective medium theory approach described in Section 3.2.4 can be applied, if the parameter field is split into subgroups, where the isolated material parts are put in several groups and the whole connected structure in the material has to be represented by one group. For simplicity we will assume that there is only one material or a continuous range of parameters which has connected paths in the material. The Maxwell approach is then applied to calculate the effective permeability for the wetting and for the non-wetting fluid.
The test fields used here are three material composites. As starting fields the test fields introduced in Chapter 2 will be used. The parameter field will be mapped onto three values for f_k, namely $f_k = -1.34$, $f_k = 0$ and $f_k = 1.34$. The volume percentage of all three materials is here $\phi_1 = 0.33$, $\phi_2 = 0.33$ and $\phi_3 = 1 - \phi_1 - \phi_2 = 0.34$. The fields are shown below in Figure 6.7.
The local Brooks-Corey relations defined in (6.29), (6.30) and (6.31) are here also valid. But the distribution of the f_k values is here different. The averaged saturation without access criteria is now

$$\langle S_w \rangle_{\text{no acc.}} = 1 - \sum_{\{i, f_{k,i} > -2\ln(P^{(0)})\}} \phi_i \left(1 - \frac{\exp\left(-f_{k,i}\right)}{(P^{(0)})^2} \right). \tag{6.39}$$

The averaged saturation with access criteria is again given by (6.36).

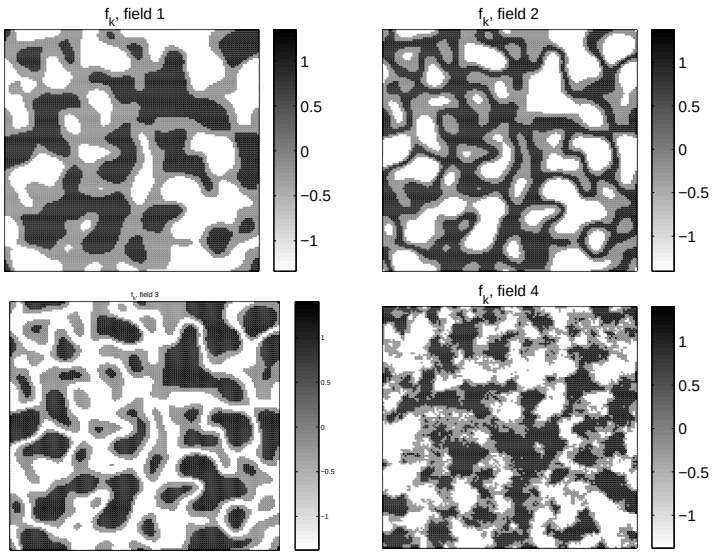

Figure 6.7: Test fields from Chapter 2 (Figure 2.4) transformed into three-material composites

The effective permeability can here be calculated in a better way than just taking the averaged value. If there is a background material and the other materials form isolated inclusions it would for example be possible to approximate the permeability with the Maxwell approach or with the differential effective medium theory approach. Otherwise the self-consistent approach or the geometric mean could be used. The geometric mean would be consistent to stochastic theory, but it will yield a permeability of zero if the non-wetting fluid has a saturation of zero anywhere in the medium. The Maxwell and the differential effective medium theory approximation will yield a non-zero effective permeability for the non-wetting phase as soon as the entry pressure of the background material is exceeded. The local values are given by (6.30) and (6.31).
From the volume percentages of the materials and the local permeability values of the materials the total permeability, effective medium theory permeabilities for both fluids can be calculated using (3.33), (3.38) or (3.47). In this example we use the Maxwell approach (3.33). It is used to calculate the capillary pressure - permeability relationships for both fluids. From the effective permeability curves the effective mobility curve Λ can be calculated according to (6.28).
The effective permeability curves for the test fields shown in Figure 6.7 are shown in Figure 6.8. The Λ-curves that result from the effective permeabilities, are shown in Figure 6.9. It is clearly visible that the geometric mean and the arithmetic mean are here no good choices to predict the effective permeabilities. The arithmetic mean overpredicts both permeabilities, the permeability of the wetting fluid as well as that of the non-wetting fluid. Therefore the mobility Λ generated with these permeabilities overpredicts the real curve. The geometric mean on the other hand vanishes if the saturation of non-wetting fluid is zero anywhere in the field. Therefore the effective non-wetting permeability is underpredicted at low capillary pressures. The mobility Λ is thus also underpredicted at

these values. The effective curves calculated with the Maxwell approach show the best results. As the background material is assigned to the material which has a connected path, the macroscopic residual saturation is captured well. The permeability at saturation one of the wetting phase (at capillary pressure $P_c^{(0)} = 0$) is not well reproduced with the Maxwell approach, as the background has a too strong influence. The differential effective medium theory approach might overcome these problems, however, the approach is difficult to handle if a part of the medium has a permeability of zero.

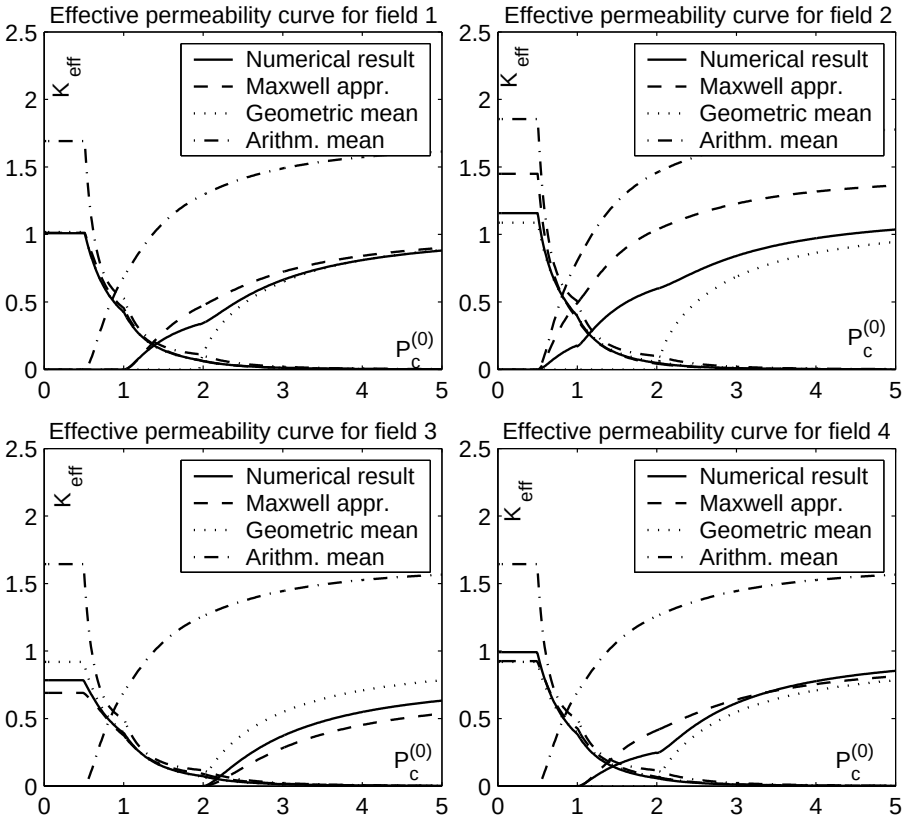

Figure 6.8: Effective permeability curves for the four test fields

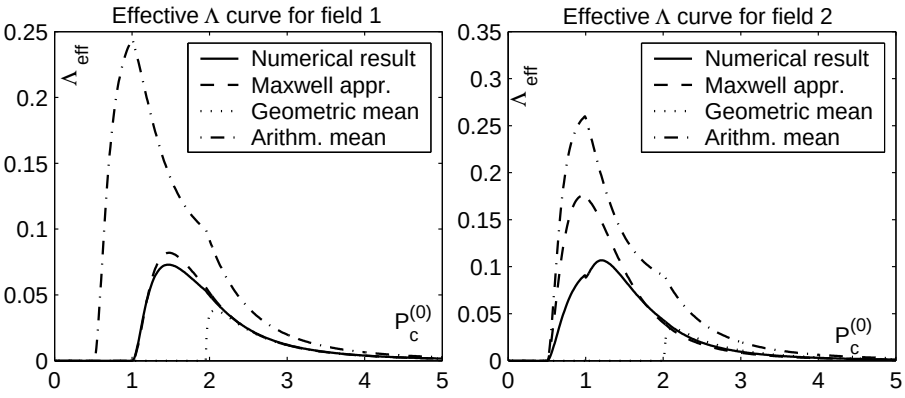

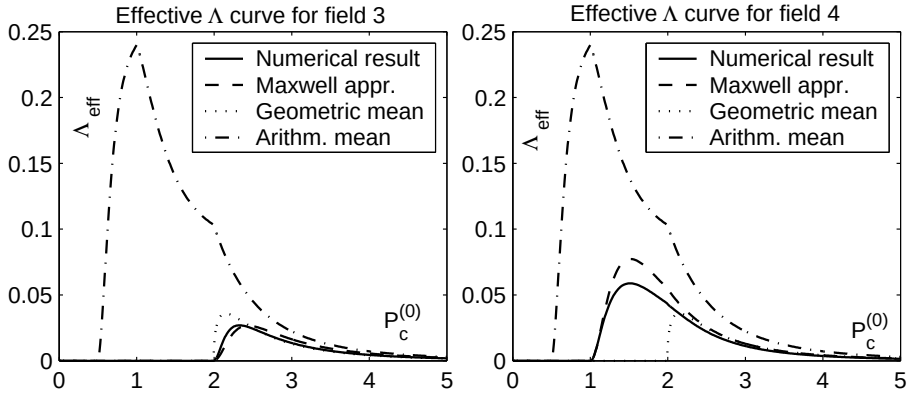

Figure 6.9: Effective Λ curves for the four test fields.

6.4 Numerical test

In order to test the applicability of the upscaling procedure described above, numerically calculated saturation fields are compared. The model MUFTE-UG (see Helmig et al. (1998)) was used to solve the two phase flow problem in the heterogeneous fields. The upscaled effective equation was solved using an integral finite difference scheme and an internal matlab solver. The one dimensional effective equation is discretized with the same resolution as the two dimensional heterogenous case.

For the heterogeneous case the infiltration of a DNAPL of density $\rho_2 = 1470.0 kg/m^3$ and viscosity $\mu_2 = 5.7 \cdot 10^{-4} kg/(ms)$) into a water saturated soil (density $\rho_1 = 1000.0 kg/m^3$, viscosity $\mu_2 = 1.0 \cdot 10^{-3} kg/(ms)$) is considered. The local relative permeability and capillary pressure curves are modeled by Brooks Corey parameter functions (Brooks and Corey, 1966) with a Brooks Corey parameter $\lambda = 2$. The residual saturations are zero. The entry pressure is related to the absolute permeability via a Leverett scaling approach as $P_{\text{entry}} = (0.007 kg\,m/s^2)/\sqrt{K_{\text{int}}}$. The porous medium has a length of $L_x = 1m$ and a height of $L_z = 1m$. The boundaries are assumed to be impermeable. At initial time the saturation of DNAPL in a zone of $1m$ length and $0.25m$ height in the top part of the medium is $S_{nw} = 0.9$ and $S_{nw} = 0$ in the rest of the medium. We compare permeability fields of the type 2 and 3 shown in Figure 2.4 in Chapter 2. The fields have in both cases a geometric mean of $K_{\text{int,g}} = 1.0 \cdot 10^{-11} m^2$ and a variance of log permeability of $\sigma_f^2 = 1.0$. In both cases the fields are isotropic and have a correlation length of $l_x = l_z = 0.02m$. A unit cell is $0.25m x 0.25m$ in size, discretized uniformly into 64 x 64 cells. This yields homogenization parameters of $\varepsilon = 0.02$ and $Bo^{-1} = 0.48$.

The effective curves are obtained here without approximations for the effective permeability, but the relative permeability curves were calculated numerically for each fluid separately. From this the Λ function for the 1d model is obtained (6.28). The residual saturation of the non wetting phase is higher for the connected field than for the disconnected field.

As the results are comparable only on a scale larger than the unit cell, the saturation for

the heterogeneous model is averaged in horizontal direction and a floating average with an averaging length of 64 cells is performed in vertical direction for the heterogeneous model as well as for the effective homogeneous model. The averaged saturations at different time steps are shown in Figure 6.10. Although in the disconnected field the residual saturation of the non wetting phase was estimated too high, the upscaled model reproduces the simulations of the heterogeneous fields in terms of the time behaviour of the front position and the averaged saturation very well. The front itself is sharper in the upscaled simulations. The spreading of the front in the homogeneous fields is due to the capillary forces on the small scale. As this is a small scale effect it is not captured by the upscaled model. The front moves much slower in the disconnected medium than in the other one. This is mainly caused by the different values of the residual saturations. The different time behaviour of the infiltration front is not negligible. The front reaches the bottom of the connected medium more than twice as fast than in the disconnected medium. This illustrates the importance of soil connectivity properties for DNAPL infiltration processes.

6.5 Summary

In this chapter an upscaled model for gravity driven counterflow of two immiscible fluids was derived. As the fluids are assumed to bypass each other in a heterogeneous medium, the effective permeabilities for the single fluids were derived first. From this the effective mobility function Λ was derived. As here the non-wetting phase is not assumed to be always mobile (as in the Richards equation), connected structures in the porous medium have a large influence on the macroscopic residual saturation of the medium. The macroscopic residual saturation can only be predicted when knowledge about connected paths is available. Effective permeabilities calculated as arithmetic means of the local permeabilities overpredict the real effective permeabilities. Effective medium theory approaches are more useful to predict effective permeabilities than stochastic averages. The effective capillary pressure curve is influenced by accessibility criteria for the non-wetting fluid, as the non-wetting fluid can infiltrate into porous medium only if it is not blocked by porous material with a higher entry pressure which is not exceeded. A comparison with a numerical test example confirms the upscaling approach employed here.

The macroscopic residual saturation of the non-wetting phase is highly sensitive to the connected structures of the soil. The fractional function Λ, which gives a measure for the mobility for buoyancy forces, depends strongly on the residual saturation of the non-wetting phase. Information about connected paths of material should be taken into account when applying upscaled models to applications such as CO_2 sequestration.

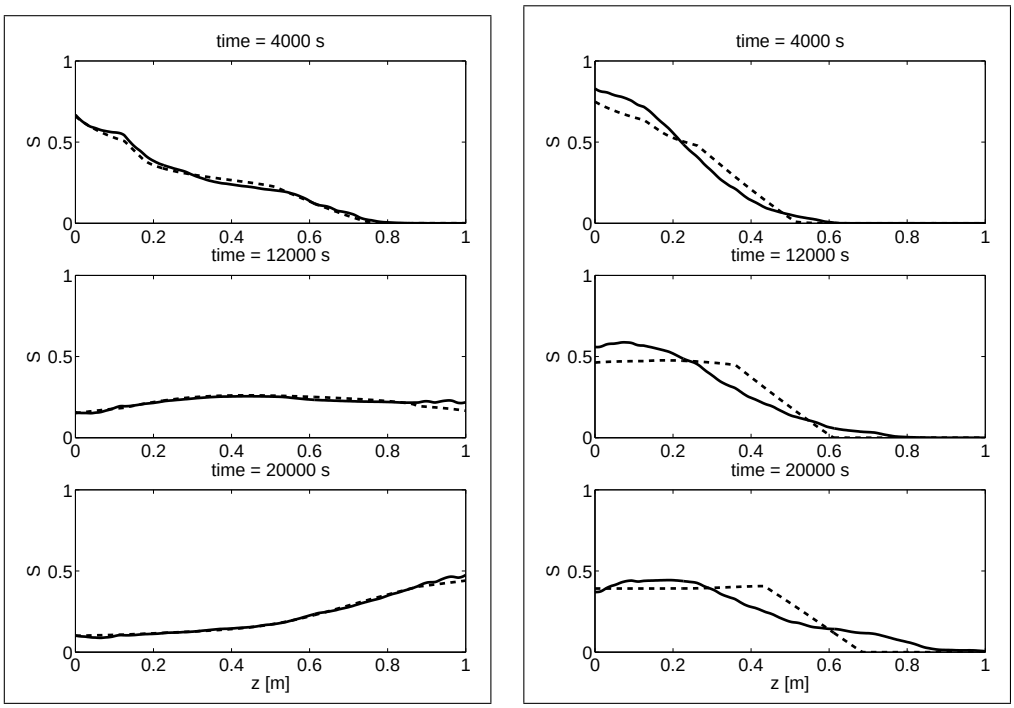

Figure 6.10: Averaged saturations at different times. Left: High permeability well connected, right: low permeability well connected. Solid lines: floating average of the saturation in the heterogeneous field, dashed lines: floating average of the saturation obtained with the effective homogeneous model.

Chapter 7

Two-phase flow on a large scale

Two-phase flow processes in the subsurface can occur on very large length scales. Several techniques for oil reservoir exploitation are based on the displacement of one fluid by another, immiscible one. Also storage of waste materials requires often to comprehend two-phase flow processes in porous of fractured media on large length scales. Nuclear waste disposition or the recently discussed sequestration of carbon dioxide are examples for such technical applications.

If two-phase flow processes occure over very large length scales (which means in practice kilometers), large pressure gradients have to be applied. Also, the relevant flow processes occur often in very deep formations and in material with very low permeability. For such flow scenarios capillary forces can often be neglected.

This section deals with upscaling of two-phase flow processes where capillary forces are not taken into account. The fully two-phase flow equations outlined in Section 1.4.3 are considered, however, the capillary forces are neglected as the capillary numbers (cf. equation (1.22)) are high.

In the following the flow equation and the solutions in a homogeneous medium are discussed. An upscaled model is then derived for the problem in a heterogeneous model. For viscous dominated flow this is done using homogenization theory, while for the case that viscous and gravity forces balance, homogenization theory is no longer applicable. For this case the stochastically averaged problem is derived. The effective parameters are analyzed qualitatively. The width of the transition zone between the two fluids is derived from the upscaled problem. The theoretically predicted values are compared to values determined from numerical multi-realization calculations.

7.1 Flow in a homogeneous medium

The flow of two immiscible fluids is described by the mass balance equation and the Darcy equation described in Chapter 1, (1.17) and (1.18).

$$\begin{aligned} & n_f \frac{\partial S_i}{\partial t} + \vec{\nabla} \cdot \vec{q}_i = 0 \\ & \vec{q}_i = -\frac{\mathbf{K}_{\text{int}}}{\mu_i} k_{r,i}(S_i) \left(\vec{\nabla} P + \rho_i g \vec{e}_z \right) \\ & S_1 + S_2 = 1, \end{aligned} \tag{7.1}$$

where P [M / (LT^2)] is the phase pressure, S_i [-] is the saturation of fluid i, μ_i [M / (L T)] and ρ_i [M / L^3] are its viscosity and density. $\mathbf{K}_{\text{int}}$ [L^2] is the intrinsic permeability of the medium and $g = 9.81 m/s^2$ is the constant of gravitation. The intrinsic permeability is in the following assumed to be isotropic and the tensor notation is dropped. $\vec{e}_z$ is the unit vector in vertical direction and n_f [-] is the porosity. $k_{r,i}$ [-] is the relative permeability of phase i. As capillary forces do not occure here, the pressure P is not distinguished between the tow phases. Also the terms wetting and nonwetting fluid are not meaningful. The fluids will be indicated with 1 and 2 instead.

7.1.1 Total velocity formulation

For many types of problems it is often better to write the two-phase flow equation in a form which corresponds to the Buckley Leverett problem. This formulation is equivalent to the total flow formulation used in Chapter 6 without the capillary pressure. By transforming the unknowns from the saturations and the pressure S_1, S_2, P to the saturations and the total flow velocity

$$\vec{q}_{\text{total}} = \vec{q}_1 + \vec{q}_2, \tag{7.2}$$

the equations (7.1) are transformed to

$$\begin{aligned} & n_f \frac{\partial S_i}{\partial t} + \vec{q}_{\text{total}} \cdot \vec{\nabla} f_i(S_i) + \vec{\nabla} \cdot \frac{K_{\text{int}} \Delta \rho_i g}{\mu_i} \Lambda_i(S_i) \vec{e}_z = 0 \\ & \vec{q}_{\text{tot}} = -K_{\text{int}}(\lambda_1(S) + \lambda_2(S)) \vec{\nabla} P - K_{\text{int}}(\lambda_1(S)\rho_1 + \lambda_2(S)\rho_2) g \vec{e}_z \\ & S_1 + S_2 = 1. \end{aligned} \tag{7.3}$$

The function f_i [-] is the fractional flow function

$$f_i = \frac{k_{r,i}(S)/\mu_i}{(k_{r,1}(S)/\mu_1) + (k_{r,2}(S)/\mu_2)} = \frac{\lambda_i(S)}{\lambda_1(S) + \lambda_2(S)} = \frac{\lambda_i(S)}{\lambda_{\text{total}}(S)}, \tag{7.4}$$

where λ_i [L T / M]is called the mobility of fluid i and $\lambda_{\text{total}} = \lambda_1 + \lambda_2$ is the total mobility of both fluids. The function Λ_i [-] is also a dimensionless function of the relative permeabilities and the viscosity of phase i

$$\Lambda_i = \frac{\mu_i \lambda_1 \lambda_2}{\lambda_1 + \lambda_2}. \tag{7.5}$$

$\Delta\rho_i = \rho_i - \rho_{\text{not i}}$ is the density difference of the two fluids. The first term in the continuity equation is the viscous part and describes the change of saturation due to the total flow. The second term accounts for countercurrent flow of both fluids due to buoyancy forces. The formulation of the type (7.3) is often of advantage, especially if problems with a flux boundary are considered. Two-phase flow problems on a large scale are often problems where a constant flux of the displacing fluid is imposed. Often a radial flux field has to be considered, if e.g. the nearer field of an injection well is considered. If buoyancy forces are negligible, the total flow velocity decreases with the inverse radius r in a 2d flow scenario,

$$\vec{q}_{\text{total}}^{\text{rad}} = \frac{Q_r}{2\pi r}\vec{e}_r. \tag{7.6}$$

Q_r [L^2 / T] is the areal injection rate and $\vec{e}_r$ is the unit vector in radial direction. However, also uniform flow fields are important e.g. for water flooding of oil reservoirs. The total flow velocity in a uniform flow field is constant

$$\vec{q}_{\text{total}}^{\text{unif}} = Q_x\vec{e}_x. \tag{7.7}$$

Q_x [L / T] is the line injection rate and $\vec{e}_x$ is the unit vector in the direction of the flux. If the medium is homogeneous, the continuity equation (7.3) can be written as

$$n_f\frac{\partial S}{\partial t} + \vec{q}_{\text{total}}\cdot\frac{df}{dS}\vec{\nabla}S + \frac{K_{\text{int}}\Delta\rho g}{\mu}\frac{d\Lambda}{dS}\frac{\partial}{\partial z}S = 0. \tag{7.8}$$

The equation can be considered a nonlinear advection equation.

Buckley Leverett solution

If buoyancy forces are not important and the buoyancy term can be neglected, the problem is the classical Buckley Leverett problem. In a quasi one-dimensional problem with constant inflow, a weak solution can be constructed. As the derivative of the fractional flow function df/dS goes typically from zero for saturation one to a maximum and then back to zero for saturation zero, the saturation develops usually a shock with a certain saturation at the front. Typical fractional flow functions and their derivatives for different viscosity ratios are shown in Figure 7.1. The shock saturation and the front velocity can be determined using the method of characteristics (see e.g. Marle (1981)).
The homogeneous Buckley Leverett solution in a homogeneous uniform flow field (which is aligned with x_1 can be written as

$$S(\vec{x},t) \;=\; S^{\text{rear}}\left(\frac{x}{V^\star t}\right)\,\Theta\left(\frac{x}{V^\star t} - 1\right). \tag{7.9}$$

where $\Theta(x)$ is the Heavyside step function as defined in Arfken and Weber (2001). $V^\star$ [L / T] is the front velocity. It is determined by the saturation at the front S_{front} and the total flow velocity

$$V^\star \;=\; q_{\text{total}}\,\frac{df}{dS}|_{(S_{\text{front}})}. \tag{7.10}$$

The saturation at the front S_{front} can be determined via the Welge tanget method

$$\left.\frac{df}{dS}\right|_{S=S_{\text{front}}} = \left.\frac{f}{S}\right|_{S=S_{\text{front}}}. \tag{7.11}$$

If we assume e.g. a quadratic functions for the relative permeabilities ($k_{\text{rel},1} = S_1^2, k_{\text{rel},2} = S_2^2$) we would have $S_{\text{front}} = \sqrt{\frac{M}{1+M}}$ (see e.g. Marle (1981)). M [-] is the viscosity ratio, $M = \mu_1/\mu_2$. The function S^{rear} describes the saturation distribution at the rear of the front. The shape of this function is determined by the derivative of the fractional flow function $f'(S) = df/dS$.

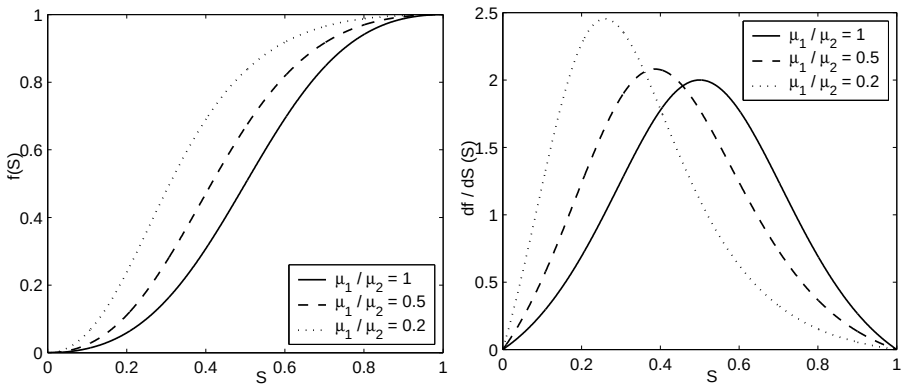

Figure 7.1: Fractional flow function (left) and derivative (right) for different viscosity ratios using quadratic relative permeabilities

Solution with gravity

If buoyancy forces have to be taken into account, a general solution cannot be constructed as strictly, especially if the mean flow is not directed vertically. If the total flow velocity is however uniform in vertical direction, the considerations for the classical Buckley Leverett problem can be transferred to the problem with gravity. The homogeneous saturation distribution depends not on the fractional flow function f, but on the features of the function $\varphi(S)$ [-]

$$\varphi(S) = \frac{df}{dS} + \frac{K_{\text{int}}\Delta\rho g}{\mu q_{\text{total}}}\frac{d\Lambda}{dS}. \tag{7.12}$$

In general this function increases monotonically with saturation. In case the function has an inflection point we obtain a self sharpening front. The front saturation $S^\star$ can be again determined by the Welge tangent method (see e.g. Marle (1981)) $\varphi(S)/S|_{S^\star} = d\varphi(S)/dS|_{S^\star}$. The general solution for an vertical injection with constant rate reads then

$$S(\vec{x},t) = S^{\text{rear}}\left(\frac{z}{V^\star t}\right)\Theta\left(\frac{z}{V^\star t} - 1\right). \tag{7.13}$$

$V^\star = q_{\text{total}}\, \varphi(S)/S|_{S^\star}$ [L / T] is the front velocity. If the function $\varphi(S)$ has a horizontal tangent at the maximum saturation, the saturation decreases continuously between the injection saturation and the front saturation. The saturation in the rear of the front is then determined by the derivative of $\varphi(S)$ with respect to S. For some gravity numbers, the function $\varphi(S)$ is not monotonically increasing but has a maximum between front saturation and maximum saturation and decreases towards the maximum saturation. The derivative $d\varphi/dS$ will then be negative behind the front. The characteristics would lead to unphysical solutions. High saturations of the displacing fluid will then be damped out. In this case the homogeneous saturation distribution is constant until it reaches a transition zone, where it decreases towards the front. The same kind of solution is obtained, if the tangent of $\varphi(S)$ at the injection saturation is larger than zero. If the function $\varphi(S)$ has a maximum at low saturations, the transition zone can be neglected and the solution is a step function with a saturation $S^{\text{rear}} = S^\star$ and a front velocity $V^\star = q_{\text{total}} 1/S^\star$.

7.1.2 Stability criteria

The solution of the continuity equation (7.8) can become unstable. Both viscous and gravity forces have an impact on the stability of the solution. In case that the total mobility λ_{total} directly behind the front is higher than that one directly ahead of the front, the interface becomes viscous unstable. The characteristic quantity is the shock mobility ratio M_{shock} [-]

$$M_{\text{shock}} = \frac{\lambda_{\text{total}}|_{(S=S_{\text{front}})}}{\lambda_{\text{total}}|_{(S=0)}}. \tag{7.14}$$

If $M_{\text{shock}} > 1$, perturbations of the saturation distribution (in particular a perturbation of the front line) are then increased with the movement of the front. The front develops fingers which grow with the movement of the front (cf. Chapter 4). Fingers can occur with different width, however, different widths move with different speed. There is a characteristic finger width which grows fastest and dominates the flow. In the opposite case that $M_{\text{shock}} < 1$, the front is viscous stabilized. If the front line is perturbed, the perturbations are damped out. Buoyancy will enforce a perturbation of the front in case that the denser fluid is above the lighter fluid. Otherwise buoyancy acts stabilizing. A criterion for stability for flow with buoyancy forces can be found by introducing a critical velocity (cf. Marle, 1981)

$$q_{\text{crit}} = \frac{K_{\text{int}}\, S^\star \Delta\rho\, g}{\mu_2 (M_{\text{shock}}^{-1} - 1)}. \tag{7.15}$$

The density and mobility ratio are meant as the rations across the front. Solutions with flow velocities q_{total} will be stable if

$$\left(1 - M_{\text{shock}}^{-1}\right)\left(q_{\text{total}} - q_{\text{crit}}\right) < 0, \tag{7.16}$$

and unstable otherwise. For unstable flow scenarios the averaged saturation is not necessarily related to the heterogeneous structure of the soil parameters, as has been discussed in Chapter 4. The averaged saturation might be modelled by a model with an artificial

term which generates a spreading of the front which is proportional to time (see e.g. Blunt et al. (1994)).

7.2 Flow in a heterogeneous medium

In a heterogeneous medium the absolute permeability K_{int} is a function of space. The total flow velocity q_{total} can therefore be treated as a heterogeneous parameter field. The heterogeneous parameters cause perturbations of saturation distribution. It is not clear how heterogeneity is influenced by the stability properties of the homogeneous problem. Depending on the stability criteria of the flow perturbations can either be enforced or damped out. If the heterogeneity is strong it can dominate, so that stability criteria do not have any influence. In the following we will proceed from the assumption that this is the case.
In order to write the continuity equation in a dimensionless way, the heterogeneous parameters have to be scaled with a typical value. The total flow velocity is written as

$$\vec{q}_{\text{total}} = U\vec{q}^{\star}_{\text{total}}(\vec{x}). \tag{7.17}$$

U [L / T] is the absolute value of the averaged total flow velocity $U = |\vec{q}_{\text{total}}|$. Quantities with a star index are dimensionless. The absolute permeabilty is written as

$$K_{\text{int}}(\vec{x}) = \mathscr{K}\,\kappa(\vec{x}). \tag{7.18}$$

$\mathscr{K}$ is a typical value for the absolute permeability. For a two-dimensional problem it would e.g. be appropriate to use the geometric mean as typical value. The permeability is often written in a log permeability formulation. In this case we would have

$$\mathscr{K} = K_{\text{int,g}} \quad \kappa(\vec{x}) = \exp(f(\vec{x})), \tag{7.19}$$

where $K_{\text{int,g}}$ is the geometric mean and f is the logarithm of the absolute permeability.
The fluctuating parameters are split into their constant average and the fluctuation part with a zero mean

$$\vec{q^{\star}_{\text{total}}}(\vec{x}) = \vec{e}_q + \tilde{q}^{\star}(\vec{x}), \quad \kappa(\vec{x}) = 1 + \tilde{\kappa}(\vec{x}). \tag{7.20}$$

$\vec{e}_q$ is the unit vector in mean flow direction. In the following it will be assumed that the mean flow is aligned in the vertical direction. However, the analysis could be performed the same way with a differently oriented mean flow. Introducing typical numbers for the time and space variable and choosing the time scale as advective time corresponding to the space variable

$$\vec{x} = L\vec{x}^{\star}, \quad t = Tt^{\star}, \quad T = \frac{L}{U} \tag{7.21}$$

where quantities with a star index are dimensionless, yields

$$n_f \frac{\partial S}{\partial t^{\star}} + \vec{q}^{\star}_{\text{total}}(\vec{x}^{\star}) \cdot \vec{\nabla}^{\star} f(S) + Gr\vec{\nabla}^{\star} \cdot \kappa(\vec{x}^{\star})\Lambda(S)\vec{e}_z = 0. \tag{7.22}$$

The dimensionless number Gr is the gravity number

$$Gr = \frac{\mathscr{K}\Delta\rho g}{\mu U}. \tag{7.23}$$

7.2.1 Upscaled problem for viscous dominated flow

To get an understanding of the shape of the upsaled equations, the heterogeneous problem (7.22) will be analyzed with the scale expansion of homogenization theory. The analysis is performed in analogy to Mauri (2003). We will assume here a random parameter field instead of periodic unit cells and perform an average over an REV. The method requires that there are two distinct length scales in the problem, one large length scale L assigned to the length scale of the medium and a small length scale ℓ assigned to the heterogeneity. There are two relevant time scales. The first one is the observation time scale T, which is associated to the large length scale $T = L/U$. There is also a fast time scale, associated to the small length scale, $\Theta = \ell/U = \varepsilon T$. Both time scales have to be taken into account.
It is assumed that the mass of the displacing fluid is completely contained in the zeroth order of the saturation expansion (cf. Mauri, 2003). This way sources and sinks due to higher order contributions are avoided. The average of the higher orders has therefore to vanish,

$$\langle S\rangle = \langle S^{(0)}\rangle, \langle S^{(1)}\rangle = 0, \langle S^{(2)}\rangle = 0, \ldots. \tag{7.24}$$

The two-phase flow problem without capillary forces (7.22) is purely advective. The homogeneous solution is characterized by a sharp front of the displacing fluid. In a heterogeneous medium the front will become irregular, and will get rougher with time. Therefore, unlike in linear advection - dispersion problems, the solution in a heterogeneous medium will not become more homogeneous with time (such as for solute transport). After a certain time scale, the roughness of the front will exceed the size of an REV. Also, as there is a moving transition zone, which has a small lateral extension compared to the large length scale, the real front cannot be recovered on a large length scale. The upscaled model will therefore only represent the large scale averaged behaviour, not the real situation. The averaging has to be considered either a spatial average over a large length scale, such as an average over the spatial direction perpendicular to the mean flow direction. For example, in a vertical displacement, a spatial average over the horizontal direction could be considered. The averaged problem could also be considered to be the ensemble average. In this case the upscaled model predicts the stochastic mean of the solution only. In this averaged sense the upscaled saturation can be considered smooth, however, in a single realization of a porous medium it will have a rough transition zone.
As the form of the upscaled equation is analyzed with homogenization theory, the solution in a single realization is considered. The irregularity on the small scale is here a problem. In order to artificially force the solution to be smooth on the large scale (so that the averaged behaviour is mimicked), a diffusion term will be added to the problem. This artificial diffusion term is supposed to be very small, so that it is not dominant in the flow problem.

In case that the fluids have similar densities and that the permeability of the material is low (which is often the case in water flooding problems), the gravity number Gr is low. In this case the flow is dominated by viscous forces. We will consider here the case that the garvity number is in the order of the scale ratio ε (see (3.1) in Section 3.1), $Gr \approx \varepsilon^1$. To handle the different orders of ε in the system of equations, it is useful to introduce a rescaled gravity number

$$Gr = Gr'\varepsilon, \tag{7.25}$$

where Gr' is of the order ε^0. As outlined above, an additional diffusion term is added, which is also scaled with ε. Introducting the separated scales (3.5) and expansionding the saturation accordingly to (3.8) and 3.7) explained in Section 3.1,

$$S = S^{(0)} + \varepsilon S^{(1)} + \varepsilon^2 S^{(2)} + \dots \tag{7.26}$$

yields

$$\begin{aligned} n_f \left(\frac{\partial}{\partial t} + \frac{1}{\varepsilon}\frac{\partial}{\partial \Theta} \right) \left(S^{(0)} + \varepsilon S^{(1)} + \varepsilon^2 S^{(2)} + \dots \right) + \\ \vec{q}_{\text{total}}(\hat{Y}) \cdot \left(\vec{\nabla}_{\hat{X}} + \frac{1}{\varepsilon}\vec{\nabla}_{\hat{Y}} \right) \left(f^{(0)} + \varepsilon f^{(1)} + \varepsilon^2 f^{(2)} + \dots \right) + \\ Gr'\varepsilon \left(\vec{\nabla}_{\hat{X}} + \frac{1}{\varepsilon}\vec{\nabla}_{\hat{Y}} \right) \cdot \left(\kappa(\hat{Y}) \left(\Lambda^{(0)} + \varepsilon \Lambda^{(1)} + \varepsilon^2 \Lambda^{(2)} + \dots \right) \vec{e}_z \right) - \\ \varepsilon \left(\vec{\nabla}^2_{\hat{X}} + 2\vec{\nabla}_{\hat{X}} \cdot \vec{\nabla}_{\hat{Y}} + \frac{1}{\varepsilon^2}\vec{\nabla}^2_{\hat{Y}} \right) \left(S^{(0)} + \varepsilon S^{(1)} + \varepsilon^2 S^{(2)} + \dots \right) = 0. \end{aligned} \tag{7.27}$$

The artificial diffusion term is given in the lowest row of equation (7.27). The star index is left out in order to avoid complex notations. The lowest order which appears is the order ε^{-1}. The equation in this order reads

$$\varepsilon^{-1}: \quad n_f \frac{\partial}{\partial \Theta} S^{(0)} + \vec{q}_{\text{total}}(\hat{Y}) \cdot \vec{\nabla}_{\hat{Y}} f^{(0)} - \vec{\nabla}^2_{\hat{Y}} S^{(0)} = 0. \tag{7.28}$$

The simplest possible solution for this equation is a locally constant zeroth order saturation, which does not depend on the fast time scale,

$$S^{(0)} = S^{(0)}(\hat{X}, t). \tag{7.29}$$

The next order to appear is the order ε^0. The terms of this order yield the equation

$$\begin{aligned} \varepsilon^0: \quad & n_f \frac{\partial}{\partial t} S^{(0)} + n_f \frac{\partial}{\partial \Theta} S^{(1)} + \vec{q}_{\text{total}}(\hat{Y}) \cdot \vec{\nabla}_{\hat{X}} f^{(0)} + \vec{q}_{\text{total}}(\hat{Y}) \cdot \vec{\nabla}_{\hat{Y}} f^{(1)} + \\ & Gr' \vec{\nabla}_{\hat{Y}} \cdot \left(\kappa(\hat{Y}) \Lambda^{(0)} \vec{e}_z \right) - \vec{\nabla}_{\hat{X}} \cdot \vec{\nabla}_{\hat{Y}} S^{(0)} - \vec{\nabla}^2_{\hat{Y}} S^{(1)} = 0. \end{aligned} \tag{7.30}$$

Averaging of this equation yields the leading order of the upscaled problem

$$\langle \varepsilon^0 \rangle: \quad n_f \frac{\partial}{\partial t} S^{(0)} + \langle \vec{q}_{\text{total}} \rangle \cdot \vec{\nabla}_{\hat{X}} f^{(0)} = 0. \tag{7.31}$$

The leading order of the upscaled problem is the advective problem with the averaged total flow velocity field. It has the same form as the homogeneous Buckley Leverett problem. The original problem has a term of order ε^1. Therefore the upscaled problem should also be considered up to that order. Therefore, the consistently upscaled problem is the leading part (7.31), plus the averaged terms of order ε^1. The second contribution is

$$\langle \varepsilon^1 \rangle : \quad \vec{\nabla}_{\hat{X}} \cdot \langle \vec{q}_{\text{total}}(\hat{Y}) f^{(1)} \rangle + Gr' \langle \kappa(\hat{Y}) \rangle \vec{\nabla}_{\hat{X}} \Lambda^{(0)} \vec{e}_z - \vec{\nabla}^2_{\hat{X}} S^{(0)} = 0. \tag{7.32}$$

The second term is the original gravity term with the averaged total permeability. Note that we have made use of the requirement that the total mass is contained in the zeroth order saturation term (cf. (7.24)). The first term yields a nonlinear dispersion term. To obtain this term, a solution for $f^{(1)}$ has to be derived. This can be achieved by subtracting the averaged zeroth order equation from the non-averaged one,

$$\begin{aligned} \varepsilon^0 - \langle \varepsilon^0 \rangle : & n_f \frac{\partial}{\partial \Theta} S^{(1)} + (\vec{q}_{\text{total}} - \langle \vec{q}_{\text{total}} \rangle) \cdot \vec{\nabla}_{\hat{X}} f^{(0)} + \vec{q}_{\text{total}} \cdot \left. \frac{df}{dS} \right|_{S=S^{(0)}} \vec{\nabla}_{\hat{Y}} S^{(1)} + \\ & Gr' \left(\frac{\partial}{\partial_{\hat{Y}_z}} \kappa(\hat{Y}) \right) \Lambda^{(0)} \vec{e}_z - \vec{\nabla}_{\hat{X}} \cdot \vec{\nabla}_{\hat{Y}} S^{(0)} - \vec{\nabla}^2_{\hat{Y}} S^{(1)} = 0. \end{aligned} \tag{7.33}$$

This equation is linear in $S^{(1)}$ and can therefore be solved in a perturbation approximation with the method of Green's functions. The Green's function G is given as

$$\begin{aligned} & \frac{\partial}{\partial \Theta} G + \vec{e}_z \left. \frac{df}{dS} \right|_{S=S^{(0)}} \cdot \vec{\nabla}_{\hat{Y}} G - \vec{\nabla}^2_{\hat{Y}} G = \delta^d(\hat{Y} - \hat{Y}') \delta(\Theta - \Theta'), \\ & G(\hat{Y}, \hat{Y}', \Theta, \Theta') = \frac{1}{\sqrt{2\pi(\Theta - \Theta')}^d} \exp \left(- \frac{\left(\hat{Y} - \hat{Y}' - \vec{e}_z \left. \frac{df}{dS} \right|_{S=S^{(0)}} (\Theta - \Theta') \right)^2}{2(\Theta - \Theta')} \right). \end{aligned} \tag{7.34}$$

The perturbation solution to first order in the fluctuating terms is then

$$S^{(1)} = - \int\int G(\hat{Y}, \hat{Y}', \Theta, \Theta') \left(\tilde{q}_{\text{total}} \cdot \vec{\nabla}_{\hat{X}} f^{(0)} + Gr' \left(\frac{\partial}{\partial_{\hat{Y}_z}} \kappa(\hat{Y}) \right) \Lambda^{(0)} \right) d^d \hat{Y}' d\Theta'. \tag{7.35}$$

Inserting into (7.32) yields:

$$\begin{aligned} & \vec{\nabla}_{\hat{X}} \cdot \langle \vec{q}_{\text{total}}(\hat{Y}, \Theta) f^{(1)} \rangle = \\ & \quad - \vec{\nabla}_{\hat{X}} \cdot \left. \frac{df}{dS} \right|_{S=S^{(0)}} \left[\int G(\hat{Y}, \hat{Y}', \Theta, \Theta') \langle \tilde{q}_{\text{total}}(\hat{Y}, \Theta) \tilde{q}_{\text{total}}(\hat{Y}', \Theta') \rangle d^d \hat{Y}' d\Theta' \right] \cdot \vec{\nabla}_{\hat{X}} f^{(0)} \end{aligned} \tag{7.36}$$

This is a macrodispersion term with a macrodispersion coefficient, which is completely analogous to the macrodisperion found in solute transport (Gelhar, 1993; Dagan, 1989). However, it is nonlinear, as it acts on the zeroth order fractional flow function.

The upscaled problem can thus be written in a general form:

$$n_f \frac{\partial}{\partial t} S^{(0)} + \langle \vec{q}_{\text{total}} \rangle \cdot \vec{\nabla}_{\hat{X}} f^{(0)} - \varepsilon \vec{\nabla}_{\hat{X}} \mathscr{D} \vec{\nabla}_{\hat{X}} f^{(0)} + Gr \vec{\nabla}_{\hat{X}} \cdot \langle \tilde{\kappa} \rangle \Lambda^{(0)} \vec{e}_z = 0. \tag{7.37}$$

The artificial diffusion term is now neglected. There are two effective parameters, the dispersion coefficient $\mathscr{D}$

$$\mathscr{D} = \left. \frac{df}{dS} \right|_{S=S^{(0)}} \left[\int G(\hat{Y}, \hat{Y}', \Theta, \Theta') \langle \tilde{q}_{\text{total}}(\hat{Y}, \Theta) \tilde{q}_{\text{total}}(\hat{Y}', \Theta') \rangle d^d \hat{Y}' d\Theta' \right], \tag{7.38}$$

and the effective permeability K_{eff}

$$K_{\text{eff}} = \langle \tilde{\kappa} \rangle. \tag{7.39}$$

Introducing the dimensional quantities back in yields

$$n_f \frac{\partial}{\partial t} S^{(0)} + U \vec{e}_q \cdot \vec{\nabla} f^{(0)} - U \ell \vec{\nabla} \mathscr{D} \vec{\nabla} f^{(0)} + \frac{K_{\text{eff}} \Delta \rho}{\mu} \vec{\nabla} \cdot \Lambda^{(0)} \vec{e}_z = 0. \tag{7.40}$$

The spatial derivatives are now only valid for the large scale $\hat{X}$.
The upscaled problem has an additional mechanism, which is not present in the original problem. This is the nonlinear macrodispersion term. This term causes a spreading of the front of the displacing fluid. The same macro dispersion term would have been found, if the flow would be horizontal, so that buoyancy froces would not appear at all. The shape of the upscaled equation is thus a nonlinear advection dispersion problem, similar to the solute transport problem described in Section 1.4.5.
The interpretation of the macrodispersion term is however different than the interpretation for solute transport. In solute transport there is always a mechanism that mixes tracer over different streamlines, as diffusion is alway active. Therefore, after a long enough waiting time, the tracer has been distributed by small scale mixing over different streamlines, so that the solute distribution is really a homogeneous plume, which is modelled by a transport equation with the corresponding macrodispersion term. The upscaled equation describes the real problem in the one realisation of the porous medium at hand. This is quite different for immiscible displacement problems. There is no mechanism, which acts towards a uniform distribution of the two fluids. Instead, the saturation profile is self-sharpening, which counteracts a uniform distribution. The macrodispersion term is here completely artificial and represents only the behaviour of the **averaged** saturation distribution. The upscaled model does not represent the real process, but only the averaged one. In the single realization there is always a sharp front, which roughens with time. In this way, the question of asymptotic behaviour, which is important for solute transport, does not arise here. In solute transport the asymptotic macrodispersion term does only model the dilution of the solute in a single realization if the solute has been transported over many correlation length of the field. Otherwise the solute cloud is irregular, but not diluted. The macrodispersion coefficient does then only represent the averaged solute

concentration, where the spreading of the averaged tracer cloud is mainly due to the different location of the center of mass of the solute clouds in the single realizations. Here the macrodispersion coefficient is supposed to model the ensemble averaged behaviour only. Therefore the question of the asymptotic limit is not relevant.
The dispersive large scale effect for the heterogeneous Buckley Leverett problem has been addressed by Cvetkovic and Dagan (1996) and Dagan and Cvetkovic (1996), who applied a Lagrangian perturbation theory approach to the immiscible displacement problem in order to determine the averaged cumulative recovery of the displacing fluid and the spatial moments of the fluid distribution. They found a dispersive large scale effect, which is not explicitly determined. A dispersive approach was also used by Zhang and Tchelepi (1999) to derive mean and covariances of the saturation fields in a uniform flow field in an unbounded domain. Pruess (1996) also analyzed a dispersive flux in the two-phase flow equation in order to model the spreading of a DNAPL plume. The spreading of the plume was investigated with numerical simulations. A dispersive approach to model the impact of heterogeneities was also addressed by Ewing (1997). The dispersion coefficient was calculated explicitly by Langlo and Espedal (1995), who applied a perturbation theory approach to the Buckley Leverett problem, where they expanded the fluid saturation around the vertically averaged saturation distribution. They investigated both flow scenarios with and without capillary forces. The autocovariance of flow velocity for single phase flow was used for the autocovariance of total flow velocities. They found a large scale dispersion effect, similar to the linear macrodispersion, however, the dispersion has to be modified by the square of the fractional flow function.
The dispersion term obtained here, given by equation (7.40), is different from the upscaled model obtained by Langlo and Espedal (1995). Transforming their notation to the notation used here, the upscaled model derived by Langlo and Espedal (1995) would yield the upscaled model:

$$n_f \frac{\partial}{\partial t} S^{(0)} + U\vec{e}_q \cdot \vec{\nabla} f^{(0)} - U\ell \vec{\nabla} \mathscr{D} \vec{\nabla} \left[\int_0^S dS' \left(\frac{d\psi(S')}{dS'} \right)^2 \right] = 0. \tag{7.41}$$

As Langlo and Espedal (1995) consider horizontal flow only, the buoyancy term is not included.

7.2.2 Upscaled problem for gravity dominated flow

The upscaled problem for the flow problem with buoyancy forces will be derived in the following. Similar problems have been addressed in the literature. The impact of density differences as well as viscosity differences on macrodispersion for miscible displacement in a heterogeneous permeability field has been investigated by Welty and Gelhar (1991). The transition zone between two fluids in miscible displacement was determined experimentally and numerically for fluids with different densities and viscosities for stable flow scenarios by Kempers and Haas (1994). They found the dispersivity to be dependent on density and viscosity. However, they found a strong decrease of the dispersivity in

case that the density difference acts stabilizing on the flow. Tchelepi and Jr. (1994) analyzed the transition zone in a heterogeneous medium for immiscible displacement with numerical methods. They included gravity effects, however, the flow configuration was horizontal. The problem considered here is different from the works mentioned above, as it is not a miscible displacement problem, and the flow is vertically oriented.
The homogenization method is no reasonable approach if the gravity number is in the range of $Gr \approx \varepsilon^0$. If the same expansion and separation of scale approach as in the viscous dominated problem (7.27) is performed, the equation of order ε^{-1} reads

$$\varepsilon^{-1}: \quad n_f \frac{\partial}{\partial \Theta} S^{(0)} + \vec{q}_{\text{total}}(\hat{Y}) \cdot \vec{\nabla}_{\hat{Y}} f^{(0)} + Gr \vec{\nabla}_{\hat{Y}} \tilde{\kappa}(\hat{Y}) \Lambda^{(0)} \vec{e}_z - \vec{\nabla}_{\hat{Y}}^2 S^{(0)} = 0. \tag{7.42}$$

The equation cannot be fulfilled if the zeroth order saturation does not depend on the small scale $\hat{Y}$. The solution would be a saturation distribution in the unit cell, where the fluids are completely segregated, so that the fluids are completely separated with the denser fluid below the lighte fluid. This is not a physically reasonable configuration in one unit cell.
The form of the upscaled equation is thus analyzed for this problem without a scale expansion, but the flow equation is ensemble-averaged without separating between large and small scale. The solutions are approximated with a perturbation approach. The solution is expanded around the homogeneous solution in terms of the fluctuation parameter. We assume that flucutations of the (dimensionless) total flow velocity are in the same order as fluctuations of the (dimensionless) absolute permeability. The flutuation parameter will be denoted as ε_σ

$$\varepsilon_\sigma \approx \sigma_q \approx \sigma_\kappa. \tag{7.43}$$

This procedure is equivalent to the method explained in Section 3.3.4. The saturation and the functions of the saturation are expanded as

$$\begin{aligned} S &= S^{(0)} + \varepsilon_\sigma S^{(1)} + \varepsilon_\sigma^2 S^{(2)} + \dots \\ f &= f^{(0)} + \varepsilon_\sigma f^{(1)} + \varepsilon_\sigma^2 f^{(2)} + \dots \\ \Lambda &= \Lambda^{(0)} + \varepsilon_\sigma \Lambda^{(1)} + \varepsilon_\sigma^2 \Lambda^{(2)} + \dots, \end{aligned} \tag{7.44}$$

where $f^{(1)}$, $\Lambda^{(1)}$, etc. are obtained from a Taylor expansion of the functions around the zeroth order of the saturation, in the same way as this was done for the scale expansion in homogenization theory.
By inserting this approach into (7.22)

$$\begin{aligned} & n_f \frac{\partial}{\partial t} \left(S^{(0)} + \varepsilon_\sigma S^{(1)} + \varepsilon_\sigma^2 S^{(2)} + \dots \right) + \\ & \quad (\vec{e}_z + \varepsilon_\sigma \tilde{q}_{\text{total}}) \cdot \vec{\nabla} \left(f^{(0)} + \varepsilon_\sigma f^{(1)} + \varepsilon_\sigma^2 f^{(2)} + \dots \right) + \\ & \quad Gr \vec{\nabla} \cdot \left((1 + \varepsilon_\sigma \tilde{\kappa}) \left(\Lambda^{(0)} + \varepsilon_\sigma \Lambda^{(1)} + \varepsilon_\sigma^2 \Lambda^{(2)} + \dots \right) \vec{e}_z \right) = 0, \end{aligned} \tag{7.45}$$

and solving for each order of the expansion parameter separately (see Section 3.3.4) we split the equation (7.22) into a system of equations, for each order ε_σ separately. The

zeroth order is simply the homogeneous equation.

$$n_f \frac{\partial}{\partial t} S^{(0)} + \vec{e}_z \cdot \vec{\nabla} f^{(0)} + Gr \vec{\nabla} \cdot \Lambda^{(0)} \vec{e}_z = 0. \tag{7.46}$$

The first and second order read

$$n_f \frac{\partial}{\partial t} S^{(1)} + \vec{e}_z \cdot \vec{\nabla} f^{(1)} + \tilde{q}_{\text{total}} \cdot \vec{\nabla} f^{(0)} + Gr \vec{\nabla} \cdot \Lambda^{(1)} \vec{e}_z + Gr \vec{\nabla} \left(\tilde{\kappa} \cdot \Lambda^{(0)} \vec{e}_z \right) = 0, \tag{7.47}$$

$$n_f \frac{\partial}{\partial t} S^{(2)} + \vec{e}_z \cdot \vec{\nabla} f^{(2)} + \tilde{q}_{\text{total}} \cdot \vec{\nabla} f^{(1)} + Gr \vec{\nabla} \cdot \Lambda^{(2)} \vec{e}_z + Gr \vec{\nabla} \left(\tilde{\kappa} \cdot \Lambda^{(1)} \vec{e}_z \right) = 0. \tag{7.48}$$

The zeroth order equation is nonlinear, however, all higher order equations are linear. In principle they can therefore be solved using the method of Green's functions. The Green's function for each order is defined by

$$\frac{\partial}{\partial t} G + \frac{\partial}{\partial z} \varphi(S^{(0)}) G = \delta(\vec{x} - \vec{x}') \, \delta(t - t'). \tag{7.49}$$

The function φ is defined as in equation (7.12). The value of the function at the front position is denoted as $\varphi^\star$. The Green's function can only be determined if the solution for the homogeneous problem is known. The homogeneous solutions have been discussed above. We will consider for simplicity the case that the homogeneous solution can be approximated as a step function. The case that the solution has a sharp front with a rearefraction wave can be treated in a similar way. The Green's function is then simply

$$G(\vec{x}, \vec{x}', t, t') = \delta^d \left(\vec{x} - \vec{x}' - \vec{e}_z 1/\varphi^\star (t - t') \right) \Theta \left(\frac{t}{t'} - 1 \right). \tag{7.50}$$

The first and second order of the saturation distribution can be obtained from (7.47) and (7.48).

$$\begin{aligned} S^{(1)} &= \int d^d x' \int dt' \, G(\vec{x}, \vec{x}', t, t') \left(\tilde{q}_{\text{total}} \vec{\nabla}' f^{(0)} + \vec{\nabla}' \tilde{\kappa} \Lambda^{(0)} \vec{e}_z \right) \qquad (7.51) \\ S^{(2)} &= \int d^d x' \int dt' G(\vec{x}, \vec{x}', t, t') \left(\tilde{q}_{\text{total}} \vec{\nabla}' f^{(1)} + \vec{\nabla}' \tilde{\kappa} \Lambda^{(1)} \vec{e}_z + \vec{\nabla}' \left. \frac{d\varphi}{dS} \right|_{S=S^{(0)}} \left(S_1(\vec{x}', t') \right)^2 \right). \end{aligned}$$

Making use of this expansion, we can construct an approximate solution of the heterogeneous solution up to a certain order in the expansion parameter.
Inserting the solutions (7.51) into the fluctuating parts of the total continuity equation (7.45) and averaging the equation to second order yields

$$n_f \frac{\partial}{\partial t} \langle S \rangle + \vec{e}_z \cdot \vec{\nabla} \langle f(S) \rangle + Gr \vec{\nabla} \cdot \langle \Lambda \rangle \vec{e}_z + \varepsilon_\sigma^2 \vec{\nabla} \langle \tilde{q}_{\text{total}} f^{(1)} \rangle + \varepsilon_\sigma^2 \vec{\nabla} \langle \kappa \Lambda^{(1)} \vec{e}_z \rangle = 0 \tag{7.52}$$

As the Green's function basically pins the perturbation to the location at the front, the last two terms in (7.52) yield as in the viscous dominated case a macrodispersiion type of term and an advective term.

The shape of the upscaled equation is thus the same as in the viscous dominated case. The equation is nonlinear and has an advective part and a dispersive part, which will cause a spreading of the averaged front.
Despite that the shape of the equation can be determined, the single terms cannot be quantified as well as in the viscous dominated case. First, the averaged equation to zeroth order is not that clear. In the viscous dominated case there was an advective term, which had the same shape as in the unperturbed problem. This is here no longer the case. The second term in the upscaled problem (7.52) reads

$$\vec{e}_z \cdot \vec{\nabla} \langle f(S) \rangle = \vec{e}_z \cdot \vec{\nabla} \left(f(S^{(0)}) + \left. \frac{df}{dS} \right|_{S=S^{(0)}} \langle S^{(2)} \rangle + \left. \frac{d^2 f}{dS^2} \right|_{S=S^{(0)}} \langle (S^{(1)})^2 \rangle + \dots \right) \neq \vec{e}_z \cdot \vec{\nabla} f(\langle S \rangle). \tag{7.53}$$

This part is not the same as in the unperturbed problem, as the averaged fractional flow function is not the fractional flow function of the averaged saturation. The expressions are equal only up to the first order. The same reasoning holds for the gravity term. To evaluate the real shape of these terms, the second order saturation would have to be taken into account explicitely. In this way the upscaled problem can be considered an advective dispersive equation in the same way as for the viscous dominated case only up to first order. It is thus a first order second moment result. If the result would be required to hold up to second order, the assumtion would have to be made that the averaged nonlinear functions are uniquely related to the averaged saturation,

$$\langle f(S) \rangle = F(\langle S \rangle), \quad \langle \Lambda(S) \rangle = \mathscr{L}(\langle S \rangle). \tag{7.54}$$

The functions are similar to the functions obtained with pseudo relative permeabilities, which are sometimes used as effective parameters to capture the effect of the heterogeneity of the permeability field in two-phase flow (see e.g. Barker and Thibeau, 1997). This might be a reasonable assumption, however, it would have to be tested. In the following the terms will be left undetermined and it will be proceeded from the first order second moment result, where the upscaled problem has the shape

$$n_f \frac{\partial}{\partial t} \langle S \rangle + \langle \vec{q}_{\text{total}} \rangle \cdot \vec{\nabla} F(\langle S \rangle) - \vec{\nabla} \mathscr{D} \vec{\nabla} f(\langle S \rangle) + Gr \vec{\nabla} \cdot K_{\text{eff}} \mathscr{L}(\langle S \rangle) \vec{e}_z = 0. \tag{7.55}$$

$\mathscr{D}$ is the dispersion coefficient and K_{eff} is the effective permeability.

7.3 Explicit results for the horizontal Buckley Leverett problem

The upscaled problem can be evaluated explicitely if a horizontal flow scenario is considered. In this case the gravity number Gr is zero and the upscaled problem has the shape as given in (7.37), however the gravity term is absent. The upscaled flow problem is simply the homogeneous problem with an additional nonlinear macrodispersion term. The

dispersive term acts on the fractional flow function. The macrodispersion coefficient $\mathscr{D}$ is in principle a tensor, which reads

$$\mathscr{D} = \left.\frac{df}{dS}\right|_{S=S^{(0)}} \left[\int G(\hat{Y},\hat{Y}',\Theta,\Theta')\langle\tilde{q}_{\text{total}}(\hat{Y},\Theta)\tilde{q}_{\text{total}}(\hat{Y}',\Theta')\rangle d^d\hat{Y}'d\Theta'\right] \tag{7.56}$$

The Green's function is without gravity given as (7.34). If the artificial diffusion term is neglected, the Green's function can be approximated as

$$G(\hat{Y},\hat{Y}',\Theta,\Theta') = \delta^d\left(\hat{Y}-\hat{Y}'-\vec{e}_x\left.\frac{df}{dS}\right|_{S=S^{(0)}}(\Theta-\Theta')\right). \tag{7.57}$$

7.3.1 Stochastic properties of the total flow velocity

The macrodispersion tensor depends on the stochastic properties of the total flow velocity field. The stoachtistic properties of the total flow velocity of the Buckley Leverett problem have been analyzed in Neuweiler et al. (2003). In a first approximation it could be assumed that the stochastic properties of the total flow velocity are similar to those of the flow velocity in a single phase flow problem. It is a question of stability of the problem, how good this approximation holds. Behind the front and at the rear of the front the flow velocity is similar to a single phase flow problem, as mainly one fluid flows. As capillary forces are neglected the saturation distribution in the rear of the front does not fluctuate much, so that it is reasonable to assume similar stochastic properties behind and ahead of the front. If the flow is mutually stable, the stochastic properties at the front can also be approximated the same way. However, if the displacement is unstable the front will develop fingers which grow with time. The roughness of the front will grow with time rather than in a dispersive way (i.e. a growth with square root of time). The stochastic properties of the flow velocity around the front will then be different from those in the other areas. Also, they will change with time, as e.g. the corrleation length of the velocity will grow with time. The opposite is the case if the flow is stabilizing. In this case the total flow veloctiy at the front will fluctuate less than in the other areas, as in this area fluctuations are damped out. That means that the variance of the total flow velocity will be reduced in the area of the front. This is illustrated in Figure 7.2. Also the correlation length of the total flow velocity will be reduced in this area.

For stabilizing flow the macrodispersion term does not give a lot of information. It is large only ahaed of the front and at the rear of the front, where the averaged saturation is constant and therefore a macrodispersive flux does not occure. In the area of the front the macrodipsersion coefficient is very small. The front does not spread because the front in each realization is stabilizing.

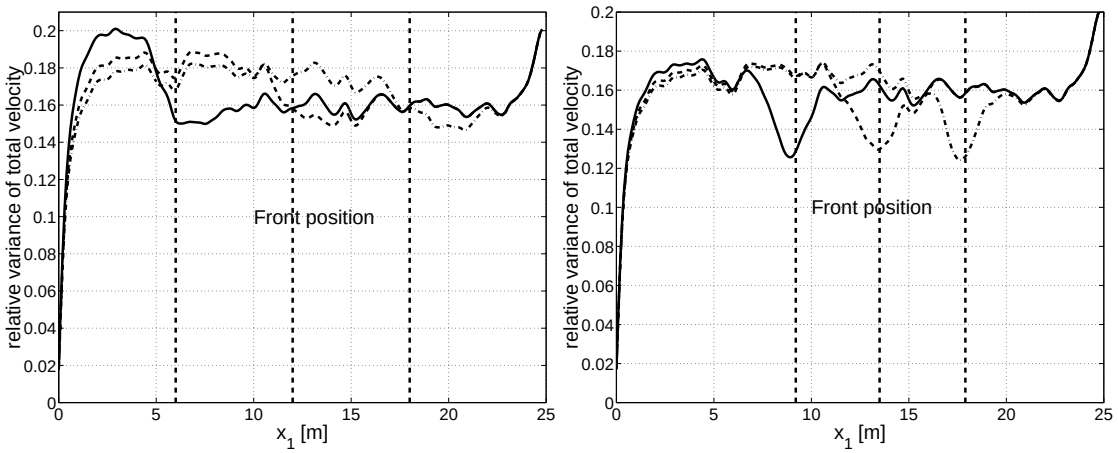

Figure 7.2: Variance of total flow velocity for an immiscible displacement with a viscosity ratio of $M = 0.5$ (left) and $M = 1.2$ (right) at three different times. The flow with $M = 1.2$ is stabilizing. Note that the viscosity ratio M is different from the shock mobility ration M_{shock} defined by (7.14).

The analysis of the macrodispersion term is therefore only really meaningful for the case that the flow is mutually stable, which is given if the shock mobility ratio of the fluids is close to one. In this case it is reasonable to assume that the total flow velocity it time independent and its stochastic properties can be assumed to be similar to those of single phase flow. For the evaluation of the macrodispersion coefficient (7.56) the autocovariance of the total flow velocity is required. We will assume here that it is stationary and can be approximated by a Gaussian function. This is supposed to capture the general features of the macrodispersion term. The autocovariance is approximated as

$$C_{qq,ij}(\hat{Y}-\hat{Y}') = \langle \tilde{q}_i(\hat{Y})\tilde{q}_j(\hat{Y}')\rangle = \sigma_q^2 \exp\left(-\frac{\left(\hat{Y}_i-\hat{Y}_i'\right)^2}{l_i^2}\right)\delta^{(d-1)}(\hat{Y}_{j\neq i}-\hat{Y}'_{\mathrm{j\neq i}})\delta_{ij}. \quad (7.58)$$

The Kronecker δ is introducted as the macrodispersion tensor is assumed to be diagonal. The variance σ_q^2, the correlation length in flow direction l_z and the correlation length perpendicular to the flow direction l_x should in principle be related to the stochastic properties of the permeability field, as they are not known a priori. The derivation of the explicit form of the correlation function for different flow configurations for single phase flow can be found e.g. in Fiori et al. (1998) or Hsu and Neuman (1997).
Using the approximation (7.58) to evaluate the macrodispersion tensor yields

$$\mathscr{D}_{ii} = \int \sigma_q^2 \exp\left(-\frac{(\Theta-\Theta')^2}{l_i^2}\right) d\Theta' = \sigma_q^2 l_i. \quad (7.59)$$

The macrodispersion term is the same as for a solute transport problem, except that it acts on the fractional flow function instead on the saturation directly.

7.3.2 Transition zone of the front

The macrodispersion coefficient is not a measurable quantity. To test the applicability of the upscaled model, quantities have to be derived, which are related to the macrodispersion coefficient. The macrodispersion coefficient can then be determined indirectly and compared to numerical simulations of the flow in a heterogeneous medium. A similar procedure is often applied for macrodispersion in solute transport. A measure for the dispersive growth of the averaged transition zone of the front is a generalized second spatial moment of the saturation distribution.

Uniform flow field

The macrodispersion coefficient for solute transport in a uniform flow field is often defined via the second spatial moment of the solute plume. From the solution of the homogeneous advection dispersion equation it can be deduced that the dispersion coefficient is

$$D_{ij} = \frac{\partial}{\partial t}\mu_{ij}^2(c), \tag{7.60}$$

where μ_{ij}^2 is the ij component of the second spatial moment of the solute concentration

$$\mu_{ij}^2 = \int x_i x_j c(\vec{x}) d^d x. \tag{7.61}$$

A similar concept can be applied for the macrodispersion coefficient in the upscaled horizontal Buckley Leverett problem. As outlined above, the nonlinear macrodispersion term in the upscaled problem is supposed to generate spreading of the front in the averaged saturation profile. So an equivalent measure as a second spatial moment can be applied to derive the macrodispersion coefficient. Only moments of the horizontal coordinate lateral to the mean flow direction (denoted by x) have to be considered, as the averaged problem is assumed to be symmetric in the direction perpendicular to that one. For the nonhomogeneous problem we have to centralize the second moment in a way that the centralized second moment of the homogeneous (not upscaled) solution vanishes. The spatial moments of the homogeneous solution read

$$\begin{aligned} m_{0,S}(t) &= \int dx\, S(x,t) = \int_0^1 d\eta\, S^{\text{rear}}(\eta) U^\star t \\ m_{n,S}(t) &= \frac{\int dx\, x^n S(x,t)}{m_{0,S}(t)} = \frac{\int_0^1 d\eta\, \eta^n S^{\text{rear}}(\eta)}{\int_0^1 d\eta\, S^{\text{rear}}(\eta)} (U^\star t)^n, \end{aligned} \tag{7.62}$$

where η is a variable given by $\eta = x/(V^\star t)$. We will use a more general definition of the centralized second moment as usually applied for solute transport, where we centralize with the first spatial moment of the fractional flow function, which has been normalized

with the mass of the saturation,

$$m_{1,f}(t) = \frac{\int dx\, x\, f(S(x,t))}{m_{0,S}(t)}. \tag{7.63}$$

With this first moment we can get a definition for the square width of the spreading zone of the front,

$$M_2(t) = \frac{m_{2,S}(t) - 2\int dt' m_{1,f}(t')}{m_{0,S}(t)}, \tag{7.64}$$

where we used a time integral instead of the square of the first moment. If the unperturbed Buckley Leverett equation (7.22) is multiplied by x^2 and integrated over space, it can be seen that this definition vanishes for all homogeneous solutions of the kind described above. With definition (7.64) we will characterize the transition zone of the averaged heterogeneous saturation distribution. Applying the definition (7.64) to the upscaled Buckley Leverett problem (7.40), we obtain

$$M_2(t) = 2\mathscr{D}_{xx} t. \tag{7.65}$$

The dispersion coefficiten can thus be defined as

$$\mathscr{D}_{xx} = \frac{1}{2}\frac{\partial}{\partial t} M_2(t). \tag{7.66}$$

If the spreading of the transition zone of the two fluids is of dispersive nature, we would expect M_2 derived from the averaged saturation $\langle S \rangle$ to grow with time, equivalently to the width of a solute plume spread by dispersion. A spreading characterized as advective would cause a growth rate proportional to square of time, similar to spreading caused by anomalous diffusion.

Radial flow field

Besides the uniform flow configuration, which is the most relevant one for practical applications, we want to consider a radial displacement process with a cylindric flow symmetrie in a two dimensional medium. This configuration occurs e.g. in single fracture air pressure tests.
The mean part of the total flow velocity is now aligned in radial direction and decreases with $1/r$. The total velocity reads

$$\vec{q}_{\text{total}}(x) = \vec{U}_r + \tilde{q}(\vec{x}) = \frac{Q}{2\pi r}\vec{e}_r + \tilde{q}(\vec{x}). \tag{7.67}$$

The homogeneous saturation for the radial flow configuration is given by

$$S(\vec{x},t) = S^{\text{rear}}\left(\frac{r^2}{V_r^\star t}\right)\Theta\left(1 - \frac{r^2}{V_r^\star t}\right). \tag{7.68}$$

The definition of the large scale dispersivity has for this case to be reconsidered.
Proceeding from the flow equation (7.40), we have to make an assumption about the nature of the large scale mixing. Spatial moments have to be defined according to this assumtion. This is equivalent to the solute transport problem in a radial flow field (cf. Attinger et al., 2001; Indelman and Dagan, 1999; Neuweiler et al., 2001). We could assume it to be diffusion-like, described by $\mathscr{D}_{rr} = D^\star$ const., or dispersion-like, with a dispersion coefficient proportional to the mean velocity, $\mathscr{D}_{rr} \propto U_r/r \cdot \alpha_r$. α_r is the dispersivity. In the second case we would like to have a definition of a large scale dispersivity α_r rather than a large scale dispersion coefficient $\mathscr{D}$. Using the same general concept for spatial moments as for the uniform flow field, we obtain different definitions for $D^\star$ and α_r.

$$D^\star_{rr} = \frac{1}{4}\frac{\partial}{\partial t}\frac{\int_0^\infty r\,dr\,r^2 S - \frac{U_r}{\pi}\int_0^\infty r\,dr\,f(S)}{\int_0^\infty r\,dr\,S}, \tag{7.69}$$

$$\alpha_r = \frac{1}{6U_r}\frac{\int_0^\infty r\,dr\,r^3\partial_t S - \frac{3}{2}\frac{U_r}{\pi}\int_0^\infty r\,dr\,rf(S)}{\int_0^\infty r\,dr\,S}. \tag{7.70}$$

Similar to the uniform flow case the approaches can be tested by applying the definitions to averaged saturation fields. If $D^\star_{rr}$ or α_r are not constant with time, this would mean a contradiction to the validity of the upscaled problem given by equation (7.37).
In Neuweiler et al. (2003) both definitions (7.69) and (7.70) were calculated analytically to second order in a perturbation approach. It could be shown that the first definition leads to contradictions, so that the additional term in the upsaled equation is really dispersive by nature.

7.3.3 Numerical example

The results are due to many approximations and have therefore to be tested by numerical multi-realization calculations for the displacement process with a heterogeneous permeability field. The simulations shown here were performed using the streamline code 3dsl (Batycky, 1997; Batycky et al., 1997). The code is based on an IMPES scheme (implicit in pressure, explicit in saturation). In 3dsl the pressure field for the flow problem is calculated using finite differences. From the pressure field the streamlines are derived and the saturation distribution is caclulated as the onedimensional Buckley Leverett solution on each streamline. The saturation is then transformed back to the regular grid. The details of the program can be found in Batycky (1997) and Batycky et al. (1997).
The example field is two-dimensional and rectangular, with an extension of 8 m in direction transversal to the mean flow direction and 25 m in mean flow direction. It was discretized as a regular grid with a grid size of 0.1 m x 0.1 m (or 80 x 250 cell grid). The heterogeneity field was generated using the code fgen by Robin et al. (1993b). The random permeability field has an isotropic correlation structure with an integral scale of 0.44

m, so that one integration scale incorporates 4.4 grid discretization lengths. The mean permeability of the field is $K_{\text{int}} = 4 \cdot 10^{-12} m^2$ and the relative variance is $\sigma_K^2 / \langle K \rangle^2 = 0.56$. The porosity is constant and set to $n_f = 0.2$. An ensemble of 200 realizations of permeability fields was analyzed. The inflow of the displacing fluid was established by 80 injection wells with a constant areal inflow rate of $1 \cdot 10^{-7} m^2/s$ in each cell of the left boundary, leading to an average flow velocity of $U = 5 \cdot 10^{-6} m/s$. This is a typical velocity for water flooding of an oil reservoir. The outflow was established by 80 production wells held at constant pressure in each cell of the right boundary. The simulation was run for an injection time span of $T = 3.5 \cdot 10^6 s$ with a time discretization step of $\Delta t = 6823 s$. The viscosity of the displacing and the displaced fluid are $\mu_1 = 1 \cdot 10^{-3} Ns/m^2$ and $\mu_2 = 2 \cdot 10^{-3} Ns/m^2$, leading to a viscosity ratio of $\mu_1/\mu_2 = 0.5$. This is a realistic viscosity ratio for a water flooding problem. A second set of simulations was performed with the parameters $\mu_1 = 1 \cdot 10^{-3} Ns/m^2$ and $\mu_2 = 0.8333 \cdot 10^{-3} Ns/m^2$ (viscosity ratio $\mu_1/\mu_2 = 1.2$). The relative permeability function are simple quadratic functions, and with these functions the flow process is stable ($M_{\text{shock}} = 0.85$ in the first case and $M_{\text{shock}} = 0.52$ in the second case, cf. (7.14)).

The variance of the total flow velocity as well as the longitudinal integral scale for the total flow velocity were calculated numerically. The variances are shown in Figure 7.2. In the first case a variance of $\sigma_q^2/U^2 = 0.2$ to $\sigma_q^2/U^2 = 0.175$ in the rear of the front was obtained. In the second case, the variance has a dip around the front. This is due to the stabilizing character of the displacement process for small mobility ratio. A variance of $\sigma_q^2/U^2 = 0.175$ far ahead of the front and $\sigma_q^2/U^2 = 0.13$ at the dip was obtained. The integral scale was found to be more constant in time and space and is approximately $l_1 = 1.0\,m$ and $l_1 = 0.9\,m$ for the first and the second case. In the second case it is slightly reduced compared to the first case as the flow is stabilizing.

In Figure 7.3 the numerically calculated dispersion coefficient according to (7.66), applied to the ensemble averaged saturation field, is plotted over time. The time derivative was calculated numerically with an upstream difference discretization. The integration was also performed numerically using summations over the grid.

In the first case the numerically calculated dispersivity reaches a plateau after 0.21 of the total travel time, which corresponds to a travel distance of 5.4 integral scales of total flow velocity. The dispersivity is not exactly constant in time, but reaches a maximum, before it drops slightly to a constant value of $D^\star = 0.175\,m \cdot U$. This can be explained by the decrease of the velocity variance at the rear of the front with time. There are still fluctuations of the dispersion coefficient, which are due to the finite ensemble of 200 realizations.

In the second case the dispersivity reaches a plateau very quickly (after one integration scale) and stays constant. The value is $D^\star/U = 0.09m$, which is much smaller than in the first case. The dispersivity obtained with the single phase flow stochastics would be too large by a factor of 3. The results of the second case suggest, that the dominant stochastic properties are the quantities at the front. This is a region of the saturation field, where the impact of the nonlinearities is high. The linear single phase flow stochastics will in these cases not be appropriate to capture the problem.

In order to estimate the effect due to numerical dispersion the same definition (7.66) was applied for the large scale dispersivity to the homogeneous solution. The result is also plotted in Figure 7.3. Here a value of $D^\star/U = 0.045m$ was obtained for the first case and $D^\star/U = 0.045m$ for the second case. This is not negligible, but much smaller than the value obtained from the heterogeneous fields. We can therefore assume that the dispersion coefficient we obtain from the heterogeneous fields is due to the heterogeneities and not a numerical artefact.

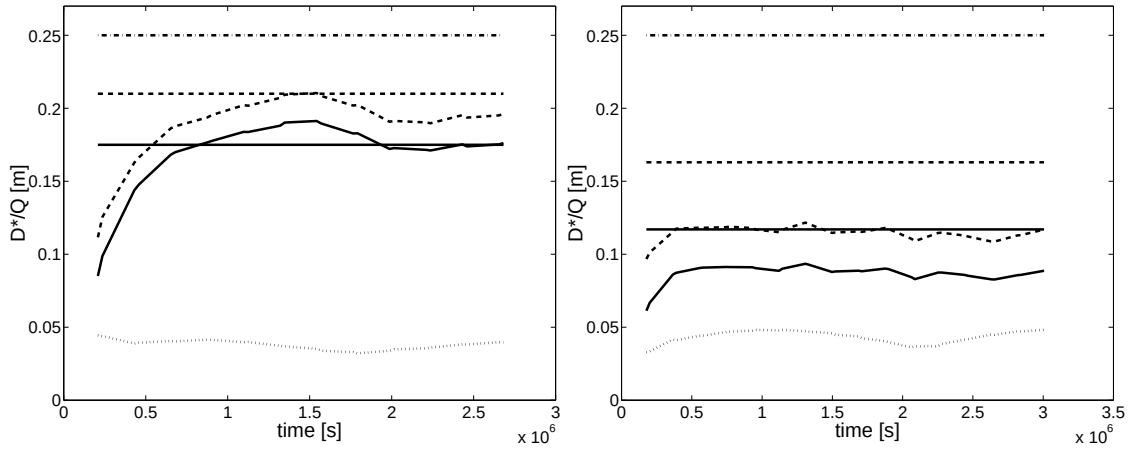

Figure 7.3: Numerically calculated dispersivity ($D^\star/U$) for viscosity ratio $\mu = 0.5$ (left) and $\mu = 1.2$ (right) plotted over time. Solid lines (-): Numerical result und theoretically expected result with approach (7.66). The stochastic properties of the total flow velocity are as given above. Dashed lines (–): Numerical result and theoretically expected result with the approach of Langlo and Espedal (1995), (7.41). Dotted line(..): Dispersivity obtained from a homogeneous medium with approach (7.66). Dashed-dotted lines (.-): Theoretical results with single phase flow stochastics (7.66).

7.4 Explicit results for vertical flow with strong gravity forces

For vertical flow with gravity, results cannot be derived as directly as for the horizontal Buckley Leverett problem. There are two general terms with effective parameters, the buoyancy term and the dispersion term. The definition of the transition zone is thus more complex here (see also Neuweiler and King (2006)). As second order results are considered, the parameters will depend on the second order stochastic properties of the total flow velocity and of the total permeability.

7.4.1 Stochastic properties of the total flow velocity

In order to analyze the averaged saturation we need the covariances of the fluctuating parameter, $\langle \tilde{\kappa}\tilde{q}_z \rangle$, $\langle \tilde{q}_z\tilde{q}_z \rangle$ and $\langle \tilde{\kappa}\tilde{\kappa} \rangle$, which characterize the heterogeneities. The covariance of the permeability is given and we assume it to be stationary, isotropic and Gaussian for simplicity.

$$\langle \kappa(x)\kappa(x') \rangle = \sigma_\kappa^2 \exp\left(-\frac{(x-x')^2}{\lambda_\kappa^2} \right). \tag{7.71}$$

The variance and correlation length λ are constants. In principle the permeability cannot be normally distributed, as the values cannot become negative. However, if the variance is small, a Gauss function is a reasonable approximation for the autocovariance. We can write the covariance of the other terms in general as the variance times a correlation function

$$\langle XY \rangle = \sigma_X \, \sigma_Y \, \rho_{XY}(l). \tag{7.72}$$

X and Y stand for $\tilde{\kappa}$ and $\tilde{q}$ respectively. ρ is a general covariance function. It is assumed that a finite integral scale exists for all cases, which is related to the correlation length l. The correlation length does not have to be finite, but we will assume that we can determine a correlation length for all cases. Both correlation length and variances can be time and space dependent. The covariances of velocities and the crosscovariance between velocity and permeability is left unspecified at this stage and numerical examples will be discussed.

7.4.2 Transition zone of the front

The transition zone can in principle be defined the same way as has been outlined for the Buckley Leverett problem. A definition is obtained by analysing the homogeneous problem and deriving an equivalent to a second spatial moment that vanishes for the homogeneous problem. Instead of centralizing with the fractional flow function the equivalent moment has here to be centralized with the function φ (cf. (7.12)). The corresponding first moment is

$$m_{1,\varphi}(t) = \frac{\int dz\, z\, \varphi\left(S(\vec{x},t)\right)}{m_{0,S}(t)}. \tag{7.73}$$

With this first moment a definition for the square width of the spreading zone of the front can be defined as

$$M^{(2)}(t) = \frac{m_{2,S}(t) - 2\int dt' m_{1,\varphi}(t')}{m_{0,S}(t)}. \tag{7.74}$$

It is a problem here, that the advective part of the upscaled equation is not the same as that of the homogeneous equation (cf. (7.55)). To evaluate the transition zone of the upscaled model by applying definition (7.74) to the averaged saturation is therefore not a reasonable approach. However, the definition (7.74) can be applied to the heterogeneous saturation distribution in each single realization. As the moments are all defined in vertical direction,

the moments will be determined by the vertical distance of the front in the heterogeneous medium from the front location in a homogeneous medium at each point in horizontal direction. The average of these displacements will be due to the roughening of the front and can be assigned to the transition zone.
If the spreading of the transition zone of the two fluids is of dispersive nature, $\langle M^{(2)} \rangle$ is expected to grow with time, equivalently to the width of a solute plume spread by dispersion. A spreading characterized be the change of the advective part of the upscaled equation would cause a growth rate proportional to square of time, similar to spreading caused by anomalous diffusion.
The ensemble average of (7.74) up to second order of ε_σ applied to the heterogeneous solution $S^{(0)} + \langle S^{(2)} \rangle$ given by equation (7.52) yields

$$\langle M^{(2)} \rangle = \frac{-2 \int d^d x \int_0^t dt' z \langle \left(\tilde{q}_z f'(S_0) + GrU \tilde{\kappa} \Lambda'(S_0) \right) S_1(\vec{x}', t') \rangle}{m_{0,S}(t)}. \tag{7.75}$$

As the homogeneous solution is approximated as a step funtion the evaluation of (7.75) gives

$$\langle M^{(2)} \rangle(t) = 2 \frac{A^1_{vv} + GrA^1_{q\kappa} + GrA^1_{\kappa q} + Gr^2 A^1_{\kappa\kappa} + GrA^2_{q\kappa} + Gr^2 A^2_{\kappa\kappa}}{m_{0,S}(t)}. \tag{7.76}$$

As a first approximation all covariances are approximated as Gaussian functions. In this case the integrals A_{ij} are

$$A^1_{ij} = \varphi'(S_0)\, \varphi(S_0) \sqrt{\pi}\, l_{ij}\, \sigma_i\, \sigma_j \frac{t^2}{2} \tag{7.77}$$

$$A^2_{ij} = -\varphi'(S_0)\, \varphi(S_0)\, \sigma_i\, \sigma_j \frac{t^3 V^\star}{3}. \tag{7.78}$$

There are contributions both of dispersive and of superdispersive nature, characterized by the different exponents of the time. Note that the approximation of the stochastic properties as Gaussian becomes questionable as soon as the flow is unstable or stabilizing. As $m_{0,S}$ grows linearly with time, $\langle M^{(2)} \rangle$ has a part which grows quadratic with time. This part is due to the fluctuations of the permeability. It has also a part which grows linear with time. The dispersive growth of the transition zone between the fluids is contained in the linear part.

7.4.3 Numerical examples

The transition zone between displaced and displacing fluid is analyzed by comparing numerical multi realization calculations to the theoretical predictions. The code 3dsl (Batycky et al., 1997; Batycky, 1997) was again used in order to simulate the saturation distribution. The same setup as for the horizontal Buckley Leverett problem was

used for all simulations, but with a vertical flow direction. The injection velocity is this time $U = 4 \cdot 10^{-5} m/s$.
200 permeability fields for each set of simulations were generated using the random generator fgen (Robin et al., 1993b). Spatially isotropic permeability fields were generated with a Gaussian distribution, characterized by a relative variance of $\sigma_\kappa^2/\langle K \rangle^2 = 0.56$ and a correlation length of $l = 0.5m$. In this way a correlation length is resolved by 5 grid cells.
The flow properties, the mean permeabilities and the stability criteria for the different flow scenarios are given in Table 7.1.

Ensemble	ρ_1	ρ_2	μ_1	μ_2	$\langle K_{\text{int}} \rangle$
	$[kg/m^3]$	$[kg/m^3]$	$[Ns/m^2]$	$[Ns/m^2]$	$[m^2]$
1	1200	700	0.001	0.0015	$4.2 \cdot 10^{-11}$
2	1000	2000	0.001	0.002	$4.2 \cdot 10^{-12}$
Ensemble	$S^\star$	$Q^\star/Q$	M_{front}	q_{crit}	Gr
	$[-]$	$[-]$	$[-]$	$[m/s]$	$[-]$
1	0.85	1.08	1.1	0.0013	-3.4
2	0.55	1.43	0.8	$4.5 \cdot 10^{-5}$	0.5

Table 7.1: Parameters for the numerical multi realization calculations
The relative permeabilities are in both cases given as quadratic functions of the saturation.

Stabilizing displacement (Ensemble 1)

The first set of simulations is gravity dominated and stabilizing due to the gravity forces. $M^{(2)}$ was calculated numerically for each realization and was then averaged over the ensemble. The results are plotted in Figure 7.4. The stochastic parameters for the theoretically predicted curve was obtained from the numerical simulations. The definition of $M^{(2)}$ was also applied to the numerically obtained homogeneous solution (dashed line), in order to estimate the effects due to numerical dispersion. The effect from the quadratic part $M_{t^2}^{(2)}$, which characterizes the effective permeability, is too small to be separated from the effect of numerical errors. In the time regime considered here, the quadratic part is not dominant. By fitting a line to the linear part, we get a proportionality factor of $M_t^{(2)} = 0.102\, Q^\star t$. This small proportionality factor of $M_t^{(2)}$ due to the stability of the flow configuration matches well to the result of Kempers and Haas (1994) for stabilizing miscible displacement.

Stable displacement with low gravity number (Ensemble 2)

In the second set of simulations q_{crit} is in the same range as q_{total}. The flow is therefore neutrally stable. The linear part of the square width, $M_t^{(2)}$, was calculated numerically for

each realization and the results were then averaged over the ensemble. The quadratic part was too small to be analyzed further. The result is plotted in Figure 7.5. The stochastic properties to calculate the theoretically predicted result were obtained from the simulations. In this case, we get a very good agreement between the theoretically expected value and the numerical result. Both values lie clearly above the effect from the numerical dispersion.

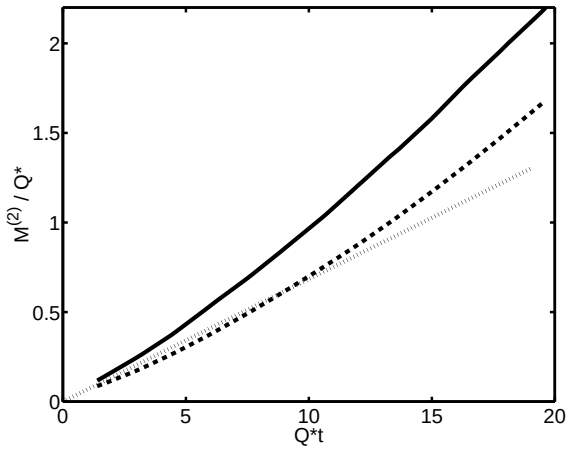

Figure 7.4: $M_t^{(2)}$ calculated numerically, Solid line: Calculated from the averaged heterogeneous saturation distribution, dashed line: Calculated from the numerical homogeneous solution, dotted line: Expected curve from equation (7.76), where the stochastic properties are obtained from the numerical simulations.

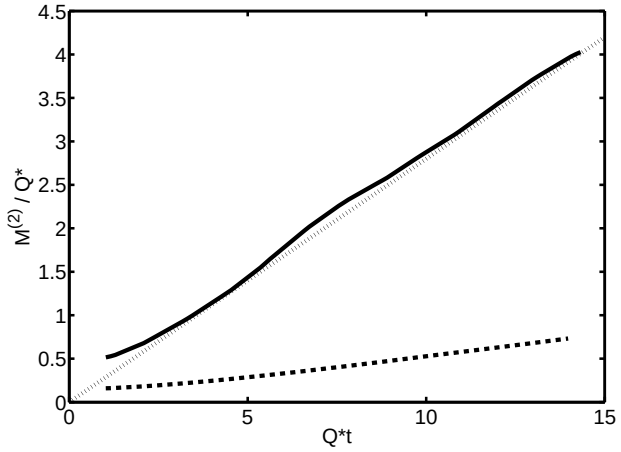

Figure 7.5: $M_t^{(2)}$ calculated numerically, Solid line: Calculated from the averaged heterogeneous saturation distribution, dashed line: Calculated from the numerical homogeneous solution, dotted line: Expected curve from equation (7.76), where the stochastic properties are obtained from the numerical simulations.

7.5 Summary

In this chapter the upscaled two-phase flow problem for large-scale flow problems where capillary forces can be neglected was derived. A typical flow scenario is water flooding of an oil reservoir. The upscaled problem has an artificial nonlinear dispersion term with a dispersion coefficient which is equivalent to the dispersion coefficient of solute transport. However, this form of the equation is only meaningful if the flow is neither stabilizing (where the front of a displacing fluid remains straight, independent of the soil structure) nor unstable (where the fingering is also independent of the soil structure). The dispersion coefficient could be reproduced with numerical multi-realization calculations.

Chapter 8

Summary, main conclusions and outlook

The study presented in the last chapters discusses the problem of the influence of scales on flow and transport processes in porous media. As soil and rock formations are usually heterogeneous, this problem is strongly coupled to the question as to how information about structure is transported over length scales. On different length scales different driving forces determine flow and transport processes. In order to derive an appropriate model for a certain scale of interest it is crucial to include information on information about the impact of structure on smaller scales into the model. The transfer from a detailed heterogeneous model to an equivalent model on a larger scale, where averaged properties are described, is called upscaling.
To derive an upscaled model the following questions have to be addressed:

- What are the relevant time scales and length scales?
- What are the relevant processes on the scale, where heterogeneities are resolved?
- How does the upscaled model look like?
- What are the effective parameters for the upscaled model?

As detailed information about the parameter distribution in the heterogeneous model is in most cases not known or it is not possible to deal with the exact distribution, further questions have to be addressed:

- How can the effective parameters be approximated based on incomplete knowledge about the parameter distribution?
- What are the relevant quantities to characterize the heterogeneous distribution and how can they be taken into account?

Another important aspect which is beyond the scope of this work is the treatment of uncertainties in the model predictions which are due to the uncertainties in the parameters of the model.

Different concepts to characterize heterogeneity are described in Chapter 2. Stochastic methods are mostly based on second order properties, while other approaches are used to quantify connected structures.
Several methods to derive upscaled models and to approximate effective parameters are discussed in Chapter 3. These methods are homogenization theory, volume averaging and stochastic averaging. Stochastic theory and different effective medium theory approaches to approximate effective parameters are outlined. In this chapter, the discussion is restricted to materials with heterogeneties with a finite typical length scale. Coarse graining approaches, which are applicable if length scales are not separated, are not taken into account.
Chapters 4 to 7 are applications of these methods, and comprise the largest part of the studies pursued by the author over the last years (Metzger et al., 1999; Neuweiler et al., 2001; Attinger et al., 2001; Neuweiler and King, 2002; King and Neuweiler, 2002; Neuweiler et al., 2003, 2004b,a; Eichel et al., 2005; Neuweiler and Cirpka, 2005; Neuweiler and King, 2006; Neuweiler and Eichel, 2007; Neuweiler and Vogel, 2007). The chapters deal with different two-phase flow scenarios.
Chapter 4 is dedicated to the discussion of how averaged properties can be modelled for unstable flow. Besides viscous instabilities the main focus is on capillary unstable flow. The problem is treated with an analogous model for drainage in an open rough walled fracture. The fracture can be considered a simplified model for a porous medium. The effect of trapping of displaced fluid and the related flow patterns are considered to be transferable from the fracture model to a heterogeneous porous medium in a qualitative sense. The flow in the fracture was analyzed with an invasion percolation model and with laboratory experiments on artificial rough walled fractures with different aperture structure. An aperture field with a finite correlation length (thus a macroscopically homogeneous field) was compared to a field with no finite correlation length. This field had structures on all length scales. The main achievements obtained in the work presented in Chapter 4 are:

- The results of the invasion percolation models allowed the conclusion that the flow patterns are irregular and the correlation function of the spatial saturation distribution has no finite correlation length, independently of the correlation structure of the underlying field.
- It has been shown that invasion percolation models capture the main flow mechanisms of drainage in an open rough walled fracture. There was a good correspondence between experiment.
- The lack of a macroscopic REV for unstable flow process makes the application of continuum models on a larger scale questionable.
- Models which describe the averaged saturation have to be used with care, when flow processes are unstable. Averaged properties are then not representative for the processes in a single realization of a porous medium. Averaged properties are, however, relevant for risk assessment.

In Chapter 5 upscaling of Richards equation is analyzed. Richards equation is a model for water flow in the unsaturated zone. The flow of air is in this model neglected. The flow occurs here typically on a length scale of meters to tens of meters. The upscaled model is derived for slow time scales using homogenization. Effective parameters were calculated with different methods for capillary dominated flow. Gravity dominated flow and the intermediate flow regime between gravity and capillary dominated flow was analyzed for a layered porous medium. The major findings are:

- The upscaled model for the Richards equation has the same shape as Richards equation in case that the flow is slow and capillary dominated.
- It was shown for the layered system that for gravity dominated flow the Richards equation pertains its form. The evaluation of different test cases showed that the parameters are not that different from the parameters obtained with the assumption of capillary equilibrium. It can be concluded that results obtained using the capillary equilibrium assumption are for slow flow processes good estimates, even if gravity forces are strong.
- For the layered system it could also be shown that in case that the separation of scales is not given, the upscaled model has no longer the form of a Richards equation. It is very likely that also for faster flow processes the form is changed.
- For the capillary dominated slow flow scenario the effective parameters were calculated with stochastic theory. Entry pressure effects of the effective parameter functions disappear due to the averaging.
- It was demonstrated that fields with connected extreme parameter values are not well represented by second order stochastic theory. Although the effective retention function is not sensitive to structure, differences are pronounced in the effective permeabilities.
- Effective medium theory approaches based on a background-inclusion description of the medium was used to calculate the effective permeability for fields with connected extreme values. Compared to second order stochastic theory the results were much improved.

A more general two-phase flow problem is analyzed in Chapter 6, namely the problem of counter-current flow in a closed medium for the condition of capillary equilibrium. The process is considered to occur on a length scale of a meter, similar to the unsaturated flow problem. Contrary to this problem, however, it is in this case not sufficient to consider the flow of one fluid only, but the coupled system for both fluids has to be taken into account. The main results are the following:

- An upscaled model for the flow problem was derived. The upscaled model has no viscous term. The local viscous term yields on average a buoyancy term. The effective parameter functions are calculated from the flow equations for both fluids

separately, where the other fluid is considered stagnant in the background. The model was validated with numerical simulations of the heterogeneous problem.

- The stochastically averaged parameter functions for the upscaled model were calculated explicitly. Only the arithmetic mean of the permeability can be used for a stochastic average, as the vanishing of non-wetting phase leads to local relative permeabilities of zero. This leads to unphysical results for the effective permeability if the geometric mean or the harmonic mean are considered. The averaged permeability functions thus overpredicts the real permeability.

- The effective parameter functions was analyzed for fields where extreme values are connected. Stochastic averages do not give good estimates especially for the parameters of the non-wetting phase. The macroscopic residual saturation depends strongly on the existence of connected paths.

- Effective medium theory approaches which are based on a background-inclusion representation of the medium are much better suited to approximate the effective parameters in case that the fields have connected extreme values.

In Chapter 7 immiscible displacement is analyzed on a large length scale, typically several kilometers, where capillary forces are negligible. This is the Buckley Leverett problem, where gravity forces and viscous forces are considered. The flow can be unstable or stabilizing. In both cases the relation between heterogeneous structure and flow patterns cannot be quantified. For neutrally stable flow the upscaled problem was investigated in more detail. The following points have been accomplished:

- The upscaled model was derived. It was found that an artificial (small) diffusion term has to be added to derive a meaningful upscaled model. The upscaled model describes the spatially averaged saturation distribution. The scenario in a real porous medium would only be represented by such a model if there was really a diffusion mechanism. The opposite is however the case, the interface between the two fluids is usually self-sharpening. The upscaled model does therefore not represent the real flow on the large scale, but only the spatially or stochastically averaged problem.

- The effective parameters were derived for the upscaled model. A non-linear dispersion term, which is not present in the small-scale model was found and the dispersion coefficient was calculated explicitly with second order stochastic theory.

- The dispersion coefficient was analyzed for a radial and for a uniform flow scenario. A generalized moment method was used to quantify the transition zone between the fluids and thus the macrodispersivity. The macrodispersion coefficient is similar to the macrodispersion coefficient found in solute transport.

- The results were compared to numerical simulations. The results of these simulations underlined the importance of stable conditions.

Upscaled models and upscaled parameters have been analyzed successfully for several two-phase flow problems on different scales. These examples contribute to the understanding of the influence of soil structrue on flow processes on different length scales. This work makes a substantial contribution to the evaluation and comparison of different upscaling methods as well as of their possibilities for application. It also makes an important contribution to the development of methods for transporting information across scales.

However, many open questions still remain. Some of them are relevant for application of these models for problems in the field. They should therefore be addressed.

The first important point to notice concerns the assumption for all upscaled models that the scales in the porous medium are clearly separated. This is often not the case in natural porous media. The exploration of methods which account for large scale heterogeneity is today at beginning stage. Especially for non-linear problems, such as two-phase flow, these methods are difficult to apply. However, progress in this field is crucial for the practical use of upscaled models.

The issue of uncertainty of the effective parameters was here not addressed. For the application of the upscaled models it is however important to have an estimate as to how reliable their prediction are. For unsaturated flow a large amount of work in this field has been done over the last years. For the full two-phase flow problem this is however not the case and there is need for further investigation.

The upscaled models in the examples considered in this work were always derived for slow flow processes. However, flow processes are often fast. As an example, the infiltration of water into the unsaturated zone after a rainfall event happens on small time scales. It is to be expected that the upscaled models have a much more complex form than the original equations. The investigation of dynamic effects is an open and young field of research.

The systems considered in this work were systems with simple boundary conditions. Future research will however be much more driven towards coupling of the different hydrologic systems. For example, the coupling of the unsaturated zone to surface flow processes and the atmosphere is nowadays one of the important problems in water research. This requires that much more complex boundary conditions which change in time and space have to be incorporated into upscaled models. It might very well be that the variability of the boundary conditions has an equally important or even larger influence on the upscaled model than the variability of the parameters of the medium.

Bibliography

A. Abdin, S. M. Chang, M. W. Kemblowski, and J. J. Kaluarchchi. Stochastic Analysis of Two–Phase Flow in Porous Media: II. Comparison Between Perturbation and Monte–Carlo Results. *Transport in Porous Media*, 19:261 – 280, 1995.

P. Adler. *Porous Media - Geometry and Transport*. Butterworth–Heinemann, Boston, 1992.

E. Aker, K. J. Maloy, and A. Hansen. Dynamics of stable viscous displacement in porous media. *Phys Rev E*, 61(3):2936–46, 2000.

H. Amundsen, G. Wagner, U. Oxaal, P. Meakin, J. Feder, and T. Jossang. Slow two-phase flow in artificial fractures: Experiments and simulations. *Water Resour Res*, 35(9): 2619–26, 1999.

G. B. Arfken and H. J. Weber. *Mathematical Methods for Physicists*. Harcourt Academic Press, San Diego, 2001.

S. Attinger. Generalized coarse graining procedures in heterogeneous porous media. *Computational Geosciences*, 7(4):253–273, 2003.

S. Attinger, M. Dentz, H. Kinzelbach, and W. Kinzelbach. Temporal behaviour of a solute cloud in a chemically heterogeneous porous medium. *Journal of Fluid Mechanics*, 386: 77–104, 1999.

S. Attinger, I. Neuweiler, and W. Kinzelbach. Macrodispersion in a radially diverging flow field with finite peclet numbers ii: Homogenization theory approach. *Water Resources Research*, 37(3):495–507, 2001.

J. L. Auriault. Effective macroscopic description for head conduction in periodic composites. *International Journal of Heat Transfer*, 26(6):861–869, 1983.

J. W. Barker and S. Thibeau. A critical review of the use of pseudo-relative permeabilities for upscaling. *SPE Reservoir Engineering*, 12:138–143, 1997.

R. P. Batycky. *A three-dimensional two-phase field scale streamline simulator*. Ph. D. dissertation, Stanford University, Stanford, California, 1997.

R. P. Batycky, M. J. Blunt, and M. R. Thiele. A 3d field scale streamline simulator with gravity and changing well conditions. *SPE Reservoir Engineering*, pages 246–254, 1997.

J. Bear. *Dynamics of Fluids in Porous Media*. Dover Publications, New York, 1972.

R. Beckie, A. a. Aldama, and E. F. Wood. The universal structure of the groundwater flow equations. *Water Resources Research*, 30:1407–1419, 1994.

A. Bellin, A. Rinaldo, W. Bosma, S. van der Zee, and Y. Rubin. Linear equilibrium adsorbing solute transport in physically and chemically heterogeneous porous formations 1. analytical solutions and 2. numerical solutions. *Water Resources Research*, 29: 4019–4043, 1993.

A. Bensoussan, J.-L. Lions, and G. Papanicolaou. *Asymptotic Analysis for Periodic Structures*. North Holland, Amsterdam, 1978.

B. Berkowitz and R. P. Ewing. Percolation theory and network modeling applications in soil physics. *Surveys in Geophysics*, 19:23–72, 1998.

P. Binning and M. A. Celia. Practical implementation of the fractional flow approach to multi-phase flow simulation. *Advances in Water Resources*, 22(5):461–478, 1999.

J. Birkhoelzer and C. Tsang. Solute channeling in usaturated heterogeneous porous media. *Water Resources Research*, 33(10):2221–2238, 1997.

M. J. Blunt and H. Scher. Pore-level modeling of wetting. *Phys Rev E*, 52(6):6387–403, 1995.

M. J. Blunt, J. W. Barker, B. Rubin, M. Mansfield, I. D. Culverwell, and M. Christie. Predictive theory for viscous fingering in compositional displacement. *SPE Reservoir Engineering*, pages 73–80, 1994.

A. Bourgeat and M. Panfilov. Effective two-phase flow through highly heterogeneous porous media: Capillary nonequilibrium effects. *Computational Geosciences*, 2:191–215, 1998.

C. Braun, R. Helmig, and S. Manthey. Determination of constitutive relationships for two-phase flow processes in heterogeneous porous media with emphasis on the relative permeability-saturation-relationship. *Advances in Water Resources*, 2004.

R. Brooks and A. Corey. Properties of porous media affecting fluid flow. *Soil Sci. Soc. Am. J.*, 39(2):61–88, 1966.

E. D. Chikhliwala, A. B. Huang, and Y. C. Yortsos. Numerical study of the linear stability of immiscible displacement in porous media. *Transport in Porous Media*, pages 257–276, 1988.

R. L. Chouke, P. van Meurs, and C. can der Poel. The instability of slow, immiscible, viscous liquid-liquid displacements in permeable media. *Petroleum Transactions AIME*, 216:183–194, 1959.

D. Cioranescu and P. Donato. *An Introduction to Homogenization*. Oxford, 1999.

O. A. Cirpka and P. Kitanidis. Characterization of mixing and dilution in heterogeneous aquifers by means of temporal moments. *Water Resources Research*, 36(5):1221–1263, 2000.

O. A. Cirpka and P. K. Kitanidis. Numerical evaluation of solute dispersion and dilution in unsaturated heterogeneous media. *Water Resources Research*, 38(11): 1220,doi:10.1029/2001WR001262, 2002.

V. Cvetkovic and G. Dagan. Reactive transport and immiscible flow in geological media. ii. applications. *Proc. R. Soc. Lond. A*, 452:303–328, 1996.

G. Dagan. Models of groundwater flow in statistically homogeneous porous formations. *Water Resources Research*, 15(1):47–63, 1979.

G. Dagan. Solute transport in heterogeneous porous formations. *Journal of Fluid Mechanics*, 145:151–177, 1984.

G. Dagan. Time dependent macrodispersion for solute transport in anisotropic heterogeneous aquifers. *Water Resources Research*, 24:1491–1500, 1988.

G. Dagan. *Flow and Transport in Porous Formations*. Springer, 1989.

G. Dagan. Transport in heterogeneous porous formations: Spatial moments, ergodicity and effective dispersion. *Water Resources Research*, 26:1281–1290, 1990.

G. Dagan. High-order correction of effective permeability of heterogeneous isotropic formations of log-normal conductivity distribution. *Transport in Porous Media*, 12: 279–290, 1993.

G. Dagan and V. Cvetkovic. Reactive transport and immiscible flow in geologic media: I. general theory. *Proc. R. Soc. London, Ser. A*, 452:285–302, 1996.

M. Dale, S. Ekrann, J. Mykkeltveit, and G. Virnovsky. Effective relative permeabilities and capillary pressure for one-dimensional heterogeneous media. *Transport in Porous Media*, 26(3):229–260, 1997.

J. C. Davis. *Statistics and Data Analysis in Geology*. Wiley, New York, 1986.

G. de Marsily. *Quantitative Hadrogeology: Groundwater Hydrology for Engineers*. Academic Press, San Diego, 1986.

M. Dentz, H. Kinzelbach, S. Attinger, and W. Kinzelbach. Temporal behaviour of a solute cloud in a heterogeneous porous medium: Point-like injection. *Water Resources Research*, 36(12):3591–3604, 2000.

A. J. Desbarats. Upscaling capillary pressure-saturation curves in heterogeneous porous media. *Water Resouces Research*, 31(2):281–288, 1995.

R. L. Detwiler, S. E. Pringle, and R. J. Glass. Measurement of fracture aperture fields using transmitted light: An evaluation of measurement errors and their influence on simulations of flow and transport through a single fracture. *Water Resour Res*, 35(9): 2605–17, 1999.

C. V. Deutsch and A. G. Journel. *GSLIB: Geostatistical software library and user's guide*. Oxford University Press, New York, 1992.

M. M. Dias and D. Wilkinson. Percolation with trapping. *J Phys A*, 19:3131–46, 1986.

P. A. Domenico and F. W. Schwartz. *Physical and Chemical Hydrogeology*. John Wiley and Sons, Inc., New York, 1990.

L. J. Durlofsky. Representation of grid block hydraulic conductivity in coarse scale models of randomly heterogeneous porous media. *Water Resources Research*, 28(7):1791–1800, 1992.

L. J. Durlofsky. Coarse scale models of two phase flow in heterogeneous reservoirs: volume averaged equations and their relationship to existing upscaling techniques. *Computational Geosciences*, 2:73–92, 1998.

H. Eichel, R. Helmig, I. Neuweiler, and O. Cirpka. Upscaling of two-phase flow processes in porous media. In D. B. Das and S. Hassanizadeh, editors, *Upscaling Multiphase Flow in Porous Media*, pages 237 – 257. Springer, 2005.

R. E. Ewing. Aspects of upscaling in simulation of flow in porous media. *Advances in Water Resources*, 20(5-6):349–358, 1997.

C. W. Fetter. *Applied Hydrogeology, 4th ed.* Prentice Hall, Upper Saddle River, 2001.

A. Fiori. On the influence of the pore-scale dispersion in nonergodic transport in heterogeneous formations. *Transport in Porous Media*, 30:57–73, 1998.

A. Fiori, P. Indelman, and G. Dagan. Correlation structure of flow variables for steady flow toward a well with application to highly anisotropic heterogeneous formations. *Water Resources Research*, 34(4):699–708, 1998.

H. B. Fischer, E. J. List, R. C. Y. Koh, J. Imberger, and N. H. Brooks. *Mixing in Inland and Coastal Waters*. Academic Press, 1979.

U. Fischer, B. Kulli, and H. Fluehler. Constitutive relationships and pore structure of undisturbed fracture zone samples with cohesionless fault gouge layers. *Water Resour Res*, 34(7):1695–1701, 1998.

I. Forrer, R. Kasteel, M. Flury, and H. Flühler. Longitudinal and lateral dispersion in an unsaturated field soil. *Water Resources Research*, 35(10):3049–3060, 1999.

R. A. Freeze and J. A. Cherry. *Groundwater*. Prentice Hall, Englewood Cliffs, 1979.

W. Gardner. Some steady state solutions of unsaturated moisture flow equations with application to evaporation from the water table. *Soil Sci.*, 85:228–232, 1958.

L. W. Gelhar. *Stochastic Subsurface Hydrology*. Prentice Hall, 1993.

L. W. Gelhar and C. L. Axness. Three-dimensional analysis of macrodispersion in aquifers. *Water Resources Research*, 19(1):161–180, 1983.

R. J. Glass and L. Yarrington. Simulation of gravity fingering in porous media using a modified invasion percolation model. *Geoderma*, 70:231–52, 1996.

R. J. Glass, M. J. Nicholl, and L. Yarrington. A modified invasion percolation model for low-capillary number immiscible displacement in horizontal rough-walled fractures: Influence of local in-plane curvature. *Water Resour Res*, 34(12):3215–34, 1998.

J. J. Gomez-Hernandez and X.-H. Wen. To be or not to be multi-gaussian? a reflection on stochastic hydrogeology. *Advances in Water Resources*, 21:47–61, 1997.

T. Harter and J. W. Hopmans. Role of vadose zone flow processes in regional scale hydrology: Review, opportunities and challenges. In R. Feddes, G. de Rooij, and J. van Dam, editors, *Unsaturated Zone Modeling: Progress, Applications, and Challenges*, chapter 6, pages 179 – 208. Kluwer, 2004.

R. Hassanein, E. Lehmann, and P. Vontobel. Methods of scattering corrections for quantitative neutron radiography. *Nuclear Instruments and Methods in Physics Research A*, 542:353–360, 2005.

S. M. Hassanizadeh and W. G. Gray. Thermodynamic basis of capillary pressure in porous media. *Water Resources Research*, 29(10):3389 – 3405, 1993.

S. M. Hassanizadeh, M. Celia, and H. Dahle. Dynamic effect in the capillary pressure-saturation relationship and its impacts on unsaturated flow. *Vadose Zone Journal*, 1: 38–57, 2002.

R. Helmig. *Multiphase Flow and Transport Processes in the Subsurface*. Springer, Berlin, 1997.

R. Helmig, H. Class, R. Huber, H. Sheta, J. Ewing, R. Hinkelmann, H. Jakobs, and P. Bastian. Architecture of the Modular Program System MUFTE_UG for Simulating Multiphase Flow and Transport Processes in Heterogeneous Porous Media. *Mathematische Geologie*, 2, 1998.

R. Hilfer. Geometric and dielectric characterization of porous media. *Physical Review B*, 44(1):60–74, 1991.

R. Hilfer. Local-porosity theory for flow in porous media. *Physical Review B*, 45(13): 7115–7121, 1992.

R. Hilfer and P. E. Øren. Dimensional analysis of pore scale and field scale immiscible displacement. *Transport in Porous Media*, 22:53–72, 1996.

G. M. Homsy. Viscous fingering in porous media. *Annual Review of Fluid Mechanics*, 19:271–311, 1987.

U. Hornung. *Homogenization and Porous Media*. Springer, 1997.

D. T. Hristopulos. Renormalization group methods in subsurface hydrology: overview and applications in hydraulic conductivity upscaling. *Advances in Water Resources*, 26:1279 – 1308, 2003.

K. C. Hsu and S. P. Neuman. Second-order expressions for velocity moments in two- and three-dimensional statistically anisotropic media. *Water Resources Research*, 33 (4):625–637, 1997.

R. G. Hughes and M. J. Blunt. Network modeling of multiphase flow in fractures. *Adv Water Resour*, 24:409–21, 2001.

A. Hunt. *Percolation theory for flow in porous media*. Springer, Berlin, 2005.

P. Indelman and G. Dagan. Solute transport in divergent radial flow through heterogeneous porous media. *Journal of Fluid Mechanics*, 384:159–182, 1999.

P. Indelman, D. Or, and Y. Rubin. Stochastic analysis of unsaturated steady state flow through bounded heterogeneous formations. *Water Resources Research*, 29(4):1141–1148, 1993.

E. H. Issaks and R. M. Srivastava. *An Introduction Into Applied Geostatistics*. Oxford University Press, New York, 1989.

C. Jackson, A. Hoch, and S. Todman. Self-consistency of a heterogeneous continuum porous medium representation of a fractured medium. *Water Resources Research*, 36 (1):189–202, 2000.

U. Jaekel, A. Georgescu, and H. Vereecken. Asymptotic analysis of nonlinear equilibrium solute transport in porous media. *Water Resources Research*, 32(10):3093–3098, 1996.

M. W. Kemblowski and J. C. Wen. Contaminant spreading in stratified soils with fractal permeability distribution. *Water Resources Research*, 29(2):419–425, 1993.

L. J. Kempers and H. Haas. The dispersion zone between fluids with different density and viscosity in a heterogeneous porous medium. *Journal of Fluid Mechanics*, 267: 299–324, 1994.

P. King. The use of field theoretic methods for the study of flow in a heterogeneous porous medium. *Journal of Physics A*, 20:3935 – 3947, 1987.

P. King and I. Neuweiler. Probability upscaling. *Computational Geosciences*, 6:101–114, 2002.

P. King, S. Buldyrev, N. Dokholyan, S. Havlin, E. Lopez, G. Paul, and H. Stanley. Using percolation theory to predict oil field performance. *Physica A*, 314:103–108, 2002.

P. R. King. The use of renormalization for calculating effective permeability. *Transport in Porous Media*, 4:37, 1989.

P. K. Kitanidis. Prediction by the method of moments of tranport in heterogeneous formations. *Journal of Hydrology*, 102:453–473, 1988.

P. K. Kitanidis. *Introduction to Geostatistics*. Cambridge University Press, 1997.

M. A. Knackstedt, A. P. Sheppard, and M. Sahimi. Pore network modeling of two-phase flow in porous rock: the effect of correlated heterogeneity. *Adv Water Resour*, 24: 257–77, 2001.

C. Knudby and J. Carrera. On the relationship between indicators of geostatistical, flow and transport connectivity. *Advances in Water Resources*, 28:405–421, 2005.

C. E. Koltermann and S. M. Gorelick. Heterogeneity in sedimentary deposits: A review of structure-imitating, process-imitating and descriptive approaches. *Water Resources Research*, 32(9):2617–2658, 1996.

B. H. Kueper and E. O. Frind. An overview of immiscible fingering in porous media. *Journal of Contaminant Hydrology*, 2:95–110, 1988.

B. H. Kueper and D. B. M. Worther. The use of macroscopic percolation theory to construct large-scale capillary pressure curves. *Water Resources Research*, 28(9):2425–2436, 1992.

R. Landauer. The electrical resistance of binary metallic mixtures. *Journal of Applied Physics*, 23:779–784, 1952.

R. Landauer. Electrical conductivity in inhomogeneous media. In J. C. Galrand and D. B. Tanner, editors, *Electrical, Transport and Optical Properties of Inhomogeneous Media*. AIP, New York, 1978.

P. Langlo and M. S. Espedal. Macrodispersion for two-phase, immiscible flow in porous media. *Advances in Water Resources*, 17:297–316, 1995.

E. H. Lehmann, P. Vontobel, and L. Wiezel. Properties of the radiography facility neutra at sinq and its potential for use as european reference facility, nondestructive testing and evaluation. *Proceedings of the Sixth World Conference on Neutron Radiography, Osaka, Japan, May 17-21, 1999*, 16:191–202, 2001.

T. Leihnse. Upscaling, why and what. In D. F. C. on Hydrological Science, editor, *Turning the Water Wheel Inside Out*, pages 26–27. Royal Netherlands Academy of Arts and Sciences, Amsterdam, 2005.

R. Lenormand and C. Zarcone. Capillary fingering: Percolation and fractal dimension. *Transport Porous Med*, 4:599–612, 1989.

R. Lenormand, E. Touboul, and C. Zarcone. Numerical models and experiments on immiscible displacement in porous media. *J Fluid Mech*, 189:165–87, 1988.

M. C. Leverett. Capillary behaviour in porous solids. *Trans. AIME Petr. Eng. Div.*, 142: 152–169, 1941.

T. Levy. *Fluids in porous media, Darcy's law*, volume 272 of *Lecture Notes in Physics*, chapter 2, pages 75 – 84. Springer, 1987.

J. Lewandowska and J.-P. Laurent. Moisture transfer in an unsaturated heterogeneous porous medium. *Transport in Porous Media*, 45:321–345, 2001.

J. Lewandowska, A. Szymkiewicz, K. Burzynski, and M. Vauclin. Modeling of unsaturated water flow in double-porosity soils by the homogenization approach. *Advances in Water Resources*, 27:283–296, 2004.

Z. M. Lu and D. Zhang. Analytical solutions to steady state unsaturated flow in layered, randomly heterogeneous soils via kirchhoff transformation. *Advances in Water Resources*, 27(8):775–784, 2004.

I. Lunati, S. Attinger, and W. Kinzelbach. Macrodispersivity for transport in arbitrary nonuniform flow fields: Asumptotic and preasymptotic results. *Water Resources Research*, 38(10):doi:10.1029/2001WR001203, 2002.

K. J. Maloy, L. Furuberg, J. Feder, and T. Jossang. Dynamics of slow drainage in porous media. *Phys Rev Letters*, 68(14):2161–64, 1992.

B. B. Mandelbrot and J. W. V. Ness. Fractional brownian motions, fractional noises and applications. *SIAM Review*, 10(4):422–437, 1968.

A. Mantoglou and L. Gelhar. Effective hydraulic conductivities of transient unsaturated flow in stratified soils. *Water Resources Research*, 23(1):57–67, 1987a.

A. Mantoglou and L. W. Gelhar. Stochastic modeling of large-scale transient unsaturated flow systems. *Water Resources Research*, 23(1):37–46, 1987b.

C. M. Marle. *Multiphase Flow in Porous Media, 1. edition*. Institut Francais du Petrole, Paris, 1981.

R. Mauri. Heat and mass transport in nonhomogeneous random velocity fields. *Physical Review E*, 68:doi: 10.1103/PhysRevE.68.066306, 2003.

R. Mauri. Dispersion, convection and reaction in porous media. *Physics of Fluids A*, 3 (5):743–756, 1991.

W. McComb. *The Physics of Fluid Turbulence*. Oxford Science Publication, Oxford, 1996.

P. Meakin. Invasion percolation and invading eden growth on multifractal lattices. *J Phys A*, 21:3501–22, 1988.

K. Mecke and H. Wagner. Euler characteristic and related measures for random geometric sets. *Journal of Statistical Physics*, 64:843–850, 1991.

D. Metzger, H. Kinzelbach, I. Neuweiler, and W. Kinzelbach. Asymptotic transport parameters in a heterogeneous porous medium: Comparison of two ensemble-averaging procedures. *Stochastic Environmental Research and Risk Assessment*, 13:396–415, 1999.

E. E. Miller and R. D. Miller. Phyiscal theory for capillary flow phenomena. *Journal of Applied Physics*, 27:324–332, 1956.

F. Miralles-Wilhelm and L. W. Gelhar. Stochastic analysis of sorption macrokinetics in heterogeneous aquifers. *Water Resources Research*, 32(6):1541–1549, 1986.

Y. Mualem. New model for predicting hydraulic conductivity of unsaturated porous-media,. *Water Resources Research*, 12(3):513–522, 1976.

I. Neuweiler and O. Cirpka. Homogenization of richards equation in permeability fields with different connectivities. *Water Resources Research*, 41(2): doi:10.1029/2004wr003329, 2005.

I. Neuweiler and H. Eichel. Effective parameter functions for richards equation in layered porous media. *Vadose Zone Journal*, 5:963–977, 2007.

I. Neuweiler and P. King. Coarse graining of the solute concentration probability distribution for advective transport in porous media. In S. M. Hassanizadeh, R. J. Schotting, W. G. Gray, and G. Pinder, editors, *14. International Conference on Computational Methods in Water Resources*, pages 1147 – 1154. Elsevier Science Publishers B.V., 2002.

I. Neuweiler and P. King. Transition zone between two fluids for vertical immiscible displacement in heterogeneous porous media. *Computational Geosciences*, page submitted, 2006.

I. Neuweiler and H.-J. Vogel. Upscaling of unsaturated flow considering connectivity. *Water Resources Research*, 43(3):W03444, doi:10.1029/2005WR004271, 2007.

I. Neuweiler, S. Attinger, and W. Kinzelbach. Macrodispersion in a radially diverging flow field with finite peclet numbers, 1.: Perturbation theory approach. *Water Resources Research*, 37(3):481–493, 2001.

I. Neuweiler, S. Attinger, W. Kinzelbach, and P. King. Large scale mixing for immiscible displacement in heterogeneous porous media. *Transport in Porous Media*, 51:287 – 314, 2003.

I. Neuweiler, O. Cirpka, H. Eichel, and R. Helmig. Infiltration of dnapl into heterogeneous water-saturated soil with different connectivity properties. In C. Miller, W. Farthing, W. Gray, and G. Pinder, editors, *15. International Conference on Computational Methods in Water Resources*, pages 313 – 324. Elsevier Science Publishers B.V., 2004a.

I. Neuweiler, I. Sorensen, and W. Kinzelbach. Experimental and theoretical investigations of drainage in horizontal rough-walled fractures with different correlation structures. *Advances in Water Resources*, 27(12):1217–1231, 2004b.

J. L. Nieber, R. Z. Dautov, and A. G. Egorov. Dynamic capillary pressure mechanism for instability in gravity-driven flows: Review and extension to very dry conditions. In D. B. Das and S. M. Hassanizadeh, editors, *Upscaling Multiphase Flow in Porous Media*, pages 147 – 172. Springer, 2005.

A. N. Norris, A. J. Callegari, and P. Sheng. A generalized differential effective medium theory. *Journal of Mechanics and Physics of Solids*, 33(6):525–543, 1985.

C.-W. Park, S. Gorell, and G. M. Homsy. Two-phase displacenemt in hele-shaw cells: experiments on viscously driven instabilities. *Journal of Fluid Mechanics*, 141:257–287, 1984.

L. Paterson. Radial fingering in a hele shaw cell. *Journal of Fluid Mechanics*, 113: 513–529, 1981.

G. E. Pickup and K. S. Sorbie. The scaleup of two-phase flow in porous media using phase permeability tensors. *Society of Petroleum Engineers, SPE*, page No. 28586, 1996.

G. E. Pickup and K. D. Stephen. An assessment of steady-state scale-up for small-scale geological models. *Petroleum Geoscience*, 6:203–210, 2000.

S. Pozdniakov and C. Tsang. A self-consistent approach for calculating effective hydraulic conductivity of a binary, heterogeneous medium. *Water Resources Research*, 40(5):doi:10.1029/2003WR002617, 2004.

W. H. Press, S. Teukolsky, W. Vetterling, and B. Flannery. *Numerical Recipes, Second Edition*. Cambridge University Press, 1988.

K. Pruess. A fickian diffusion model for the spreading of liquid plumes infiltrating in heterogeneous media. *Transport in Porous Media*, 24(1):1–33, 1996.

H. Rajaram and L. W. Gelhar. Plume scale-dependent dispersion in heterogeneous aquifers, 1: Lagrangian analysis in a stratified aquifer. *Water Resources Research*, 29(9):3249–3260, 1993.

P. Renard and G. de Marsily. Calculating equivalent permeability: a review. *Advances in Water Resources*, 20(5-6):253–278, 1997.

M. J. L. Robin, A. L. Gutjahr, E. A. Sudicky, and J. L. Wilson. Cross-correlated random field generator with the direct fourier transform method. *Water Resour Res*, 29(7): 2385–97, 1993a.

M. J. L. Robin, A. L. Gutjahr, E. A. Sudicky, and J. L. Wilson. Cross-correlated random field generator with the direct fourier transform method. *Water Resources Research*, 29 (7):2385–2397, 1993b.

N. Romano, B. Brunone, and A. Santini. Numerical analysis of one-dimensional unsaturated flow in layered soils. *Advances in Water Resources*, 21(4):315–324, 1998.

K. Roth, W. A. Jury, H. Flühler, and W. Attinger. Transport of chloride through an unsaturated field soil. *Water Resources Research*, 27(10):2533–2541, 1991.

Y. Rubin. *Applied stochastic hydrogeology*. Oxford University Press, 1997.

Y. Rubin, A. Sun, R. Maxwell, and A. Bellin. The concept of block-effective macrodispersivity and a unified approach for grid-scale- and plume-scale-dependent transport. *J. Fluid Mech.*, 395:161–180, 1999.

J. Ruge and K. Stüben. Algebraic multigrid (amg). In S. F. McMormick, editor, *Multigrid methods*, pages 73–130. SIAM, 1987.

D. Russo. Determining soil hydraulic properties by parameter estimation: On the selection of a model for the hydraulic properties. *Water Resources Research*, 24(3):453–459, 1988.

D. Russo. Upscaling of hydraulic conductivity in partially saturated heterogeneous porous formation. *Water Resources Research*, 28(2):397–409, 1992.

D. Russo. Upscaled conductivity in gravity-dominated flow through variably saturated heterogeneous formations. *Water Resources Research*, 39(9):1255 doi:10.1029/2002WR001857, 2003.

D. Russo. Stochastic analysis of flow and transport in unsaturated heterogeneous porous formations. *Water Resources Research*, 34:569–581, 1998.

P. G. Saffman. Viscous fingering in hele-shaw cells. *Journal of Fluid Mechanics*, 173: 73–94, 1986.

P. G. Saffman and G. Taylor. The penetration of a fluid into a porous medium of hele-shaw cell conatining a more viscous liquid. *Proc Royal Soc Ser. A*, 245:312–31, 1958.

M. Sahimi. *Flow and Transport in Porous Media and Fractured Rock*. VCH, Weinheim, 1995.

E. Sanchez-Palencia. *Non-homogeneous media and vibration theory*, volume 127 of *Lecture Notes in Physics*, chapter 7, pages 129 – 157. Springer, 1980.

E. Sanchez-Palencia and A. Zaoui. *Homogenization Techniques for Composite Media*. Springer, Lecture notes in Physics 272, 1987.

T. M. Shaw. Movement of a drying front in a porous material. In C. J. Brinker, D. E. Clark, and D. R. Ulrich, editors, *Mat. Res. Soc. Symposium Proc. (73)*, pages 215–223. 1986.

H. E. Smith. The influence of small-scale heterogeneity on average relative permeability. In *Reservoir Characterization II*, pages 52–76. Academic Press Inc., 1991.

G. Sposito and W. Jury. Miller similtude and generalized scaling anaysis. In ed. by D. Hillel and D. Elrick, editors, *Scaling in Soil Physics: Principles and Applications*, volume 25, pages 13–22. SSSA Spec. Publ., 1990.

R. Srivastava and T. Yeh. Analytical solutions for one-dimensional, transient infiltration toward the water-table in homogeneous and layered soils. *Water Resources Research*, 27(5):753–762, 1991.

D. Stauffer. *Introduction to percolation theory*. Taylor & Francis, London, 1992.

E. A. Sudicky. A natural gradient experiment on solute transport in a sand aquifer: Spatial variability of hydraulic conductivity and its role in the dispersion process. *Water Resources Research*, 22(13):2069–2082, 1986.

A. Szymkiewicz and J. Lewandowska. Unified macroscopic model for unsaturated water flow in soils of bimodal porosity. *Hydrological Sciences Journal*, in press, 2006.

D. M. Tartakovsky, S. P. Neuman, and Z. Lu. Conditional stochastic averaging ofsteady state unsaturated flow by means of kirchhoff transformation. *Water Resources Research*, 35(3):731–745, 1999.

G. Taylor. Dispersion of soluble matter in solvent flowing slowly through a tube. *Proceedings of the Royal Academy Society London*, A219, 1953.

H. A. Tchelepi and F. M. O. Jr. Interaction of viscous fingering, permeability heterogeneity, and gravity segragation in three dimensions. *SPE Reservoir Engineering*, pages 266–271, 1994.

V. C. Tidwell and R. J. Glass. X-ray and visible-light transmission for laboratory measurement of 2-dimensional saturation fields in thin-slab systems. *Water Resour Res*, 30 (11):2873–82, 1994.

S. Torquato. *Random Heterogeneous Materials*. Springer, New York, 2002.

S. Torquato, J. Beasley, and Y. Chiew. Two-point cluster function for continuum percolation. *Journal of Chemical Physics*, 88(10):6540–6547, 1988.

K. Unlu, D. Nielsen, and J. Biggar. Stochastic-analysis of unsatruated flow - one-dimensional monte-carlo simulations and comparison with spectral perturbation analysis and field observations. *Water Resources Research*, 26(9):2207–2218, 1990.

N. Ursino and T. Gimmi. Combined effect of heterogeneity, anisotropy and saturation on steady state flow and transport: Structure recognition and numerical simulation. *Water Resources Research*, 40:WO1415, doi:10.1029/2003WR002180, 2004.

M. T. van Genuchten. A closed-form equation for predicting the hydraulic conductivity of unsaturated soils. *Soil Science Society Am. Journal*, 44:892–898, 1980.

N. G. van Kampen. *Stochastic Processes in Physics and Chemistry*. North-Holland Personal Library, Amsterdam, 1992.

C. J. VanDuijn, A. Mikelic, and I. S. Pop. Effective equations for two-phase flow with trapping on the micro scale. *SIAM Journal of Applied Mathematics*, 62(5):1531–1568, 2002.

H.-J. Vogel. Topological characterization of porous media. In K. Mecke and D. Stoyan, editors, *Morphology of Condensed Matter - Physics and Geometry of Spatially Complex Systems, Lecture Notes in Physics, 600*, pages 75–92. Springer, 2002.

R. F. Voss. Random fractal forgeries. *Fundamental Algorithms for Computer Graphics*, F 17:805–34, 1985.

G. Wagner, P. Meakin, J. Feder, and T. Jossang. Invasion percolation on self-affine topographies. *Phys Rev E*, 55(2):1698–1703, 1997.

C. Welty and L. W. Gelhar. Stochastic analysis of the effects of fluid density and viscosity variability on macrodispersion in heterogeneous porous media. *Water Resources Research*, 27(8):2061–2075, 1991.

A. Western, G. Bloeschl, and R. B. Grayson. Toward capturing hydrologically significant connectivity in spatial patterns. *Water Resources Research*, 37(1):83–97, 2001.

S. Whitaker. Flow in porous media i: A theoretical derivation of darcy's law. *Transport in Porous Media*, 1:3–25, 1986a.

S. Whitaker. Flow in porous media ii: The governing equations for immiscible, two-phase flow. *Transport in Porous Media*, 1:105–125, 1986b.

S. Whitaker. *The Method of Volume Averaging*. Kluwer Academic Publishers, Dordrecht, 1999.

D. Wilkinson and J. F. Willemsen. Invasion percolation: a new form of percolation theory. *J Phys A*, 16:3365–76, 1983.

T. A. Witten and L. M. Sander. Diffusion-limited aggregation. *Phy Rev B*, 27(9):5686–97, 1983.

S. Wolfram. *Mathematica*. Addison-Wesley, Reading MA, 1991.

B. Xu, Y. C. Yortsos, and D. Salin. Invasion percolation with viscous forces. *Phy Rev E*, 57(1):739–51, 1998.

T. C. J. Yeh, L. W. Gelhar, and A. L. Gutjahr. Stochastic analysis of unsaturated flow in heterogeneous soils, 1, statistically isotropic media. *Water Resources Research*, 21(4): 457–464, 1985.

Y. C. Yortsos. Stability of displacement processes in porous media in radial flow geometries. *Physics of Fluids*, 30(10):2928–2935, 1987.

Y. C. Yortsos. Instabilities in displacement processes in porous media. *Journal of Condensed Matter*, 2:443–448, 1990.

Y. C. Yortsos and A. B. Huang. Linear stability anlysis of immiscible displacement: Part 1 - simple basic flow profiles. *SPE Reservoir Engineering*, pages 378–390, 1986.

D. Zhang. *Stochastic Methods for Flow in Porous Media*. Academic Press, San Diego, 2002.

D. Zhang. Nonstationary stochastic analysis of transient unsaturated flwo in randomly heterogeneous media. *Water Resources Research*, 35(4):1127–1141, 1999.

D. Zhang and H. Tchelepi. Stochastic analysis of immiscible two-phase flow in heterogeneous media. *SPE Journal*, 4(4):380–388, 1999.

D. Zhang, T. C. Wallstrom, and C. L. Winter. Stochastic analysis of steady-state unsaturated flow in heterogeneous media: Comparison of the brooks-corey and gardner-russo models. *Water Resources Research*, 34(6):1437–1449, 1998.

R. Zimmerman and G. Bodvarsson. Hydraulic conductivity of rock fractures. *Transport in Porous Media*, 23:1–30, 1996.

R. W. Zimmerman, D. Chen, and N. Cook. The effect of contact area on the permeability of fractures. *Journal of Hydrology*, 139:79–96, 1992.

B. Zinn and C. F. Harvey. When good statistical models of aquifer heterogeneity go bad: A comparison of flow, dispersion and mass transfer in connected and multivariate gaussian hydraulic conductivity fields. *Water Resources Research*, 39(3): doi10.1029/2001WR001146, 2003.